Optical and Morphological Characterization of Copper Zinc Tin Sulfide (CZTS) Nano-crystal Thin Film Solar Cell

Afrina Sharmin

A thesis submitted in partial fulfillment of the requirement for the Degree of Doctor of Philosophy (Ph.D.) in

Department of Electrical and Electronic Engineering (EEE), University of Dhaka, Dhaka, Bangladesh.

Registration no: 24/2019-20 (new)

04/2014-15 (old)

July, 2023

To Qazi Ishtiaq Hossain

Declaration

I hereby proclaim that the research project, titled "Optical and morphological characterization of Copper Zinc Tin Sulfide (CZTS) Nano-crystal Thin film Solar cell," is the consequence of my research, which was conducted under the supervision of Professor Dr. S.M. Mostafa Al Mamun, Professor, Department of Electrical and Electronic Engineering, University of Dhaka and Dr. Samia Tabassum, Principal Scientific Officer, IFRD, BCSIR. The facts from other research have been correctly cited. I further declare that this project was not submitted for the purpose of acquiring a research degree from this university or any other university or institution in the country or overseas.

_____

Afrina Sharmin

Department of Electrical and Electronic Engineering

University of Dhaka.

_____

Co-Supervisor

Dr. Samia Tabassum

Principal Scientific Officer

IERD, BCSIR, Dhaka

_____

Supervisor

Dr. S.M. Mostafa Al Mamun

Professor

Department of Electrical and Electronic Engineering

University of Dhaka

Certificate of Approval

This is to ensure that Ms. Afrina Sharmin, Ph.D. scholar, Department of Electrical and Electronic Engineering, University of Dhaka, has conducted research in the above-mentioned department and Institute of Fuel Research and Development (IFRD), BCSIR, Dhaka-1205, under our guidance and supervision. The result of research work has been acquiesced by Ms. Afrina Sharmin in this thesis entitled 'Optical and Morphological characterization of Copper Zinc Tin Sulfide (CZTS) Nano-crystal Thin film Solar cell' for the degree of Doctor of Philosophy.

Ms. Afrina Sharmin has contented all the necessities under the PhD Regulations of the University of Dhaka and encounterssatisfactoryperformance standards. This thesis, in its entirety or in part, has not been submitted to any other academic or institution for any other degree or diploma, to the best of our knowledge.

_____

Co-Supervisor

Dr. Samia Tabassum

Principal Scientific Officer

IERD, BCSIR, Dhaka

_____

Supervisor

Dr. S. M. Mostafa Al Mamun

Professor

Department of Electrical and Electron Engineering

University of Dhaka

Abstract

Development of economical and highly proficient solar cells is crucial to gratify the rising global call. Solar energy generation is a technologically feasible method, though primarily it's expensive. Copper-zinc-tin-sulfide (CZTS) is another alternative compound that fascinates all soalr cell material researchers. To date, the best CZTS solar cell converts only 11% (for CZTSe, it's 12.6% for ACZTSSe, 13.8%.) of light into electricity, paralleled to above 27.6% for single crystal silicon concentrator type solar cells. As the theoretical efficiency of CZTS is about 30%, therefore, it can be said that CZTS solar cells are still in a premature enquiry stage where much of the area is yet to be explored. The rapid advancements in the efficiency of CZTS solar cells are accredited to a trial-and-error methodology to module assembly. This has led to a fundamental knowledge gap of CZTS. This thesis aimed to reduce this knowledge gap to its best. Throughout the study, the ability to regulate the composition, crystallinity and stoichiometry of CZTS thin films has been demonstrated and preliminary efforts in pre and post annealing treatment towards crystalline films are promising indeed. In the context of this project, tunable band gap absorber material, specifically, Cu_2ZnSnS_4 (CZTS) is fabricated by three different methods to find out better morphology, composition, stoichimetry and other opto electronic properties for photovoltaic application. Kesterite CZTS is collection of plentiful fundamentals and non-toxic substantial, with necessary attributes for photovoltaic (PV) uses, for example, high absorption coefficient ~10^{-4} cm^{-1} and a band gap energy (E_g) adjacent to 1.5 eV. The effect of various deposition techniques and annealing parameters on film growth was explored using optical, morphological, and structural material characterizations along with composition analyses. The sputtered kesterite which reveals best quality thin film for this study, must be annealed to produce device-grade films. Moreover, sputter system provides the facilities achieving a desired thickness of the film. The prepared film is undergoing post-annealing treatment with different temperatures (250-560° C) and pressure (150- 450 Torr). XRD pattern shows preferential characteristics peak along (112), (220), and (312) and phase purity is inveterate by Raman studies. The granules are compact, and as the annealing temperature rises, agglomeration increases, boosting the absorption coefficient. The band gap energy (E_g) differs between 1.47-1.51 eV which is compatible with optimum values. Sputtered films have uniform surface topography and thickness. As a result, the film has significantly better covering than the sol deposited film. RMS roughness increases with annealing heat and base pressure. The chemical composition of the fabricated sample shows good atomic stoichiometry of the film. The elemental composition is observed as Cu and S enriched Zn and Sn deficient without sulfurization. SnS loss occurs at temperatures of above 500 °C which results cavities on film surface and affects the stoichiometry of the film. The current study shows that sputter deposition may be used to produce CZTS thin films on soda lime glass (SLG) with molybdenum (Mo) back contact for prospective solar cell applications. In addition, impurity doped ZnO (ZnO: Al or AZO), which has been examined for this thesis, is currently the best indium-free contender for an alternative TCO compound. In particular, the study is concentrated on the consequence of depositions factors and techniques with extensive analysis of AZO fabrication to find an equally transparent, efficient, cheap, more readily available, and electrically conductive alternate to Indium. The findings of the research work encompasses a range of significant contributions, from discovering empirical evidence to optimizing different key parameters for CZTS and AZO thin films, and finally, developing a complete and optimized **SLG/ Mo/CZTS/CdS/i-ZnO/AZO** solar cell fabrication process. Moreover, A comprehensive theoretical model of CZTS solar cell has been developed and anlyzed. From the Simulations, the maximum PCE is shown as 23.74% with V_{oc}= 1.62 V and J_{sc}= 28.37 mA/cm^2 for 3000 nm CZTS absorber layer. The research not only advances the understanding of solar cell technology but also has practical implications for sustainable energy solutions in the future.

Acknowledgement

The Solar Energy Technology Research Laboratory of the Institute of Fuel Research and Development (IFRD) of the Bangladesh Council of Scientific and Industrial Research (BCSIR) was responsible for a great deal of this study. This applies to the production of all films as well as the majority of characterization and analysis.

First and foremost, I want to express my gratitude to Dr. S.M. Mostafa Al Mamun, my supervisor, for his advice and assistance throughout the academic research and writing of my thesis. I'd want to express my gratitude to Dr. Samia Tabassum, PSO, IERD for her assistance during the investigation.

I'd like to thank M. S. Bashar, PSO, IERD, BCSIR for his diligence and direction in providing technical support for characterisation using XRD, AFM, HE, UV-Vis, and Surface profilometer, as well as film deposition procedures.

It was a pleasure for me to participate in numerous fruitful exchanges that fueled my research efforts. I gladly acknowledge the discussions with Dr. Zahid Hassan Mahmood, Professor, Department of Electrical and Electronic Engineering, University of Dhaka, M.S. Bashar, PSO, IFRD, BCSIR and Dr. S.M. Mostafa Al Mamun for their patience and immense support.

Last but not least, I owe a debt of gratitude to my parents and spouse for their unwavering support throughout my PhD studies.

Scientific publications

Journal:

1. **'Influence of annealing conditions on the performance of sputtered grown CZTS thin film solar cells',** Afrina Sharmin, Koushik Kumar, S. M. Mostafa Al Mamun, *and* Mainul Hossain, AIP Advances 12, 115025 (2022); https://doi.org/10.1063/5.0130395

2. **Sputtered single-phase kesterite Cu_2ZnSnS_4 (CZTS) thin film for photovoltaic applications: Post annealing parameter optimization and property analysis'**, Afrina Sharmin, M. S. Bashar, Munira Sultana, S.M. Mostafa Al Mamun. AIP Advances 10(1), 015230 (2020). https://doi.org/10.1063/1.5129202

3. '**Low Cost and Sol-Gel Processed Earth Abundant Cu_2ZnSnS_4Thin Film as an Absorber Layer for Solar Cell: Annealing without Sulfurization'**, Afrina Sharmin, M. S. Bashar, Samia Tabassum, Zahid Hasan Mahmood. International Journal of Thin Film Science and Technology, 8 (2),65-74, 2019. http://www.naturalspublishing.com/ContIss.asp?IssID=1600

4. '**Depositions and characterization of sol gel processed Al-Doped ZnO (AZO) as Transparent Conducting Oxide (TCO) for solar cell application'**Afrina Sharmin, Samia Tabassum, M. S. Bashar, Zahid Hasan Mahmood. Journal of Theoretical and Applied Physics. 13(2),123-132, 2019https://doi.org/10.1007/s40094-019-0329-0

5. **Properties of Cu_2ZnSnS_4 Thin Films Fabricated by Dip Coating Technique for Solar Cell Application'**. Sabiha Dilruba, Tabassum Perveen Ananna, Afrina Sharmin, M. S. Bashar, Zahid Hasan Mahmood. American International Journal of Research in Science, Technology, Engineering & Mathematics, 26(1), 170-178, 2019. http://www.iasir.net.

6. **'Study on the Effect of Varying Film Thickness on the Transparent Conductive Nature of Aluminum Doped Zinc Oxide Deposited by Dip Coating'**; Rosaleena Rafique,Kaniz Naila Tonny, Afrina Sharmin, Zahid Hasan Mahmood; Materials Focus 7(5),7070-713, 2018.https://doi.org/10.1166/mat.2018.1572

7. '**Electrical, optical and structural properties of transparent conducting Al doped ZnO (AZO) deposited by sol-gel spin coating'**, Kaniz NailaTonny, RosaleenaRafique, Afrina Sharmin, Muhammad Shahriar Bashar,Zahid Hasan Mahmood; AIP Advances 8, 065307, 2018. . https://doi.org/10.1063/1.5023020

8. **'Progress in Major Thin-filmSolar Cells: Growth Technologies, Layer Materials and Efficiencies.'** Abu Kawser, Syed Farid Uddin Farhad , Mashudur Rahaman , Md. Saidul Islam, Abdullah Yousuf Imam, Sumon Chandra Debnath, Munira Sultana, Md. Azizul Hoque, Afrina Sharmin, Zahid Hasan Mahmood. **InternationalJournal of Renewable Energy Research (IJRER), 9(2), 579-597, 2019.** www.ijrer.org/ijrer

9. '**Analysis and Theoretical Efficiencies of $GaInP_2$/GaAs/Ge Multijunction Solar Cell'**; Abu kowser, Md. Abul Hossin, Md Sofikul Islam, Afrina Sharmin, Zahid Hasan Mahmood; **Dhaka University Journal of Applied Science and Engineering (DUJAPSE)**, 3(1), 1-5. 2015. http://journal.library.du.ac.bd/index.php?journal=DUJAPSE

Conference:

1. International Leadership Talk on "**Design and Fabrication of Cu_2ZnSnS_4(CZTS) Thin Film Solar Cell**", **Keynote Speaker**, Department of mechanical Engineering, Synergy Institute of Technology, Bhubaneswar, India, 26 Dec, 2022.

2. '**Working Principle of Semiconductor based Solar Cell**'; ***Keynote Speaker*** at Synergy International Leadership Talk at Synergy Institute of Technology, Bhubaneswar, India, 01 Oct, 2021.

3. **'Mg nano particle doping effect on cadmium sulfide (CdS) thin film to enhance photoconversion efficiency for CdTe based solar cell'**; Sadat Islam Khan, Munshi Sajidul Islam, Afrina Sharmin, Syed Shafquat Mahmood, Munira Sultana, Imtiaz Ahmed* and M S Bashar*. International Conference on Science and Technology for celebrating Birth Centenary of Bangabandhu(ICSTB-2021)" , 11-13 March, 2021.

4. **'Recent advances in Thin Film Solar Cell Research for Energy and Environment', Keynote Speaker,** Synergy International Leadership Talkorganized by Department of Mechanical Engineering, Synergy Institute of Technology, Bhubaneswar, India in collaboration with Institute of Innovation Council (Ministry of HRD), 11 September, 2020.

5. **'Aspects of Numeral Value of Cu_2ZnSnS_4 (CZTS) Absorber Layer Fabricated in Sol-gel Process by Dip Coating Technique'**, S Dilruba, A Sharmin, TP Ananna, ZH Mahmood. 1st International Conference on Advances in Science, Engineering and Robotics Technology (ICASERT), IEEE, Dhaka, Bangladesh, 2019.

6. **'Effect of annealing temperature on different properties of CZTS thin film synthesized by sol-gel spin coating'**, Afrina Sharmin, M S Bashar, Samia Tabassum, Zahid Hasan Mahmood.International Conference on Material Sciences and Semiconductor Device (ICMSSD), 7-8 September, 2018

7. **'Effect of Zn concentration on different properties of Al doped ZnO Thin film deposited by Sol-gel Method'** , Afrina Sharmin, Samia Tabassum, M S Bashar, Zahid Hasan Mahmood.International Conference on Engineering Materials and Metallurgical Engineering (ICEMME), 22- 24 December, 2016.

8. '**Emerging Solar Energy Technologies in Bangladesh and Research activities of IFRD, BCSIR'**, **Keynote speaker**, Renewable related energy focusing on Microalgae Technology Using Ocean Resources including Solar and Fuel Cell, Iran (31Oct-02 Nov, 2016). Organized by IROST, COMSATS and USB, Iran.

Poster

1. **'Effect of annealing temperature on earth abundant Cu_2ZnSnS_4 thin film for photovoltaic application synthesized by low cost sol-gel spin coating.'**

'International Conference on Advanced Materials for Clean Energy and Health applications' (AMCEHA 2019), February 6-8, 2019, University of Jaffna, Jaffna, Sri Lanka.

2. **'Solar Thermal and Solar Photovoltaic Technologies and Application in Bangladesh.'**

Indian Nanoelectronics Users Program(INUP) Familiarization Workshop, 10-12 Sep, 2018, Indian Institute of Science (IISc), Bangalore, India.

Table of Contents

List of Figures

List of Tables

Chapter 1: Introduction

1.1.General Introduction

i. Global Warming: A vital warning to mankind!

One of the main causes of global warming is the excessive generation of greenhouse gases that develops during the production of energy from fossil fuels. International Panel on Climate Change (IPCC) has been issuing reports intermittently on the communal scientific considerate of climate change since 1990 [1] and its correlation to human activity as UN Secretary General Ban Ki-Moon remarked in 2007 "the IPCC has now unequivocally confirmed the warming of our climate system and linked it directly to human activity"[2]. It is now obvious that humanity must modify its way of life, notably in terms of energy generation and utilization, in addition to the limited quantity of fossil fuels. So several so-called renewable energy options are predictable to become more significant in near future (Fig.1.1). By 2100, it is anticipated that traditional fossil fuels including coal, oil, and natural gas will still be available. Their relative share in the future energy will, however, significantly decrease. Renewable resources of energy options like wind, biomass, water, and solar energy is expected to be dominating the energy supply in the twenty-second century [3]. Even more energy than 60% is predicted to come from solar sources. Heat and electricity can be produced from solar energy. However, Becquerel's discovery of the photovoltaic effect in 1839, allows direct conversion of sun light to electric energy[4].

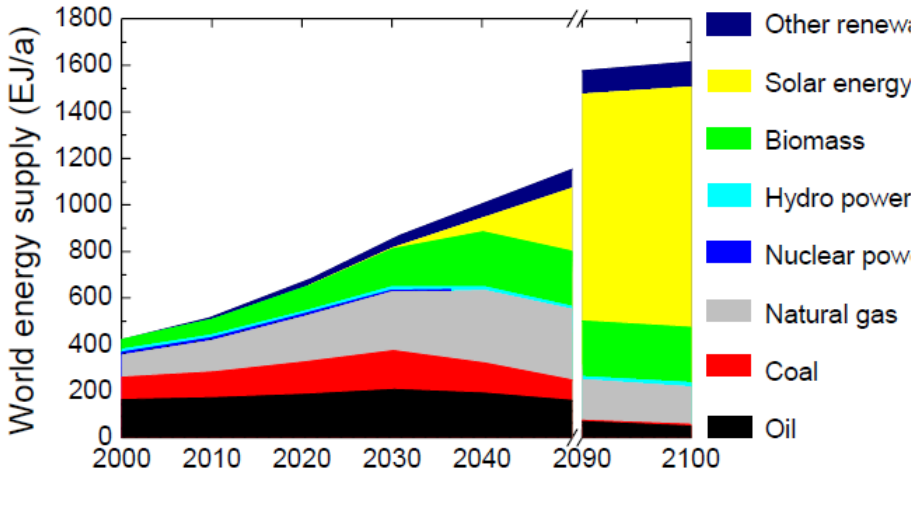

Fig.1.1: *The upcoming energy assortment anticipated by German Advisory Council on Global Change***.**[5]

ii. Energy from sunlight: The global solution

It is commonly acknowledged that generating energy by burning things does not bode well for future generations. The key to solving the problem is the worldwide reliance on renewable sources of energy. Photovoltaics (PV) is one of the replacements being studied. PV is the method of directly altering solar energy into electrical energy. The PV "product" is a solar cell, which is basically an optoelectronic device. The majority of solar cells have their highest conversion efficiency when operating between 0.6 and 1.1 volts [6].

For a variety of reasons, photovoltaic is a particularly appealing option-

1. Solar energy has no limit. Additional renewable energy sources, like wind, biomass, and hydropower, simply cannot compete with solar energy's widespread availability. The current global energy required to command the world per unit time is roughly 20 TW, and this amount is rapidly

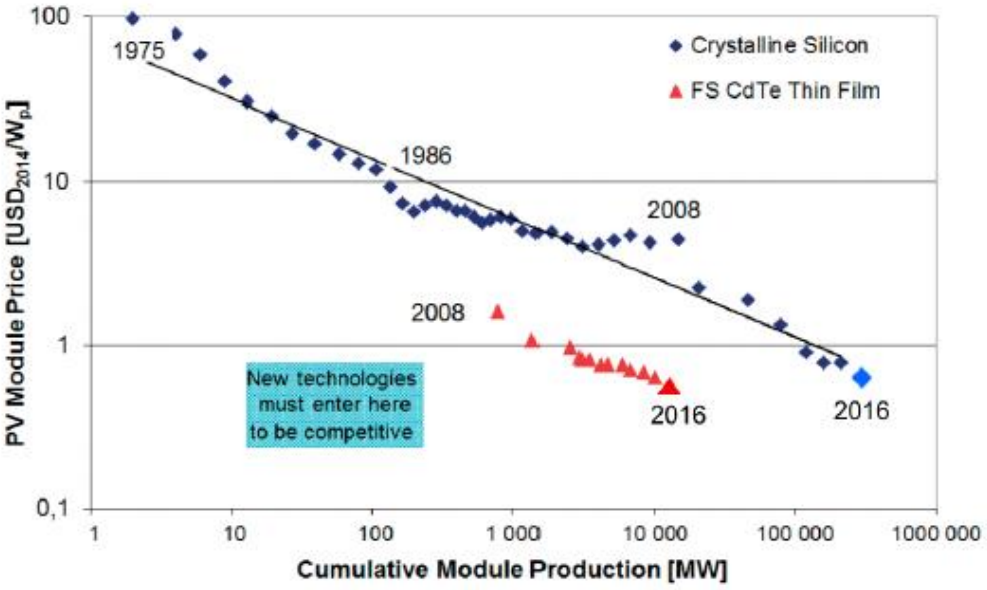

(a)

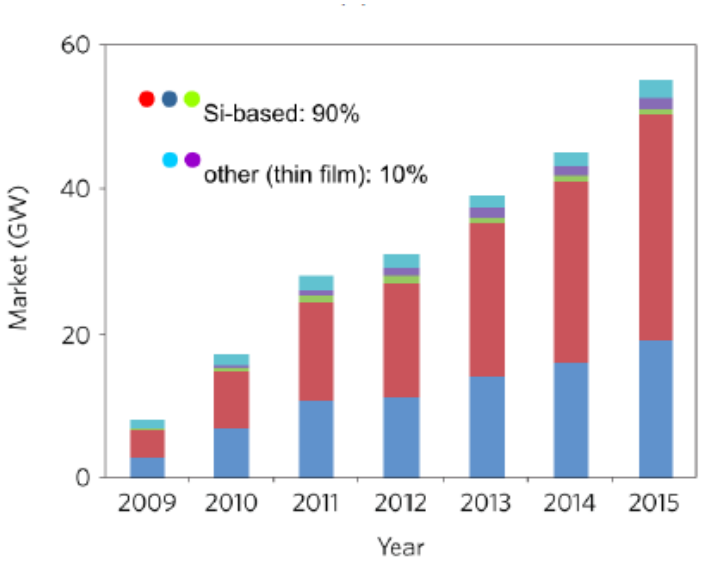

(b)

Fig.1.2 (a). *PV module pricing [7,8],* ***(b):*** *Breakdown of the PV market [6].*

growing. According to a study by Hegedus S and Luque, if PV can transform solar energy into electricity at an average efficiency of 1% immediate solar irradiance and 0% at night, and solar panels cover 0.6 % of the surface of the earth area, they could supply the whole need. [19].

2. Solar energy is free. Once solar energy was used to be pricey but as you can see from Fig.2(a), it is reduced day by day. It is currently over 10 times less expensive than it was 35 years ago. Solar energy has attained grid parity in areas of the world with the highest solar irradiation. As a result, it is now less expensive than the electrical energy supplied by traditional electrical dispersal arrangements.

3. Solar energy is safe, sound and ecofriendly. It does not necessitate substantial landscape changes and appears to be rather attractive. There may be certain concerns with nuclear, hydro, and wind energy, respectively.

4. Solar energy can be used to power GW-scale power plants that feed the grid, or it could be installed on a roof or reserved property and afford a few kW of power to a homeowner or manufacturing plant, which can trade the excess to the nationwide grid. It might be utilized to power similar devices with less than a Watt of power in calculators and backpacks, or as a micro-energy mower to command microchips in wireless sensor that necessitate power in the μW . Various PV equipment constructed on different photovoltaic constituents are already available. They offers a specific use in which they excel [20, 9].

5. Solar energy is the most available, available, unrestricted and direct source of energy on the planet. The proportion at which solar energy is captured by the earth is approximately 10,000 times faster than the ratio at which humans consume energy. Solar energy is not distributed evenly throughout the globe. Many solar energy techniques is being used as a source of energy almost anywhere on the planet. For a long time, photovoltaic system is being utilized in dedicated applications. Furthermore, PV systems that are both stand-alone and grid-connected has been utilized since 1990.

There is a very common problem of most renewable energy sources. Like other renewable energy sources, it is subject to fluctuations with different parameters and even with locations. If there is no wind, there is no energy from wind. If it's dark, there is no energy from sun. Conventional fuels do not behave like this which gives a great flexibility. Given these constraints, significant advancements in energy storing technology are required aforegradually terminated CO_2 emitting fuels. However, it is possible that conventional power plants could be used as a backup energy source in the first stage if renewable energy sources are unavailable.

iii. Solar Cell: Nanotechnology application

Electrons could engage with electromagnetic radiation, as demonstrated by the photovoltaic effect [4]. The physical principle of photovoltaic (PV) devices, which transform solar light into electricity, is this communication. The use of solar panels to generate electricity is now a global trend. It is a process which converts solar energy into electricity directly.The annual growth rate for PV production was more than 50% in the last decade, thanks to a supportive pricing policy. It is one of the wildest risingtechnologies with market prices that are already competitive. Nonetheless, there is still room for new resources, knowledge, and idealistic technology to be explored.
In 1959, Richard Feynman conveyed a speech in CalTech where he said '*There is plenty of room at the bottom.'* Feynman won the Nobel Prize in 1965 for his concept of nano science and nanotechnology. Scientists have been studying and working with nanoparticles for centuries. But to understand the

structure and success of nano particles took a long time. Microscopes that can display particles as small as atoms have enabled scientists to see what they're working on, allowing them to really explore nano-sized materials. And as a result of that episode, a whole new universe of possibilities has opened up in a range of sectors and scientific efforts. Nanotechnology, which is typically a collection of strategies that allows manipulation of properties at a very small scale, has a wide range of uses, counting drug delivery, fabrics, the study of material reactivity and strength, Micro/Nano Electro Mechanical Systems (MEMS, NEMS), Molecular Manufacturing, medicine, food, fuel cells, solar cells, water quality, a chemical sensor, and so on. Through the utilization of nanoparticles in the production of solar cells provides significant advantages:

- Manufacturing costs are reduced as a result of adopting a low temperature technique rather than the high temperature vacuum deposition procedure that is generally utilized to make traditional cells composed of crystalline semiconductor material.
- It lowers the cost of implementation. Flexible rolls were used instead of stiff crystalline panels to save money. This is also a feature of semiconductor thin films.

Traditional solar cell is not as competitive as nanotechnology solar cells. Traditional technologies are rather inexpensive. As a result, nanotechnology alternatives should be less expensive. Advanced technologies, such as quantum dots, are expected to able to achieve higher proficiency compared to traditional ones.

The first Photovoltaic device with a rational conversion efficiency was established in 1954 by Chapin *et al.* at Bell laboratory [5]. It was founded on crystalline silicon (c-Si). This c-Si solar cell revealed an energy alteration efficiency of ~6 % [5] and the record efficiency has been improved up to 24.7 % [6]. While c-Si solar cell is once thought to be prohibitively expensive for use on the ground, they nevertheless control the PV market with a share of over 90% today. Solar cells based on thin films, such as a-Si:H, CdTe, CuIn(Ga)Se_2, and most recently Cu_2ZnSnS_4, are responsible for the remainder of the PV market.

Table1.1.The list of some companies and materials they used for manufacturing a solar cell.

Company	**Materials Used**
Global Photonics	Organic solar cells
Innovalight	Silicon nano crystalline ink
EnSol	Nanocrystals implanted in a thin film compound
Solarmer Energy	Nanoparticles in plastic solar cells
Nanosolar	Copper-Indium-Diselenide semiconductor ink
Bloo Solar	Nano-cables has developed on thin film materials

iv. CZTS Thin Film Solar Cell: A new approach

Solar cell prepared from amorphous hydrogenated silicon (a-Si:H) has been on the market for nearly 40 years. Carlson and Wronski reported on the first production of amorphous hydrogenated silicon in 1976. [10]. The technology is broadly employed in different applications. However, only low power is necessitated and economic expense are desired like handheld calculators, solar caps or solar charger for small gadgets. Due to the growing interest in photovoltaic technology in recent years, a-Si:H based solar cells have caused quite a stir due to their prospective applications and low cost per watt. This is particularly inspiring for hugeefficacyscale Photovoltaic projects. Combining a-Si:H devices with hydrogenated microcrystalline (mc-Si:H) silicon solar cells, that is first designated by Faraji et al. [11] and Flückiger et al. [12], could considerably improve their efficiency. Meier et al. [13] demonstrated that combining both cells into the a-Si:H/mc- Si:H technology leads to greater efficiencies of up to 12.3 %[14]. Using an a-Si:H/mc-Si:H/mc-Si:H triple cell technique, even greater efficiencies of up to 13.4 percent were demonstrated [15]. These record efficiencies are still modest when matched to other solar cell technologies. The fact that the total expense of a photovoltaic system typically scales with the system's area rather than the deployed electrical power. As a result, better adaptation efficiencies of thin film silicon solar cells are crucial.

CIGS- and CdTe solar cells, like a:Si:H photovoltaics, have a 40-year track record (Fig 1.3). As a result of their present production numbers and current regulation, they are destined to dictate the thin film photovoltaic sector. The availability of the relatively uncommon elements, on the other hand, is a major worry. In the case of photovoltaic cells, demand for In, Ga, Te, and Se should spike [16, 17]. Additionally, Cd is a dangerous heavy metal for mankind. In certain regions of the world, legislation is already moving toward outright prohibition of Cd. CdTe modules are not permitted on domestic rooftops in Japan. Weighty elements like Cd and Pb were specifically excluded from saleable items in the European Union under the Restriction on Hazardous Substances (RoHS) regulation [18]. PV modules are now excluded from the RoHS requirements, although this may change in the future. As a result, it appears that neither CIGS nor CdTe solar cells represent a viable extensive standing answer to the world's energy shortage. Because the causes behind this are inherent in their essential elements, the solitary way to fix them is to move to another materials.

Commercially accessible thin film modules have a number of drawbacks, including poor efficiency (a-Si), a scarcity of raw materials (Te in CdTe and In in CIGS technology), and resources noxiousness (Cd in CdTe technology). In current situation, CZTS/Se proved to be an interesting and promising material for usage as a chalcogenide absorber in photovoltaic cells. Furthermore, it is created from non-toxic (no Selenium), plentiful and cost effective raw ingredients, has an ideal absorption coefficient and band gap energy, and has demonstrated great efficiency in lab studies. [21].

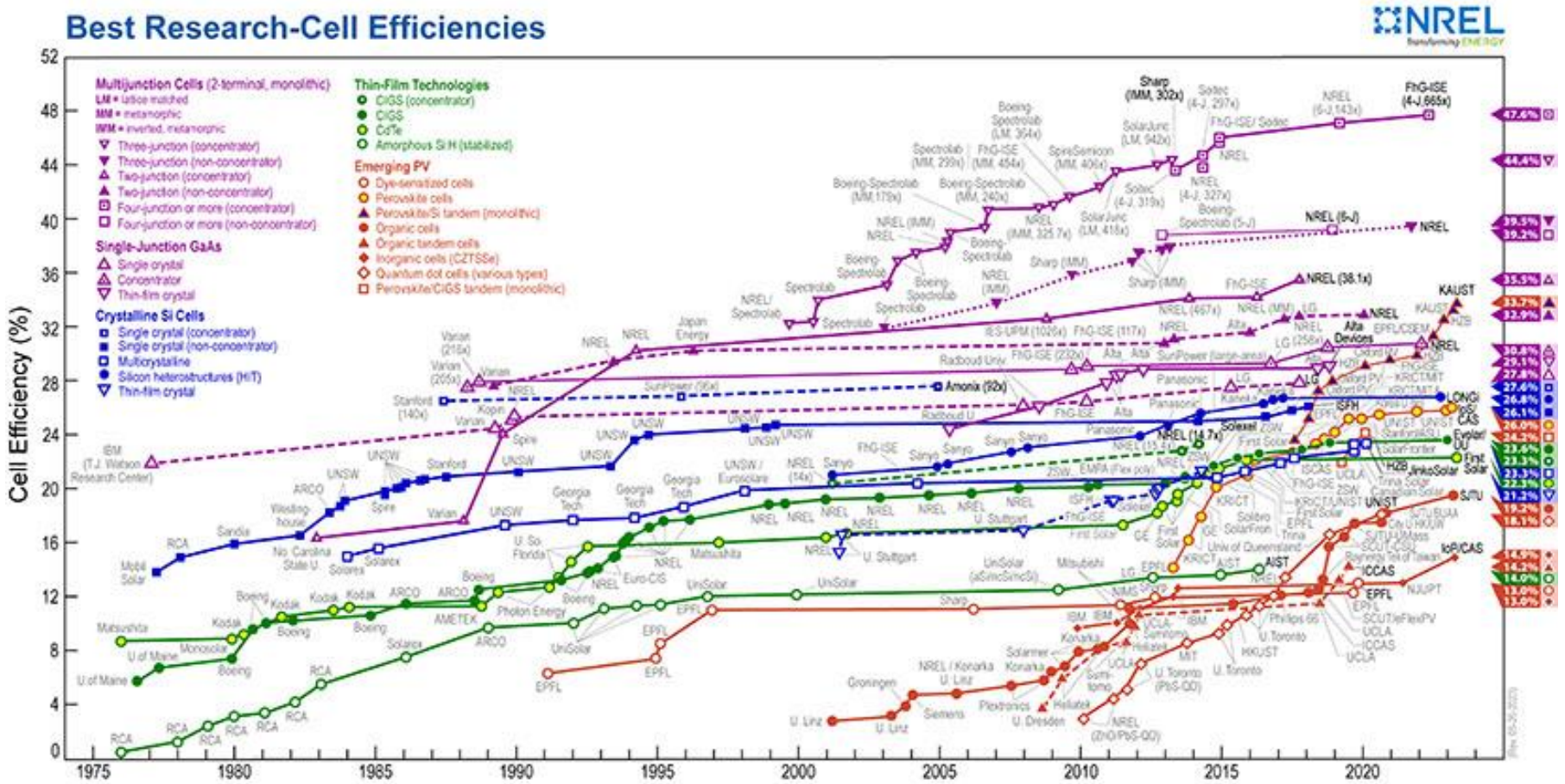

Fig.1.3. *Solar cell power conversion efficiencies (PCE) [28]*

1.2. Motivation

Hypothesis

Sustainable chalcogenide based, CZTS thin film solar cells have concerned a lot of interest in recent times due to the due to low cost, non-toxic nature high abundance, and excellent absorption characteristics (band gap 1.4-1.5eV) of CZTS. Last 10 years have seen a significant enhancement in the performance of CZTS solar cells. However, despite promising efforts, CZTS solar cells had a limited power conversion efficiency (PCE) of~ 10% until only recently. For example, using 600 nm CZTS absorber layer, fabricated by a vacuum process, Shin *et al.*[29] achieved 8.4% PCE. The PCE was improved to 9.4% by controlled deposition and annealing of a 40 nm CdS layer, as reported by Tajima *et al.*[30]. Non-radiative recombination within the CZTS heterostructure results in large voltage loss and has been a major limiter, in enhancing the PCE. In 2018, Yan *et al.*[31,32] reported a record PCE of 11.3% by using heat treatment to reduce the recombination. Several strategies are yet to be explored, in depth, which may enhance the performance of CZTS thin film solar cells. These include minimizing defects, reducing interfacial recombination, minimizing series resistance, and using a highly reflective back contact [33]

Several key deposition method parameters can be attuned to regulate the CZTS thin films solar cell attributes. Numerous series of sample prepared using various deposition techniques are employed in this research in order to illustrate the function and impact of the major deposition parameters. There appear to be two crucial factors in this situation that merit consideration if production costs are to remain competitive. First, the deposition at low substrate temperatures marginally shortens the deposition time and costs and primarily pave the way for the use of plastic substrates, which are intriguing because of their inexpensive cost and their mechanical qualities i.e. flexibility. Second, a significant rise in the deposition rate could result in a further reduction of the production costs. This work addresses each of these problems. The electrical characteristics of each layer of solar cell are directly influenced by its structure. And multiple thickness series of samples individually are explored to study the impact of the structure.

Research Questions

a. What is the impact of crystallographic defects?
b. Which deposition process does show great morphology?
c. What solution processing technique yields highest PCE?
d. What is the impact of deposition and annealing parameters on film stoichiometry?
e. How does stacking faults at CZTS layer influence solar cell's performance?
f. For a low cost approach, does plastic really work as an alternate to glass substrate?

1.3. Aim of this study

Cu_2ZnSnS_4, called as "CZTS" is a relatively new and also suitable material with some benefits over the technology that now benefits consumers along with silicon(Si), the best-understood material for PV on the planet. CZTS and Silicon(Si) are the light-absorbing compound of respective solar cell. There are some essentials for an ideal solar cell device as follows.

i. Enhance the quality of each material by producing it in the most efficient manner possible;
ii. considering the smartest combination of materials that work well together;

iii. High absorption coefficient
iv. Junction formation ability
v. Long diffusion length
vi. Absorbing as many photons as possible
vii. Low recombination velocity
viii. Reduce the defect formation
ix. To maximize the number of carriers created and extracted
x. Ecofriendly and low cost materials

The points to be noted for solar panel manufacturing-

i. To minimizing materials cost (<1$/watt)
ii. Minimum material/ watt
iii. Minimum Energy input/watt
iv. Ensuring mechanical integrity.
v. High stability and long life (>20years)
vi. Energy payback period (< 2 years)

Meanwhile, there are some interesting advantages of CZTS with respect to silicon i.e.

I. Involves 200 times less solid
II. It can be fabricated with economical methods
III. The deposition or fabrication temperature is lower;
IV. Capable of fabricating an unobtrusive-looking solar cell.

The research of a trade-off between low processing cost and high performances CZTS has motivated the consideration of the scientific society through CZTS solar cells. To date, the best CZTS solar cell converts only 11% (for CZTSe, it's 12.6%) of light into electricity whereas it is over 27.6% for single crystal silicon concentrator type solar cells. Then the question may arise, 'why CZTS?' Yes, it is still CZTS as CZTS solar cells are still in the development stage. When equated to other materials, CZTS has the benefit of having optical and electrical attributes that enable the development of photovoltaic thin film technology that could scale up to several GW/year [23]. Moreover, it does not comprise any critical chemical elements. As a result, CZTS solar cell performance must be strengthened for manufacturing output. CZTS Nanocrystal was first reported in 2009 and the conversion efficiency was recorded as 7.2% in 2010. In 2012, the CZTSSe solar cell predicated on nanocrystals achieved an energy conversion proficiency of 9.85 % [24]. Hence, further research needs to be done in the field of enhancement of the synthesis of CZTS nanocrystal inks and the corresponding film technology [25]. Todorov*et al*. informed an enhancement of the module performance by adjustment of the chemical composition of CZTS/Se absorber layer [26]. This could be the perfect choice for this research work as well. However there are some limitations that still existed such as insufficiency in open circuit voltage (V_{oc}), fatalities in fill factor (FF) which offer plenty of room for improvement. Taking all these into consideration, high improvements in device performance are expected from this endeavor which will be cost effective as well. Moreover, the vast analysis and characterization techniques would reveal some mechanisms like grain rotations and re-crystallization [27], which control the evolution of the nanostructure.

So, here comes the aim of this thesis:

i. Understand the different fabrication processes like (a) Sol Gel Spin and Dip coating and (b) Sputtering to find the most apposite deposition process for solar cell fabrication.
ii. Optimization of deposition parameters to fabricate CZTS absorber layer.
iii. Optimization of annealing parameters to obtain device grade CZTS thin film.
iv. Investigation of AZO as a possible alternative to expensive ITO or FTO.
v. Modelling, Simulation and Fabrication of complete CZTS solar cell.

1.4.Outline

In the **second chapter** of this thesis, the detailed description of thin films solar cells and the background of photovoltaic is narrated. The physics of solar cells via light-to-current conversion, as well as the main properties and parameters of photovoltaic devices are covered in detail. And the working principles and the evolution of CZTS material are recounted.
The experimental instruments and methodologies employed in this study are designated in **Chapter 3**. It includes different processes used for thin film fabrication. Different characterization tools are also described here which are used in thin film analysis.
Chapter 4 contains a thorough investigation and analysis of the Al doped ZnO (AZO) as a see through conductive oxide of CZTS solar cell. This chapter provides a wide-ranging interpretation of the electrical possessions of the AZO thin film. Successively, the chapter evaluates the principal features of the consequence of the fabrication parameters on electrical, optical, and morphological attributes with the deviation of film wideness.
The optical properties of CZTS is described in **Chapter 5** along withmorphology, and composition of absorber layer. Finally, the degradation of the morphology and configuration of materials with the change of annealing parameter is described. The nature of this phenomena is described, as well as a possible solution based on the optimization of the deposition parameter is reported.

1.5.Bibliography

[1] International Panel on Climate Change, http://www.ipcc.ch/
[2] United Nations Secretary General Ban Ki moon,
http://www.un.org/News/Press/docs/2007/sgsm11175.doc.htm
[3] German Advisory Council on Global Change, World in Transition, TowardsSustainable Energy Systems, www.wbgu.de
[4]E. Becquerel, "On Electron Effects under the Influence of Solar Radiation,"Compt. Rend. 9, 561, 1839.
[5] D. M. Chapin, C. S. Fuller, and G. L. Pearson, J. Appl. Phys. 25, 676 , 1954.
[6]M A Green, K Emery , Y Hishikawa , W Warta and E D Dunlop, " Solar Cell Efficiency Tables (Version 45)," Progress inPhotovoltaics: Research and Applications, 24, 905-913, 2016.
[7] Jager-Waldau A 2014 PV Status Report JRC 92477
[8] Module prices for selected models in Germany Photon International, fraunhofer ISE, 42, 2016.
[9] M AGreen,"Commercial progress and challenges for photovoltaics,"Nature Energy, 1 15015, 2016.
[10] D. E. Carlson and C. R. Wronski, "Amorphous silicon solar cell," Applied Physics Letters 28(11) 671 –673 1976.
[11] M. farazi et al., "High mobility hydrogenated and oxygenated microcrystalline silicon as a photosensitive material in photovoltaic applications," Applied Physics Letters, 60(26) 3289–3291,1992.
[12] R. Fluckiger et al., "Microcrystalline silicon prepared with the very high frequency glow discharge technique for p-i-n solar cell applications,"11th EC Photovoltaic Solar Energy Conférence, p. 617,1992.

[13] J Meier et al.,"On the Way Towards High Efficiency Thin Film Silicon Solar Cells by the 'Micromorph' Concept," MRS Proceedings, p. 420, 1996.
[14] U kroll et al., "Recent Developments of High-Efficiency Micromorph Tandem Solar Cells in KAI-M/ Plasmabox PECVD Reactors," 26th European Photovoltaic Solar Energy Conference and Exhibition (3BO.2.6) 2011.
[15] S. W. Ahn, S. E. Lee and H. M. Lee, "Toward commercialization of triple-junction thin-film silicon solar panel with >12% efficiency,"27th European Photovoltaic Solar Energy Conference, 3AO5.1, Frankfurt, 2012.
[16] "Rare Earth Elements|Critical Resources for High Technology" USGS Fact,Sheet 087-02, 2005
[17] P C K Vesborg andT F Jaramillo, "Addressing the terawatt challenge: scalability in the supply of chemical elements for renewable energy," RSC Advances 2 7933, 2012.
[18] Directive 2011/65/EU of the European Parliament and of the Council of 8 June 2011 on the restriction of the use of certain hazardous substances in electrical and equipment (recast).
[19] S Hegedus and A Luque, "Achievements and Challenges of Solar Electricity from PhotovoltaicsHandbook of Photovoltaic Science and Engineering," (Chichester, UK: John Wiley & Sons, Ltd) pp 1-38, 2011.
[20] S Hegedus and A Luque, "Achievements and Challenges of Solar Electricity from Photovoltaics Handbook of Photovoltaic Science and Engineering," Chichester, UK: John Wiley & Sons, Ltd, pp 1-38, 2011.
[21] W. Ki, H. W. Hillhouse, "Earth-Abundant Element Photovoltaics Directly from Soluble Precursors with High Yield Using a Non-Toxic Solvent,"Adv. Energy Mater.,1(2011), pp. 732–735, 2011.
[22] www.epia.org
[23] H. Katagiri, K. Jimbo, S. Yamada, T. Kamimura, W.S. Maw, T. Fukano, T. Ito,T. Motohiro, "Solar cell without environmental pollution by using CZTS thin films,"Proceedings of Photovoltaic Energy Conversion Conference Vol. 3, 2003.
[24] Q. Guo, H. W. Hillhouse, and R. Agrawal, "Synthesis of Cu_2ZnSnS_4 Nanocrystal Ink and Its Use for Solar Cells,"J. Am. Chem. Soc., 131, 11672–11673, 2009.
[25] C. Leidholm, C. Hotz, A. Breeze, C. Sunderland, and W. Ki, "Wurtzite CZTS nanocrystals and phase evolution to kesterite thin film for solar energy harvesting," NREL Subcontract Report NREL/SR-5200-56510, 2012.
[26] T.K. Todorov, J. Tang, S. Bag, O. Gunawan, T. Gokmen, Y. Zhu, D.B. Mitzi, "Beyond 11% Efficiency: Characteristics of State-of-the-Art $Cu_2ZnSn(S,Se)_4$ Solar Cells," Advanced Energy Materials, 3,34-38, 2013.
[27] I. Petrov, P. B. Barna, L. Hultman, and J. E. Greene, "Microstructural evolution during film growth,"Journal of Vacuum Science and Technology A21, 117, 2003.
[28]NREL Website: http://www.nrel.gov.
[29] S. J. C. and S. G. Byungha Shin, Oki Gunawan, Yu Zhu, Nestor A. Bojarczuk, "Thin film solar cell with 8.4% power conversion efficiency using an earth-abundant Cu_2ZnSnS_4 absorber," Prog. Photovoltaics Res. Appl. 21, 72–76 ,2013.
[30] T. M. and T. I. Shin Tajima, Mitsutaro Umehara, Masaki Hasegawa, "Cu_2ZnSnS_4 photovoltaic cell with improved efficiency fabricated by high-temperature annealing after CdS buffer-layer deposition," Prog.Photovoltaics Res. Appl. 25, 14–22 ,2017
.[31] C. Yan, J. Huang, K. Sun, S. Johnston, Y. Zhang, H. Sun, A. Pu, M. He, F. Liu, K. Eder, L. Yang, J. M. Cairney, N. J. Ekins-Daukes, Z. Hameiri, J. A. Stride, S. Chen, M. A. Green, and X. Hao, "Cu_2ZnSnS_4 solar cells with over 10% power conversion efficiency enabled by heterojunction heat treatment," Nat. Energy 3(9), 764–772, 2018.
[32] M. A. Green, E. D. Dunlop, J. Hohl-Ebinger, M. Yoshita, N. Kopidakis, and X. Hao, "Solar cell efficiency tables (version 56)," Prog. Photovoltaics Res. Appl. 28(7), 629–638 , 2020.
[33] A. Polman, M. Knight, E. C. Garnett, B. Ehrler, and W. C. Sinke, "Photovoltaic materials: Present efficiencies and future challenges," Science (80-.). 352(6283), 2016.

Chapter 2: State of the art

2.1. Physics of solar cell

The photovoltaic cell is an optoelectronic device that transform sunlight into electric energy. It can be utilized with both direct sunlight and artificial or ambient light. The term light, on the other hand, refers to the electromagnetic radiation emitted by the Sun and experienced by us on the Earth's surface [44]. Nonetheless, only a small portion of this radiation spreads the Earth. The air mass coefficient (AM1.5) is an index that is utilized to calculate the Sun's active electromagnetic radiation at ocean surface. (fig.2.1)[45]. The reductions in terms of emission that occurred here is for the absorption by the Earth's atmosphere. The key absorbing substances that avert the ultraviolet (UV) and some portions of the infrared (IR) sections of the sun spectrum are ozone, water vapor, oxygen, and carbon dioxide. The AM1.5 spectrum reflects the highest quantity of energy that may be turned into electrical energy by a solar cell. To maximize the production of photogenerated current, an efficient photovoltaic cell must be capable to transform the entire spectrum.

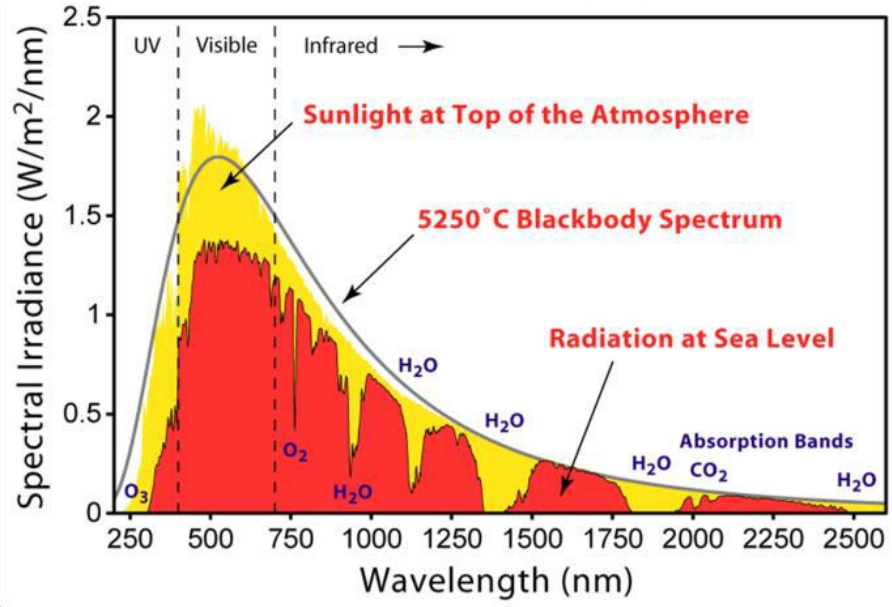

***Fig.2.1**.Solar irradiance spectrum [45]*

A solar cell can be thought of as a "black box" where light enters, electrons are generated, and electrons exit. The various categories of solar cells e.g. Silicon(Si) solar cells, thin film solar cells, dye manufactured solar cells are differentiated by the nature of the "black box." The following aspects must be observed by all types of solar cells: [44]

1. **Absorbance of the incident light:** The core compound used to fabricate the solar cell has a property that allows it to absorb light. It is inextricably linked to the material's absorption spectrum. Before being transformed into electric current, sunlight must be absorbed. The absorption spectrum shows how much of the incident radiation is collected by the substantial over a wide collection of frequency. The atomic and molecular structure of the substance determines this phenomenon. The absorption spectrum of an optimum contender core substantial for the current production in a solar cell matches the AM1.5 spectrum.

2. **Generating charges:**The initial stage in generating energy is to absorb sunlight in a solar cell. The second stage is to create photocarriers. With the energy provided by light absorption, the core of a solar cell should be capable to produce both electrons and holes. Photogeneration can occur inside a solar cell through a variety of ways. And it is through these processes that the various varieties of solar cells are defined. In this phenomona, different types of semiconductors with various band structures can generate pairs of electrons and holes.

3. **Transportation of the charges:** After the light has been absorbed, the charges have been created. This is when the solar cell, which requires a driving force, must be capable to accumulate them. The photogenerated electron and hole reunite when there is no driving force. An internal electric field must be generated to the solar cell to gather them efficiently. The built-in field is what it's called. The electrons and holes are transported in reverse directions by this electric field. The built-in field can be improved by improving the solar cell. It could be an improvement in the core material's thickness, alternative production procedures, or the addition of other materials that works as carrier selectors.

In a simple electrical circuit, a solar cell could be connected to a battery. The distinction is that the simple electric circuit performs nothing in the dark [46]. The cell develops a photovoltage when it is lit. The open circuit voltage is the photvoltage formed while the two terminals of the cell are quarantined with an infinite load resistance (V_{oc}). The current is generated by the cell under radiance while the two terminals are linked. When the two terminals are joined, the cell generates current under illumination. The short circuit current is what it's called (Isc). According to Ohm's law, the cell provides a current I(V) for load resistance (R_L) for voltages between 0 and V_{OC}: V = RL. I. The current-voltage characteristic of the cell under a given light is defined by I(V). The short circuit current density (J_{sc}) exchanges the I_{sc}, as the current is regularized above this region, because the current engendered by the cell is proportionate to the lit zone.

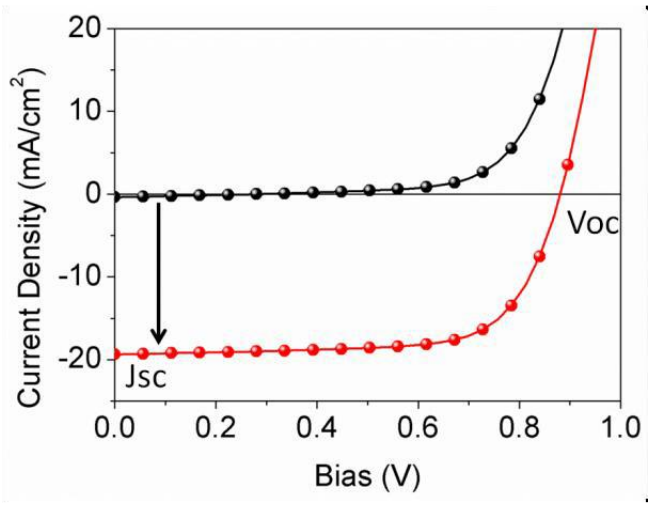

Fig.2.2*.Current-voltage characteristic of an ideal solar cell in light (red) and in dark (black)[53]*

A conventional solar cell drives as a diode in dark with a altered quantity of current with forwarding bias (V > 0) compared to reversing bias (V 0). (Fig.2.2). Photovoltaic devices have this rectifying behavior as a feature. It's also a result of the asymmetric junction required to distribute charges.

The diode's I(V) characteristic shifts by a feature hypothetically equivalent to the short circuit current when exposed to sunshine. The photocurrent and the dark current are superimposed to produce the total current. The phoyovoltaic cell is electrically equal to a current generator in series with a diode (Fig. 2.3). The photocurrent generated by a photovoltaic cell is split between the diode's changing resistance and the load applied. If there is no diode, there is no photovoltage . So there is also nothing to guide the photocurrent through the load.

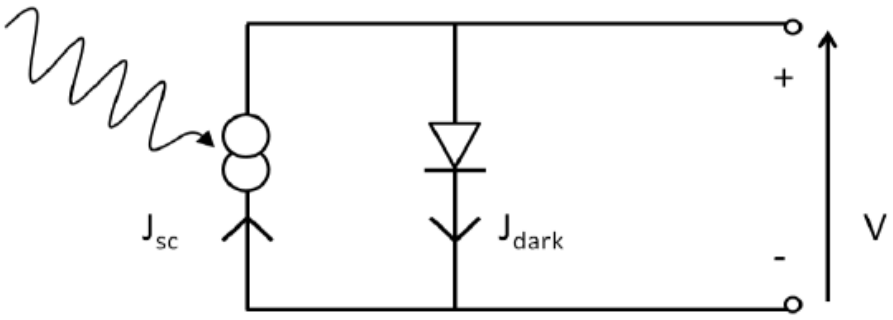

Fig.2.3. *Comparable circuit of ideal solar cell* [53]

The choice of bias from 0 to Voc is the working zone of a solar cell. Inside this limit, the cell provides power. The power density is defined as

$$P = JV \qquad (2.1)$$

The extreme value of P is demarcated as the supreme power point of the cell. This happens at some voltage V_m with the resultant current density J_m. It indicates that the optimal load for a solar cell shows a resistance agreed by V_m/J_m. The Fill Factor (FF) might be estimated from J_m and V_m as

$$FF=\frac{Jm\,Vm}{Jsc\,Voc} \qquad (2.2)$$

which defines the "squareness" of the J-V curve.
The efficiency, η of a photovoltaic cell is the power supplied at the supreme power point as a portion of the incident light power density, P_s:

$$\eta= \frac{Jm\,Vm}{Ps} \qquad (2.3)$$

Utilizing the characterization of Fill Factor in Eq (2.3):

$$\eta=\frac{Jm\,Vm\,FF}{Ps} \qquad (2.4)$$

These four measures as J_{sc}, V_m, FF, and η are the key enactment features of a photovoltaic cell. And the quantities should be demarcated under typical radiance environments using the AM1.5 spectrum with an incident power density of 1000 W/m^2.

2.2. Physics of Semiconductor:

Two atoms combine to biuld a molecule. Consequently, their atomic orbitals also conglomerate to generate pairs of molecular orbitals with slightly different energy levels than the prototypes. If more

than two atoms combine to create a solid, the parting energy of all orbitals is so near that they create a continuous range of reachable levels. The band energy phrase is used to define this *continuum*. To convert sunlight into electricity, a suitable photovoltaic substance must absorb visible light. This evolution necessitates a gap in the material's bands. The band gap is the energy variance between the maximum occupied state and the lowermost unoccupied state. A band gap exists in all semiconducting and insulating compound. Only semiconductors, on the contrary, have the correct band gap energy for solar cell light absorption. In solar cells, the band gap of insulators is too large, and the band gap of metal is too little[47]. If there is no band gap (for example, in metals), the excited electrons do not have adequate time to be captured while they have been excited. As a result, electrons falloff through a series of intermediate states. When an electron is agitated in a semiconductor with a band gap, it swiftly decays to the conduction band's minimum energy. And it just takes a few femtoseconds to complete this path [48]. As a result, the recombination to the valence band happens at a gentler rate, taking quite a few microseconds, resulting the solar cell abundant time to extract the electron. Figure 2.4 depicts the process.

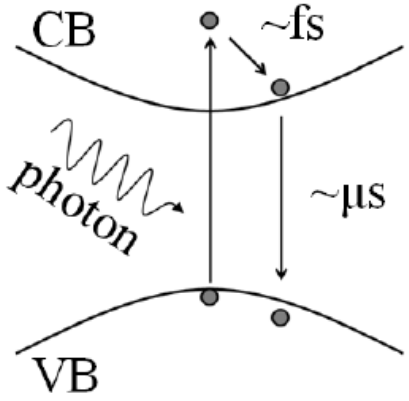

Fig.2.4. *Excitation mechanism of an electron from the valence band (VB) to the conduction band (CB)[53]*

The band gap features of a certain material are linked to its atomic features [11]. While two atoms come together to construct a molecule, their electron orbitals merge to produce molecular orbitals, which have new energy levels. Each atomic orbital splits into a continuum of levels when this method is repetitive to create a solid. It's referred to as a 'band'. Due to the energy distribution, these bands may or may not overlap. This is a representation of the underlying electronic characteristics of the atoms. The tenancy of these bands is determined by the molecular orbitals' initial occupation. The valence band is considered as the highest occupied band (VB). The conduction band is characterized by a low vacant band (CB). The solid is metal when the valence band and the conduction band converge. If the band energies of the two bands are separated by a band gap, the solid is a semiconductor. If the band gap is sufficiently large, as seen in Fig.2.5, it becomes an insulator.

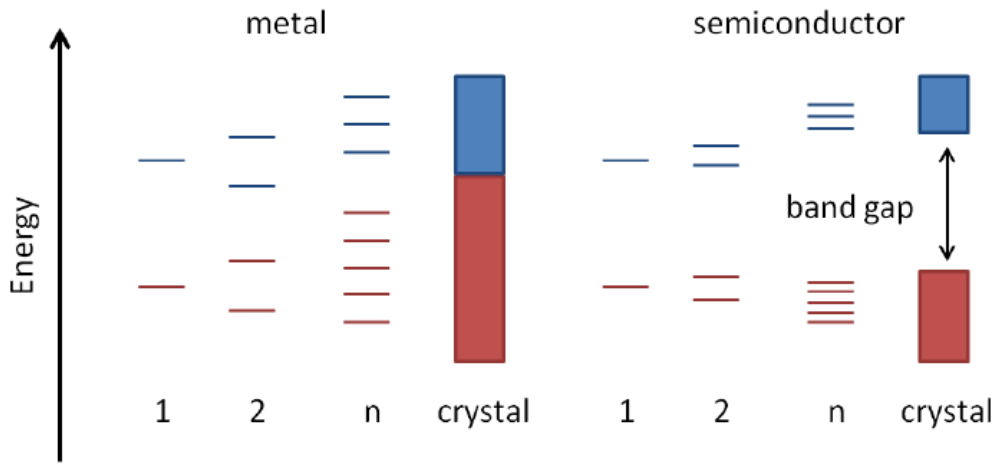

***Fig.2.5**. Band structure for a metal and a semiconductor[53].*

The type of material is determined by the difference in band energy (eV) between the two bands. It is 0 eV for metals, less than 0.5 eV for semimetals, within 0.5 to 3 eV for semiconductors, and more than 3 eV for insulators. A positively charged vacancy is generated in the VB when the electron is propelled from the VB to the CB. The neighboring electrons in the VB normally fill this hole. This shifts the vacancy to a nearby location. As a result, this process could become repeated with the accompany of an electric field. This causes current to flow, which is symbolized by the vacancy moving in the opposite direction of the excited electron. The relative current might be regarded as the current of positive holes in the VB since this vacancy consequences from a deficiency of negative charge (missing one electron). The electron and the corresponding hole have opposite-sign charges. In general, these two charges are thought to be independent of one another. Nonetheless, they can sometimes interfere in certain circumstances. The Coulomb contact, which is disclosed between charges of opposite sign, links the electron and the holes in a exclusive state known as an exciton under these conditions [48]. Within some materials, these excitons can be stationary. It may, meanwhile, be portable. It displays a sequence of intra-band gap states that are a little overhead the VB and slightly below the CB. Though excitonic states are irrelevant for electrons and holes in isolation, it is significant for semiconductor optical characteristics.

The absorption of light and the creation of charges are two of the key ways in the solar cell, as we described formerly. The third option is to transfer them in a current. Unevenness is required in an ideal solar cell to move electrons and holes in opposite directions. That is why an active solar cell requires an internal electric field.

The classic model of a solar cell is a p-n junction. The type of solar cell determines and characterizes the p-n junction's operating manner. The junction is made up of a semiconductor with two doped p (with a lack of electrons) and n (with an abundance of electrons) zones. The valence and conduction bands of the two sections of the semiconductor are twisted when the two zones (p and n) come into contact with each other. Within the junction, the distinction between the two work functions produces an electric field.

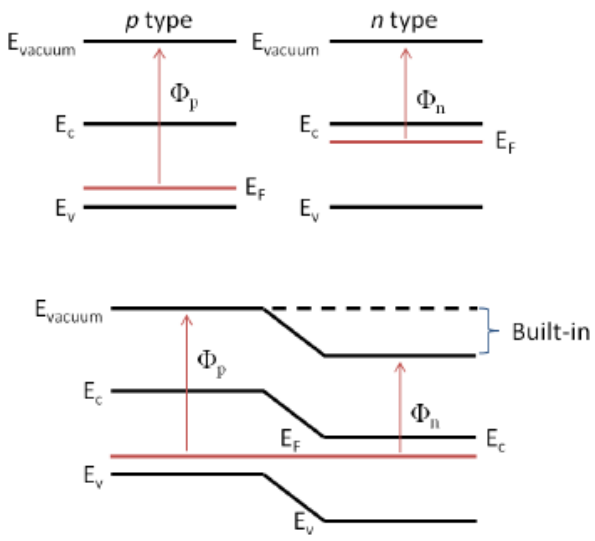

Fig.2.6. *Energy band for a p-type and n-type semiconductor (top). The energy arrangement of a p-n junction (bottom)*[53].

2.3. Generation and Recombination

Electronic stimulation develops and enhances the number of free carriers offered to transport the charge along the circuit. The mechanism of generation necessitates the use of energy. And this energy can come from phonons (vibrations) or light (photons). Recombination, on the other hand, is an electrical relaxation process that lowers the amount of free carriers in the medium [48]. It's a method that uses reversed generation techniques to liberate energy. For each creation of electrons, there is a recombination mechanism.

Photo generation is the process of generating charges from light absorption in solar cells. The absorption of a photon is the first step in this process. This causes an electron to be promoted from the VB to the CB, forming an electron-hole pair. Recombination, on the other hand, is the return of an electron from the CB to the lower state.

The absorption coefficient, which specifies how light is diminished as it passes through the absorber material of the solar cell, is another key mechanism. There is a flow of photons *(I)* with energy E and intensity *I (0).* According to the relative thickness *dx*, a portion of this flux is absorbed through the absorber compound. So the absorbed flux is calculated as

$$\frac{dI}{dx} = -\alpha I \tag{2.5}$$

Integrating Eq (2.5) offers with a uniform α the Lambert-Beer law (figure 2.7):

$$I(x) = I(0)e^{-\alpha x} \tag{2.6}$$

Here, *I(0)* is the intensity classified for the surface.

If all photons are enchanted to produce free carriers, the degree of carrier generation per unit volume as a utility of the distance*x* is measured as follows

$$g(E,x) = b(E,x)\alpha(E,x) \tag{2.7}$$

Here, *b* is the photon flux at *x*. It should be emphasized that the rate of generation is controlled by the amount of photons rather than their energy.

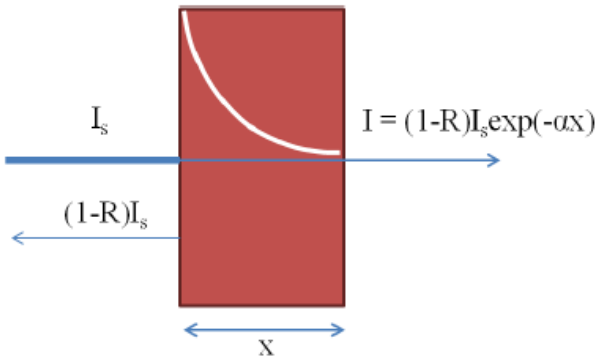

Fig.2.7. *Diminution of light intensity (white line) through the absorber layer of the solar cell[53].*

It's worth noting the importance of the quantity of photons in terms of the energy carried. The energy must be greater than the band gap; else, photons would be absorbed. Photons with a higher energy than the band gap keep electrons in the CB with an surplus of energy (Fig.2.5), which is wasted in a quick thermalization technique. And relaxes the electron in the CB band's minimal level. Meticulously, this energy is transformed to phonons by colliding with the lattice. The quantity of photons, on the other hand, is proportional to the amount of excitation events that occur. It also has something to do with the quantity of electrons stimulated in the CB. Recombination is a term that refers to one or more mechanisms which diminish the amount of movable electrons and holes. Therefore, two types of recombination process are there as follows-

Unavoidable recombination

Unavoidable recombination is correlated to the inherent physical properties of the compound. There are two kinds of unavoidable recombination as follows-Radiative recombination and Auger recombination (Fig.2.8).

i. **Radiative recombination**: One of the most significant recombination process in photovoltaic solar cells is radiation recombination. Radiative recombination is the unprompted emission of a photon caused by the recombination of an electron with a hole at the conduction band's lowest and valence band's maximum (VB). The band gap energy is proportional to the energy of the emitted photon.

ii. **Auger recombination**: Auger recombination occurs when two comparable carriers collide (i.e. electrons). Evidently, this is a non-radiative procedure. The first carrier transmits its kinetic energy to the second carrier, causing the first carrier to degrade in the valence band (VB). Consequently, immediately before degrading and dropping its energy in the arrangement of phonons, the second carrier is promoted to high-energy excited states.

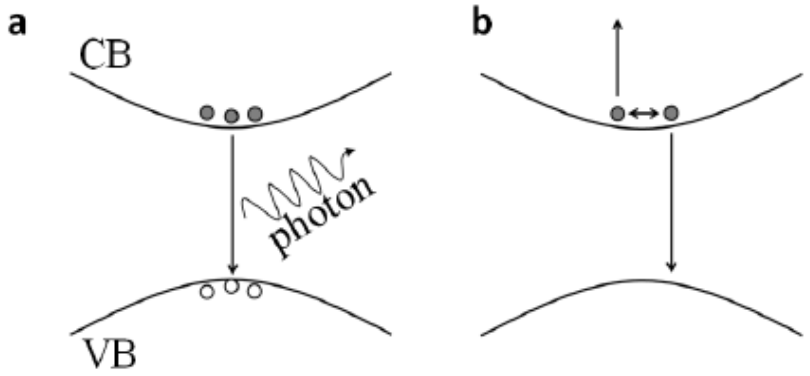

(a) (b)

Fig.2.8. *Unavoidable recombination mechanisms: (a)Radiative recombination, (b)Auger recombination[53].*

Avoidable recombination

Avoidable recombination are associated to structural imperfections and impurities in the compound. That's why these are avoidable. There are two types of avoidable recombination through trap states and grain boundaries as follows(Fig.2.9)-

i. **Traps state:** Sub-band gap levels are known as trap states. Like a potential well, these levels operate as a sink for excited electrons and holes. When the state's energy is deep within the band-gap, these states may perform as recombination centers. Recombination with the contrary carrier is preferable to thermal detrapping back into the band when the state's energy is low. Aside from that, electrons and holes might be freed, causing in a relaxed current flow.

ii. **Grain boundaries recombination**: Surfaces and grain boundaries are flaws affecting areas in polycrystalline films. Recombination centers, such as trap states, can be generated by localized states such as broken bonds or external contaminants. In addition, the time it needs for electrons and holes to be captured is reduced.

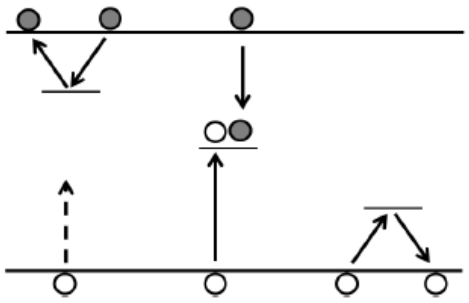

Fig.2.9*. Avoidable recombination aided by trap state[53].*

2.4. Current-voltage characteristics of a diode

A diode is a p-n junction with two contacts linked to it. The current-voltage (I-V) features of diodes (Fig.2.10) are as shown below:

$$I(V) = I_0\left(e^{\frac{qV}{nkT}} - 1\right) \tag{2.8}$$

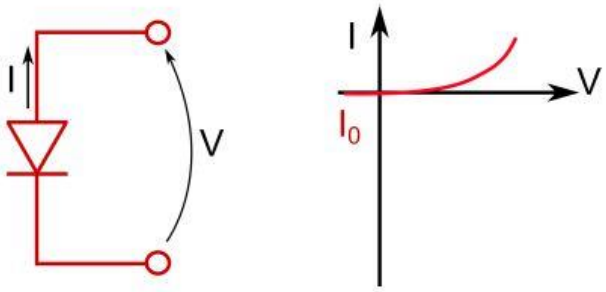

Fig.2.10: *Static I-V characteristics of a diode [54].*

here*I* is the gross current flow in the diode. I_0 is the dark saturation current and *V* is the realistic voltage across the diode.in addition, *n* is the diode ideality factor, *k* is the Boltzmann constant, and *T* is the temperature.
I_0 can be defined as:

$$I_0 = I_{00}\left(e^{\frac{-E_A}{nkT}} - 1\right) \tag{2.9}$$

I_0 is the diode saturation current. When there is no light, it is the diode leakage current. The activation energy E_A, which is the energy of the predominant recombination process, activates it. Moreover, I_{00} is called "*reference current*" which is faintly temperature reliant only. The *n* regulates the voltage reliance of the current density [49].

2.5. Ideality factor

The slope of the dark I-V characteristics is usually employed to compute the ideality factor (n). The ideality factor in an ideal solar cell is ~1. Different ideality factor (n) values indicate that a certain recombination strategy is overriding.

2.6. Light I-V characteristics

Additional electron-hole pairs are created when a solar cell is irradiated with the sun spectrum. The photo produced current (Iph) is generated as a current generator in comparable with the diode as a result of this (Fig.2.5). The photo generated current, I_{ph} is measured as

$$I_{ph}(V) = -qA \int G(z)\eta_c(z,V)dz \tag{2.10}$$

Here, *G(z) is* carrier generation function and $\eta_c(z,V)$ *is* the collection probability. In addition, the fundamental charge is q, and the solar cell's surface is A. The "collection probability" (ηc) is interpreted as an indication that a carrier created by photon absorption in a definite location of the p-n junction will be together. Because the electric field efficiently splits the electron-hole pairs in the SCR, the collection probability$\eta_c(z,V)$ is enhanced to maximum. Diffusion is the most important process in QNR. Only carriers produced at a detachment from the SCR less than the minority carrier diffusion length (Ln,p) might be captured in these locations. The regular space a carrier may cross from the site of creation to the point of recombination is reffered to as Ln,p.
In most solar cells, p type material is utilized as the light absorber material. As a result, solar cells have an absorber layer(p) that is significantly thicker than the other layer(n) that makes up the p-n junction [49].

I_{ph} has the impact of flowing down the I-V characteristics into the fourth quadrant (Fig. 2.11). While a cell is illuminated, Eq.2.8 (diode law) is revised considering the addition of the photogenerated current. The output current I(V) is then measured as

$$I(V) = I_0\left(e^{\frac{qV}{nkT}} - 1\right) - I_{ph}(V) \tag{2.11}$$

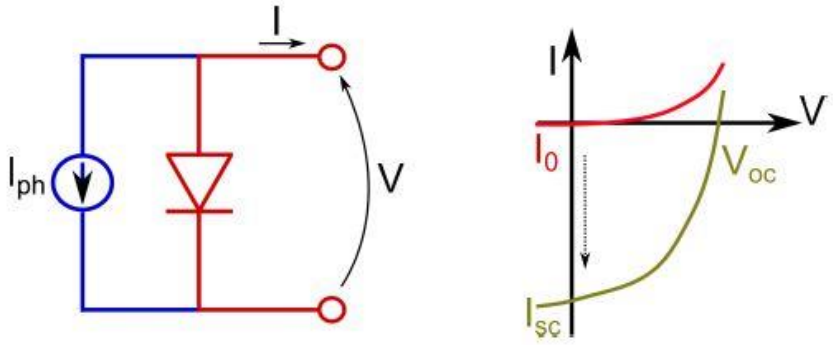

Fig.2.11*: Model and I-V curve of a solar cell with radiance[54].*

Short-circuit current

The short circuit current, I_{sc} in Fig.2.11 is considered as the current throughout the PV cell if the terminals are in a short circuit i.e. the voltage of the solar cell is zero. That is a significant figure of merit, which quantify the performance of a solar cell as a device. Undoubtedly, I_{sc} is alike to $I_{ph}(0)$. The significant factors that influence short circuit current, I_{sc} are the light intensity, the optical attributes, the thickness of the *p* and *n* junction along with the assemblage probability [49].

Open-circuit voltage

Besides Short circuit current, I_{sc} , another significant figure of merit is the *"open-circuit voltage"* (V_{oc}). While there is no load connected, it is the voltage at the output of the cell circuit. Therefore, the output current is zero ($I=0$), so the open circuit voltage, V_{oc} is measured as

$$V_{oc} = \frac{nkT}{q} \ln\left(\frac{I_{ph(Voc)}}{I_0} + 1\right) \quad (2.12)$$

Again, V_{oc} can be modified as:

$$V_{oc} = \frac{E_A}{q} - \frac{nkT}{q} \ln \frac{I_{00}}{I_{ph(Voc)}} \quad (2.13)$$

Eq 2.8 shows that V_{oc} leans on both I_{00} and I_{ph}. The differences of I_0 recombination reliant within the photovoltaic cell. As a result, variability in Voc could be contingent on the portion of recombination in the photovoltaic cell.

Fill Factor

The third figure of merit for a solar cell's performance as a module is the fill factor (FF). It is estimated as the ratio between the values of the supreme power point ($P_{MP}=V_{MP}\times I_{MP}$) and the product of $V_{oc}\times I_{sc}$ in Fig.2.12 as

$$FF = \frac{V_{MP}\times I_{MP}}{V_{OC}\times I_{SC}} \quad (2.14)$$

Here, I_{MP} and V_{MP} is the current and voltage respectively of the solar cell. An ideal solar cell should have a *fill factor(FF)* ~1. It can be comprehend that *FF* grows along with V_{MP} and I_{MP} impending respectively V_{oc} and I_{sc}. To achieve FF as 1, it is obligatory to drop the fatalities due to parasitic resistances within the solar cell. Thereby it is another way to represent the *fill factor (FF)* as a degree of the fatalities or thelosses of a solar cell.

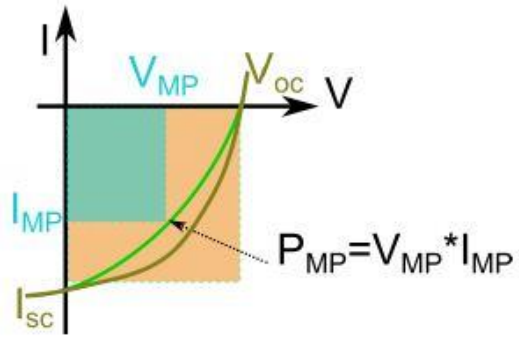

Fig.2.12: *Fill Factor of a PV cell: the green square is consequent from the supreme power point (Vmp,Imp), the yellow square is acknowledged by (Voc, Isc)[54]*

Power Conversion Efficiency

The power conversion efficiency (*PCE*) is one of the furthermost significant figure of merit of photovoltaic module. This value permits associating solar cells conversion efficiency to each other. It can be estimated as the ratio amid the produced electrical power (P_{MP}) and the solar energy (P_{IN}) as

$$PCE = \frac{P_{MP}}{P_{IN}} = \frac{V_{OC} \times I_{SC} \times FF}{P_{IN}} \quad (2.15)$$

The intensity of the incident radiation, the nature of solar spectra, the operational temperature of the solar cell, and even the geographical region and weather all affect power conversion efficiency. As a result, to identify the I-V characteristics of two or more photovoltaic modules, all of the state of affairs under which the power conversion efficiency, PCE, is evaluated must be carefully controlled. At a temperature of 25°C, an AM1.5G spectrum is a comprehensive analytical setup for outdoor solar cells.

2.7. Losses in solar cell

Eq 2.11 is deliberated for an ideal solar cell. There are series (R_s) and shunt resistances (R_{sh}) which is obvious in real solar cell. By integrating the resistances, the output current I(V) should be as follows-

$$I(V) = I_0 \left(e^{\frac{q(V - IR_S)}{nkT}} - 1 \right) - I_{ph}(V) - \frac{V - IR_S}{R_{sh}} \quad (2.16)$$

It can be noted that with the presence of these resistances, there is a diminution in the *FF* of the solar cells.

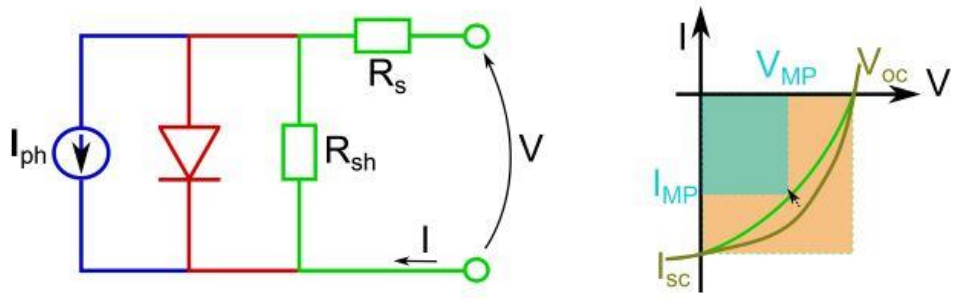

Fig.2.13*. PV cell counting parasitic resistances[54].*

Series resistance

The series resistance, Rs, of a solar cell is primarily influenced and altered by the resistances of the forward-facing and rear contacts. Moreover, there is resistance at the interface of the solar cell's several layers[49]. In contrast to open circuit voltage, Voc, higher standards of series resistance, R_s, may diminish the short circuit current, Isc. (Fig.2.14).

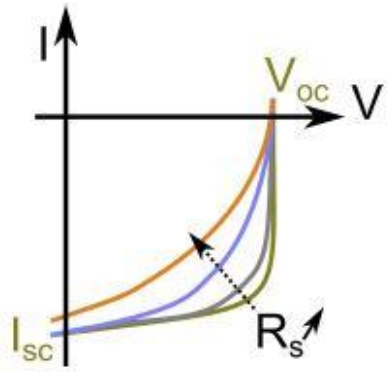

***Fig.2.14**. Impact of R_s on photovoltaic characteristics with lights[54].*

Shunt resistance

Shunt resistance, often known as R_{sh}, is a distinct type of current path, i.e. short-circuits. There are a variety of reasons why a solar cell might have this type of resistance. It's possible that the interface between the doped areas and the metal contacts isn't flawless. As a result, there is a fluctuation in shunt resistance, R_{sh}. Recombination in Shockley-Read-Hall (SRH) imperfections into the QNR could also cause shunt resistance. Shunt resistance, R_{sh}, should be as great as feasible to evade losses in open circuit voltage, V_{oc}, in contrast to series resistance, R_s(Fig.2.15).

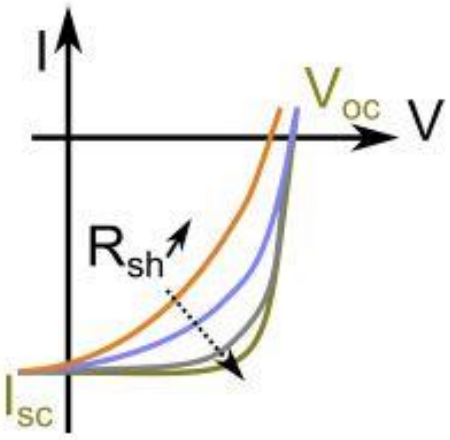

***Fig.2.15**. Impact of R_{sh} on photovoltaic characteristics with lights[54].*

2.8. Current trends in PV Technology:

To make the world safe and sound for future generations, the requisite to accomplish lessening fossil fuel reserves is the biggest challenge facing the planet today. And the phrase "climate change" has largely been ascribed to recent apparent changes in the climate initiated by global warming as well as the greenhouse gas impact. According to the IPCC, the scope of climate change effects on individual regions will definitely vary over time. And there will be no hope if we don’t change our life style right

now. The greenhouse effect is indispensable for human survival on earth. However, this biological event has been credited with leading to multiple ancient extinction events since the 1950s. It has now been accelerated as a result of rising levels of greenhouse gases in the air, mainly carbon dioxide and other greenhouse gases. Therefore, the other renewable sources of energy that both compete the growing energy consumption and offer a CO_2–neutral know-how are necessary. Due to several aspects, the nuclear power plant is not a really long term alternative. Consequently, conventional fuels such as oil, coal, and other fuel is inadequate. Likewise, the subject of eventual storage for radioactive waste remains unaddressed. [1]. Solar energy is now the supreme anticipated renewable source, as it has the capability to meet up the global energy needs while also being abundant and non-polluting. Only 0.1 percent of the earth's area could be shielded with roughly 10% effective solar cells to encounter the world's energy need. Only 0.1% of the earth's surface area could be roofed with roughly 10% effective solar cells to meet the world's energy need. Solar cells' light-to-electricity transformation is one of the utmost well-developed environmentally approachable renewable energy technologies to date.

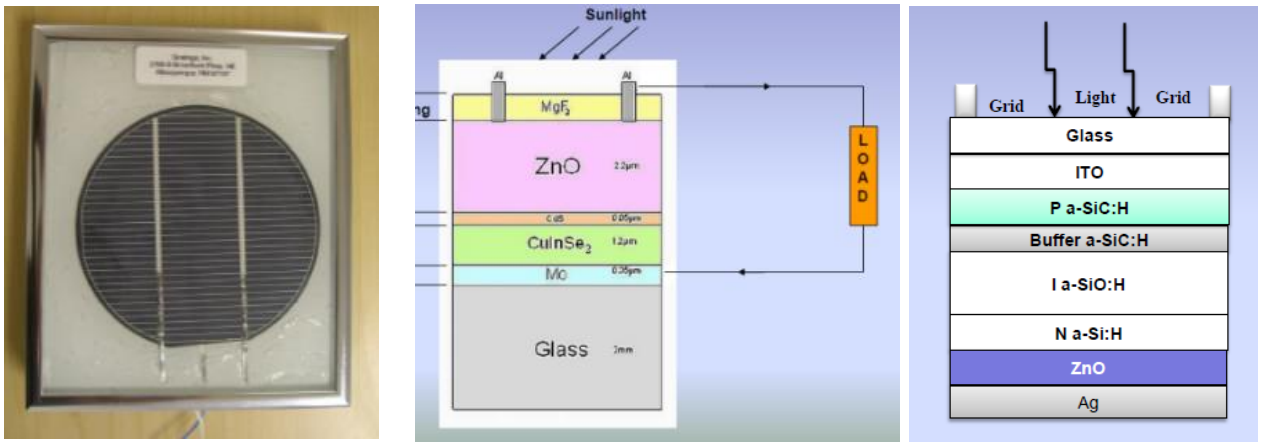

(a) (b) (c)

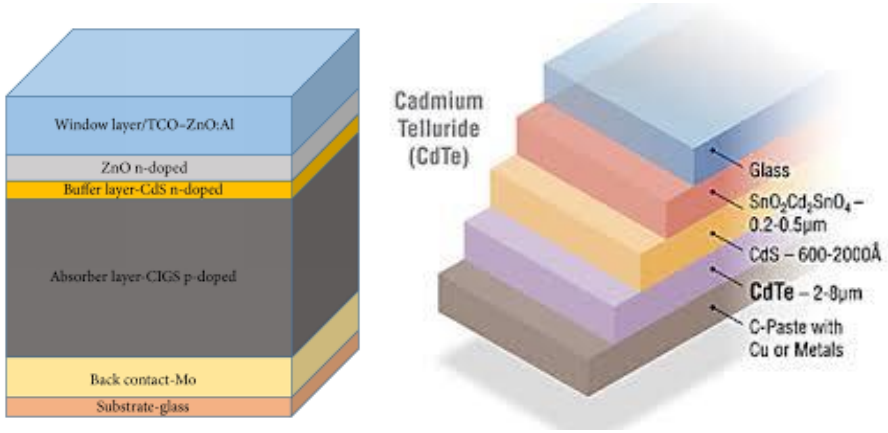

(c) (d)

Fig2.16*.(a) c-Si, (b)a-Si, (c)CIS , (d) CIGS and (e)CdTe solar cell.*

Solar modules are primarily manufactured from highly pure crystalline silicon (**first generation**). Manufacturing of this silicon (Si) is highly exclusive that rises the overall production cost of the solar panels. In that case, thin film solar cell (**second generation**) is emerging as an alternative technology.

.

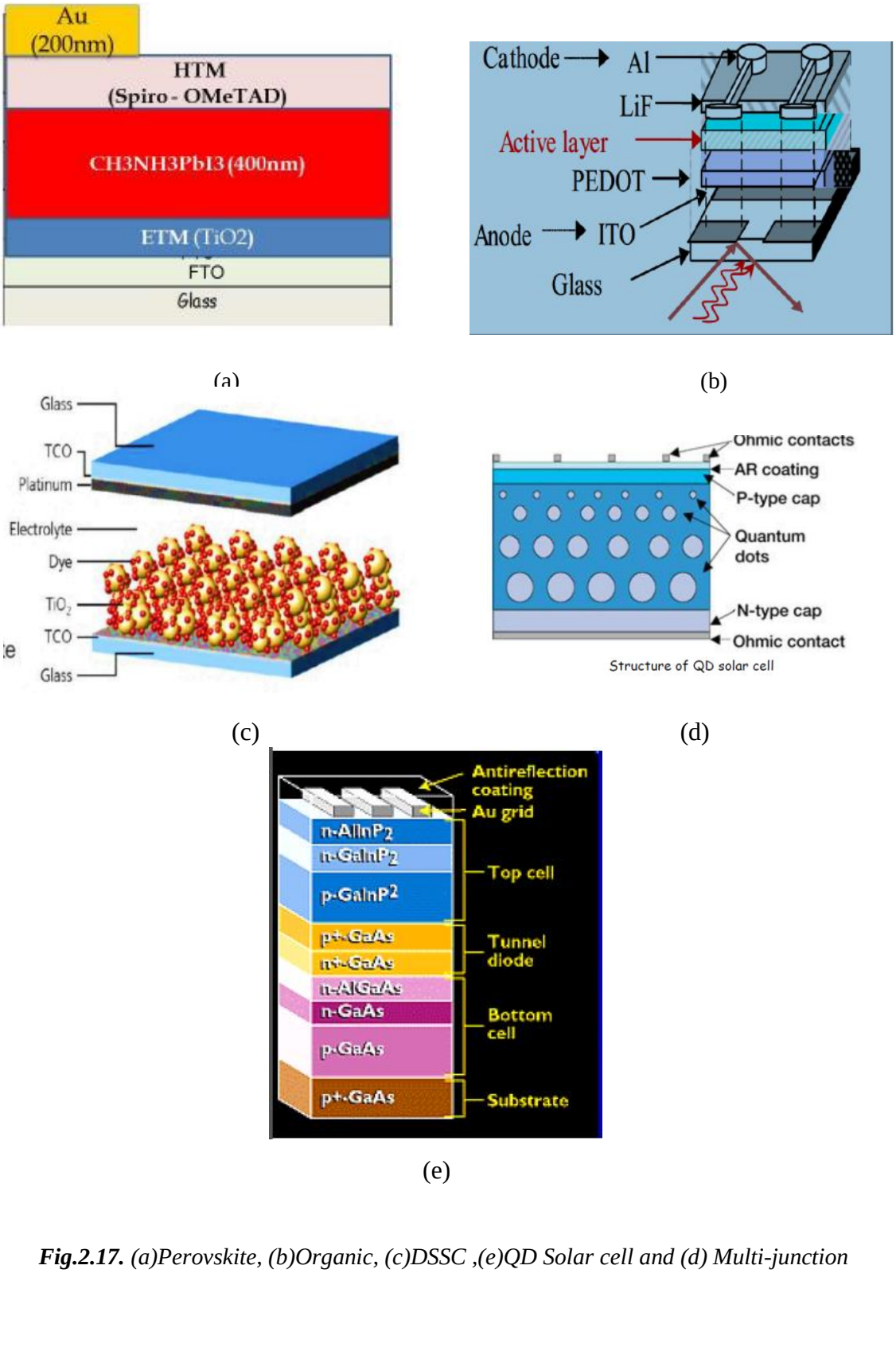

Fig.2.17. *(a)Perovskite, (b)Organic, (c)DSSC ,(e)QD Solar cell and (d) Multi-junction*

In solar cell module, thin (~1 μm) films of semiconductor materials i.e. cadmium telluride (CdTe) and copper indium gallium diselenide ($CuInGaS(e)_2$ or CIGS) are utilized instead of a thick (~100 μm) silicon wafer. Thin film ingredients, which are 100 times thinner than crystalline silicon(Si), may absorb the same quantity of energy whereas the absorption coefficient(α) of characteristic thin film absorber materials is ~100 times higher than crystalline silicon [2]. However, the **third generation** of solar cell includes polymeric, organic, quantum dot(QD), and dye-sensitized solar cells. The third generation emerged in the last decade with the hope of enabling the fabrication by less-complex technologies and cost effective resources and apparatus. Efficiency-cost trade-off for the three generations of solar cells is shown in Fig 2.18.[43]

Till now three kinds of thin film material has been used for industrial manufacture of solar cells- Amorphous silicon (a-Si), Cadmium telluride (CdTe), and Copper-Indium-Gallium-Selenide/Sulfide (CIGS/Se), where CIGS touched the uppermost efficacies that may contest with commercial polycrystalline silicon

Today the efficiency of multicrystalline Silicon(Si) is 20.4% and 19.4% for CIGS [3]. But there are still some issues like the absence of Grid Parity or Socket Parity. Again the photovoltaics are based on an inconstant energy supply occurring problems of energy storage.

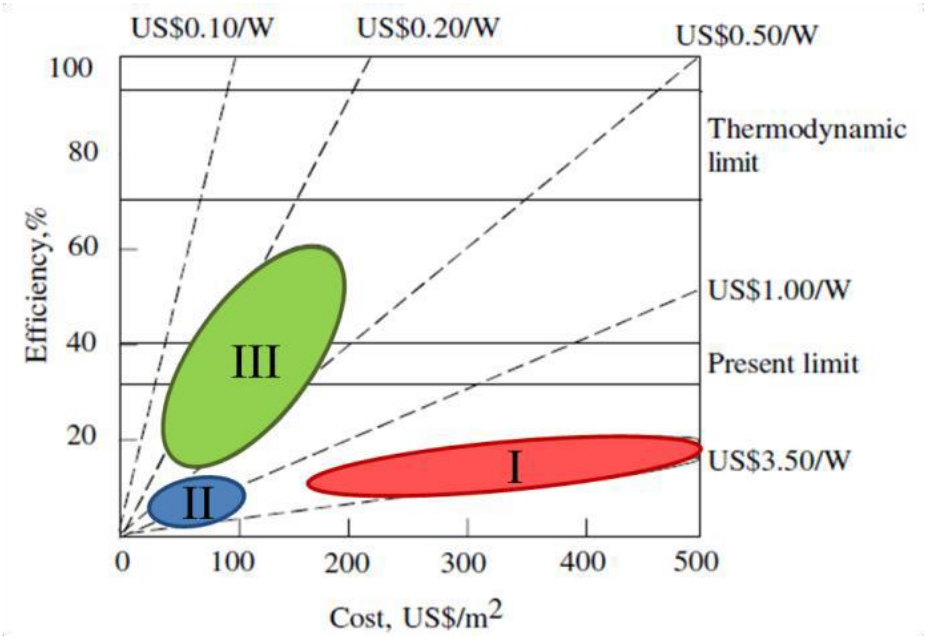

***Fig.2.18**. Efficiency-cost trade-off for the three generations of PV cells* [43].

There are issues with the semiconductor materials commonly used for the production of CdTe or CIGS. Cadmium is toxic and in addition Indium and Tellurium is rare in the world's crust. Indium's avalibility is infrequent and it would be limited within the next 12-18 years, while the expense is growing hastily. Replacing Indium by Zinc and Tin, Copper Zinc Tin chalcogenide (CZTS/Se) is evolving as a prominent contender to develope thin film PV to its bursting prospective [4, 5].CZTS is a compound whose inherent

point defects initiates it typical semiconductor behavior. The ideal band energy level for transforming the supremequantity of energy from the solar spectrum into electric energy is 1.5 eV [6]. CZTS has a similar band gap with a higher absorption coefficient ($>10^4$ cm^{-1}) in the visible region of the electromagnetic spectrum. As a result, even with a few micron thick film of CZTS may absorb photons with energy over the band gap.

However, further research is needed to be done with different fields of the solar cell, especially with the materials. CZTS would be a perfect choice to go ahead that is indicative of the development of the greatest efficiency for CZTS solar cells along with other photovoltaic devices.

2.9. Evolution of CZTS

The hunt for an alternate light-absorbing material has been an ongoing field of study after the materialistic approach of Silicon(Si) solar cells since 1950. Silicon (Si) is an element of an indirect band gap energy and comparatively small optical absorption coefficient. To avoid these drawbacks, a material with a higher absorption coefficient (with direct band gap energy) was in demand for the production of second-generation thin film photovoltaic cells at a reasonable rate. [7]. There are mainly two major thin-film knowledge that have developed in the past decades centered on CdTe [8, 9] and CuInGaSe or in short CIGS [10–13]. Definitely, considering to more intricate resources compromises a greater degree of freedom. If we follow the previous research study of Ito and Nakazawa, [14] over the previous ten years, the investigation of the quaternary chalcogenide semiconductor Cu_2ZnSnS_4 (CZTS) for solar cells has intensified. This material of CZTS contents the basic demand of photovoltaic device [15–25] since CZTS conglomerates an optimam bandgap energy of 1.5eV and a high optical absorption coefficient(α) of $10^4\,cm^{-1}$.

When Hall et al. announced the X-ray diffraction configuration of the organic crystals kesterite and stannite, CZTS appeared to be in the running as a photovoltaic material. In 1978, he determined that they were structurally similar but separate minerals [26]. Shinshu University of Japan's Iko and Nakazawa [27] developed a heterojunction diode in 1988. It contained of a see through cadmium-tin-oxide thin film and a CZTS thin film on a stainless as absorber material. It was the first study of CZTS' photovoltaic impact. In 1997, Katagiri*et al*. [28] declared the very first CZTS photovoltaic module with a amalgamation of ZnO:Al/CdS/CZTS/Mo/glass. They used SLG as a substrate. The device that team of Katagiri fabricated, exposed an open circuit voltage of 400 mV and power conversion efficiency of 0.66%. The CZTS thin films were produced by sulfurization of the electron beam fabricated as Cu/Sn/Zn stacked precursors. Friedlmeier *et al*. [29] also reported CZTS thin film photovoltaiccell in 1997. They used CZTS as the light absorbing film with the greatest power conversion efficiency of 2.3% at that time. The open circuit voltage, V_{oc} was shown as 470 mV. Katagiri*et al*.[30] established a new record in 1999 who produce the CZTS thin films by sulfurization of Cu/Sn/ZnS stacks method generated emplying vacuum technique. The power conversion efficiency is 2.62 %. The efficiency has been increased to 5.45 % in 2003 by optimizing the annealing method [30].

Later in 2008, it was discovered by Katagiri *et al*. that soaked CZTS films in deionized water permits the etching of the metal oxide particles into the CZTS film. It was revealed that this process results high efficiency device of 6.7 % PCE [31]. This efficiency was the highest until Mitzi*et al*. described a 9.6 %

efficient solution treated CZTSSe photovoltaic cells [32] in 2010. Mitzi employed a solution method by spin-coating precursors enclosing metal binary chalcogenides liquefied in hydrazine. Sulfurization or selenization methods were also followed for these devices fabrication.

The PCE was improved up to 10.1 % by the group [33, 34] in 2011. In 2013, the greatest power conversion efficiency for CZTS(Se) based photovoltaic cells till date has reported as 12.6 % in IBM by Mitzi and the team.[51]

2.10.Best CZTS Solar Cell (Experimental)

	Efficiency	**Stack**	**Method**
1	13.8%, 14.1%	Mo/ACZTSSe/CdS/ZnO/ITO/Ni/ Al/MgF_2	Sol-gel Spin coating [68]
2	13.59%	Mo/ACZTSSe/CdS/ZnO/ITO/Ni/ Al/MgF_2	Sol-gel Spin coating [69]
3	12.87%	Mo/ACZTSSe/CdS/ZnO/ITO	Sol-gel Spin coating [70]
4	12.6%	Mo/CZTSSe/CdS/ZnO/ITO/Ni-Al/MgF_2	Hydrazine solution approach, Spin coat [55]
5	11.4%	FTO/MoO_2/(CZTSSe, CZTSSe(Na))	Sol-gel Spin coating[71]
6	11.1%	glass/Mo/CZTSSe/CdS/ZnO/ITO/ Ni-Al	Hydrazine processed CZTSSe, Spin Coat [56]
7	10.2%	Mo/CZTSSe/CdS/i-ZnO/AZO/Ni/Al	Magnetron sputtering [57]
8	10%	CZTS/CdS/i-ZnO/ITO/Al/ MgF_2	Magnetron Sputtering [58]
9	9.6%	CZTSSe/CdS /ZnO /ITO.	Hydrazine processed CZTSSe, Spin Coat [59]
10	8%	Mo/ CZTSSe/NaF/CdS/i-ZnO/AZO/ Ni/Al/MgF2	Magnetron Sputtering [60]
11	7%	glass/Mo/CZTS/CdS/i-ZnO/AZO	Co-electrodeposition [61]
12	6.7%	Mo/CZTS/CdS/ZnO	RF Magnetron Co sputtering [62]

2.11.Best CZTS Solar Cell (Simulation)

	Efficiency	Stack	Study
1.	24.8%	MoS_2/CZTSSe/ZnS/ITO	ZnS buffer layer, Impact of different layer thickness and band gap [63]
2.	23.72%	ZnO/CdS/CZTS/Mo	The influence of device parameters and temp.[64]
3.	17.59%	MgF_2/AZO/ZnO/CdS(n)/ ACZTS(p)/CZTS(p+)/ITO	Ag incorporation to CZTS [65]
4	16.28%	SLG/Mo/CZTSSe/CdS/ZnO	CdS, **SnS_2**,ZnO, ZnTe, ZnS, Zn(O,S), (Mg,Zn)O, In_2S_3,TiO_2 &CdTe buffer layer [66]
5.	11.20%.	CZTS/CdS/ITO	CdZnS buffer Layer [67]

2.12.CZTS Nano-crystal

Solution processed CZTS nanocrystals are likely the solitary method that allows phase development to happen earlierof film creation. In a very careful and precise conditions, phase formation takes place in the liquid phase. As a result, it permits much higher diffusivity levels to surpass the activation energy barrier and touch a more stable phase. For most solution-based techniques, meanwhile, one or more solid state reactions are required for phase development. Other solution-phase processes, on the other hand, leave certain unanticipated remnants in deposited films. This has a significant impact on device performance [39]. Kesterite, Stannite, and pre-mixed Cu-Au (PMCA) configurations are the three different crystal structures of CZTS. Because of its stability, Kesterite (A_2BCX_4) is the furthermost auspicious to replace the present light-absorbing resources.

The Quantum dot sensitized solar cell (**QDSSC**) is a variant of this nano-crystal approach with the advantage of quantum mechanical effects (called Quantum Confinement) to perform better. Dye-sensitized solar cell (**DSSC**) is also a related approach where nano-structuring is part of the substrate.

Deposition of nano-crystal CZTS

It needs several steps for the development of CZTS absorber layer.

i. **Synthesis:** Parallel syntheses of ZnS, SnS, and CTS are required for the stack technique. The most versatile approach for making CZTS nanocrystals is colloidal thermolysis growth. This approach produces nanocrystals that are as-synthesised and have well-controlled phase, size, shape, and composition. There's also a lot of dispersion. CZTGeS nanocrystals were produced and utilized to make CZTGeSSe thin films. They discovered

incredible device performance values of up to 8.4% [42]. Precursors are also used to prepare the fluid for the sol gel procedure.

ii. **Deposition:** CZTS thin films will be formed by spin coating ZnS, SnS, and CTS nanoparticles separately. Alternatively, a solution containing all of the precursors is put on a glass substrate. A complex target could be utilized for single sputtering. To make a CZTS thin film, three distinct targets of ZnS, SnS, and CTS could be employed for co-sputtering. Nanocrystal coatings are used to generate 1 to 2 mm thick layers by periodic spin coating or doctor blading. [40].

iii. **Heat Treatment:** Heat treatment is needed to carry out with a range of 200-400°c. The preferred thickness can be obtained by recapping steps ii and iii.

iv. **Annealing and Sulfurization**: Under a sulfur or selenium environment, an annealing process will be carried out at temperatures varies between 450°C to 600°C. For nanocrystal films, high-temperature thermal annealing methods are always used. It produces exceptional grain growth, which is necessary to evade disproportionate recombination and carrier scattering at nanocrystal borders. According to research, if a grain-growing thermal annealing procedure is not used, solar cells' performance will not reach even 1% of PCE [41].

2.12.1. CZTS crystal structure

CZTS is a quaternary chemical with the formula I_2-II-IV-VI_4. CZTS can be generated by swapping the trivalent In/Ga with a bivalent Zn and IV-valent Sn in the chalcopyrite CIGS configuration. CZTS could also be detected in the composition of stannite. The conditions beneath which a stannite structure can form, however, are still unknown. The crystal energy of stannite is just 2.86 meV/atom higher than that of kesterite, according to first-principles calculations. As a result, it is clear that both forms can persist together.

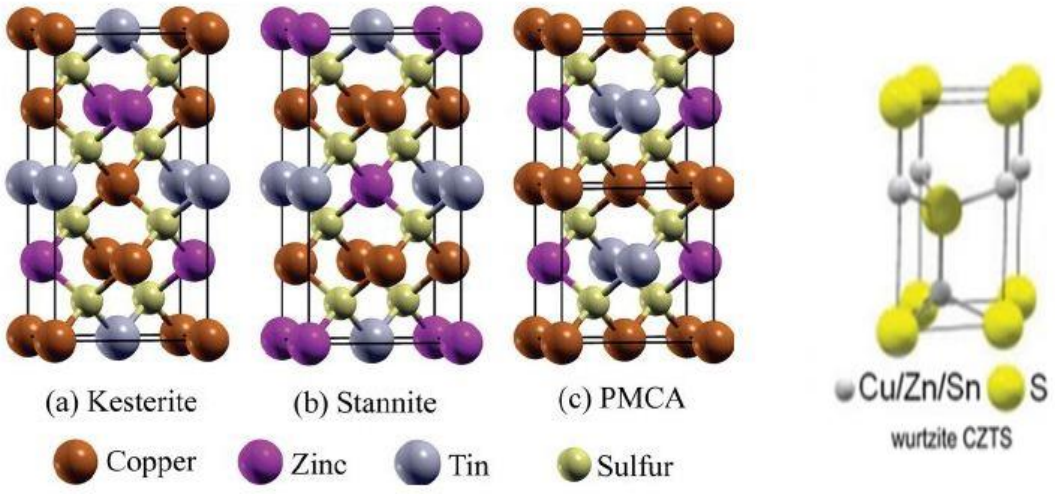

Fig 2.19.. *Different Crystal structure of CZTS [50]*

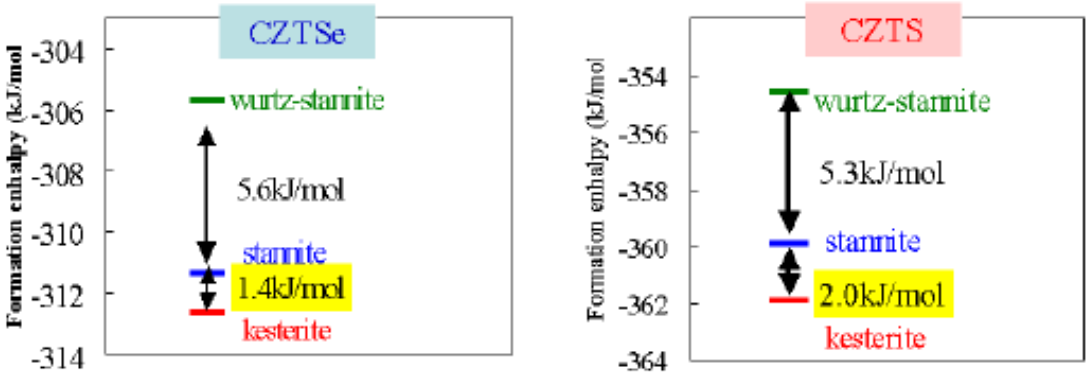

Fig 2.20. *Speculative enthalpies (-ΔH) for development of kesterite, stannite and wurtz-stannite of CZTSe and CZTS* [50]

The predicted materialization enthalpy (Δ*H*) of the kesterite phase (-312.7 kJ/mol) is slightly less compared to that of the stannite phase (-311.3 kJ/mol) and significantly less than that of the Wurtz-stannite phase (-305.7 kJ/mol) for CZTSe[52]. The kesterite phase's Δ*H* (-361.9 kJ/mol) is lower than the stannite phase's (-359.9 kJ/mol) for CZTS. CZTS has a higher variation in Δ*H* between the kesterite and stannite phases than CZTSe. This indicates that in CZTS, the kesterite phase is more steady compared to the stannite phase when paralleled to CZTSe.

The valence band maximums (VBMs) of the kesterite, stannite, and Wurtz-stannite-type CZTS/Se are antibonding orbitals of Cu 3d and S 3p (Se 4p), as disclosed by their electronic structures. Antibonding orbitals of Sn 5s and Se 4p (S 3p)form the conduction band minimums (CBMs). In either CZTSe or CZTS, the Zn atom has no effect on the VBM or CBM. The Sn 5s orbital in the band structure of CZTS/Se is somewhat confined. Nonetheless, due to the inert pair effect, the electrons of Sn 5s do not donate much to chemical bonding [52].

2.12.2. CZTS band gap energy

The band gap energy (Eg) of kesterite-type CZTSe and CZTS is much more widely distributed than that of stannite and Wurtz-stannite-type CZTSe and CZTS [50]. In addition, the considered band gap of CZTSe in the kesterite, stannite, and Wurtz-stannite structure are lesser compared to that in CZTS. The tunable bandgap of kesterite absorber layers is ~ 0.95 eV for CZTSe and its around ~1.5 eV for CZTS. It may vary from 1.48 to 1.63 eV for CZTS.

2.13. Device Structure

1.1.1. **Substrate:** There is a substrate on which different layers of thin films are deposited applying various techniques. This part (substrate) is mainly due to protect the cell. Liable on the material of the absorber film and others, the fabrication assembly may vary. However, a generalized structure has been discussed here. A substrate might be glass, metal foils, or even plastic. However, reflection losses might be abridged by anti-reflection coating and non-reflecting glass.

1.1.2. **Back contact:** For achieving the property of good conductivity, oxidation, and stability against corrosion, a back contact[35] is needed on the substrate. Generally, for CIGS and CZTS solar cells, molybdenum (Mo) is used.

1.1.3. **Absorber layer/ p-layer:** There is a very significant part of a solar cell is called absorber layer. The efficiency mostly depends on this layer. Depending on the material chosen, the thickness of this layer may be different. For CIGS/Se, co-evaporation of the four constituents

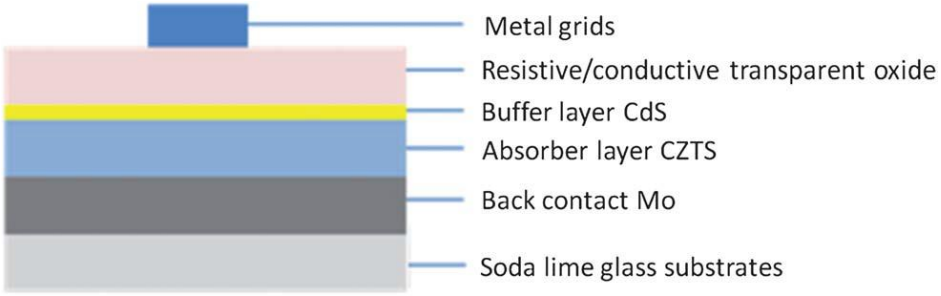

Fig.2.21. *Structure of CZTS solar cell*.

(Cu, In, Ga, S/Se) is a renowned process. There are some other techniques like sputtering, chemical vapor deposition that is applicable for deposition [36]. For sputtering, it requires another deposited layer by sulphurization or selenization to produce the concluding compound from the solid precursor for optimal grain growth.

1.1.4. **Buffer layer:** it is observed that adding a buffer layer in the cell improves the performance. It improves the lattice similarity between the absorber *p* type layer and the n-doped-layer. For CIGS and CZTS, there is a buffer layers of cadmium sulfide (CdS; n-type buffer layer) fabricated by chemical bath deposition (CBD) and pure (without doping) zinc oxide (i-ZnO, deposited by sputtering). But the fact that can't be hiding is the proper explanation or function is not completely found till now [37].

1.1.5. **Window layer/ n-layer:** The solar cell structure needs an *n* type layer to form the p-njunction to carry away the charge carriers. It is utilized in CZTS, CIGS, CdTe, and a-Si cells while these materials can not absorb sufficient of the arriving sunlight. It is actually a layer of *TCO* (*Transparent Conducting Oxide*) which perform this nicely. It is also reffered to as 'window layer' as visible light is transmitted through it. For CIGS, heavily Al-doped ZnO (ZnO:Al) is used as TCO [36] which is deposited by sputtering. Heavy doping provides good conductivity.

1.1.6. **Back contact:** There are photons that are with longer wavelengths. These photons might be transmitted through the absorber layer of a solar cell. Again the absorption coefficient will determine how strong the absorption per depth is. A thin film photovoltaic cell, on the other hand, is designed to be as lean as possible in order to conserve material and costs. Therfore a reflecting back-contact might be the solution here. Generally, Aluminium(Al) is widely used for a-Si and Zirconium Nitride (ZrN) for CIGS [38] and Mo or MoS_2 is used for CZTS [67].

.

2.14. Bibliography

[1] IAEA: The Long Term Storage of Radioactive Waste: Safety and Sustainability.

http://www-pub.iaea.org/MTCD/publications/PDF/LTS-RW_web.pdf.Version: 2003.

[2] J. B. Li, V. Chawla, and B. M. Clemens, "Investigating the Role of Grain Boundaries in CZTS and CZTSSe Thin Film Solar Cells with Scanning Probe Microscopy,"Adv Mater 24, 720 , 2012.

[3] M A Green, K Emery, Y Hishikawa, W Warta, "Solar cell efficiency tables, Version 35," Progress in photovoltaics: Research and applications 18, S. 144–150, 2010.

[4] D. B. Mitzi, O. Gunawan, T. K. Todorov, K. Wang, and S. Guha, "The path towards a high-performance solution-processed kesterite solar cell," Sol. Energy Mater. Sol. Cells 95, 1421 2011.

[5] H. Katagiri, "Cu_2ZnSnS_4 thin film solar cells," Thin Solid Films 480-481, 426, 2005.

[6] W. Shockley, and H. J. Queisser, "Detailed Balance Limit of Efficiency of *p-n* Junction Solar Cells," J. Appl. Phys. 32, 510, 1961.

[7] A. Luque , S. Hegedus , "Handbook of Photovoltaic Science and Engineering,"Wiley , Sussex 2011 .

[8] K. Mitchell , A. L. Fahrenbruch , R. H. Bube , "Relative carrier densities and trap effects on the properties of CdS/CdTe,"J. Vacuum Sci. Technol., 12 , 909, 1975 .

[9] D. Cusano , "CdTe solar cells and photovoltaic heterojunctions in II VI compounds,"Solid-State Electronics,6 , 217, 1963.

[10] A. Shah , P. Torres , R. Tscharner , N. Wyrsch , H. Keppner , " Photovoltaic technology: the case for thin-film solar cells," Science , 285 , 692, 1999.

[11] A. V. Shah , R. Platz , H. Keppner, "Thin-film silicon solar cells: A review and selected trends," Sol. Energy Mater. Sol. Cells, 38 , 501, 1995 .

[12] L. L. Kazmerski , F. R. White , G. K. Morgan , " Thin-film $CuInSe_2$/CdS heterojunction solar cells", Appl. Phys. Lett.,29, 268, 1976.

[13] H. W. Schock , R. Noufi , " CIGS-based solar cells for the next millennium," Prog. Photovoltaics: Res. Appl. ,8, 151, 2000 .

[14] K. Ito , T. Nakazawa ," Electrical and Optical Properties of Stannite-Type Quaternary Semiconductor Thin Films," Jpn. J. Appl. Phys. 1988 , 27 , 2094, 1988.

[15] J. J. Scragg , P. J. Dale , L. M. Peter , G. Zoppi , I. Forbes , " New routes to sustainable photovoltaics: evaluation of Cu_2ZnSnS_4 as an alternative absorber material,"Phys. Stat.Solidi B , 245 ,1972, 2008 .

[16] C. Steinhagen , M. G. Panthani , V. Akhavan , B. Goodfellow , B. Koo ,B. A. Korgel , "Synthesis of Cu_2ZnSnS_4 Nanocrystals for Use in Low-Cost Photovoltaics," J. Am. Chem. Soc. , 131 , 12554, 2009 .

[17] S. Schorr , H.-J. Hoebler , M. Tovar , " A neutron diffraction study of the stannite-kesterite solid solution series," Eur. J. Mineral.,19, 65, 2007 .

[18] T. K. Todorov , K. B. Reuter , D. B. Mitzi , "High-Efficiency Solar Cell with Earth-Abundant Liquid-Processed Absorber,"Adv. Mater. ,22 , E156, 2010 .

[19] R. Haight , A. Barkhouse , O. Gunawan , B. Shin , M. Copel ,M. Hopstaken , D. B. Mitzi , " Band alignment at the $Cu_2ZnSn(S_xSe_{1-x})_4$/CdS$Cu_2ZnSn(S_x\ Se_{1-x})_4$ /CdS interface," Appl. Phys. Lett.,98, 253502, 2011 .

[20] T. Tanaka , T. Nagatomo , D. Kawasaki , M. Nishio , Q. Guo ,A. Wakahara , A. Yoshida , H. Ogawa , J.,"Preparation of Cu_2ZnSnS_4 thin films by hybrid sputtering," Phys. Chem. Solids **2005** , 66 , 1978, 2005.
[21] J. S. Seol , S. Y. Lee , J. C. Lee , H. D. Nam , K. H. Kim ,"Electrical and optical properties of Cu2ZnSnS4 thin film prepared by RF magnetron sputtering process," Sol. EnergyMater. Sol. Cells,75, 155, 2003 .
[22] H. Katagiri , K. Saitoh , T. Washio , H. Shinohara , T. Kurumadani ,S. Miyajima , "Development of thin film solar cell based on Cu_2ZnSnS_4 thin films," Sol. Energy Mater. Sol. Cells,65, 141, 2001 .
[23] M. Kurihara , D. Berg , J. Fischer , S. Siebentritt , P. J. Dale ,"Kesterite absorber layer uniformity from electrodeposited pre-cursors,"Phys. Stat.Solidi, 6, 1241, 2009 .
[24] A. Redinger , S. Siebentritt ," Coevaporation of **$Cu_2ZnSnSe_4$** thin films," Appl. Phys. Lett., 97 , 092111, 2010 .
[25] A. Redinger , D. M. Berg , P. J. Dale , S. Siebentritt ," The Consequences of Kesterite Equilibria for Efficient Solar Cells,"J. Am. Chem. Soc., 133 , 3320, 2011 .
[26] S. R. Hall, J. T. Szymanski, and J. M. Stewart, " Kesterite, Cu_2 (Zn,Fe)SnS_4 , and stannite, $Cu_2Fe,ZnSnS_4$, structurally similar but distinct minerals," Can. Mineral. 16, 131, 1978.
[27] K. Ito, and T. Nakazawa, " Electrical and Optical Properties of Stannite-Type Quaternary Semiconductor Thin Films," Jpn. J. Appl. Phys. 27, 2094,1988.
[28] H. Katagiri, N. Sasaguchi, S. Hando, S. Hoshino, J. Ohashi, T. Yokota, Preparation and evaluation of Cu_2ZnSnS_4 thin films by sulfurization of E-B evaporated precursors, solar Energy Materials & Solar Cells, 49, 407-414,1997.
[29] T. M. Friedlmeier, N. Wieser, T. Walter, H. Dittrich, and H. W. Schock, "Heterojunctions based on Cu_2ZnSnS_4 and $Cu_2ZnSnSe_4$ thin films," 14th European PVSEC, Belford, UK ,pp. 1242, 1997.
[30] H. Katagiri, K. Jimbo, W.S. Maw, K. Oishi, M. Yamazaki, H. Araki, A. Takeuchi, "Development of CZTS-based thin film solar cells," Thin Solid Films, 517, 2455-2460,2009.
[31] H. Katagiri, K. Jimbo, S. Yamada, T. Kamimura, W.S. Maw, T. Fukano, T. Ito, T. Motohiro, "Enhanced Conversion Efficiencies of Cu_2ZnSnS_4-Based Thin Film Solar Cells by Using Preferential Etching Technique, " Applied Physics Express, 1,041201, 2008.
[32] D.B. Mitzi, M. Yuan, W. Liu, A.J. Kellock, S.J. Chey, V. Deline, A.G. Schrott, "A High-Efficiency Solution-Deposited Thin-Film Photovoltaic Device," Advanced Materials, 20, 3657-3662, 2008.
[33] S. Bag, O. Gunawan, T. Gokmen, Y. Zhu, T.K. Todorov, D.B. Mitzi, "Low band gap liquid-processed CZTSe solar cell with 10.1% efficiency," Energy & Environmental Science, 5, 7060, 2012.
[34] D.A.R. Barkhouse, O. Gunawan, T. Gokmen, T.K. Todorov, D.B. Mitzi, "Device characteristics of a 10.1% hydrazine-processed Cu2ZnSn(Se,S)4 solar cell," Progress in Photovoltaics: Research and Applications, 20, 6-11, 2012.
[35] Emmanuel Van Kerschaver, and Guy Beaucarne, "Back-contact Solar Cells: A Review",Prog. Photovolt: Res. Appl., 14:107–123,2006. DOI: 10.1002/pip.657.
[36] Lewerenz, H.-J. ; Jungblut, H.: Photovoltaik - Grundlagen und Anwendungen.Springer-Verlag, 1995.
[37] R N Bhattacharya, K Ramanathan,"Cu(In,Ga)Se2 thin film solar cells with buffer layer alternative to CdS,"Solar Energy ,77, S. 679–683, 2004.
[38] S Schleußner, "Cu(In,Ga)Se2 Thin Film Solar Cells with ZrN as a Back Contact," Universität Stuttgart, Diplomarbeit, 2003.
[39] W. Ki and H. W. Hillhouse, " Earth-Abundant Element Photovoltaics Directly from Soluble Precursors with High Yield Using a Non-Toxic Solvent," Adv. Energy Mater.,1, 732–735, 2011.
[40] Huanping Zhou, Wan-Ching Hsu, Hsin-Sheng Duan, Brion Bob, Wenbing Yang,Tze-Bin Song, Chia-Jung Hsu and Yang Yang, "CZTS nanocrystals: a promising approach for next generation thin film photovoltaics," Energy Environ. Sci., 6, 2822, 2013.DOI: 10.1039/c3ee41627e.
[41] C. Steinhagen, M. G. Panthani, V. Akhavan, B. Goodfellow,B. Koo and B. A. Korgel, "Synthesis of Cu_2ZnSnS_4 Nanocrystals for Use in Low-Cost Photovoltaics," J. Am. Chem. Soc., 2009, 131,12554.

[42] Q. Guo, G. M. Ford, H. W. Hillhouse, and R. Agrawal, "A generalized and robust method forefficient thin film photovoltaic devices from multinary sulfide nanocrystal inks,"37th IEEE PVS Conf., 2011, pp. 003522–003526.
[43] M. A. Green, Third Generation Photovoltaics, Springer, 2006.
[44] A. Luque, S. Hegedus, Handbook of Photovoltaic Science and Engineering, Wiley-VCH, 2003.
[45] P. Würfel, "The Chemical Potential of Radiation," J. Phys. C - Solid State Physics, 15, 3967, 1982.
[46] P. Würfel, Physics of Solar Cells, Wiley-VCH, Weinheim, 2005.
[47] J. Nelson, The Physics of Solar Cells, Imperial College Press, 2004.
[48] P.T. Landsberg, Recombination in Semiconductors,Cambridge University Press, 1991.
[49] A. Luque, S. Hegedus, Handbook of Photovoltaic Science and Engineering ,2011.
[50] T. Maeda, S. Nakamura and T. Wada, "Phase stability and electronic structure of In-free photovoltaic semiconductors, $Cu_2ZnSnSe_4$ and Cu_2ZnSnS_4 by first-principles calculation,"Mater. Res. Soc. Symp. Proc. Vol. 1165 Materials Research Society, 2009.
[51] W Wang, M T Winkler, O Gunawan, T Gokmen, T K Todorov, Y Zhu, D B Mitzi, "Device Characteristics of CZTSSe Thin-Film Solar Cells with 12.6% Efficiency,"Advanced Energy Materials. 4 (7): 1301465, 2013. doi:10.1002/aenm.201301465.
[52] T. Maeda, S. Nakamura and T. Wada; 'Phase stability and electronic structure of In-free photovoltaic semiconductors, $Cu_2ZnSnSe_4$ and Cu_2ZnSnS_4 by first-principles calculation' ,1165-M04-03, Mater. Res. Soc. Symp. Proc. Vol. 1165 Materials Research Society, 2009.
[53] Michele De Bastiani, "Ph.D. Thesis: The stability of third generation solar cells", Università degli Studi di Padova,Dipartimento di Scienze Chimiche,Center for Nanoscience and Technology, CNST, PoliMi, Istituto Italiano di Tecnologia, 2016.
[54] Giovanni Altamura, "PhD Thesis: Development of CZTSSe thin films based solar cells", Equipe Nanophysique et Semiconducteurs(NPSC), Universite de Grenoble, 2014.
[55] Wei Wang , Mark T. Winkler , Oki Gunawan , Tayfun Gokmen , Teodor K. Todorov , Yu Zhu , and David B. Mitzi , Device Characteristics of CZTSSe Thin-Film Solar Cells with 12.6% Efficiency Advanced Energy Materials **2014,** 4, 1301465.
[56] T. K. Todorov , J. Tang , S. Bag , O. Gunawan , T. Gokmen , Y. Zhu , D. B. Mitzi, "Beyond 11% Efficiency: Characteristics of State-of-the-Art $Cu_2ZnSn(S,Se)_4$ Solar Cells," Adv. Energy Mater., 3 , 34, 2013.
[57] J. Li et al., Solar Energy Materials and Solar Cells, "10% Efficiency $Cu_2ZnSn(S, Se)4$ thin film solar cells fabricated by magnetron sputtering with enlarged depletion region width,"
149, 242-249, 2016.
[58] C . Yan et al. , "Cu_2ZnSnS_4 solar cells with over 10% power conversion efficiency enabled by heterojunction heat treatment," Nature Energy, 3, 764–772, 2018.
[59] T. K. Todorov , K. B. Reuter , D. B. Mitzi , High-Efficiency Solar Cell with Earth-Abundant Liquid-Processed Absorber,"Adv. Mater., 22 , E156, 2010 .
[60] H.K. Park et al. , "Chemical tailoring of sodium content for optimization of interfacial band bending and alignment in flexible kesterite solar cells," Solar Energy Materials and Solar Cells , 230 ,111243, 2021.
[61] J. Tao et al., "7.1% efficient co-electroplated Cu_2ZnSnS_4 thin film solar cells with sputtered CdS buffer layers," Green Chemistry,18, 550-557, 2016.
[62] H. Katagiri , K. Jimbo , S. Yamada , T. Kamimura , W. S. Maw , T. Fukano , T. Ito , T. Motohiro , "Enhanced Conversion Efficiencies of Cu_2ZnSnS_4-Based Thin Film Solar Cells by Using Preferential Etching Technique," Appl. Phys. Express , 1 , 041201, 2008.
[63] Sadanand , D.K. Dwivedi, "Numerical modeling for earth-abundant highly efficient solar photovoltaic cell of non-toxic buffer layer," Optical Materials , 109 , 110409, 2020.
[64]Y. H. Khattak et al., "Enhancement of the conversion efficiency of thin film kesterite solar cell,"
Journal of Renewable and Sustainable Energy , 10, 033501, 2018.
[65] Uday Saha and Md. Kawsar Alam , "Boosting the efficiency of single junction kesterite solar cell using Ag mixed Cu_2ZnSnS_4 active layer," RSC Adv., 8, 4905, 2018.
[66] S. E. Maklavani et al. , "Enhancing the open-circuit voltage and efficiency of CZTS thin-film solar cells via band-offset engineeringOptical and Quantum Electronics ,52:72, 2020.

[67] F. A Jhuma et al., “Towards high-efficiency CZTS solar cell through buffer layer optimization” Materials for Renewable and Sustainable Energy , 8:6, 2019.
[68] Jiazheng Zhou et al. Control of the phase evolution of kesterite by tuning of the selenium partial pressure for solar cells with 13.8% certified efficiency Nature Energy, 8,526–535, 2023.
[69] Yixiong Ji & Fangyang Liu, „Single-phase evolution path to new record efficiency of kesterite solar cells“ , Sci China Chem, 66, 2023.
[70] Hang Geng et al., “Two-Step Cooling Strategy for Synergistic Control of CuZnand SnZnDefects Enabling 12.87% Efficiency (Ag,Cu)2ZnSn(S,Se)4 Solar Cells”, Adv. Funct. Mater., 33, 2210551, 2023
[71] Yage Zhou et al., “11.4% Efficiency Kesterite Solar Cells on Transparent Electrode,” Adv. Energy Mater. 13, 2300253, 2023

Chapter 3: Modelling

3.1.Thin Film Fabrication Method

Thin Film Fabrication is a nano- skill of depositing a lean film of compound. The thickness can differ between a few nanometers to about 100 micrometers. The deposition can be on a "substrate" surface or on a previously deposited coating to form different layers. It has a wide range of uses in optics, such as reflecting, anti-reflective, or self-cleaning glass, electronics (various layers of insulators, semiconductors, and conductors to construct integrated circuits), wrapping (aluminum-coated PET film, for example), and other fields. Similar types of methods are employed where value of film width is not significant. The decontamination of copper by electroplating and the fabrication of silicon and enhanced uranium by a CVD-like method after gas-phase treating- for these type of process thin film fabrication is employed too. Thin Film manufacturing methods are one of the prominent features in semiconductor manufacture plant, solar panels, CDs, DVDs, and other optoelectronic device industries.

Reliant on the deposition technique is predominantly chemical or physical,fabrication procedures fall into two comprehensive categories [1]. Physical deposition method employed mechanical, electromechanical, or thermodynamic means to manufacture a thin film. In a chemical process, nonetheless, a fluid precursor involves chemical change at a solid surface, occasioning in the fabrication of a solid layer.

The fabrication procedures might be categorized into two natures based on the basic principles that cause film fabrication: Physical Vapor Deposition (PVD) and Chemical Vapor Deposition (CVD).

A material is evaporated or sputtered using a physical vapor deposition (PVD) process. It generates a gaseous plume or beam that falls onto the subject. The electron beam evaporator, thermal evaporator, molecular beam epitaxy (MBE), pulsed laser deposition (PLD), sputtering, and co-sputtering etc. are included in this system.

Reactive and volatile chemicals are used as precursors in the chemical vapor deposition (CVD) process. On a heated surface, it dissipates. The initial ingredients are usually organo- or hydrido-compounds which are collected into a non-volatile component at low temperatures. The residual vapor or gas is driven out of the arrangement. This method includes atomic layer deposition (ALD), plasma enhanced CVB (PECVD), metal organic vapor phase epitaxy (MOCVD), etc.

Some of the deposition technique i.e. sol gel spin coating, dip coating, sputtering system and electrodeposition is discussed which are related to this work. Sol gel spin coating and dip coating system is a low cost process but we have not achieve good quality film by these processes. Moreover, these processes can not provide a particular thickness which is the the main drawback. In this scenario, Sputtering system shows the best performance to achieve desired thickness though it is an expensive method to follow. However, we have also tried electrodepostion system to fabricate CZTS thin film and it was not an successful attempt at all as we coulnot achieve goot stoichiometry CZTS thin film. The merits and demerits of these deposition process in elaboartly discussed in chapter 4 and 5. In current chapter we have discuedd the basic of these deposition process.

3.1.1.Sol-gel: Spin Coating

Sol–gel is a method of synthesizing tiny molecules into solid materials. The method[2] is used for the deposition of different oxides of metals. It converts the monomers into a colloidal solution (which is called *sol*). This solution performs as the precursor for an integrated web (it is called *gel*). This integrated network might be some distinct particles. Distinctive precursors that are used for sol gel are metal alkoxides.

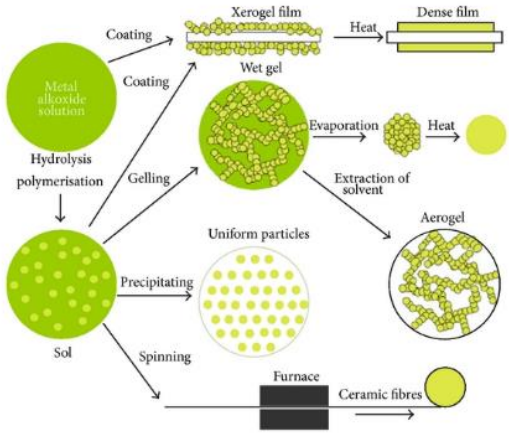

Fig.3.1. *Schematic of sol-gel method and their yields* [14]

Spin coating [3,4] comprises deposition of a minor pool of a fluid in the middle of a base material. The base is revolved horizontally at a high speed of ~3000 rpm. It is centripetal acceleration that origins the solution to extent all over the substrate. Thus, a thin film is fabricated onto a suitable substrate. The film thickness, morphology and other characteristics are governed by the attributes of the solution. Internal properties of the solution i.e. viscosity, solid portion, drying rate, nature of cooling, density and surface tension etc. are the constraints that contributes significantly on surface texture of produced thin film. In addition, external parameters e.g. fume exhaust, ultimate rotational speed and acceleration etc. subsidize the characteristics of sol gel spin layered thin film is distinct. Sol gel spin coating technique is efficaciously used in different applications of thin film for several decades.

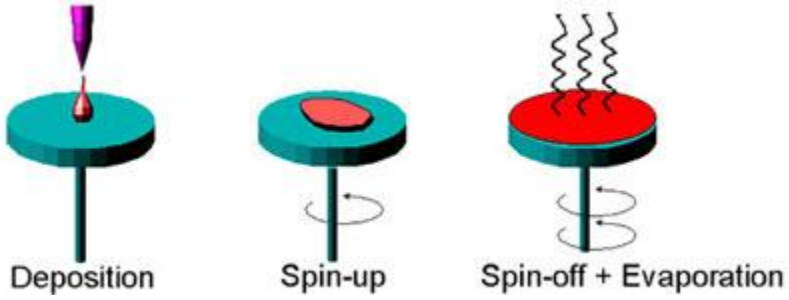

Fig.3.2*. Spin coating system.*

The reproducibility of the spin coating is another important factor. Minor differences in the parameters mentioned in the previous paragraph for the spin technique may result in dramatic changes in the spin treated film.

A classic spin coating technique contains of a dispense step in which the precursor solution is spread on the subject at a high rotation speed. The step of spinning made the solution thin. Then it is dried to eradicate extra solvents from film. There are two typical techniques of this dispense methods as (a) Static dispense and (b) Dynamic dispense.

Static dispense is merely leaving a trivial drop of precursor solution at the midpoint of suitable subject. The amount of fluid can vary from 1 to 10 cc reliant on the viscosity and density of the liquid. The required amount of fluid also vary with size and shape of the base that need to be layered. Generally, solution with high viscosity and or bigger base involve a huge drop of solution to confirm better attention of the substrate. On the other hand, dynamic dispense is the method of dispensing when the base material is rotating at a lower speed around ~500 rpm. Normally this process fabricate a film with less waste of solution or material. Dynamic dispense is a predominantly advantageous for the liquid or base that has poor moistening facilities. So that they can eradicate cavities.

Fig.3.3*. Spin coater*

After the dispensing step, the rotating speed is accelerated to thin the sol gel to achieve preferred thickness of the film. Reliant on the attributes of the sol gel and the base, spin speeds for the acceleration may vary from 1500-6000 rpm. Time for step might ranges between 10 seconds to quite a few minutes. The amalgamation of spin time and rpm designated for each stage will describe the film width and texture.

Typically, higher spin speeds for longer times produce comparatively thin solid films. This spin coating technology has a lot of factors that cancel out and average out during the spinning process. So sufficient time should be spend for experiment with new fluids as well as for a substrate to find out optimal time and spinning rate and acceleration rate for better coverage.

There is another vital step for spin coating called drying. A distinct drying step is followed by the high-speed spinning. Without substantially thinning the film, this step is carried out. Without drying, the solution might pour off the substrate. This step of drying is also essential to upsurge the physical stability of the film for further treatment of coating or annealing. Drying is applicable and beneficial for both

thick and thin film coating. Typically, a reasonable spin speed of about 25% of the high speed spin serve to benefit in dehydrating film. Spin speed of about 25% of the high speed would not change the film thickness. Fig.3.3 has shown a spin coater used for this work. This spin coater's programs can have up to ten unique process phases.

3.1.2. Sol-gel: Dip Coating

Sol gel dip coating route is a commonly used for modest and fast fabrication on an enormous zone. This method has a vast application in conventional dyeing. In addition, sol gel dip coating is much appropriate technology for the large scale manufacture of organic solar cells which is also of low budget.

An appropriate device detains a substrate that is to be covered. A precursor solution or fluid is arranged. Then the substrate is immersed into the sol or fluid. The dipping and drying procedure might be continual to achieve perfect or required thickness. Several dipping arrangements are obtainable for a system. It can be done manually or even mechanically. There are sophisticated devices, which hold the individual substrates apart, done the dipping as required and hold them until drying is accomplished.

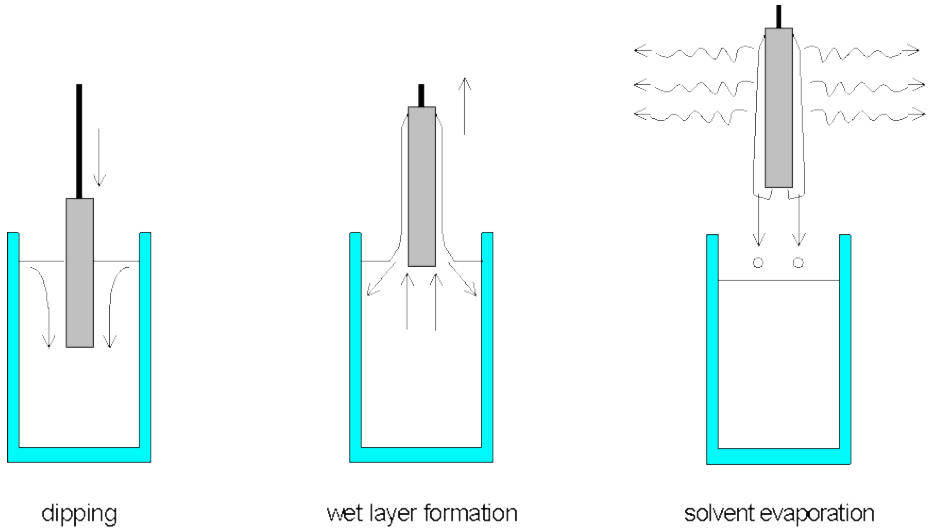

Fig.3.4. *Steps of the dip coating method.*

As shown in Fig.3.4, dip coating method is designated as a process where the substrate to be covered with desired material is submerged in a sol gel of that material (dipping). Then it's removed from the sol gel at a set speed under highly monitored temperature and environmental conditions. And a wet layer of precursor solution is formed. At the third step, the substarte is withdrawn from fluid. Evaporation of the sol gel occurs, finally a dip coated thin film is fabricated. So the parameters those play a vital role in dip coating are withdrawn speed, solid content, density and viscosity of the fluid. The width of the film is resoluted by these parameters. The film thickness might be estimated by the Landau-Levich equation[7] in the Newtonian regime as follows-

$$h = 0.94 \cdot \frac{(\eta \cdot v)^{2/3}}{\gamma_{LV}^{1/6} (\rho \cdot g)^{1/2}}$$

Where, h = film thickness, v = fluid viscosity, γ_{LV} = liquid-vapour surface tension, ρ= fluid density and g = gravity.

James and Strawbridge [5] reported that film thicknesses, which is in good agrrement with theoretical values for an acid catalyzed silicate sol. One of the exciting part of dip coating method is that if we can maintain a high optical quality, by selecting an fitting fluid viscosity, the film width might be ranged from 20 nm to 50 µm.

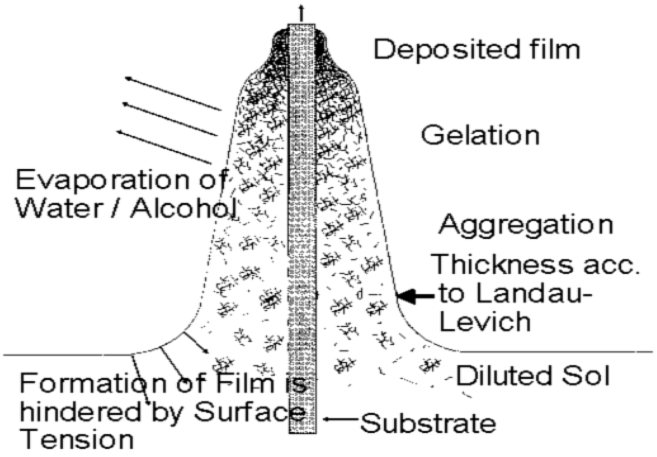

Fig. 3.5*. Gelation procedure of dip coating method.*

As we mentioned earlier, in sol-gel type of coatings, utilizing alkoxides or pre-hydrolyzed system is being used. Therefore, if the reactive system is selected, the regulattion of the atmospheric condition is indispensable. The experimental condition regulates the evaporation of the sol gel and the successive destabilization as well. By solvent evaporation process, it tips to a gelation formation and fabricates a see through film due to the minor particle dimension of sols in the scale of nanometer [6]. The phenomenon is depicted in Fig.3.5.

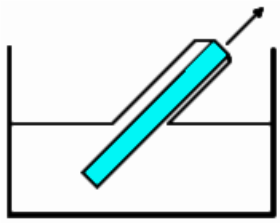

Fig. 3.6*. Schematic of angle dependent dip coating.*

Various firms use the dip coating process all around the world. Schott uses it for plate glass, founded on Schroder's [8] and Dislich's [9,10] breakthroughs in solar energy regulator systems (Calorex®) and anti-reflective coatings (Amiran®) for windows. Optical coatings, such as on bulbs, can also be covered with the dip coating. Dip coating is a process used by SMEs and other manufacturing businesses to assemble multilayer systems with up to 30 or 40 coatings with extreme accuracy, such as optical filters or dielectric mirrors. A dip coating technique that is angle-dependent has also been developed [8,11], where thickness adjustment is necessary for high precision. It is clearly depicted by Landau-Levich's equation [7]. The film width varies on the angle between the liquid surface and the substrate. Film width might be determined from the dipping angle. In addition, width of different layers can be calculated from the upper and end of the base (Fig. 3.6).

In general, there are five steps in a typical the dip-coating method[12] as follows-

(a) **Immersion:** The preferable substrate is immersed into the precursor sol with a persistent speed. This fluid contains the materials that need to be coated on the substrate.

(b) Start-up: The substrate is kept intimate the fluid for a particular time. After immersion, it is pulled up from the solution or fluid (sol) with a constant speed.

(c) Deposition: While the substrate is pulled up, there is a thin layer of desired materials on the substrate. The procedure of extracting is performed again with a persistent speed. A persistent speed is required to evade any kind of jitters. The thickness is determined by the speed as comparatively faster withdrawal produces thicker film.[13]

(d) Drainage: Excess solution or fluid will drain from the surface of the substrate automatically.

(e) Evaporation: After the drainage of excess solution, the solvent disappears from the substrate. It results thin film. If we use unstable substrate like alcohol as fluid (sol), evaporation begins even at the time of deposition.

These procedure (a)-(e) are repeated to obtain desired thickness and uniformity.

Fig.3.7. *Dip coater*

There are different parameters that donate to shaping the product by dip coating method. There are parameters like initial substrate surface, immersion and time of submersion, withdrawn speed, number of dipping process, solutions in each dipping arrangement, fluid concentration, composition, viscosity,

ambient temperature, , volatility of the fluid and environment humidity. It is probable to acquire high quality and unfluctuating films even on the substrates of bulky and complex shapes. Moreover, this process is of low cost. Therefore, dip coating is used worldwide for a vast type of applications. Fig.7 shows a dip coating system of MTI Corporation (PTL-MM01) used for this work.

3.1.3. Electro-deposition

Electro-deposition [22] is a well-known traditional surface alteration process that involves depositing a thin layer on top of another metal to alter its surface attributes. It's a simplified form of electrolytic deposition in which electrical current is used to diminish the cations of a target material in an electrolyte and deposit them as a thin film on a conductive surface. Researchers have spent a lot of time looking at how nuclei produce on the electrode substrate. The electrode substrate's crystal structure, unique free surface energy, adhesion energy, electrode surface lattice orientation, and crystallographic lattice incongruity at the nucleus-substrate interface boundary are all factors that influence the nucleation of nanostructures on the electrode for electro-deposition[24,25].

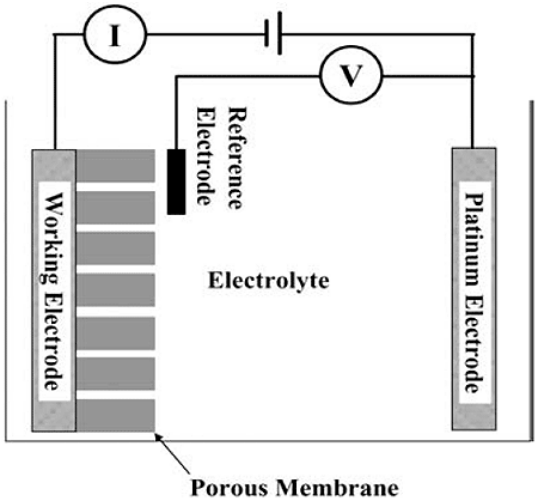

Fig.3.8. *Schematic Diagram of three electrode electrodeposition system* [23]

For thin film photovoltaic cell, The electro-deposition (ED) of the absorber layer is a promising route to cost effective production with the aptitude to produce thin films of metals, metallic alloys, and compounds which might be used in the generation of precursor layer by layer of a photovoltaic cell. The equipment for electro-deposition is low-cost and energy efficient as the method is acted upon near room temperature. Moreover, control of grain size, conformal coverage, crystallinity, and mingling of precursors etc. is employed in ED without difficulty. Thin films deposited by the ED process, on the other hand, do not have the same high crystalline perfection as those deposited by CVD or MBE. [26]. There is a lot of research work reported which used the electrodeposition method for the fabrication of thin film. There are several solution based approaches to assemble CZTS thin film [28-30]. Using Hydrazine with precursors exhibits the highest efficiency of12.8% to date [27]. Among solution based techniques, the Successive Ionic Layer Adsorption and Reaction (SILAR) method can study the synthesis of binary sulfide thin films more extensively [31-33]. The SILAR method is a fairly young

and understudied method. Moreover, the other methods used to fabricate CZTS thin film, require sulfurization, in which either N_2or H_2S atmosphere is essential for post heat treatment. To counter the disadvantage, (SILAR) method is much preferable.

3.1.4.Physical Vapor Deposition

PVD systems use a technique in which a target solid is vaporized, transferred, and condensed onto a substrate to deposit thin films on a substrate and fabricate coatings on a sample. Sputtering[18], Electron beam[18], and Thermal Evaporation[18] are examples of PVD processes.

Electron Beam Evaporation

Electron beam evaporation involve mechanisms that use a high-energy electron beam to evaporate the base material, characterized by extremely higher deposition rates up to 25000 Å/min. A magnetic field concentrates the electron beam onto the desired substrate, and the bombardment of electrons produces adequate temperature to vaporize an extensive variety of compounds with extremely higher melting

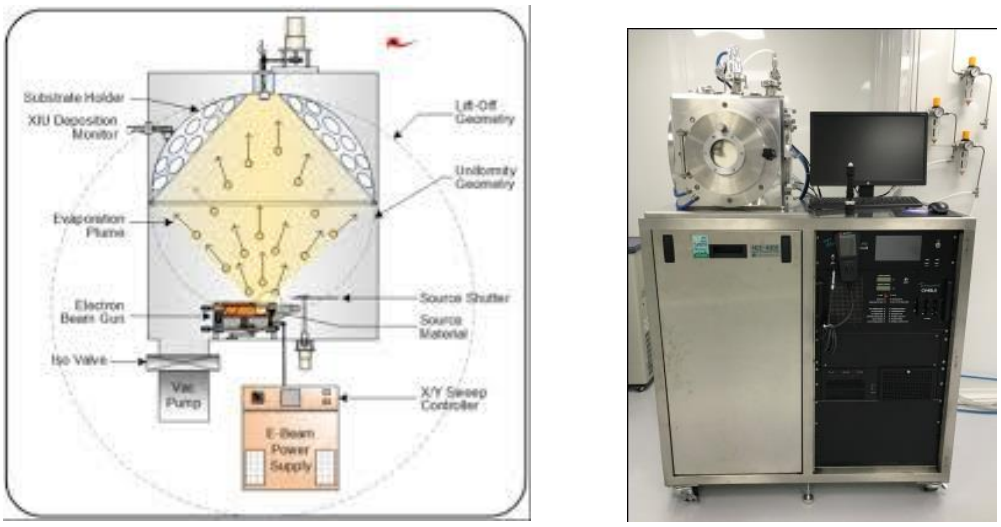

(a) (b)

Fig.3.9 (a) *Diagram of electron beam evaporation process [15],* ***(b)*** *Electron Beam Evaporator*.

points. The chamber pressure is kept lower as probable during normal e-beam evaporation to avert background gases from chemically interacting with the film or bulk evaporant. Reactive e-beam evaporation can produce films with a diverse chemical composition than the bulk when partial pressures of reactive gases are closely regulated.An electron beam source, hearth, and top cover are usually included in the basic setup, together with accessory feed throughs and appropriately sized power supplies. Depending on the evaporation material, evaporation may well be achieved straight from the hearth.

Electron beam evaporation is a really flexible process utilized in various thin film applications for its capability to regulate fabrication rate, lower impurityand outstanding utilization of material.

Thermal Evaporation

Thermal Evaporation is a popular technique of Physical Vapor Deposition (PVD). Thermal evaporation sources include modules that use resistive element for heating to evaporate the base material. The bulk material is usually put in a refractory metal source such as evaporation boat, basket, or filament-heated crucible and the temperature rises as power is supplied to promote evaporation. Fitting and hardware costs are low relative to other fabrication methods. Since, temperature regulation might be hard, and some evaporants even possesses a propensity to blend with the source materials. Therefore, it makes this method less universal than other.

The chamber pressure is reduced as prabable, similar to other methods, to avert background gases from chemically interacting with the film or other bulk evaporant. Reactive thermal evaporation might produce thin solid films with a diverse chemical composition than the bulk material if partial pressures of reactive gases are carefully regulated.

A boat, filament, or crucible source with auxiliary feed throughs (water-cooled if necessary), cross-contamination shielding, shutters, and power supplies are usually included in the basic setup of a thermal evaporator. A thermal evaporator is illustrated in Fig.3.10.

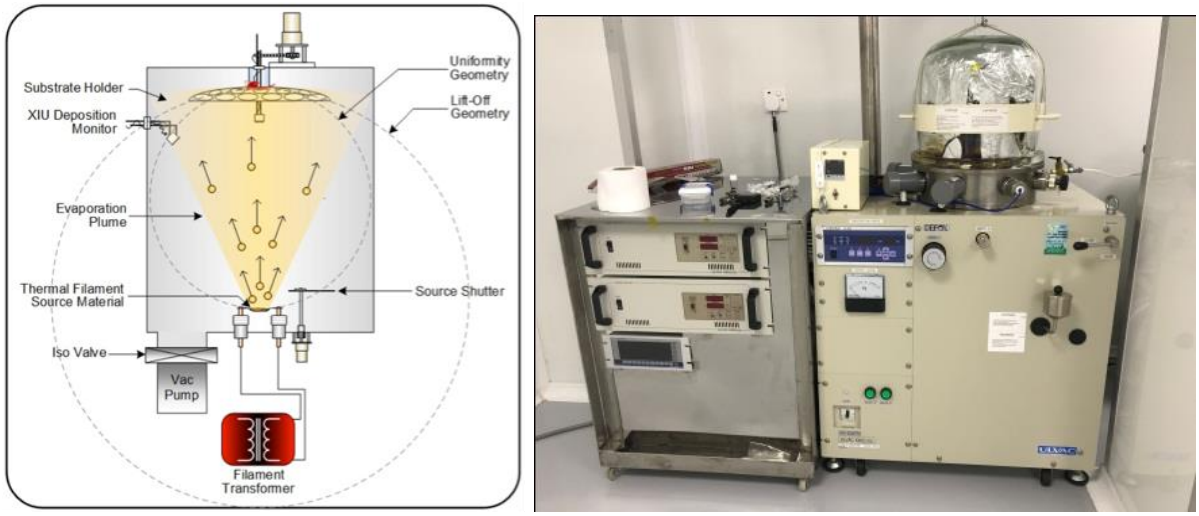

(a) (b)

Fig.3.10. (a) *Diagram of thermal evaporation process [16],* ***(b)*** *Thermal Evaporator*.

Sputtering

When Peter J. Clarke invented the first "Sputter gun" in 1970, he changed the scientific world by allowing the precise and efficient fabrication of compounds on an atomic level utilizing a charged plasma of electrons and ions in a vacuum condition. Sputter deposition, also known as sputtering, involves projecting atoms or molecules from a solid target's surface into the gas . And finally these molecules coalesce on a substrate. The verb “To Sputter” originates from the Latin word Sputare means

“To emit saliva with noise.” Sputtering does not involve melting of the target compound, rarely "spits" lumps just at base material, and the source might be placed in any configuration. In the sputtering method, the covering is not purely line-of-sight, and elemental mixtures, alloys, and compounds might be sputtered deprived of influencing their stoichiometry.

There is a target material (cathode) and the substrate (anode)in a sputtering system. A voltage is applied between them. Plasma is produced when electrons from the target's surface induce ionization in the selected gas. Sputtering sources are available in a variety of dimensions and profiles, ranging from small 1" round design R&D cathodes to larger planar output cathodes. And sources are companionable with vacuum levels ranging from a few mTorr to UHV.

There is a small voltage drop through the plasma since it is both electrically neutral and highly conductive. Crosswise thin "dark space" area, the voltage drops between the plasma and each electrode. The negative potential of the target draws positive ions from the plasma's edge, which strike the base materials with enough kinetic energy to expel neutral target atoms or molecules by transferring energy. Each expelled atom collides with various gas atoms or molecules on its way from target to substrate. This collision causes them to deflect and energy loss occurs. The atoms moves to the substrate's surface from partly randomized ways due to the optimized target-substrate gap. This phenomenon results in a unchanging film width over a textured surface.

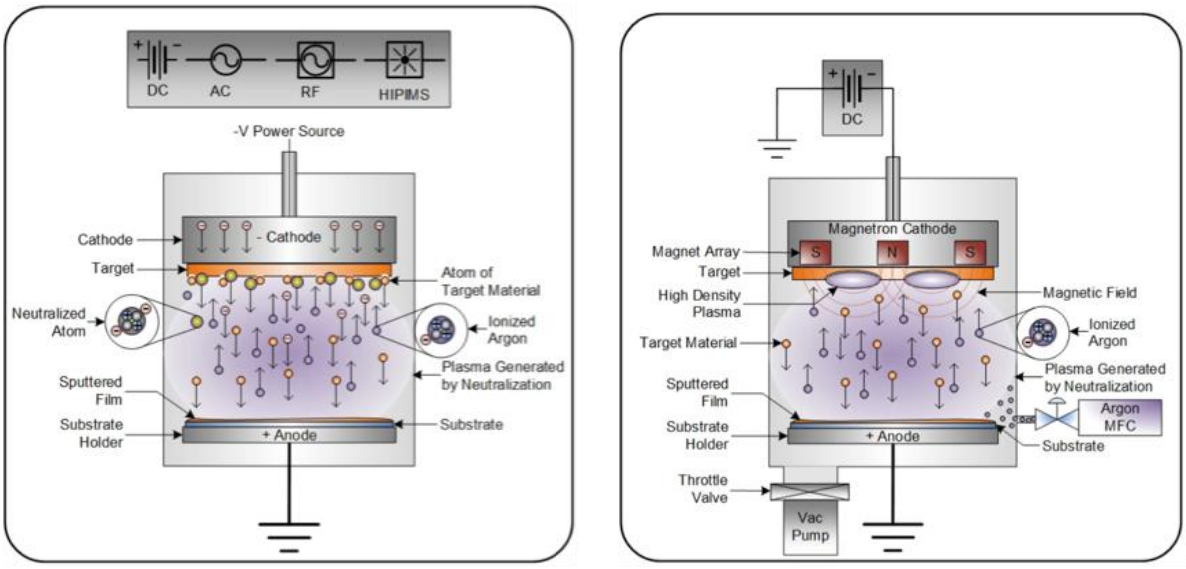

(a) (b)

Fig.3.11. Diagram of (a) Sputtering Process and (b) DC Magnetron sputtering process[17]

Fig. 3.12.Sputtering System

To "smooth out" the source's ring-like fabrication configuration, the ideal throw length between target and base material is broader than the target's diameter. A linear production source, on the other hand, has a much shorter optimum throw length when it is used to coat wide area substrates.

A TORUS® sputtering source with a target of the anticipated coating material; shutters; deposition chimney and/or gas injection; and suitably sized DC, Pulsed DC, and RF power supplies are usually included in the basic configuration. Fig. 3.12 shows PVD75 Pro Line, Kurt J Lesker which is used for this work.

There are various kinds of Sputtering Power Sources [17] i.e. DC or Direct Current Sputtering, Pulsed DC Sputtering, RF or Radio Frequency Sputtering, MF or Mid Frequency AC Sputtering, and HIPIMS or High Power Impulse Magnetron Sputtering.

Co sputtering

Co-Sputtering is a technique that involves sputtering two or more target materials at the same time in a high vacuum. It is often utilized in conjunction with Reactive Magnetron Sputtering to create thin films e.g. alloys or composites.

In the optical and architectural glass industries, the method of co-sputtering is extensively used. The refractive index or shading effect of the glass might be accurately monitored on applications. In addition, it ranges from large scale exteriors as skyscraper, architectural glass to googles where Reactive Co-Sputtering of two target like Silicon and Titanium with dual Magnetron Sputtering system has been employed.

Reactive Sputtering

The method of applying gas to a vacuum compartment that experiences a chemical change formerly approaching to other materials to be covered is known as reactive sputtering. Usually stable and inert ases such as nitrogen and oxygen, converted to ionized and reactive in the plasma atmosphere as a consequence of the higher energy collision.

3.2. Thin Film Characterization Method

Various characterization techniques are applied in the thesis to discover the structural, electrical, morphological, and optical attributes of the CZTS absorber and device. X-ray diffraction (XRD) is used to examine the crystal structure and secondary phases. The structural morphology is studied employing scanning electron microscopy (SEM). The energy dispersive X-ray spectroscopy (EDS) in the SEM systems is adopted to evaluate the chemical composition of CZTS absorbers. The external quantum efficiency (EQE) measurement indicates the spectral response of CZTS thin films. The sheet resistance of Mo back contacts is examined by the four point- probe method. For some cases, sheet resistance, resistivity, and mobility are calculated by the Hall Effect Measurement unit. And the width of the produced film is estimated with a surface profilometer.

In this section, these aforementioned techniques will be discussedin detail. These applied characterization methods are critical to understanding the attributes of the CZTS absorber and the finished CZTS device, therefore paving the way for further improving the conversion efficiency.

3.2.1. Structural

X-ray diffraction measurement (XRD)

XRD is a methodical tool that affordsstatistics on the construction of materials. In 1912, Max von Laue revealed that crystalline substrates act as three-dimensional diffraction gratings for X-ray wavelengths, which are comparable to the spacing of lattice planes in a crystal. X-ray diffraction is founded on constructive interference of single wavelength x-rays and lattice planes when situations mollify Bragg's law that is proposed by W. L. Bragg in 1912 and used to explain the interference pattern. Fig.3.13 shows the schematic representation of Bragg's law. The affiliation between the wavelength of radiation, the incidence angle of the X-rays, and the lattice spacing in the crystal can be expressed as shown in equation (3.1)

$n = 2d \sin$ (3.1)

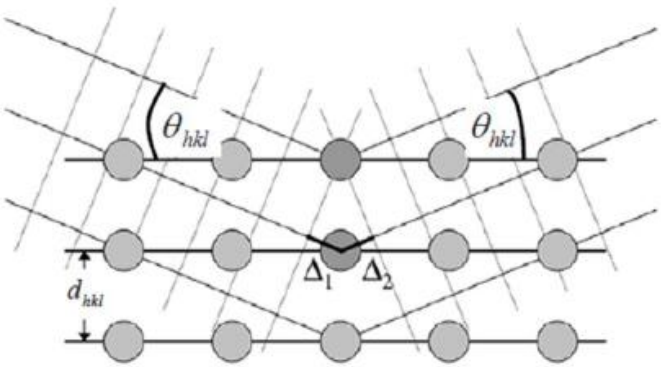

Fig.3.13*. Schematic representation of Bragg's law*. [140].

n is an integer, λ is the wavelength of the x-rays, d is the spacing between planes in the atomic lattice, and θ is the diffraction angle in degrees [139]. The resulting diffraction pattern is analyzed, with standard patterns having been available by the International Centre for Diffraction Data, USA (previously, Joint Committee on Powder Diffraction Standard) [139, 140].

Fig.3.14*.XRD System*

In this work, XRD patterns were measured by using GBC, ƐMMA research diffraction system (Fig.3.14), operating at a voltage of 35 kV and a current of 28 mA with Cu K_α radiation (λ=1.54 Å). The peak intensity, position of 2θ and full-width at half-maximum (FWHM) are fitted in the software package HighScore.

3.2.2. Morphological

Scanning electron microscopy (SEM)

Scanning Electron Microscope (SEM) is a powerful tool for seeing the invisible worlds of micro-scale and nano-scale structures. Resolution relies on the wavelength of the incident beam used to see a sample material. As electrons have much shorter wavelengths than light photons, a focused beam of electrons is applied in SEM to reveal complex details that are inaccessible by using light microscopy. This technology is extensively used to perceive the exterior plane and cross section morphology of thin films. This work utilized a SEM of Zeiss, EVO 18 (Fig.3.15(a)) which includes secondary electron and backscattered electron in-lens detection.

It is also furnished with an Energy Dispersive X-ray microanalysis system (EDAX, AMETEK) for elemental investigation (Fig.3.15(b)). For advanced morphology and chemical analysis, a seamless integration of particle analysis and identification solution is available. With the five segment BSE detector, a researcher can get more topographical detail. Variable pressure activity is also available for analyzing dry or hydrated samples. In the spacious chamber, EVO 18 can handle large specimens with versatile stage travel. The 5 segment diode BSE detector on EVO 18 provides improved low kV performance and advanced topography information.

(a) (b)

Fig.3.15*. (a) SEM and (b)EDX*

The secondary electron mode is used to obtain SEM images in the thesis. When the incident electron beam intermingles with material, secondary electrons may be produced by collisions with the nucleus, which result in significant energy loss. Electron can also be prompted by the ejection of loosely bound electrons from the sample atoms. For the improvement of the conductivity of CZTS films and prevent charging effects, the CZTS films were coated with a few nanometer thick Au (Gold) layers in the Quorum Sputter Coater, SC7620.(Fig.3.16)

Fig.3.16 *Sputter coater*

Surface Profilometer

Microscopical technologies such as scanning- or transmission-electron microscopy are the most direct approach to determine layer thickness . The downside of these procedures is their high complexity, which is attributable to the fact that they are performed under vacuum and require additional complex preparatory processes, making them time demanding and thus unsuitable for a large sample size. Furthermore, because it is a destructive measurement, the samples are frequently worthless after the experiment. Profilometry is a common and more practical technique for evaluating thickness of the film.

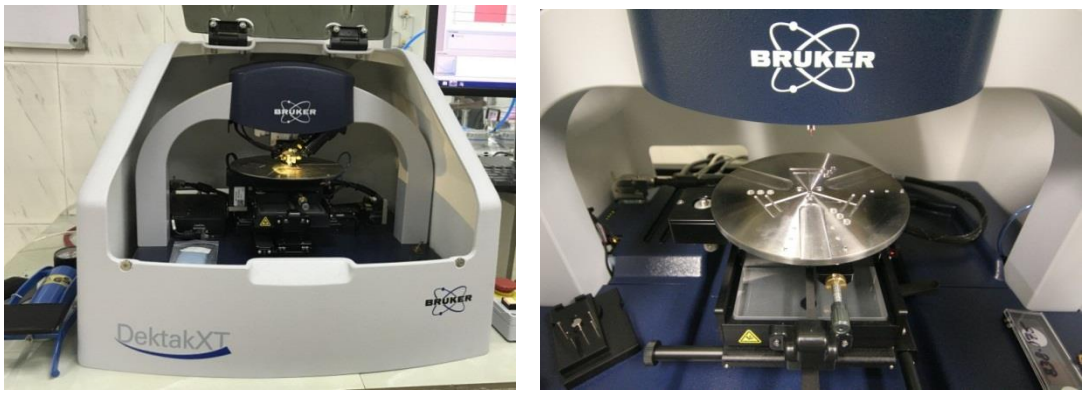

Fig.3.17*. Surface Profilometer*

A surface profilometer is a equipment that can be used to determine the profile of a surface to compute its roughness and critical dimensions such as step, curvature, and flatness of a surface. A stylus profilometer, often known as a mechanical profilometer, DektakXT, Bruker, shown in Fig.3.22 is employed to calculate the thickness of film fabricated for this research work. A diamond stylus is stimulated perpendicularly in contact with a film, then horizontally across it for a selected space and contact force. A profilometer may detect minute changes in vertical stylus movement as a role of location on a surface. A profilometer may detect microscopic upright topographies with heights varying between 10 nanometers to 1 millimeter. The diamond stylus produces an analog signal that is translated into a digital signal, collected, evaluated, and exhibited based on its height position.

The diamond stylus has a radius of 20 nm to 50 micrometers, and the horizontal resolution is determined by the scan speed and data signal sampling rate. The tracking force of the stylus can varies between less than 1 to 50 mg.

The DektakXT reduces measurement scan durations by 40% while retaining industry-leading quality thanks to a revolutionary direct-drive scan stage. Furthermore, using a single-arch structure strengthens the DektakXT, reducing sources of environmental noise.

3.2.3. Optical

Ultra-Violet-Visible Spectroscopy (UV-Vis/NIR)

Optical transmission, absorbance, and reflection were calibrated using a GBC Cintra 2020 Spectrophotometer Fig.3.17(a) ranges up to 1100nm. Another one is UH4150, Hitachi Fig.3.17(b) ranges from 190 to 2600nm. The measured wavelengths varies between 300 nm to 1100 nm with an interval of 10 nm. In the integrating sphere of the UH4150, several detectors are mounted to conduct measurements for a wide-ranging wavelengths, from ultraviolet to visible to near infrared. Prism-grating (P-G) double monochromator optical device is used here. In addition, for low transmittance and reflectance tests, the device provides low noise measurements. A background correction is applied to calibrate the baselines of 0% and 100% of transmission and reflection prior to sample measurements. The absorbance, reflectance, and transmittance can be direct. The optical absorption can also be calculated as absorbance=1-(transmittance + reflectance) given the initial light intensity is equal to unity.

(a) (b)

Fig.3.18.(a) UV Vis-GBC and (b) UV Vis-Hitachi

This system's collimated light beam permits precise quantification of reflected and scattered light. When evaluating the specular reflectance of solid samples, the incident angle is the key.

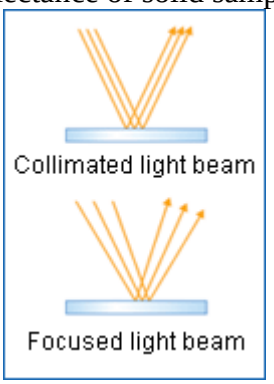

Fig.3.19 *Specular Reflectance measurement example*

The incident angle of a focused light beam varies depending on the focal length of the lens, among other factors. As a result, simulations of optical thin film designs, such as dielectric multilayer film and prisms, can vary from actual estimated values. Conversely, for a collimated

light beam, the incident angle with respect to sample is often the same, resulting in a extremely precise calculation of specular reflectance. Furthermore, the collimated light beam is employed for determining diffusivity and measuring lens transmittance (%T).

3.2.4.Electrical

Four-point-probe

The four-point probe (Fig.3.19(a)) is a specific device used to measure the resistivity of semiconductor. The substrate's resistivity can be assessed by flowing current through two outer probes and estimating voltage through the inner probes. Using a "four point probe," the sheet resistivity of the top emitter layer can be commonly accomplished by experiment. A current flows through the outer probes, causing a voltage to be induced in the inner voltage probes. Here the junction between the n and p-type semiconductor acts like an insulator. For experimentation, the cell must be preserved in dark.

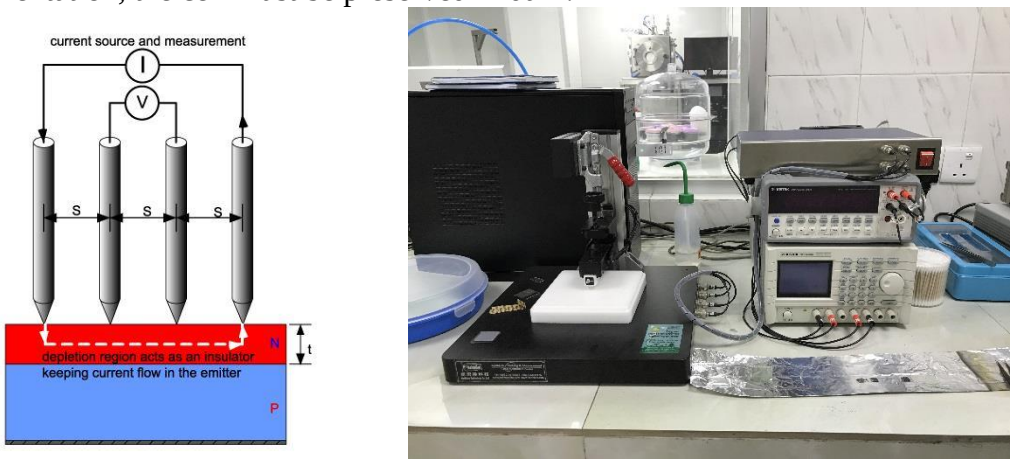

(a) (b)

***Fig.3.20**. **(a)** Schematic Diagram of four point probe **(b)** A Four point probe system*)

In an experiment, sheet resistance is estimated using a four-point-probe. The sheet resistance might be estimated using the equation (3.4).

$$\rho = 4.53\frac{V}{I} \qquad (3.4)$$

here V is the voltage across the probes, and I is the current flow in the probes [19].

The current is decreased for high resistivity samples to avoid an unnecessarily higher voltage at the contacts. It is recommended that the inner probes have a voltage of less than 100 mV/mm. Since the contacts to the silicon are ohmic, low resistivity samples are typically much easier to measure. We rise the current to 45.3 mA and set the voltmeter low if the resistivity is very low. The current moving through a material with a very low resistivity induces resistive heating, which raises the measured resistivity. KeithLink, Probing and Measurement System was used for this work (Fig.3.19(b)).

Hall Effect Measurement System

The Hall Measurement System is a comprehensive technique for determining both low and high resistance, bulk and sheet carrier concentration and mobility, and semiconductor Hall Coefficient (See Fig. 3.21). This study used HT55T3, Ecopia, and the Van der Pauw method [20]. To employ this approach, five conditions must be met [21] -

1. The specimen must be of uniform thickness and have a flat shape.
2. There must be no isolated holes in the specimen.
3. The specimen must be isotropic and homogeneous.
4. The sample's four contacts must all be at the pattern's edges.
5. Each individual contact must have an area of contact that is at least an order of magnitude less than total sample zone.

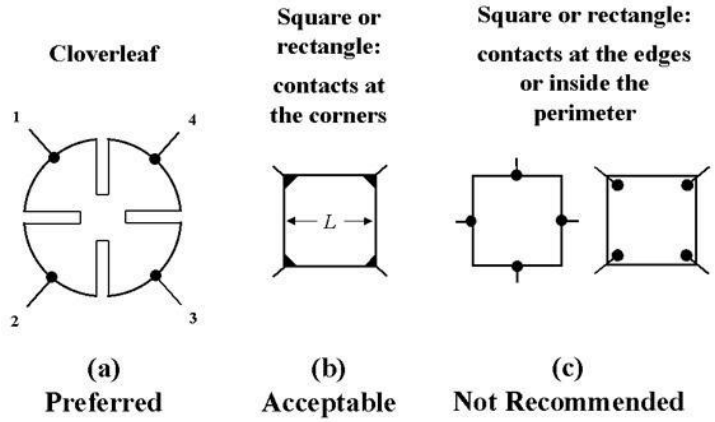

Fig.3.21. *A few probable connection locations for Van der Paw process.*

A continuous current supply, film holder, enduring magnet set, Hall effect measurement program (Windows), and liquid nitrogen funnel are included in the facility.

The Hall effect measurement system used for this work is shown in Fig.3.21. The HMS-3000 comes with software that can assess the ohmic integrity of material contacts using an I-V curve, as well as a Heating Controller (HMS3300). The system can analyse semiconductors and compound semiconductors (n-type and p-type) such as Si, Ge, SiC, GaAs, InGaAs, InP, GaN, ZnO, TCOs, metals, and other materials at room temperature (300K) and liquid nitrogen temperature (77K) as well. The resistivity ranges of HMS 3000 are 10^{-4} to 10^{7} (ohm-cm).

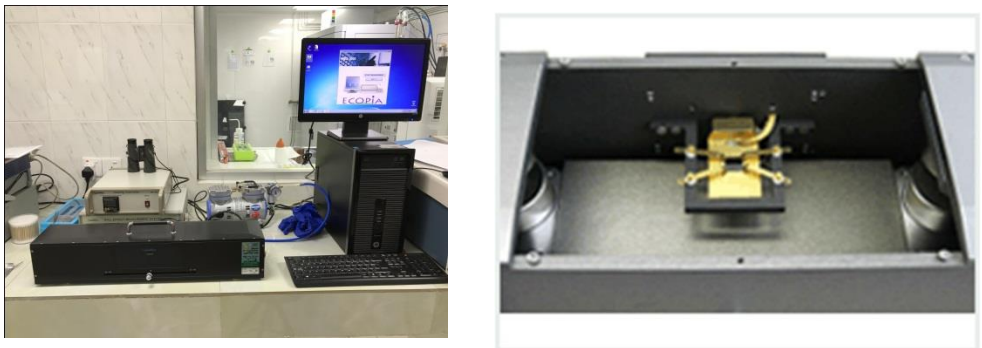

Fig.3.22*. A Hall Effect Measurement System*

3.2.5. Sun Simulator

For cutting-edge PV cell testing and related research, solar light is necessary. Solar Simulators generate a Class A Air Mass 1.5 Emission Spectrum that perfectly mimics full spectrum sunlight with a single solar output intensity. This work utilized a Solar Simulator shown in Fig.3.23 (McScience, K201, Lab55). This system includes a solar simulator with multiple irradiation zones, a photovoltaic power meter with multiple current ranges, a test jig, and assessment software for standard measurement of solar conversion efficiency. Voltage, Current, Temperature, Irradiance (Ref), etc measurement data can be calculated with various analysis parameters such as I_{sc}, V_{oc}, I_{max}, V_{max}, P_{max}, FF, Efficiency, R_s, and R_{sh}.

Fig.3.23*. Sun Simulator*

There are three types of lamp available for Solar Simulator on which the system model can differ. The lamps can be Xenon Lamp (Xe), Metal Halide Lamp (MH), or Plasma Lamp (PLS).

3.2.6. Quantum Efficiency Measurement System

Spectral response provides critical information on the spectral dependence of the photocurrent and is used to determine the mechanisms responsible for reductions in the short-circuit current [140]. The quantum efficiency is closely related to the spectral response. External quantum efficiency (EQE) is the ratio of the number of composed carriers to the number of incident photons of given energy [156]. The EQE includes the effect of transmitted and reflected photons. However, it is more useful to estimate the carrier collection efficiency by investigating the internal quantum efficiency (IQE). The IQE refers to the quantum efficiency that can be generated with the photons which is not reflected and transmitted. The IQE can be calculated using equation (3.3).

$$IQE(\lambda) = \frac{EQE(\lambda)}{1-R(\lambda)-T(\lambda)} \quad (3.3)$$

In order to remove the discrepancies between short circuit current measured in different current-voltage (I-V) tester, the short circuit current density (J_{sc}) is calibrated by incorporation of the EQE curve through the AM1.5 Global solar spectrum.

Fig.3.24*.Quantum Efficiency Measurement System*

The EQE was measured with Spectral IPEC Measurement System (McScience K3100) shown in Fig.3.24. The measured wavelength diverses from 300 nm to 1100 nm, with an increment of 10 nm.

3.3. Bibliography

[1] Functional Polymer Films Eds. R. Advincula and W. Knoll – Wiley, 2011, ISBN 978-3527321902.
[2] D A H Hanaor, I Chironi, I Karatchevtseva, G Triani, C C Sorrell,"Single and Mixed Phase TiO2 Powders Prepared by Excess Hydrolysis of Titanium Alkoxide, "Advances in Applied Ceramics. 111 (3): 149–158, 2012.
[3] D B Hall, P Underhill, J M Torkelson, "Spin Coating of Thin and Ultrathin Polymer Films, ,Polymer engineering and science, , Vol. 38, No. 12, 1998.
[4]L E Scriven , "Physics and applications of dip coating and spin coating". MRS proceedings. 121.1988.
[5]I. Strawbridge, P. F. James, "Thin silica films prepared by dip coating," J. Non-Cryst. Solids, 82, 366 – 372, 1986.
[6]C. J. Brinker, A. J. Hurd, K. J. Ward ,"Ultrastructure Processing of Advanced Ceramics", eds. J. D. Mackenzie and D. R. 4Ulrich, Wiley, New York 223, 1988.
[7]L. D. Landau, B. G. Levich, Acta Physiochim, "Infrared Spectroscopy of Titania Sol-Gel Coatings on 316L Stainless Steel,"Acta Physicochimica U.R.S.S., 17 ,42-54, 1942.
[8]O. Stern, " Theory of a double-electric layer with the consideration of the adsorption processes," Z. Elektrochem. (1924) 508, 1924.
[9]H. Schröder, " Oxide layers deposited from organic solutions," Physics of Thin Films, Academic Press, New York - London, vol. 5, 87 - 141, 1969.
[10]H. Dislich, New Routes to Multicomponent Oxide Glasses,"Angew. Chem. Int. Ed. 6 ,363,1971.
[11]H. Dislich, "Sol-gel: Science, processes and products,"J. Non-Cryst. Solids, 80 , 115 - 121, 1986.
[12]M N Rahaman, "Ceramic Processing,". Boca Raton: CRC Press. pp. 242–244. ISBN 0-8493-7285-2, 2007.
[13] DQuéré,"fluid coating on a fiber". Annual Review of Fluid Mechanics. 31 (1): 347–384, 1999. ISSN 0066-4189, doi:10.1146/annurev.fluid.31.1.347.

[14] A. Cannavale, F. Fiorito, M. Manca, G. Tortorici, R. Cingolani, and G. Gigli, “Multifunctional bioinspired sol-gel coatings for architectural glasses,” Building and Environment, vol. 45, no. 5, pp. 1233–1243, 2010.
[15] Matt Hughes - President - Semicore Equipment, Inc.,Published: 15 June 2016
http://www.semicore.com/news/89-what-is-e-beam-evaporation
[16] Norm Hardy - Process Engineer - Semicore Equipment, Inc., Published: 30 September 2013
http://www.semicore.com/news/71-thin-film-deposition-thermal-evaporation
[17] Matt Hughes - President - Semicore Equipment, Inc.Published: 24 November 2014
http://www.semicore.com/what-is-sputtering
[18] Thin Film Deposition Techniques & Capabilities
https://www.lesker.com/newweb/ped/techniques.cfm
[19] S. Wenham, M. Green, M. Watt, and R. Corkish, "Applied Photovoltaics," 2ndedition ed. UNSW centre for Photovoltaic Engineering, p. 61, 2006.
[20]Van der Pauw, "A method of measuring specific resistivity and Hall effect of discs of arbitrary shape" Philips Research Reports. 13: 1–9, 1958.
[21]J G Webster, "The measurement, instrumentation, and sensors handbook".New York: CRC Press LLC. pp. 43–1, 1999. ISBN 3-540-64830-5
[22] A Piegari and F Flory,"Optical thin films and coating, From Materials to application, "A volume in Woodhead Publishing series In Electronic and Optical Materials.Pg-815-835, 2013.
[23] D. Bera, S.C. Kuiry, and S. Seal, "Synthesis of Nanostructured Materials Using Template-Assisted Electrodeposition,"JOM volume 56, pages49–53 ,
[24] A. Milchev, S. Stoyanov, and R. Kaischew ,“Atomistic Theory of Electrolytic Nucleation," Thin Solid Films, 22 , pp. 255–265.1974.
[25] A. Milchev,"Electrocrystallization Fundamentals of Nucleation and Growth", Boston: Kluwer Academic Publishers, 2002.
[26] Abhijit Ray, " Electroplating of Nanostructures, Chapter 7: Electrodeposition of Thin Films for Low-cost Solar Cells," 2015. DOI: 10.5772/61456
[27] W Wang , M T Winkler, O Gunawan, T Gokmen, T K Todorov , Y Zhu, D B Mitzi, "Device Characteristics of CZTSSe Thin- Film Solar Cells with 12.6% Efficiency," Advanced Energy Material, 2013. https://doi.org/10.1002/aenm.201301465
[28] Y Cao et al. " High-efficiency solution-processed Cu2ZnSn(S,Se)4 thin-film solar cells prepared from binary and ternary nanoparticles," J Am Chem Soc. 26;134(38):15644-7, 2012.
[29] M.C. Rao, Sk. Shahenoor Basha, "Structural and electrical properties of CZTS thin films by electrodeposition, " Results in Physics 9, 996–1006, 2018.
[30] H W Tsai et al. "Facile Growth of Cu2ZnSnS4 Thin-Film by One-Step Pulsed Hybrid Electrophoretic andElectroplating Deposition,"Scientific Reports, 6:19102, 2016. DOI: 10.1038/srep19102.
[31] S S Mali, P S Shinde, C A Betty, P N Bhosale, Y W Oh, P S Patil, "Synthesis and Characterization of Cu2ZnSnS4 thin films by SILAR Method," Journal of physics and Chemistry of solids, 73(6), 735-740, 2012.
[32] , J Henry, K Mohanraj, G Sivakumar, "Electrical and optical properties of CZTS thin films prepared by SILAR method," Journal of Asian Ceramic Societies, 4(1), 81-84, 2016.
[33] M P Suryawanshi et al., "Improved solar cell performance of Cu2ZnSnS4 (CZTS) thin films prepared by sulfurizing stacked precursor thin films via SILAR method,"Journal of Alloys and Compounds, 671, 509-516, 2016.

Chapter 4: Fabrication and characterization of Al doped ZnO (AZO) thin film

4.1. Al doped ZnO (AZO) by sol-gel spin coating technique with thickness variance.

Because of its strong optoelectronic properties, Al doped ZnO(AZO) is regarded a suitable choice for translucent conductive oxide (TCO). It has a wide spectrum of uses in optoelectronic devices as a transparent conductive oxide with low resistance and outstanding optical transmittance in the observable wavelength area [1] [2]. ITO has become the most widely used TCO material in current history, even though it is expensive, and indium may become scarce in the future[3] [4]. So far, a handful of materials have been studied as possible approaches to ITO. ZnO films, for example, offer excellent electrical and optical attributes and can be chemically integrated with economic, nonpoisonous materials. However, if similar ZnO film is doped with contaminations such as Al or Ga, the resulting films have a substantially higher conductivity. Zinc oxide with an Al dopant (AZO) is less expensive than zinc oxide with a Ga dopant. As a result, out of all of these films, AZO is the best ITO substitute because it has strong electrical and optical attributes, contains nonpoisonous, plentiful, low-cost ingredients, and is easy to construct [5].

Several approaches can be used to produce Al doped ZnO films. Pulsed laser deposition chemical vapor deposition, sputtering, electron beam evaporation, molecular beam epitaxy, sol-gel, spray pyrolysis and other techniques are some examples. Sol-gel is the approach that is favored over the others [6]. Sol-gel spin coating [7] is a simpler and less economical practice of developing a layer on a glass substrate. During this technique, concentration, doping level, and uniformity may all be reasonably adapted.

The research is aimed at the structural, optical and electrical attributes of AZO thin films produced by spin coating as a function of width of thin film to analyze optimum width having the best attributes. This study is published at AIP Advances in 2018[18]

4.1.1.Growth of AZO

Zinc acetate dehydrate ($Zn(CH_3COO)_2.2H2O$) and aluminum nitrate nonahydrate ($Al(NO_3)_3.9H2O$) were liquefied in a solution of 2-Methoxy ethanol to make the AZO solution. Then there was the addition of monoethanolamine (MEA). Chemical precursors, dopant precursors, solvents, and stabilizers were employed as zinc acetate dehydrate ($Zn\ (CH3COO)_2.2H2O$), aluminum nitrate nonahydrate ($Al(NO_3)_3.9H_2O$), 2-Methoxy ethanol, and monoethanolamine. Monoethanolamine (MEA) has a molar ratio of 1 to zinc acetate. With regards to Zn, the concentration of Al as a dopant is 2 wt%, and the concentration of zinc acetate is 0.75 M. This fluid was agitated for 1 hour on a magnetic stirrer at 60-70^{0}C. For aging, the colorless and homogeneous AZO mixture was kept for 24 hours. A spin coater was used to deposit AZO coatings on the glass substrate. The SPS Spin 150 spin coater was used for the deposition process at 3000 rpm for 30 seconds. The AZO films were baked for 10 minutes at 300° C in the ED53 electric oven before being allowed to cool naturally for 10 minutes. Several layers of film were fabricated on the substrate to alter the thickness. The technique was repeated 5,10,15, and 20 times to generate different thicknesses which were labeled as L5, L10, L15, and L20. The resulting thin film samples were then annealed in the KLS 10/12 furnace for 1 hour at 500°C.

The consequence of modifying film width on the attributes of the films was explored in this work, with the doping concentration and annealing temperature remaining unchanged.

4.1.2. Results & Discussion:

The width of the produced AZO thin layer was estimated using a Bruker Dektak XT Stylus Profiler. The thickness of the L-5, L-10, L-15, and L-20 AZO samples was 296 mm, 585 nm, 895 nm and 1030nm correspondingly.

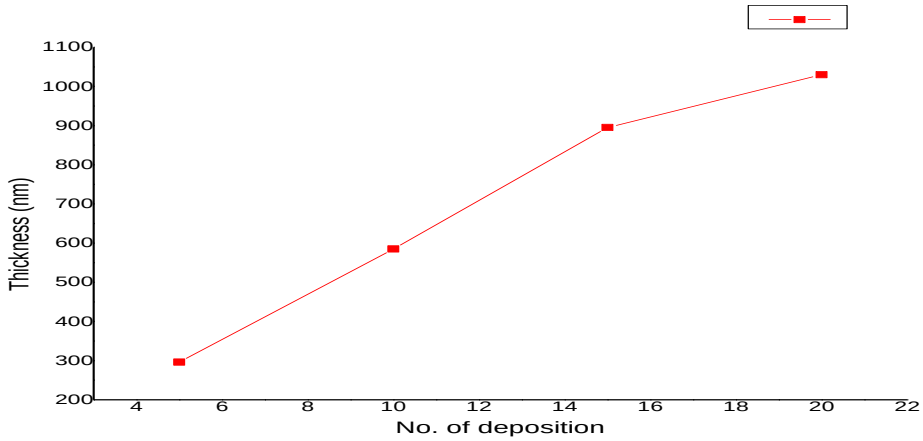

Fig.4.1.1. *Film width of sample L-5, L-10, L-15 and L-20 AZO thin film.*

The structural attributes of an AZO thin film were analyzed using a GBC EMMA 147 X-Ray diffractometer (XRD) with CuK radiation, λ= 0.154 nm, and the grain dimensions were examined in proportion to film width. The produced film's sheet resistance and conductivity were examined using the four-point probe method. A Hitachi UH4150 spectrometer was utilized to quantify the film's optical transmittance.

4.1.2.1. Structural characterization

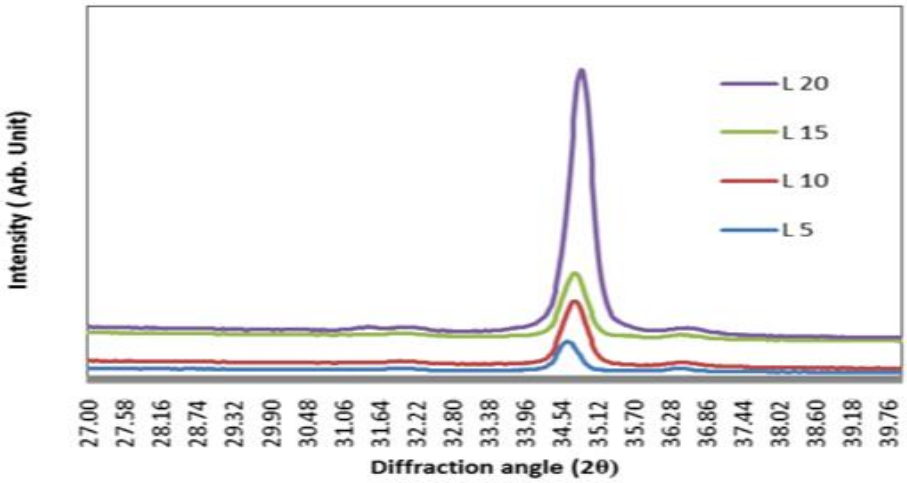

Fig.4.1.2. *XRD configuration for AZO thin film with various film width.*

The X-ray diffraction spectra for L-5 (296 nm), L-10 (585 nm), L-15(895 nm), and L-20 (1030 nm) Al:ZnO films is shown in Figure 4.1.2. The peak with a diffraction angle of 34.80, 34.820, 34.850, and 34.990 is provided by the L-5, L-10, L-15, and L-20 samples in this XRD spectrum, that meets card no ICDD-00-051-0037 for AZO. The (002) plane with a c-axis orientation is referred to the 2θ peak angle. It was discovered in a recent research study that when the AZO film is annealed below 500° C, there is no prominent diffraction peak. As a result, in this case, the AZO film was annealed at 500°C and a prominent diffraction peak was seen in the (002) plane in the c-axis orientation for AZO films.[1]

For L-5, L-10, L-15, and L-20 films, the value of diffraction angle 2θ upsurges faintly from 34.80 to 34.990 as film thickness increases. This occurs because the crystal grain's stress is reduced, resulting in a decrease in interplanar spacing [2][3][4].Grain boundary hypothesis [12] [13] states that, the film is made up of tiny crystallites during the early stages of film growth. Small crystallites can have a lot of stress. Tensile stress is produced when they consolidate, and the gap between them narrows until cohesion develops between the crystals as the film grows. With growing film width, the interaction between them becomes sufficiently robust to fill the break by elastic deformation of the film's crystallites, releasing stress.

For all four samples, two additional peaks were observed about 31.90 and 36.50, corresponding to the (100) and (101) planes, respectively. A peak shift occurs at 36.990 in the (101) plane for the L-10 sample. Peak shift might happen for a variety of causes, including strain involvement from planar stress, temperature, and XRD zero drift. For equally compressive and tensile stress, strain could be seen. Another cause of peak shift is zero error, which occurs when the sample is not standardized at the same location each time. Peak shift has happened for zero error if both the high and low angle peaks have been displaced by the equal quantity. Both the high and low angle peaks are displaced by the similarquantity in the L-10 sample. As a result, the shift can be stated to have happened here for zero error.

There is an supplementary peak for L-20 at a diffraction angle of roughly 30.990. The L-20 sample contains Al_2O_3, according to card number ICDD 00-002-1420. This could be induced by a little change in the oven's heating temperature or a lack of adhesion between the substrate and the liquid.

The FWHM (full width at half maximum) value of the L-5, L-10, and L-20 films were 0.42°, 0.40°, 0.39°, and 0.33°, respectively. The strain, ε is associated to FWHM as

$$\varepsilon = \frac{\beta cos\theta}{4} \text{.....4.1.1}$$

Here β is the FWHM in radian. Stress is directly proportional to FWHM, as depicted by Eq. 4.1.1. As the film width grows and the FWHM lowers, the tension on the film lowers as well. The influence on crystalline characteristics was not explored because the annealing temperature was constant for the L-5, L-10, L-15, and L-20 samples.

This FWHM is inversely related to grain size. The Scherrer formula can be employed to calculate grain size as[5]:

$$D = \frac{K\lambda}{\beta Cos\theta} \text{.....4.1.2}$$

Here k(=0.9) is a constant and D is grain size. λ, θ and β are respectively X-ray wavelength, Bragg angle in degree and full width at half maximum(FWHM) of the (002) plane in radian.

AZO thin film with a bigger grain size and a lower FWHM in the (002) plane have a more consistent c-axis orientation and better crystalline quality. The computed grain size of L-5, L-10, L-15, and L-20 AZO thin films is 19.59 nm, 20.82 nm, 21.38 nm, and 25.25 nm, correspondingly, based on the XRD spectrum. The value of FWHM decreases with increasing film thickness in these three Al:ZnO samples, grain size rises as well. This shows that the crystalline quality has improved [11] [14]. It can be assumed that as the film wdth upsurges, the structural properties of the film has been enhanced. The consequence of annealing temperature has not been investigated rather it has been left unchanged. When estimating grain size, imperfections are not taken into account. Due of technological issues, the SEM picture is not produced.

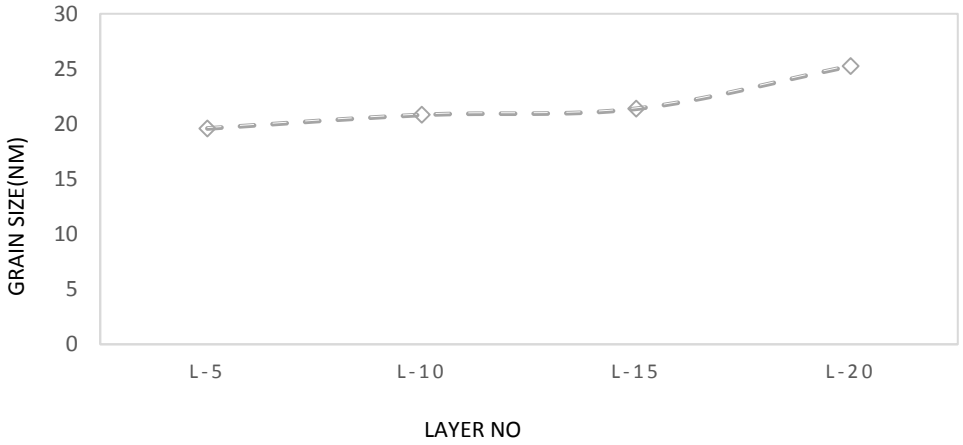

Fig.4.1.3. *Grain size(D) of Al-ZnO film with various film width.*

4.1.2.2. Electrical characterization

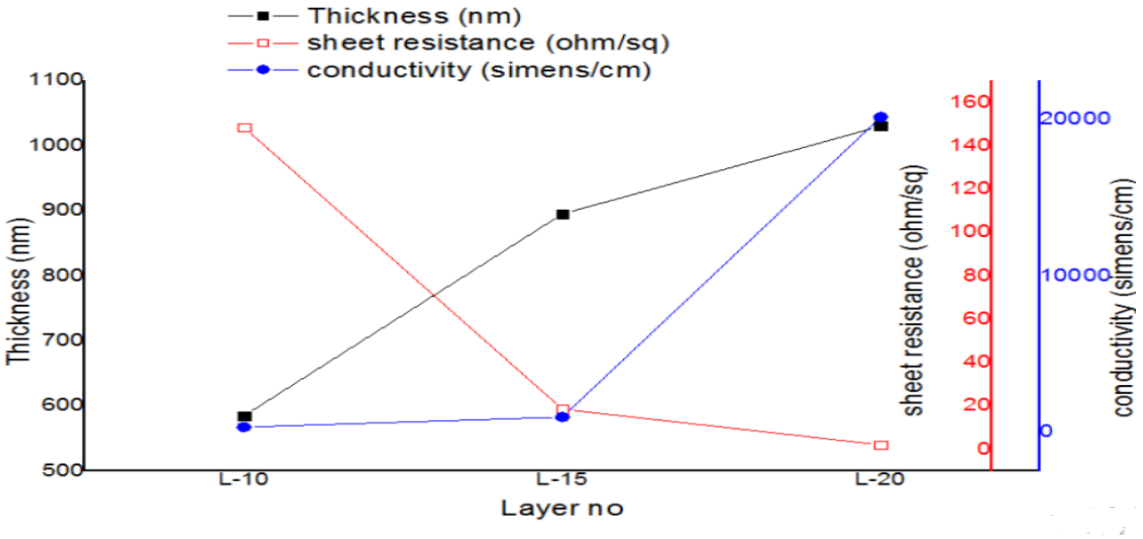

Fig.4.1.4. *Sheet resistance(R_{sh}) and conductivity(σ) of Al-ZnO with diverse film width.*

The sheet resistance and conductivity of the L-5 are correspondingly606300 (ohms/sq.) and 2.34 (Siemens/cm). Fig.4.1.4 shows that the conductivity of L-10(585 nm), L-15(895 nm), and L-20(1030 nm) AZO thin films was 315.05 (Siemens/cm), 961.50 (Siemens/cm), and 20156.27 (Siemens/cm), respectively, with sheet resistance decreasing to 148.43 (ohm/sq.), 18.58

(ohm/sq.), and 2.08 (ohm/sq.). This means that the sample with the highest thickness is more conductive than the others among these Al doped ZnO samples. The resistivity of four-point probe data is estimated as below [6]:

$$\rho = R_{sh}t \text{.....4.1.3}$$

$$\text{Again } \rho = \frac{\pi tVF}{\ln(2)I} \text{.....4.1.4}$$

ρ is resistivity (Ω-cm), R_{sh} is the sheet resistance (Ω/sq.), t is the film width, V is the voltage, I is current, F is the correction factor. Sheet resistance has a counter relationship with film width, according to Eq.4.1.3, providing all other factors remain constant. Sheet resistance is reduced as film thickness increases. This is depicted in Fig.4.1.4 where L-20(1030 nm) AZO film had the lowest sheet resistance of 2.08 (ohm/sq.) and maximum conductivity of 20156.27 (Siemens/cm) than the others.

For a given sample, resistivity is constant since the thickness and sheet resistance are both constant. The resistivity fluctuates along with the sheet resistivity in this investigation as the thickness is altered. Specific conductance is well-distinct as

$$k = 1/\rho \text{.....4.1.5}$$

From Eq.4.1.3 and Eq.4.1.5

$$k = 1/R_{sh}t \text{ .....4.1.6}$$

In this situation, the sheet resistance of an AZO film reduces drastically as its thickness increases. As a result, the conductivity of AZO film rises.

4.1.2.3. Optical characterization

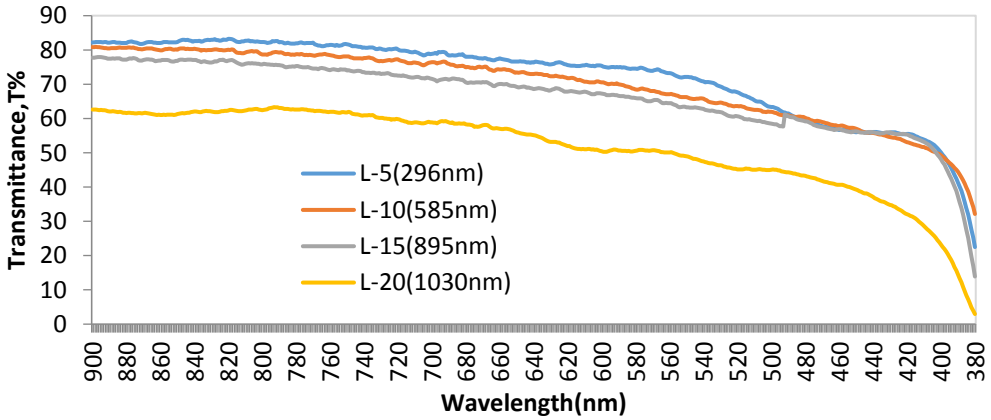

Fig.4.1.5. *Optical transmittance spectra of Al doped ZnO thin film with diverse film width.*

The sample L-5 showed a extreme transmittance of around 82 % between 900 nm and 770 nm wavelengths, according to Fig.4.1.5. The transmittance steadily declines below 770 nm wavelength, reaching 70% at 533 nm. From 500 to 380 nm, the transmittance is relatively low. Between 900 nm to 533 nm, L-5 has a high average transmittance of 78%, covering a significant portion of the visible spectrum.

The greatest transmittance of the sample L-10 was recorded between 900 nm and 861 nm wavelength, that is somewhat lesser compared to that of L-5. In addition, when compared to the L-5, the transmittance of L-10 drops quicker as the wavelength lowers. The transmittance is less than 70% below 596 nm, whereas L-5's transmittance is less than 70% for wavelengths beneath 533 nm. Between 900 and 590 nm, the regular transmittance is 76 %, and between 900 and 533 nm, it is 75.41%. The transmittance decreases below 590 nm, reaching as small as 32% at 380 nm.

The greatest transmittance for the L-15 is 77 % between 900 and 818 nm. The transmittance decreases more quickly below 818 nm wavelength than in the other two samples. Between 900 and 659 nm, the average transmittance is 74.6%. In comparison to earlier samples, the L-20 sample showed a low transmittance. At 900 nm, it has a maximum transmittance of 62%, which is not ideal. As a consequence of the optical results, regardless of the width of the samples, the transmittance decreases with decreasing wavelength. The spectrum with desired transmittance is higher for samples with reduced thickness. Transmittance decreases as the thickness of the material increases.

It has been observed in various prior research work on AZO thin films that this AZO film possesses optical transmittance near or above 80% [9] [15]. In this case, it's equivalent to the transmittance spectra of the Al:ZnO films.

Optical transmittance can be communicated as [7, 8]:

$$T = \frac{I}{I_0} = e^{-\alpha t} \text{.....4.1.6}$$

where I_o is incident light on film, I is the light leave-taking from the opposite side of the film. The ratio of these two light is optical transmittance, T and t is the film width and α is absorption coefficient. Optical transmittance has a converse relationship with film width, according to this equation. As the thickness of the film expands, more light is absorbed, and optical transmittance reduces. This variation can be seen in the transmittance curve above. The thinner film, L-5, exhibited the maximum average transmittance of 82 % among all these samples.

Table 4.1.1. *Figure of merit for AZO thin film*.

Sample no.	Film thickness (nm)	Sheet resistance (ohm/sq.) R_{sh}	Transmittance T%	Figure of merit φ_{tc} (Ω^{-1})
L-5	296	606300	72.12	6.27*10^-8
L-10	585	148.43	66.23	1.09*10^-4
L-15	895	18.58	63.23	5.49*10^-4
L-20	1030	2.08	48.99	3.82*10^-4

4.1.2.4. Performance assessment

As a TCO material, Al doped Zinc Oxide (AZO) necessitates a thickness that affords both good electrical and optical behavior. An essential measure termedas the figure of merit is utilized to appraise the enactment of TCO compound [7][9]:

$$\varphi_{tc} = \frac{T^{10}}{R_{sh}} \text{.....4.1.7}$$

Where $\varphi_{tc}$is the figure of merit and it demonstrate the best AZO which offers better optical and electrical attributes for a precise film width. T is optical transmittance at 550 nm and R_{sh} is the sheet resistance.

Table 4.1.1 demonstrates that the figure of merit for L-15 AZO film was the highest, φ_{tc}. A sample with a higher figure of merit value, φ_{tc}, might be deemed a good TCO material. As a result, the L-15 AZO thin film outperforms the other three in terms of optical and electrical qualities.

4.1.3. Remarks

Merits:

- The structural characteristics of AZO films enhance as the film thickness increases.
- L-20 AZO film own the maximum conductivity of 20156.27 Siemens/cm.
- In order to have appropriate optical and electrical attributes as a TCO material, the film thickness must be optimal. Among the four AZO thin film samples developed, L-15 (895 nm thick) has the best conductivity and optical transmittance. As a result, the film thickness for AZO thin film as an effective TCO material should be in the range of 895 nm.

Limitations:

- The Al doped ZnO thin films that weredeveloped has a robust electrical conductivity and an excellent optical transmittance in the observable wavelength range.
- The conductivity of this AZO film grows as the film widthupsurges, but the optical transmittance diminishes.
- Although the L-20 AZO film own the maximum conductivity of 20156.27 Siemens/cm, its optical transmittance was only about 65%, which was insufficient.
- It's harder to manage a steady temperature in the electric oven while heating the fabricated film inside an oven.
- Raman spectroscopy could not be performed because of the unavailability of the instrument which could confirm the phase purity of AZO thin films.

To do next

Another deposition technique i.e. sol gel dip coating may be tried to achieve

i. Better coverage of the film to ensure better transmittance.
ii. Better electrical property.

Reference:

[1] P.L. Gareso, N. Rauf, E. Juarlin, Sugianto and A. Maddu, "Characterization of nanocrystalline ZnO:Al films by sol-gel spin coating method," *Journal of Applied Physics*, vol. 1617, no. 1, 2014.

[2] F. Wang, M.Z. Wu , Y.Y. Wang , Y.M. Yu, X.M. Wu, L.J. Zhugeb, "Influence of thickness and annealing temperature on the electrical, optical and structural properties of AZO thin films," *Vaccum*, vol. 89, pp. 127-131, 2013.

[3] Dong BZ, Fang GJ., "Effect of thickness on structural, electrical, and optical properties of ZnO:Al films deposited by pulsed laser deposition," *Journal of Applied Physics*, vol. 101, no. 3, 2007.

[4] F. A. Garcesa*, N. Budiniaa, R. D. Arceab, J. A. Schmidtab,, "Thickness dependence of crystalline structure of Al-doped ZnO thin films deposited by spray pyrolysis," *Procedia Materials Science*, vol. 9, p. 221 – 229, 2015.

[5] Young-Sung Kim, Weon-Pil Tai, "Electrical and optical properties of Al-doped ZnO thin films by sol–gel process," *Applied Surface Science*, vol. 253, no. 11, p. 4911–4916, 2007.

[6] V.I. Kondratiev, I. Kink, A.E. Romanov, "LOW TEMPERATURE SOL-GEL TECHNIQUE FOR PROCESSING AL-DOPED ZINC OXIDE FILM S," *Materials Physics and Mechanics*, vol. 17, p. 38–46, 2013.

[7] G. Haacke, "New figure of merit for transparent conductors," *Journal of Applied Physics*, vol. 47, no. 9, pp. 4086-4089, 1976.

[8] Islam MM, Ishizuka S, Yamada A, Matsubara K, Niki S, Sakurai T, "Thickness study of Al:ZnO film for application as a window layer in Cu(In1-xGax)Se2 thin film solar cell," *Applied Surface Science*, vol. 257, pp. 4026-4030, 2011.

[9] A R Babar, P R Deshamukh, R J Deokate, D Haranath, C H Bhosale, "Gallium doping in transparent conductive ZnO thin films prepared by chemical spray pyrolysis," *Journal of Physics D:Applied Physics*, vol. 41, no. 13, 2008.

[10] F. Wang, M. Wu, Y. Wang, Y. Yu, X. Wu and L. Zhuge, "influence of thicness and annealinf temperature on the electrical, optical and structural properties of AZO thin films," *Vaccum*, vol. 89, pp. 127-131, 2013.

[11] G. Gordillo, C. Calderon, "Properties of ZnO thin films prepared by reactive evaporation," *Solar Energy Materials and Solar Cells*, vol. 69, no. 3, p. 251–260, 2001.

[12] P. Nunes, D. Costa, E. Fortunato, R. Martins, "Performances presented by zinc oxide thin films deposited by R.F. magnetron sputtering," *Vacuum*, vol. 64, p. 293–297, 2000.

[13] E. Fortunato, D. Ginley, H. Hosono, D. C. Paine, "Transparent Conducting Oxides for Photovoltaics," *MRS Bulletin*, vol. 32, no. 3, p. 242–247, 2007.

[14] Bayraktaroglu B, Leedy K, Bedford R., "High temperature stability of post growth annealed transparent and conductive ZnO:Al films," *Applied Physics Letter*, vol. 93, no. 2, 2008.

[15] H. Liu, V. Avrutin, N. Izyumskaya, Ü. Özgür, H. Morkoç, "Transparent conducting oxides for electrode applications in light emitting and absorbing devices," *Superlattices and Microstructures*, vol. 48, no. 5, p. 458–484, 2010.

[16] Gil Mo Nam and Myoung Seok Kwon, "Al-doped ZnO via Sol-Gel Spin-coating as a Transparent Conducting Thin Film," *Journal of Information Display*, vol. 10, no. 1, 2009.

[17] R. Hoffman, Phys Thin Flms, vol. 3, 1968, p. 211.

[18] R. Hoffman, Phys Thin Films, vol. 34, 1976, p. 185.

4.2. Al doped ZnO (AZO) by sol-gel dip coating technique with thickness variance

See-through Conductive Oxide (TCO) is a thin film material of prime importance due to its wide range of bids starting from electronics, smart windows for energy efficient buildings, and the window layer of the solar cells [1]. Different materials can be used as transparent conductive oxide for different purposes mentioned above. However, transparency and conductivity are two contradicting properties rendering the development of effective material for TCO a difficult challenge. The trade-off between these two properties becomes more impeding when it comes to the application as the window material of the solar cell high transparency is needed for effective transmission of the photon to the base absorber layer and good conductivity is required for collecting the photo-generated carriers at the front contact. It is normally expected that a TCO film will have a bandgap of more than 3eV and high mobility of carriers and lower sheet resistance. A high optical bandgap ensures high transmittance but It will have an impact on electrical characteristics. The mobility of the carriers should be around 100 cm2V-1s-1. If the mobility is much higher then resistance will increase and this will lower the solar cell performance creating a shunt path reducing fill factor and open circuit voltage [2] . Tin (II) oxide (SnO) is one of the first materials to be used as the window layer for thin film photovoltaic cells [3]. Tin oxide possesses a wide band gap energy of 3.5 eV, a high value of transmittance in the visible spectrum [4] and a n- type conductivity due to the oxygen deficiency in the crystal structure. Tin-oxide itself has a low electrical resistance. However, the electrical property can be increased further by doping it with certain dopants like fluorine which is termed as fluorine doped tin oxide or FTO[5]. FTO is also utilized as a window layer of the layer [6] because it provides high transmittance in the visible spectrum but lower electrical resistance. Higher doping condition supports these properties as the fluorine dopant occupy the tin sites and together with oxygen deficiency they provide good electrical properties [7] . Doping SnO with Indium creating Indium Doped Tin Oxide or (ITO) improves the electrical property to great extent [8].

FTO and ITO could both be utilized as a window layer in thin film photovoltaic cells and have been shown to be efficient. But ITO uses Indium which is expensive but also extensively used in the electronic industry for flat plate displays.

Recent researches have focused on using zinc oxide as the TCO material and it has shown good performance in PV cell applications. The electrical property like resistance and mobility of Zinc Oxide can be improved dramatically by doping it with aluminum [9] [10] . AZO is a suitable replacement for ITO or FTO because it shows lower resistivity than ITO, indium is very rare on earth and expensive as well [11]. AZO uses low cost, non-toxic earth abundant material and is the best replacement for ITO or FTO to be employed as the window layer of the photovoltaic cell [12] [13].

Various processes have been used to deposit un-doped and doped zinc oxides such as chemical vapor deposition, RF and DC magnetron deposition [14], plasma deposition [15], pulsed laser evaporation [16] and metal organic chemical vapor deposition (MOCVD) [17], spray pyrolysis [18] and sol-gel process [19]. While these processes have been effectively used to deposit un doped and doped zinc oxides but processes like chemical vapor deposition needs high temperature [20], pulsed laser deposition needs high vacuum condition, and precise and complex instruments [21]. Thus all of these processes are rather expensive and toilsome. Aluminum doped zinc oxide has been fabricated by sol-gel dip coating technique because it

avoids most of the complicated setup conditions mentioned above. The process has the advantage of providing good adhesion to the substrate, uniform homogeneity, temperature below 1000 C for deposition and preparation of the precursor solution and ability to be deposited over a large area [22]. This study is published at Materials Focus in 2018 [38].

4.2.1. Growth of AZO

Zinc Acetate (CH3COO)2Zn.2H2O and Aluminum Nitrate Al(NO3)3.9H2O were used as a component precursor and dopant precursor to formulate 2% wt. Zn .075 M AZO solution. 2-Methoxy Ethanol is working as a solvent and Mono Ethanolamine(MEA) as a stabilizer. 45.91 g 2-Methoxy Ethanol was stirred with 8.065 g. of Zinc Acetate and 1.465 g. of Aluminum Nitrate in a magnetic stirrer for 1 hour at 600 -700 C. 5.65 gm of MEA was added at the beginning of stirring to stabilize the solution. The molar ratio of Zn: MEA is preserved as 1. The solution is maintained at ambient temperature under suitable conditions for 24 hours for aging.

Previous research done on AZO deposited by dip coating yielded 1%. wt. of Al to Zn with the highest transmittance and lowest resistivity. However, the crystal structure for 2% wt. concentration showed better grain size and improved stability [23]. Other studies have varied doping concentration up to 5%. wt but the transmittance reduced too much and electrical resistivity increased main fold [24]. Considering these the doping concentration was maintained at 2%. wt. and molar ration of Zn: MEA was maintained at 1.

Soda lime glass slides each having a dimension of 2.5 cm ^{x} 5 cm was used as substrates. Substrates washed with deionized water were scrubbed inside an ultrasonic bath in methanol for 10 minutes, in ethanol, and then again in methanol for 10 minutes, and finally in distilled water for 10 minutes. AZO was deposited by dip coating with a withdrawal speed of 150 mm/min and by varying the number of times the substrates were dipped, the thickness of the samples could be altered. Samples were dipped in solution 5, 10, 15, and 20 times and were marked L-5, L-10, L-15, and L-20 respectively

AZO films were post-baked at 3000 C in an electric oven ED53 for 10 minutes each time it was dipped to drive any extra solution off the surface. A minimum of 10 minutes was given for the samples to be cooled down before depositing the next layer. The prepared AZO films are annealed at 5000 C in the air inside an arch furnace KLS10/12 to permanently form the crystal structure.

4.2.3. Result and Discussion

The samples are characterized based on their thickness for their electrical, optical, and structural properties. The results conformed with previous works done on AZO. The film width is estimated by using a Diamond Tip surface Profilometer DextaXT Bruker. Optical transmittance is characterised by UV- Vis UH Hitachi spectrometer in transmittance mood. A four-point probe measurement techniques and an HT55T3 Hall effect measurement instrument are used to determine electrical attributes. The sheet resistance, conductivity are calculated by four point probe measurement process [25] and the mobility of carriers in the sample is given by the Hall Effect meter [26] . The XRD of the samples was also done using an GBC EMMA spectrometer.

The width of the samples is varied and the properties obtained from the characterization are thus in relation to the width of the film. A surface profilometer was employed to quantify the

thickness of the samples. Fig.4.2.1 shows the thickness of L-5, L-10, L-15, and L-20 thin film samples.

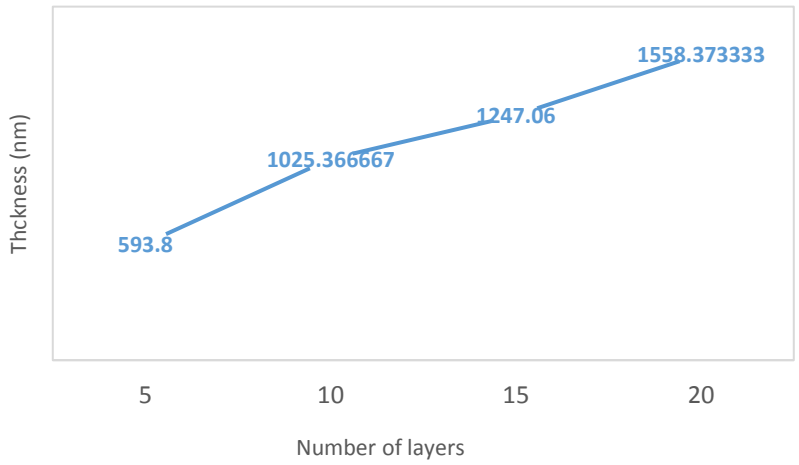

***Fig.4.2.1**. Film thickness with the number of deposited layers.*

The stylus profilometer measures thickness along the width of the sample. To determine the uniformity in thickness the film width is estimated at three points. The average thickness from the L-5 sample to the L-10-layer sample increases by 431.567 nm. Between the L-10 and L-15 samples, there is a 221.693 nm difference in thickness. L-15 and L-20 layered samples show the least difference of 244.533 nm difference in thickness.

4.2.3.1. Optical Characterization

The films annealed at 500 o c were measured for their transmittance between the wavelength of 1200 nm to 223.79 nm with alternating steps of 0.44 nm and 0.4467 nm. Figure 4.2.2 shows the plot of transmittance sample vs wavelength. L-5 sample shows a high value of transmittance of about 79.06 at 910 nm. The transmittance increases slightly after as wavelength is reduced from 910 nm. Transmittance increases from 79.06% at 910 nm to 84% at approximately 587 nm. This makes it suitable to transmit light in the upper part of the visible spectrum between 500 nm to 900 nm. Below 587 nm the transmittance reduces by a small margin. Transmittance is about 83.93% to 59.47% as the wavelength reduces from 586.88 nm to 400 nm. So this layer is suitable to transmit light between wavelength 900 nm to 600 nm. The transmittance for the L-10 sample shows a high transmittance of 73.95%. The transmittance increases gradually from wavelength reduces from 910 nm and becomes a maximum of 79% for a wavelength of 574 nm. After that, the transmittance reduces gradually. Between 910 nm to 400 nm the average transmittance is about 74.90%. For the L-15 sample at the wave length of 910 nm, the transmittance is about 75.43 %. The transmittance does not increase from this point and reduces to a low value of 25.99% at 400 nm wavelength. The average transmittance between 910 nm and 400 nm is about 60.05 %. Previous results on AZO showed that post-heating temperature does not show any primary consequence on the absorption spectra of the samples for a variety of temperatures [27][28]. However, if the temperature is reduced to a lower annealing temperature then the transmittance improves significantly and about 80-90% transmittance is obtained for films deposited between 400 to 5000 C [29]. However, the transmittance is more closely linked to the doping concertation as given by previous works lower doping concentration gives higher transmittance of 90 % at around 400 nm. In this study, the doping concentration was maintained at 2%. wt. of Al to Zn. This gave a transmittance of 83% for the L-5- sample and around 79% for the L-10 sample. This result is consistent with previous findings only the highest transmittance is obtained at

around 570 nm for both samples. As the annealing temperature was 5000 C, compared with previous results it can be inferred that higher annealing temperature shifts the transmittance spectra at higher transmittance [29]. The transmittance of the samples reduces with increasing thickness as given by the study and previous results. However, by comparison, it can be said that by keeping lower doping concentration of 0.5% to 1% wt. Al and lower post annealing temperature the transmittance can be still maintained well over 80% [24].

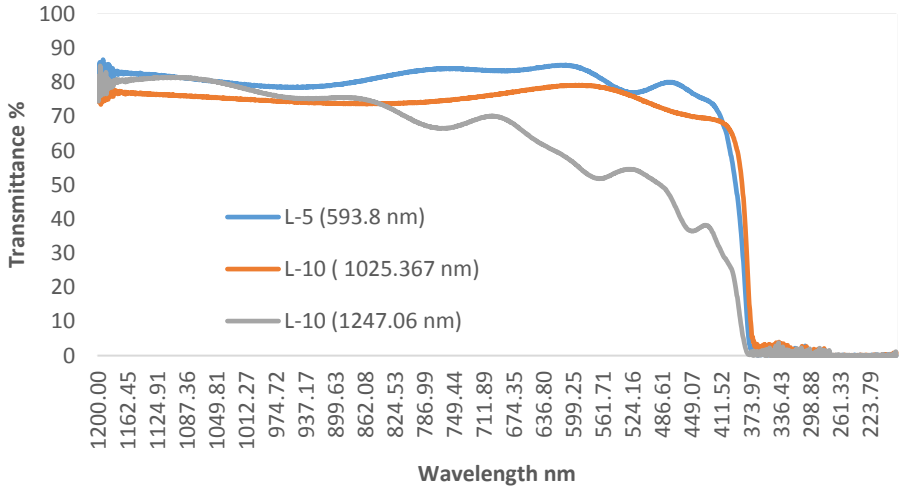

Fig.4.2.2*. plot of Transmittance Vs. Wavelength for L-5, L-10 and L-15 layered film.*

4.2.3.2. Electrical Characterization

Electrical characterization of the samples is done by utilizing a four-point probe measurement technique and the Hall effect measurement unit. Resistance, sheet resistance, and volume resistance decrease with increasing thickness of the samples. For L-5 sample having deposited film of a mean thickness of 593.8 nm has the highest mean resistance of 4.45e2 Ω. Resistance for the L-10 sample is 3.49e2 Ω reducing slightly from the L-5 sample. However, the value of resistance for L- 15 to 1.22e1 Ω is a drastic change as compared to the previous two samples.

Fig.4.2.3 displays the disparity of sheet resistance, conductivity, and mobility of carriers for the samples. Sheet resistance follows a similar pattern as that of resistance with a high value of 2.26e3 Ω -2 for L-5 sample, 1.48e3 Ω -2 for L-10 sample, and 5.18e1 Ω -2 for L-15 sample. The volume resistance changes from 1.15e-1 Ω/cm to 6.47e-3 Ω/cm from L-5 sample to L-15 sample. The reduced sheet resistance can be ascribed to the fact that it reduces with the growth in the AZO film width given by the following equation [30]

$$\rho_s = \frac{1}{q\mu_e N_D t} \text{.....4.2.1}$$

The mobility of carriers in the samples decreases as the film width rises. The effect of reduced mobility is offset by increases in the conductivity. The sheet concentration of the samples also improves and it is more than the decrease in mobility. As a result, overall the sheet resistance reduces following Eq.4.2.1. The conductivity of the samples increased with increasing thickness having values of 1.14e1 siemens/cm, 6.62 siemens/cm, and 1.55e2 siemens/cm for samples L-5 (593.8 nm), L-10 (1025.367 nm), and L-15 (1247.06 nm) respectively. The sheet resistance is related to the post heating temperature and doping concentration. Previous results show that increased annealing temperature to a certain extent reduces the sheet resistance and

Table 4.2.2. *Electrical attributes of AZO thin films.*

Sample no	Thickness (nm)	Resistance (Ω)	Volume Resistance (Ω/cm)	Conductivity (siemens/cm)	Mobility (cm2/V.s)	Sheet Concern-traction (/cm2)
L-5	593.8	4.55e2	1.15e-1	5.51	4.49e4	6.83e5
L-10	1025.367	3.49e2	1.03e-1	6.62	1.73e2	5.56e8
L-15	1247.06	1.22e1	6.47e-3	1.55e2	2.96e0	1.58e11

hence improves the film quality. A single-layered sample annealed at 650 °C shows sheet resistance of around 2-2.5 e3 ohm $^{-2}$ [27] . This is much higher than an L-10 sample annealed at 5000 C with a doping concentration of 2% as obtained from this study.

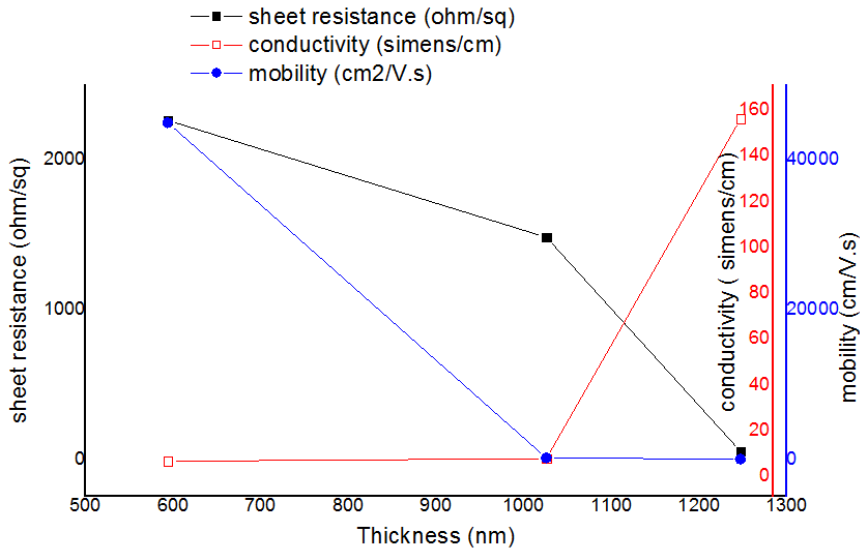

Fig.4.2.3. *Deviation in Conductivity, Sheet Resistance and, mobility of carries of the sample.*

A sheet resistivity of 1.87 e5Ω^{-2} for an L-20- sample annealed at 5000 C was obtained in a study conducted at Chang Gung University Taiwan [29]. This is much higher than the results obtained for even the samples of the lowest thickness which may be attributed to that as chemical precursor used in this research is different and also the pre-heating temperature was much lower. Lower pre-heating temperature is preferred for good electrical properties.

The mobility of the carriers of the sample reduces by four orders as the thickness increases with the L-5 sample having high mobility of 4.4195 e4 cm2/V.s. Mobility reduces to only 2.98 cm2/V. s for L-15 sample which is too low and such low mobility of carriers is likely to reduce the performance if performance in a solar cell is considered while L-10 sample has preferred mobility of 173.6 cm2/V.s.

4.2.3.4. Structural Characterization

Fig. 4.2.4 depicts the XRD pattern against the degree of the crystallographic plane of L-5, L-10, L-15 film revealing a peak roughness at 34.560 which refers to (002) crystallographic plane matching with card no ICDD-00-051-0037 [22]. It refers to crystalline wurtzite structure and a preferable c- axis orientation. There are also two minor peaks at 2θ of 320 and 360 indicating (100) and (101) planes respectively. Also, no peaks for Aluminum oxide are observed at (200) and (220) planes indicating the doping of aluminum did not create any oxide participation, and the aluminum dopant occupied interstitial space between the zinc oxide crystal[31].

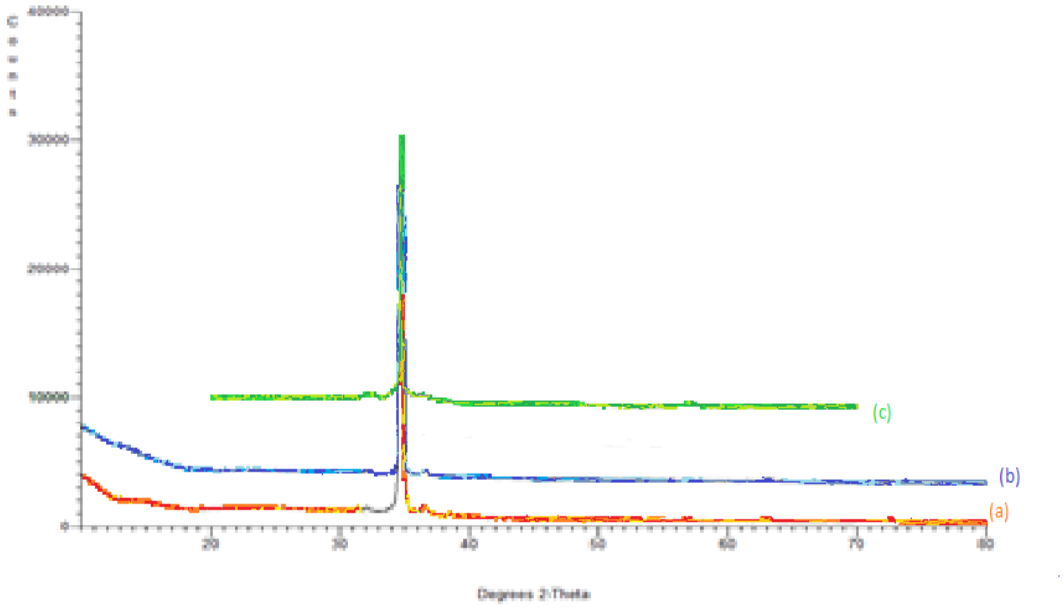

Fig. 4.2.4. *XRD configuration of AZO film of three different film width (a)L-5 (593.6 nm) (b) L-10 (1025.367 nm) (c)L-15 (1247.06 nm).*

From the XRD spectrum revealed in Fig.4.2.5, it is also evident that the full width half maximum decreases with increasing thickness of the doped aluminum zinc oxide sample. The 2θ of for the samples for the peak intensity increases from 34.560 to 34.60 which is very small and such a small variation in the angle of the peak intensity is preferable. This increase in film intensity is caused inter planer stress which reduces with increasing thickness. Initially, films are composed of small crystals and they gradually coalescence is developed between the crystals to form a uniform layer of the material. So at an initial stage, the stress is quite high and the L-5 sample as was dipped for only 5 times had lesser material to form effective coalescence and eventually higher stress due to a larger gap between the molecules. As the thickness increased in L-10 and L-15 samples more materials were present to allow effective coalescence and as result stress was reduced [32].

The FWHM shrinkages with growing film width showing that the structural possessions of the samples upgraded as the thickness enlarged. This is caused due to reduced stress on the crystal and improvement of the grain size as depicted by earlier results[33] [34]. FWHM can be related to stress using the following equation

$$\varepsilon = \frac{\beta cos\theta}{4} \quad \text{.....4.2.2}$$

Here β is the FWHM in radian and θ is the angle of the diffraction peak in degree. From Eq 4.2.2 it can be inferred that stress is released as FWHM increases and FWHM upsurges with growing film width.

FWHM is in reverse proportional to the grain size so reduced FWHM means increased grain size and hence improved crystal structure. For the three samples, the FWHM is 0.580, 0.520, and 0.480 for the L-5, L-10, and L-15 samples respectively. The reduced FWHM indicates good structural property and larger grain size as the film width enlarged.

The particle size is not affected much as the thickness is increased which can be depicted by Debey- Scherrer formula [35]. In calculating the grain size, the effect of various defects was not considered because the SEM images of the sample could not be obtained due to technical difficulties.

$$D = \frac{k\lambda}{BCos\theta} \ldots\ldots\ldots\ldots\ldots\ldots\ldots\ldots\ldots\ldots 4.2.3$$

Where λ is the X-ray wavelength, θ is Bragg Angle K is a fixed number .9 and B is the FWHM. λ is taken to be 0.15418 nm as the x-ray source is Cu-k –alpha.

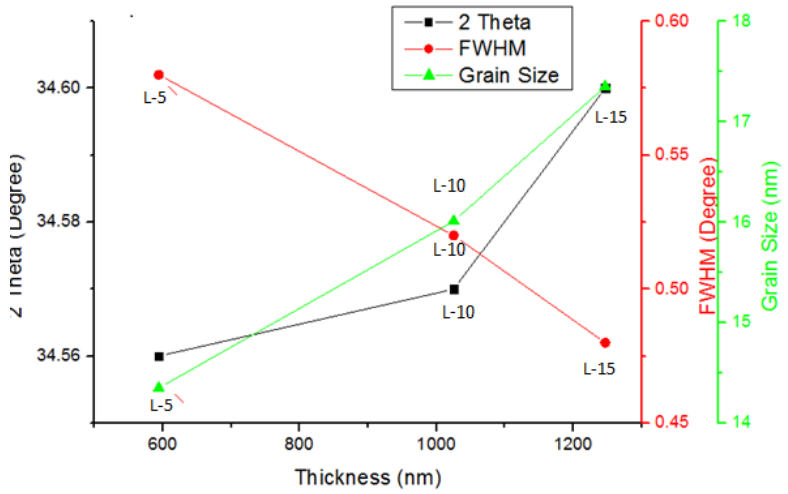

Fig.4.2.5*. Variation of Diffraction angle, FWHM and Grain size of the Samples with thickness.*

The grain dimension of the samples improved with growing film width. L-5 (593.6 nm) films had a grain size of 14.35 nm, L-10 (1025.367 nm) films had a grain size of 16.01 nm and L-15 (1247.06 nm) films had a grain dimension of 17.35 nm. The grain dimension is contrariwise proportionate to the FWHM and as the FWHM upsurges with thickness, the grain dimension improves. So larger grain dimension is preferred as the stress of the films is abridged with it [36].

The annealing temperature has also a consequence on the crystalline properties of the film. As depicted by previous studies at a lower annealing temperature of 400 0 c the peak is not distinct at the (002) plane and the (100) and (101) plane peak is completely absent and 5000 c shows all the three distinctive peaks [29]. A higher annealing temperature than 5000 improves the peak intensity linearly for all the diffraction angles [27].

4.2.3.5. Evaluation of AZO as a transparent conductive oxide

One of the effective ways to categorize TCO based on their contradicting qualities is employing a figure of merit with the obtained data. A figure of merit is the measure of the ratio between the average transmittance and sheet resistance of the thin film, that is combining both electrical and optical properties. Since transmittance reduces with increasing film thickness while the electrical property improves a tradeoff needs to is considered based on film thickness which is given by the proposed figure of merit given by the following equation [37].

$$\sigma Tc = \sigma t \exp(-10\ \alpha t) \ldots\ldots\ldots\ldots 4.2.4$$

where α is the average absorption coefficient within the spectrum of 900 nm to 400 nm and σ is the average conductivity and t is the thickness. The corresponding figure of merit for all the films are listed in Table.4.2.2. The absorption coefficient can be considered as the contrary of the average transmittance.

Table 4.2.2. *Figure of merit for the samples depending on transmittance and conductivity*

No of layers	Thickness (nm)	Average Transmittance (%)	Average Absorption co-efficient	Conductivity (Siemens/cm)	The proposed figure of merit Ω-1
L-5	593.8	84	11.90e-3	1.41e1	8.37e-6
L10	1025.367	79	12.65e-3	6.62	6.78e-6
L-15	1247.06	75.43	13.25e-3	1.55e2	193e-6

From the table, it can be inferred that the L-5- sample gives a reasonably high quantity of the figure of merit and for the L10 sample it reduces. A figure of merit greatly increases for the L-15 sample and it is very much preferable property for a TCO.

4.2.3. Remarks

Merits

- The deposited samples exposed better bond to the SLG and good electrical and optical properties.
- L-15 sample had the highest value of conductivity of 1.55e2 siemens/cm.
- L-5 sample had high optical transmittance of 84% in the observable spectrum.
- It is observed L-10 sample with a thickness of 1025.367 nm had good conductivity of 6.62 siemens /cm and transmittance of 74.90% on average between the visible spectrum. So it can be suitably used as a TCO.

Limitations

- L-15 sample had the highest value of conductivity of 1.55e2 siemens/cm. but poor transmittance 65% within the visible spectrum of 400 nm 900 nm.

- L-5 sample had high optical transmittance of 84% in the observable spectrum but a lower value of conductance.
- The dip coater relies on manual operation. The digital microelectronic based operation can reduce human error and give better results.
- Raman spectroscopy could not be performed because of the unavailability of the instrument which could confirm the phase purity of AZO thin films

To do next

- For future studies, different chemical precursors can be studied to find the consequence on the quality of the films by sol gel spin coating as this process shows better coverage. The annealing environment (preferably N_2) can also be varied to discover its influence on the excellence of the fabricated film.
- In this study deionized water was not used to clean the substrates. Using deionized water can improve the film quality as given by the XRD and its effect on the other properties on the film can also be evaluated. The temperature of the oven during post baking could not be controlled accurately.
- More accurate temperature control can ensure a better result.

References

[1] Z. Q. Xu, H. Deng, Y. Li, Q. H. Guo, and Y. R. Li, "Characteristics of Al-doped c-axis orientation ZnO thin films prepared by the sol–gel method," *Materials Research Bulletin*, 41, 2, 354-358, 2006.

[2] H. Liu, V. Avrutin, N. Izyumskaya, U. Özgür, and H. Morkoç," Transparent conducting oxides for electrode applications in light emitting and absorbing devices,"*Superlattices and Microstructures*, 48, 5, 458-484, 2010.

[3] M. Mohammad, M. Bagheri, and S.-S. Mehrdad, "The electrical, optical, structural, and thermoelectrical characterization of n- and p-type cobalt-doped SnO2 transparent semiconducting films prepared by spray pyrolysis technique,"*Physica B: Condensed Matter*, 405, 19, 4205-4210, 2010.

[4] B. Saturi, C. Abdullah and F. M. Yassin,|"Study on Optical Properties of Tin,"*Journal of Science and Technology*, 4, 1, 2008.

[5] Z. Hu, J. Zhang, Z. Hao, Q. Hao, X. Geng and Y. Zhao,"Highly efficienct organic photovoltaic devices uding F-Doped SnO2 anodes,"*Applied Physics Letters*,98, 11, 123305, 2011.

[6] C.-Y. Kim and D.-H. Riu," Texture control of fluorine-doped tin oxide thin film;In (*Thin Solid Films*, 591, no. 10, pp. 3081-3085, 2011.

[7] K. Subba Ramaiah and V. Sundara Raja,"Structural and Electrical Properties of Fluorine doped tin oxide films prepared by spray-pyrolysis technique," *Applied Surface Science* 253, pp. 1451-1458, 2006.

[8] B. N. joshi, H. Yoon and S. S. Yoon,"Structural, optical and electrical properties of tin oxide thin films by electrostatic," *Journal of Electrostatics* vol.17, pp. 48-52, 2013.

[9] D.-J. Lee, H.-M. Kim, J.-Y. Kwon, H. Choi, S.-H. Kim and K.-B. Kim,"Structural and Electrical Properties of Atomic Layer Deposited Al-Doped ZnO Films,"*Journal of Advanced functional Materials*, 21, 3, 448-455, 2010.

[10] G. Luka, L. Wachnicki, B. Witkowski, T. Krajewski, R. .Jakiela, E. Guziewicz and M. Godlewski,"The uniformity of Al distribution in aluminum-doped zinc oxide films grown by atomic layer deposition,"*Matrial Science and Engineering*, 176, 3, 237-241, 2011.

[11] J. Hüpkes, B. Rech, B. Calnan, O. Kluth, U. Zastrow, H. Siekmann and M. Wuttig; Material study on reactively sputtered zinc oxide for thin film silicon solar cells,"*Thin Solid Films*, 502, 1-2, 286-291, 2006.

[12] G. Luka, B. Witkowski, L. Wachnick, R. Jakiela, I. Virt, M. Andrzejczuk and M. G. Lewandowska,"Electrical and mechanical stability of aluminum-doped ZnO films grown on flexible substrates by atomic layer deposition,"*Metrial Science Engineering B*, 186, 15-20, 2014.

[13] T. Nam, L. C. Wan, H. J. Kim and H. Kim,"Growth characteristics and properties of Ga-doped ZnO (GZO) thin films grown by thermal and plasma-enhanced atomic layer depositio,"*Applied Surface Science*, 295, 260-265, 2014.

[14] O. Kluth, G. Schope, B. Rech, R. Menner, M. Oertel, K. Orgassa and W. H. Schock,"Comparative material study on RF and DC magnetron sputtered ZnO:Al films," *Thin Solid Films*, 502, no. 1-2, pp. 311-316, 2006.

[15] R. Groenen, J. L. Linden, H. v. Leirop, D. C. Schram, M. C. Kuypers and M. V. Sanden,"An expanding thermal plasma for deposition of surface textured ZnO:Al with focus on thin film solar cell applications,"*Applied Surface Science*, 173, no. 1-2, pp. 40-43, 2001.

[16] E. S. Shim, S. H. Kang, J. S. Kang, H. J. Kim and S. Y. Lee," Effect of the variation of film thickness on the structural and optical properties of ZnO thin films deposited on sapphire substrate using PLD," *Applied Surface Science*, 186, 1-4, 474-476, 2001.

[17] Z. Fu, B. Lin and J. Zu,"Photoluminescence and structure of ZnO films deposited on Si substrates by metal-organic chemical vapor deposition," *Thin Solid Films*, 402, 1-2, 302-306, 2002.

[18] P. Nunes, B. Fernandes, E. Fortunato, P. Vilarinho and R. Martins,"Performances presented by zinc oxide thin films deposited by spray pyrolysis,"*Thin Solid Films*, 337, 1-2, 176-179, 1999.

[19] W. Tang and D. Cameron,"Aluminum-doped zinc oxide transparent conductors deposited by the sol-gel process," *Thin Solid Films*, 238, 1, 83-87, 1994.

[20] J. Hu and R. G. Gordon; Textured aluminum-doped zinc oxide thin films from atmospheric pressure chemical-vapor deposition," *Journal of Applied Physics*, 71, 2, 880-889, 1992.

[21] J.-H. Shin, D.-K. Shin, H.-Y. Lee and J.-Y. Lee," Properties of multilayer gallium and aluminum doped ZnO(GZO/AZO) transparent thin films deposited by pulsed laser deposition process,*Transactions of Nonferrous Metals Society of China*, 21, 1, 96-99, 2011.

[22] M. Ohyama, H. Kozuka and T. Yoko,"Sol-Gel Preparation of Transparent and Conductive Aluminum-Doped Zinc Oxide Films with Highly Preferential Crystal Orientation," *Journal of American Ceramic*, 81, 6, 1622-1632, 1998.

[23] H.-m. Zhou, D.-q. Yi, Z.-m. Yu, L.-r. Xiao and J. Li,"Preparation of aluminum doped zinc oxide films and the study of theirmicrostructure, electrical and optical properties,"*Thin Solid Films*, 515, 6909-6914, 2007.

[24] V. Balaprakash, R. Rajkumar, S. Sudha and P. Gowrisankar,"Influence of Aluminum Doping on Structural,Morphological and Optical Properties of AZO Thin Films Prepared by Sol-Gel Dip Coating, "*Indian Journal of Applied Physics*, 5, 6, 443-445, 2016.

[25] S. Badwal, F. Ciacchi and D. Ho,"A fully automated four-probe d.c. conductivity technique for investigating solid electrolytes,"*Journal of Applied Electrochemistry*, 21, 8, 721-728, 1991.

[26] E. Hall,"On a new action of the magnet on electric currents,"*American Journal of Mathematics*, 2, 3, 287-292, 1879.

[27] M.-C. Juna, S.-U. Parka, k.-J. Lee, b.-M. Moon and j.-H. koha,"The microstructure of Al-doped ZnO thin films by a sol-gel dip-coating method,"*Jornal of Ceramic Processing and research*, 13, 6, 721-724, 2012.

[28] S. M. Mihaiub, A. Toader, M. Anastasescu, M. Gabor, M. Stoica and M. Zaharescu, "Al-doped and undoped zinc oxide films obtained by soft chemistry," *Processing and Application of Ceramics*, 3, no. 1-2, pp. 79-84, 2009.

[29] G. Wu, Y. Chen and H. Lu ,"Aluminum-Doped Zinc Oxide Thin Films Prepared by Sol-Gel and RF Magnetron Sputtering," *Proceedings of the VIII International Conference ION*, Dolny, Poland, 2010.

[30] R. Bhattarai and S. P. Shrestha,"Construction of Sheet Resistance Measurement Setup for Tin Dioxide Film Using Four Probe Method, "*American Journal of Applied Physics and Applications*, 5, 5, 60-65, 2017.

[31] B. R. Strohmeier and D. M. Hercules,"Surface spectroscopic characterization of manganese/aluminum oxide catalysts," *The Journal of Physical Chemistry*, 88, no. 21, 4922-4929, 1994.

[32] R. Hoffman, "Physics Thin Film," 1968.

[33] B.-Z. Dong, G.-J. Fang, J.-F. Wang, W.-J. Guan and X.-Z. Zhao,"Effect of thickness on structural, electrical, and optical properties of ZnO: Al,"*Journal of Applied physics*, 101, 3, 033713, 2007.

[34] F. Wang, M. Wu, Y. Wang, Y. Yu, X. Wu, L. J. Zhuge and F. Wang,"Influence of Annealing Temperature on the electrical, optical and structural properties of AZO thin films, " *Vaccum*, 89, 127-131, 2013.

[35] M.-C. Jun and j.-h. koh, "Effects of Annealing Temperature on Properties of Al-Doped ZnO,"*Journal of Electrical Engineering and Technology*,8, 1, 163-167, 2013.

[36] F. Wang, M. Wu, Y. Wang, Y. Yu, X. Wu and L. Zhuge, "Influence of thicness and annealing temperature on the electrical, optical and structural properties of AZO thin films, " *Vaccum*, 89, pp. 127-131, 2013.

[37] G. Haacke, "New Figure of Merit for Transparent Conductors," *Journal of Applied Physics*,47, 4086 -4088, 1976.

[38] R Rafique, K N Tonny, A Sharmin, ,Z H Mahmood,"Study on the Effect of Varying Film Thickness on the Transparent Conductive Nature of Aluminum Doped Zinc Oxide Deposited by Dip Coating,"Materials Focus 7,5,,707-713, 2018. https://doi.org/10.1166/mat.2018.1572.

4.3.Al doped ZnO (AZO) with variance of precursor concentration

Because of its widespread and potential applications, ZnO has glinted a lot of consideration in the research communal during the last decade. Biomedical science, ceramics, cosmetics, concrete manufacturing, and even culinary products all employ this compound. Solar cells, touch screens, LCDs, plasma display panels (PDPs), and OLEDs all use ZnO as a translucent electrode, which is in fierce competition [1,2]. With its unique optoelectronic properties, impurity doped ZnO [3,4] is an excellent option for transparent conducting oxide (TCO), that has superseded ITO and FTO. TCO acts as a window layer in a solar cell, allowing more than 80% of incident light to pass through. Quantum dot LED [5], Lithium-Ion battery anodes [6], piezoelectric modules e.g. surface-acoustic wave (SAW) and piezoelectric sensors, antireflection coatings, field-effect transistors, voltage dependent resistor (VDR), chemical and biological applications are just a few of the many uses for ZnO. [7].

The n-type ZnO has a large exciton binding energy of 60 meV, is chemically and thermally stable[8] and has a wide band gap energy (Eg=3.37 eV). To increase its optical properties, it can be doped or co-doped. When Al is doped into ZnO, the free charge carriers are elevated, and the optical band gap is widened [41]. Group 3 elements (e.g., Al, Ga) are utilized as doping materials to increase the number of carriers and hence lower the resistivity. Impurity doped ZnO has gotten a lot of interest since it has a lower resistivity and a higher transmittance, that is what a researcher expect from a solar cell's window layer. Furthermore, AZO is made up of harmless and abundant elements, as well as a low growing temperature [9], making it an ideal for low-cost large-scale coating. Although ITO has been investigated for over 50 years and has the utmost favorable features as TCO, AZO has been the material of choice for solar cell manufacturing. In recent years, ZnO nanoparticles have been employed in a self-washing coating on a metal panel [37] and even in an anti-corrosion nano-coating for carbon steel [38]. AZO has emerged as the most attractive translucent electrode choice for photovoltaic [39] and plasmonic solar cells due to its exceptional electric and optical characteristics. [40]

AZO Thin films might be arranged by various methods like Spray pyrolysis [19], Chemical Vapor Deposition(CVD)[20], Sputtering [21] , Laser ablation [22], plasma-enhanced CVD (PECVD) [23], single-source CVD (SSCVD) [24], metal-organic CVD (MOCVD) [25], pulsed laser deposition (PLD) [25], molecular beam epitaxy (MBE) [25], thermal oxidation of Zn or ZnS [26-27] and atomic layer deposition (ALD) [28]. Yang et al. [34] used magnetron sputtering to create high-quality transparent and conducting AZO films at ambient temperature and investigated the consequence of thermal annealing in a varied environment. Tabassum et al. [44] published a report comparing the oxidation kinetics of sputtered and sol gel produced AZO films. Most of these methods, such as physical or chemical vapor deposition, necessitate a high temperature to produce high-quality films, that is not necessarily suited for lift-off manufacturing. The manufacturing cost must be minimal and the process complexity must be overcome. The method like Sol-gel [29-30] method is not only cost effective, rather a humble and smooth method for synthesizing huge range thin films and also can be performed at ambient temperature. It permits outstanding compositional mechanism, a high degree of homogeneousness in the molecular state, and a low crystallization temperature. Khan et al. [31] used the sol-gel process to produce highly aligned and transparent ZnO thin films. Tonny et al. [13] studied the structural, optical and electrical attributes of AZO films formed using the sol-gel spin coating process with varied film thickness.

Lee et al. [47] used the vacuum evaporation method to investigate the effect of Al doping on optical and structural characteristics of Al-ZnO, while Tabassum et al. [10] used the sol-gel method to investigate the consequence of Al doping on optical and structural characteristics of Al-ZnO. When the Al concentration was amplified by 3-4 wt%, the resistivity arises. Another study [11] looked at the electrical steadiness of AZO films at various annealing temperatures and times. It is concluded that

annealing time has no significant influence and that high temperature annealed films are more stable. Several research on AZO thin films of various thickness [13-14] and annealing atmosphere [14-18] have also been published. Controlling crystallite size, form, and crystallinity, as well as several other characteristics, remains a mystery. Material stoichiometry (compositional uniformity of a metallic precursor) is one of the most important aspects in producing high-quality see-through AZO thin films. To date, only a few research have been published on the consequence of Zn concentration on the characteristics of AZO. Considering these factors into account, an easy and cost effective process such as sol-gel spin coating is used to manufacture AZO thin films for a thorough analysis. The goal of this project is to produce a high-quality translucent AZO thin film and to investigate the possibility of strengthening the thin film's capabilities as TCO. To have a better grasp of film stoichiometry, a deeper understanding of the interrelationship between distinct properties of a thin film is expected. The consequence of film width on various AZO attributes has been studied in order to determine an optimal AZO film thickness. Second, the consequence of Zn precursor molar concentration on the electro-optical quality of AZO films as transparent and conductive electrodes is evaluated. Furthermore, the use of a cost effective sol-gel spin coating process to produce AZO thin films as an equivalent to more luxurious ITO or FTO is a unique component of the study. This manuscript is published in the Journal of Theoretical and Applied Physics in 2019[50].

4.3.1. Growth of AZO

To produce the sol-gel, zinc acetate dehydrates ($Zn(CH_3COO)_2.2H_2O$) and aluminum nitrate nonahydrate ($Al(NO_3)_3\ 9H_2O$) were employed as the ZnO and dopant precursors, respectively [10]. The concentration of the precursor was changed between 0.35-0.75 mol/L. First, dehydrate Zinc acetate and nonahydrate aluminum nitrate are liquefied in 2 Methoxyethanol (solvent). Monoethanolamine (MEA) is applied in a few drops. The molar ratio of MEA to zinc acetate was adjusted at 1. MEA works as a complexing negotiator in this case. A magnetic stirrer is used to agitate the solutions at 60° C for 1 hour to obtain a clean and uniform solution. For ageing process, the precursor solution is placed for 15-20 hours. Methanol, ethanol, and again methanol were used to clean the soda lime glass (SLG) substrates for 10 minutes each, accompanied by 15 minutes in an ultrasonic bath with DI water [49]. For depositionof thin film , a spin coater (SPS SPIN 150) is used at 3000 rpm for 30s at room temperature. After each coating, the synthesized films were warmed with an oven Binder (ED 53) at 300 °C for 5 minutes. It is gradually dehydrated and chilled. To enhance the thickness, the operation was done five, ten, fifteen, and twenty times. The fifth, tenth, fifteenth, and twenty layers were used to generate samples of four different film width for each concentration. After that, the films are treated to 500°C for 1 hour in a closed N_2 environment to achieve crystallized AZO.

4.3.2. Results and Discussion

Fig.4.3.1 displays the film width of a sol-gel processed AZO thin film with the number of coating and error bars. It rises in a linear fashion as the coating number rises from 295 to 1039 nm.

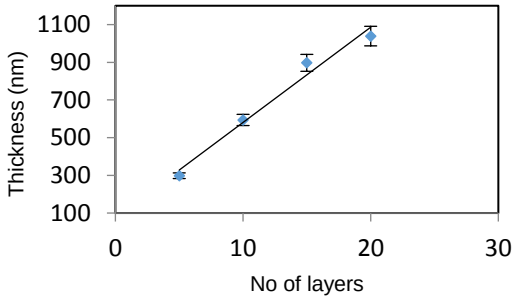

Fig.4.3.1.*Film width deviation with number of film*

4.3.2.1. Structural properties

Fig.4.3.2 shows the X-ray diffraction configuration for an AZO thin film annealed at 500°C. AZO does not display any prominent peaks beneath 500°C. AZO crystallites in this work shows a hexagonal wurtzite structure (ICDD-00-051-0037). The XRD configuration show a prominent peak at 34.60°, indicating that the crystallographic axis is preferred (002). At the axes (100) and (101), there are other, less intense peaks at 31.80° and 36.30°, respectively. The c-plane is the favored orientation in every sample. Peak intensity and sharpness upsurge with film width, as can be seen. Peak sharpness indicates that crystallite size improves as thickness increases [12-13].

To evaluate the structural parameters of AZO film, the full width at half maximum (FWHM) of XRD (002) peak, Crystallite size (D), d Spacing (Δ), Strain (Ɛ) and Dislocation density (δ) is listed in Table 1. The Crystallite size, D is evaluated from Scherrer's Formula [31]

$$D=\frac{k\lambda}{\beta Cos\theta} \qquad (4.3.1)$$

Where $\boldsymbol{\lambda}$ is the wavelength of XRD, D is the Crystallite size, $\boldsymbol{\theta}$ is the angle of diffraction and $\boldsymbol{\beta}$ is the value of Full width at half maximum (FWHM) in radians.

The **dislocation density, δ** which is the number of dislocations per unit volume of a crystalline material is calculated [31] as

$$\delta=\frac{1}{D^2} \qquad (4.3.2)$$

Dislocations cause a crystal's usual pattern to be interrupted[32].Strain, Ɛ of the thin film is calculated [31] as

$$Ɛ=\frac{\beta Cos\theta}{4} \qquad (4.3.3)$$

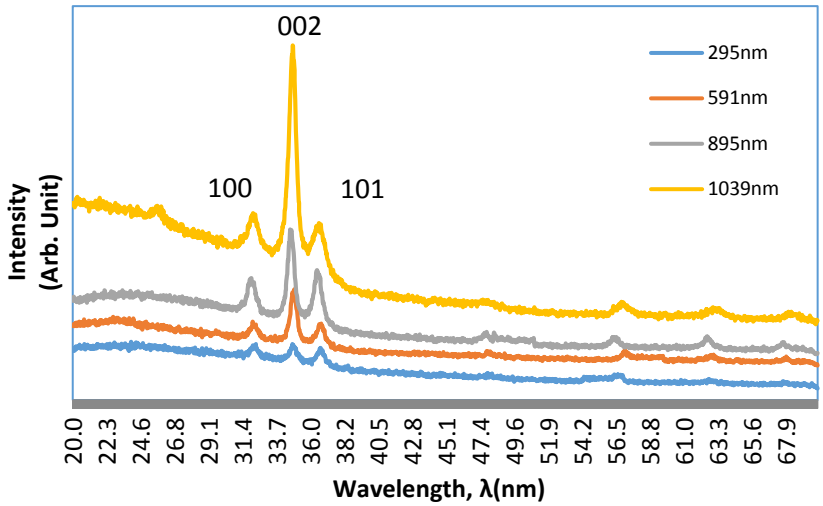

Fig.4.3.2*. X-ray diffraction spectra of AZO film with Zn concentration of 0.75mol/L*

Lesser FWHM (β) and higher Crystallite Size(D) imply superior AZO thin film crystallization. Table 1 shows that crystallite size (D) upsurges as film width grows, ranging from 9.25 to 9.81 nm. The magnitude of the crystallite (D) is mostly determined by the annealing temperature and environment [34]. Because this study is conducted at a fixed annealing temperature, no significant changes in crystallite size are detected. Furthermore, the influence of imperfections is not taken into account when estimating crystallite size. With increasing thickness, dislocation density(δ) decreases, indicating fewer lattice flaws and less strain in the AZO thin film. Table

4.3.1 shows that with the increase of the film width, the number of flaws in crystal structure diminishes.

4.3.2.2. Electrical properties: Effect of Zn concentration

The electrical characteristics of AZO thin films are exhibited in Fig.4.3.3, Fig.4.3.4, and Fig.4.3.5 as a role of film width with varied Zn concentrations of 0.35, 0.50, and 0.75m/L, accordingly. As can be seen in Fig.4.3.3, resistivity (ρ) reduces with film thickness, whereas sheet concentration (n) increases. These occurrences can be explained by an elevation in sheet concentration (n) as a outcome of free electron production and a growth in mobility (μ). The number of carriers per unit square is known as sheet carrier concentration. The number of carriers per unit volume is known as bulk carrier concentration. If the film width is identified,

$$n_s = n_b * h \quad (4)$$

Where, n_s = sheet carrier concentration, n_b= bulk carrier concentration, h = thickness of the films. In 2010, Yang W et al. published a paper explaining the dependency of electric attributes on carrier concentration, a contribution from Al^{3+} on replacement sites of Zn^{2+} ions, oxygen vacancies, and Zn interstitial atoms [34]. The presence of an annealing environment has a

Table 4.3.1. *Micro-structural parameters of AZO thin film with Zn concentration 0.75mol/L*

No of layers	d-spacing Δ Å	FWHM β (º)	Crystallite size D nm	Dislocation Density, δ Lines/m^2	Strain, Ɛ 10^{-3}
5	2.69	0.8912	9.25	1.16	3.89
10	2.70	0.8792	9.55	1.09	3.63
15	2.71	0.8660	9.67	1.06	3.60
20	2.69	0.7940	9.81	1.01	3.30

significant impact on carrier concentration [46]. The annealing environment is the same for all samples in this investigation, and 2 wt% Al doping is used. When related to 1, 3 and 4 wt% Al doping, 2 wt% Al doping has the lowest resistance and best electrical stability[10]. Excess Al doping is examined to result in non-conducting Al2O3. As a result, it behaves like a carrier trap, resulting in a higher in resistivity [33]. As a result, the decrease in resistivity (ρ) in Fig.4.3.3, Fig.4.3.4, and Fig.4.3.5 can be accredited to a alteration in Zn concentration, which increases the generation of free electrons.

The range of resistivity (ρ) reduces (i.e. conductivity rises) steadily with Zn concentration from 0.35mol/L to 0.75mol/L, as shown in Fig.4.3.3, Fig.4.3.4, and Fig.4.3.5. And the Zn concentration of 0.75mol/L has the lowest value of resistivity(ρ). Although it can be enhanced

by adjusting the annealing environment [46] and guaranteeing regulated doping concentrations, the lowest resistivity among twelve samples is 1.3x10^2 Ω-cm for the 20th layer (1039 nm). [10].However, up until the 15th layer, the mobility (μ) improves progressively with film width and then starts to decline (Fig.4.3.3). Mobility is mostly determined by layer thickness, according to Guillen et al. [46]. Until there is adequate carrier concentration, mobility (μ) extents significantly to a definite value with thickness. When carrier concentration extents a specific state, it interferes with the carrier's mobility. As a result, mobility(μ) is reduced. With increasing thickness, Fig.4.3.4 and Fig.4.3.5 show comparable features. In Fig. 4.3.4, mobility (μ) rises with film width up to 10th (591 nm) before decreasing towards the 20th layer (1039 nm). In Fig.4.3.5, the maximum mobility is 1.81x103 cm^2/Vs for the 10^{th}

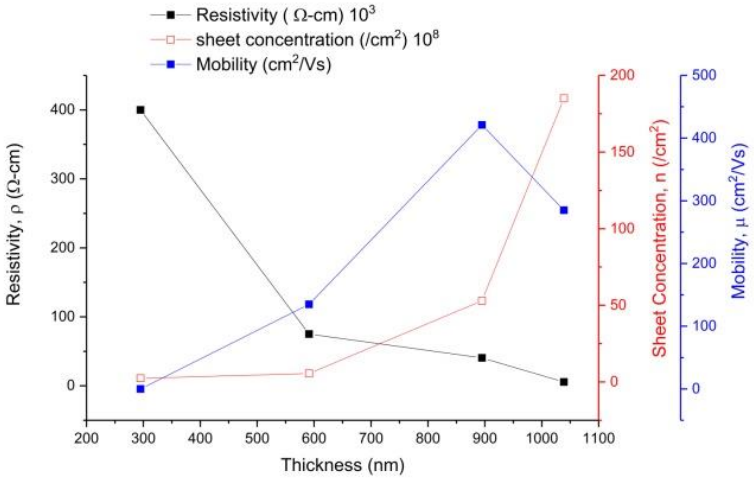

Fig.4.3.3. *Deviation of electric attributes with film widthof AZO samples with Zn concentration 0.35mol/L*

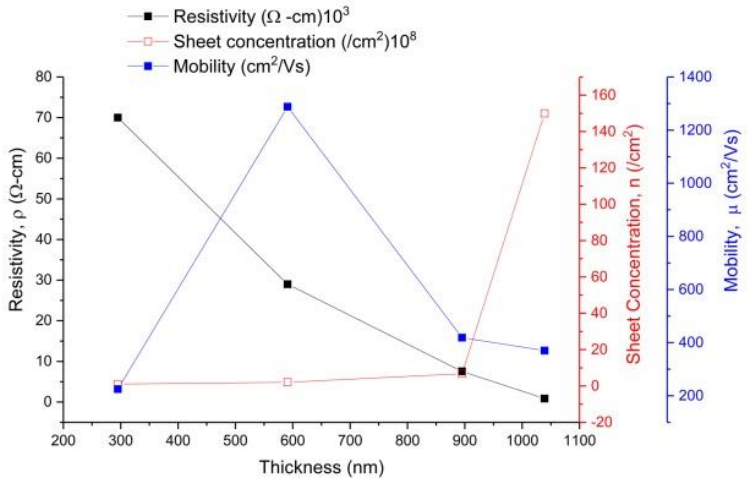

Fig.4.3.4. *Deviation of electric attributes with film width of AZO samplewith Zn concentration 0.50 mol/L*

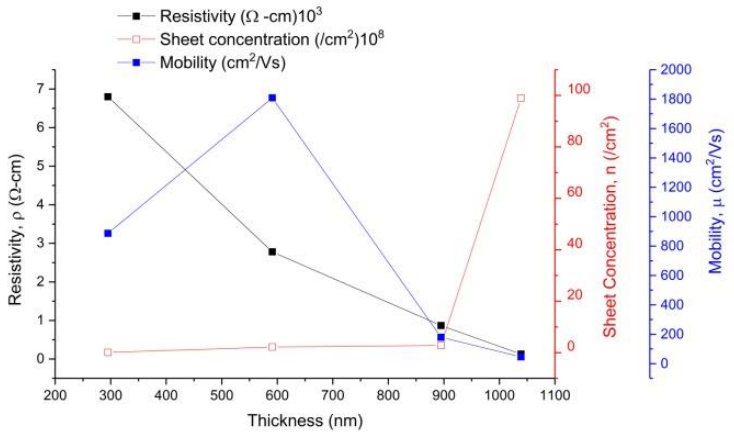

Fig.4.3.5. *Deviation of electric attributes with film width of AZO sample with Zn concentration 0.75mol/L*

layer (591 nm) at 0.75mol/L Zn concentration. The Hall Effect Measurement system measures the electric property at room temperature. Adsorption of oxygen and water molecules by the AZO layer in the annealing gas may reduce the carrier concentration, affecting the sample's conductivity [35]. The electric properties of annealed film (post heat treatment) with Argon (Ar) or pure Hydrogen (H_2) flow are more steady [10]. The electrical attributes of an AZO film is directly reflected by the number of O_2 vacancies. Because annealing in H_2 promotes O_2 annihilation, the film develops O_2 vacancies. As a result of the vacancies acting as a carrier, the resistivity(ρ) decreases. The paper reveals that in a pure H2 annealing environment, the resistivity of the AZO film reduces much more than in an Ar+5% H_2 annealing environment [11].

4.3.2.3. Optical properties: Effect of Zn concentration

Fig.4.3.6, Fig.4.3.7, and Fig.4.3.8 show the optical transmittance spectra for different number of layers (5, 10, 15, and 20th layer) of the AZO thin film developed on SLG with Zn concentrations of 0.35.0.50 and 0.75 mol/L, accordingly. At about 380 nm, a severe ultra violet cut-off is noticed. The average value of transmittance (% T) for 5 layers (295nm) is 90-92 %, as shown in Fig.4.3.6 (295nm). So as the layer thickness increases, transmission diminishes until it reaches its lowest point for 20 layers. When comparing Fig.4.3.6, Fig.4.3.7, and Fig.4.3.8, it can be seen that average transmittance (%T) declines progressively as Zn concentration rises, that is accurately indicated by band gap energy calculation. The absorption coefficient is estimated

as $(\alpha h\nu)^2 = A(h\nu - E_g)^{1/2}$ (4.3.5)

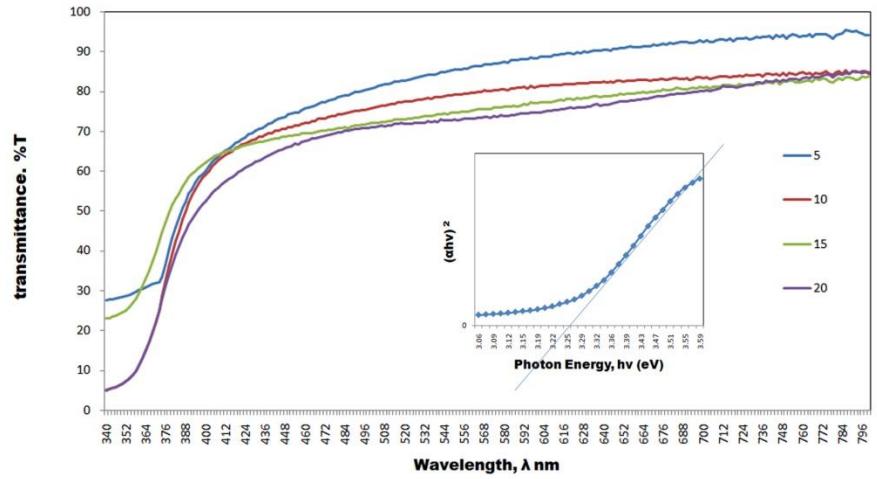

Fig.4.3.6. *Optical Transmittance (%T) of AZO with Zn concentration 0.35mol/L*

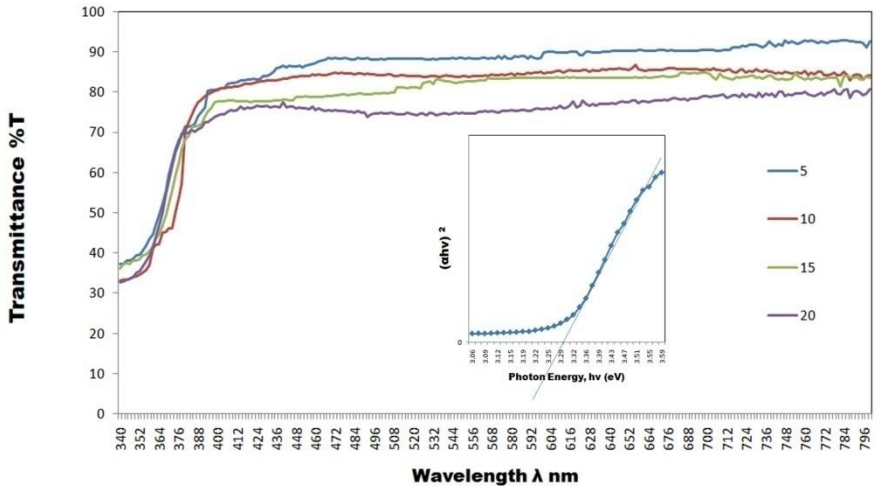

Fig.4.3.7. *Optical Transmittance (%T) of AZO with Zn concentration 0.50mol/L*

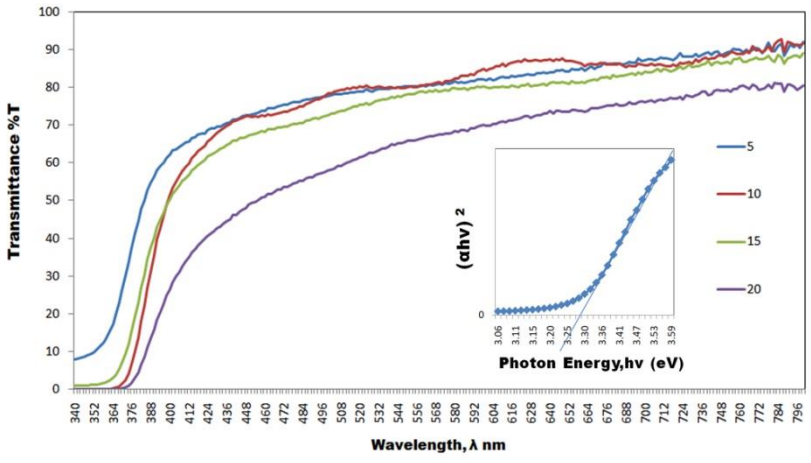

Fig.4.3.8. *Optical Transmittance (%T) of AZO with Zn concentration 0.75mol/L*

Here E_g is the band gap, *v* is the frequency of incident radiation, *h* is Plank's constant and A is a constant. For each concentration indicated inset of Fig.4.3.6, Fig.4.3.7, and Fig.4.3.8, the Tauc plot is drawn. With increasing Zn content, the optical band gap upsurges from 3.25 to 3.29 eV (see Table 4.3.2). The increase in carrier concentration is likewise linked to the broadening of the band gap energy. Furthermore, it has a direct impact on a film's transmittance. Burstein-Moss' theory explains why there is an growth in transmittance when the band gap widens[42,43]. Fig.4.3.9 demonstrates the relation between band gap energy, Eg, and refractive index (n) and molar concentration.

Semiconducting materials' band gap (E_g), refractive index (n), and dielectric constant () are critical for developing heterostructure lasers in optoelectronic devices and solar cell applications[48]. Organic solar cells are nonetheless less efficient than inorganic PV cells due to their small dielectric constant.

A material's refractive index(n), often known as its index of refraction, is a dimensionless quantity, specifies how quickly light perpetuates through it. Adding i-ZnO (anti-reflection coating) between the absorber and window layer in a photovoltaic cell reduces the refractive index [45]. Refractive index is defined as

$$n = c/v \qquad (4.3.6)$$

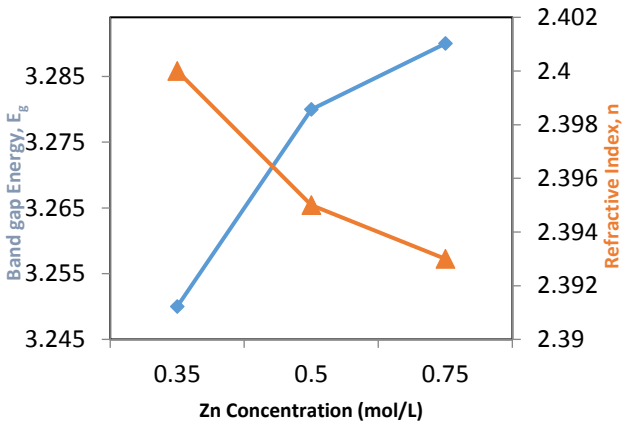

Fig.4.3.9. *Deviation of Band gap Energy, E_g(eV)and Refractive index (n) with Zn concentrations*

Where ***v*** is the phase velocity of light in the medium ***and c*** is the speed of light in vacuum. It is directly related to band gap by ***Moss relation***

$$E_g n^4 = \mathbf{k} \qquad (4.3.7)$$

Here, **k** is a constant with a value of 108eV. A substance's ability to accumulation electrical energy in an electric field is assessed by the dielectric constant. It is the ratio of a material's permittivity to the permittivity of free space. Controlling the medium dielectric constant can help enhance solar cell device performance by eliminating Voc loss. The high frequency dielectric constant (ε_∞) is measured as

$$\varepsilon_\infty = n^2 \qquad (4.3.8)$$

The static dielectric constant (ε_o) of the film is obtained as

$$\varepsilon_o = 18.52 - 3.08\, E_g \qquad (4.3.9)$$

The value of optical dielectric constant (ε_o) and optical high frequency dielectric constant (ε_∞) of AZO film is shown in **Table 4.3.2**.

Table 4.3.2*. Optical dielectric constant ($\mathcal{E}_o$) and optical high frequency dielectric constant ($\mathcal{E}_\infty$) values for AZO film*

Zn Concentration (mol/L)	Band gap Energy E_g(eV)	High Frequency Electrostatic Constant, ε_∞	Static Dielectric Constant, ε_o
0.35	3.25	8.51	5.76
0.50	3.28	8.42	5.73
0.75	3.29	8.39	5.72

4.3.2.4. Morphological properties

SEM pictures of the surface morphology of the films with 5, 10, 15, and 20 layers are depicted in Fig.4.3.10 (a,b,c,d). The film has fully surrounded the substrate, but it appears to be rough in most areas. Some areas appear wrinkled, and cavities can be seen. The preferred diffusion path for oxygen and water molecules entering the film is through the vacancies. The phenomena boost the AZO film's resilience. [44]. In Fig.4.3.10, users can see the asymmetrical AZO rod (d). Khan et al. [29] and Znaidi et al. [36] both discovered a similar pattern. The EDX graph of the proportion of the substance vs X-Ray energy is depicted in Fig.4.3.11. The synthesis of AZO with 57.7% O2, 41.9 % Zn, and 0.4 % Al is verified by EDX measurements. To improve the performance of AZO films, uniform composition is critical [45]. The AZO film composition obtained is quite similar to the values reported by Lee et al [47].

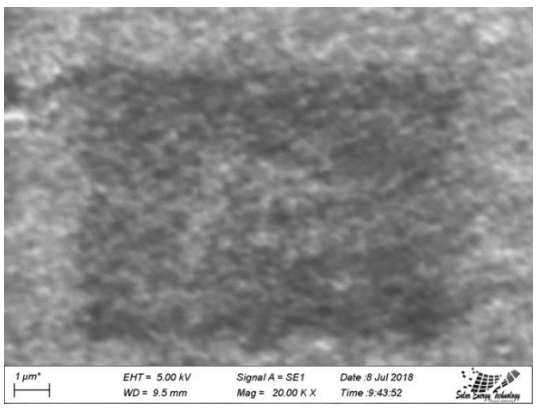

(a)

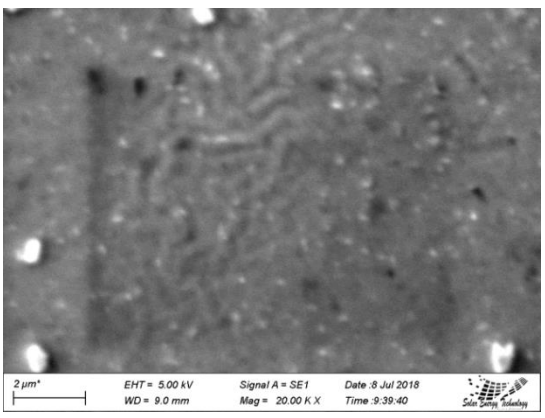

(b)

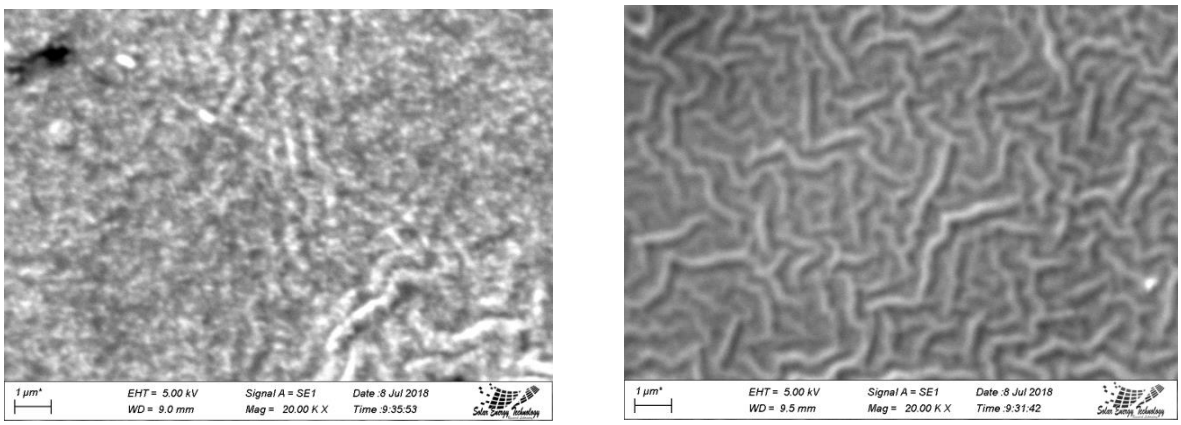

(c) (d)

Fig.4.3.10. *SEM images of AZO sample with film width of (a)295 nm,(b)591 nm,(c)895 nm and (d)1039 nm*

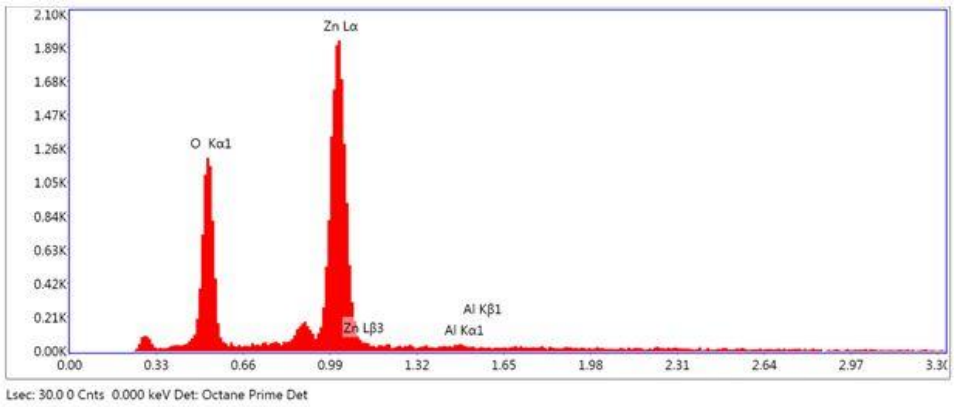

Fig.4.3.11. *EDX Spectrum for AZO film*

4.3.3. Remarks

Merits

- A unique sol-gel spin coating process is utilized to form a highly translucent AZO thin film on SLG at room temperature in this investigation. The attributes of AZO film are examined meticulously.
- The XRD investigation exposed that the AZO film possesses a hexagonal crystal configuration with a c-axis(002) orientation.
- With expanding film thickness, the grain dimension (D) of the film rises while the strain(Ɛ) diminishes.
- The impact of different Zn concentrations on the electrical and optical attributes of Al doped ZnO thin films has been investigated. In the visible region, AZO films have a transmittance (%T) of more than 90%, which progressively declines with film width and Zn content.

- Doping concentration, carrier concentration and mobility influence the electrical properties of AZO. This research was done conducted for a specific doping concentration. As a result, a alteration in Zn concentration accompanied the generation of additional free electrons, demonstrating that increasing Zn concentration is beneficial in enhancing AZO's electric behavior. For 0.75mol/L Zn concentration, the film with a width of 1039 nm has the lowest resistivity (ρ) and the film with a width of 595 nm has the highest mobility (μ).
- As the Zn concentration rises, the band gap energy (E_g) expands (3.25-3.29 eV) and the refractive index (n) lowers.
- EDX investigation examines AZO thin films qualitatively and quantitatively. In addition, the layer with a thickness of 1039 nm has scarcer voids and better covering than that of others.
- Based on the optical and electrical attributes, it is concluded that a Zn concentration of 0.75mol/L is the best for AZO film as a translucent conduction oxide for window layer of CZTS solar cells.

To do next

- Raman spectroscopy could not be performed because of the unavailability of the instrument. Raman analysis can confirm the phase purity of prepared AZO thin films.

Reference

[1] D. C. Plain, H. Y. Yeom, and B. Yaglioglu, "Flexible Flat Panel Displays," Edited by G.P. Crawford. John Wiley & Sons Ltd, Singapore: 94,2005.

[2] B. G. Lewis, D. C. Plain," Applications and Processing of Transparent Conducting Oxides," MRS Bulletin, 25, 8, 22, 2000.

[3] S. M. Park, , T. Ikegami, K. Ebihara, "Investigation of Transparent Conductive Oxide Al-Doped ZnO Films Produced by Pulsed Laser Deposition," Japanese Journal Applied Physics.44,8027, 2005.

[4] B. G. Lewis, D. C. Plain," Applications and Processing of Transparent Conducting Oxides," MRS Bulletin, 25, 8, 22, 2000

[5] Y Wang, W. Zhao, M. Zou, Y. Chen, L.Yang, L. Xu, H. Wu, A. Cao," MOF-Derived ZnO Nanoparticles Covered by N-Doped Carbon Layers and Hybridized on Carbon Nanotubes for Lithium-Ion Battery Anodes,"ACS Appl Matter Interfaces, 9, 43, 37813-37822, 2017.

[6] Y. Sun, W. Wang, H. Zhang. Q. Su, J. Wei, P. Liu, S Chen, S. Zhang, "High-Performance Quantum Dot Light-Emitting Diodes Based on Al-Doped ZnO Nanoparticles Electron Transport Layer," ACS Appl. Mater. Interfaces,10,22,18902–18909,2018.

[7]O. Lupanet al., "Nanostructured zinc oxide films synthesized by successive chemical solution deposition for gas sensor applications," Materials Research Bulletin,44,63–69, 2009.

[8] C Klingshirn," ZnO: From basics towards applications," Physica Status Solidi B, 244,9, 3027-3073, 2007.

[9] G. Fang, D. Li, B.L. Yao, " Fabrication and vacuum annealing of transparent conductive AZO thin films prepared by DC magnetron sputtering," Vacuum, 68,4,363–372, 2002),.

[10] S. Tabassum, E.Yamasue, H.Okumura, K.N. Ishihara," Damp heat stability of AZO transparent electrode and influence of thin metal film for enhancing the stability," Journal of Material Science: Materials in Electron, 25, 3203–3208, 2014.

[11] . Tabassum, E.Yamasue, H.Okumura, K.N. Ishihara,"Electrical Stability of Al-doped ZnO Transparent electrode prepared by sol-gel method," Applied Science Surface, 377, 355-360, 2016.

[12]R. Rafique,K. N. Tonny, A Sharmin, Z. H. Mahmood ,"Study on the Effect of Varying Film Thickness on the Transparent Conductive Nature of Aluminum Doped Zinc Oxide Deposited by Dip Coating," Materials Focus 7,5,7070-713, 2018.
[13]K.N. Tonny, R. Rafique, A. Sharmin, M. S. Bashar, Z.H. Mahmood, "Electrical, optical and structural properties of transparent conducting Al doped ZnO (AZO) deposited by sol-gel spin coating," AIP Advances, 8, 065307, 2018.
[14] M Ohyama, H. Kozuka,T. Yoko," Sol-Gel Preparation of Transparent and Conductive Aluminum-Doped Zinc Oxide Films with Highly Preferential Crystal Orientation," Journal of the American Ceramic Society, 81, 1622-1632 ,1998.
[15] T. Schuler, M.A. Aegerter,"Optical, electrical and structural properties of sol gel ZnO:Al coatings," Thin Solid Films 351,125-131,1999.
[16] G.G. Valle, P. Hammer, S.H. Pulcinelli, C.V. Santilli," Transparent and conductive ZnO:Al thin films prepared by sol-gel dip-coating," Journal ofthe European Ceramic Society, 24, 6,1009-1013, 2004.
[17] R.B.H. Tahar, " Structural and electrical properties of aluminum-doped zinc oxide films prepared by sol–gel process.,"Journal of the European Ceramic Society, 25,14, 3301-3306, 2005.
[18] K.M. Lin, P. Tsai, "Growth mechanism and characterization of ZnO: Al multi-layered thin films by sol–gel technique,"Thin Solid Films, 515, 24, 8601-8604, 2007.
[19] F.D. Paraguay, W.L. Estrada, D.R.N. Acosta, E. Andrade, M. Mikiyoshida, "Growth, structure and optical characterization of high quality ZnO thin films obtained by spray pyrolysis," Thin Solid Films 350,192-202,1999.
[20] A. Moustaghfir, E. Tomasella, S.B. Amor, M. Jcquet, J. Cellier,T. Sauvage,"Comparison of the structural and optical properties of zinc oxide thin films deposited by d.c. and r.f. sputtering and spray pyrolysis,"Surf ace CoatingTechnology, 200,293-296, 2005.
[21] K. Haga et al.,"ZnO thin films prepared by remote plasma-enhanced CVD method," Journal of Crystal Growth, 214,77-80, 2000.
[22]K.L. Narasimhan, S.P. Pai, V. R. Palka, R. Pinto,"High quality zinc oxide films by pulsed laser ablation ,"Thin Solid Films, 295, 104-106, 1997.
[23] M.D. Barankin, E. Gonzalez, A.M. Ladwig, R.F. Hicks, "Plasma-enhanced chemical vapor deposition of zinc oxide at atmospheric pressure and low temperature," Solar Energy Material and Solar Cells, 91,924–930, 2007.
[24]L.P. Dai, et al.," The effect of annealing temperature on the properties of ZnO films with preferential nonpolar plane orientation by SSCVD," Journal of Material Science, 43, 312–315, 2008.
[25]R Triboulet, J. Perrière," Epitaxial growth of ZnO films. Progress of Crystal Growth and Characterization of Materials" 47,65–138, 2003.
[26] A. Sekar, S.H. Kim, A. Umar, Y.B. Hahn, " Catalyst-free synthesis of ZnO nano wires on Si by oxidation of Zn powders," Jounal of Crystal Growth, 277,471–478, 2005.
[27] E.J. Ibanga, C. le Luyer, J. Mugnier, "Zinc oxide waveguide produced by thermal oxidation of chemical bath deposited zinc sulphide thin films," Materials Chemistry and Physics, 80:490–495, 2003.
[28] C.Y. Yenet al.," Influence of annealing temperature on the structural, optical and mechanical properties of ALD-derived ZnO thin films,"Applied Surface Science, 257, 7900–7905, 2011.
[29] D. Bao, H. Gu, A. Kuang, "Sol-gel-derived *c*-axis oriented ZnO thin films,"Thin Solid Films, 312, 37-39 ,1998.
[30] N. Sakti, P.S.Gupta," Structural and optical properties of sol-gel prepared ZnO thin film,"Applied Physics Research, 2,1,19-28, 2010.
[31] Z.R. Khan, M.S. Khan, M. Zulfequar, M.S. Khan," Optical and Structural Properties of ZnO Thin Films Fabricated by Sol-Gel Method," Materials Sciences and Applications, 2, 340-345, 2011.
[32]G.S. Thool, A.K. Singh, R.S. Singh, A. Gupta, M.A.B.H. Susan," Facile synthesis of flat crystal ZnO thin films by solution growth method: A micro-structural investigation," Journal of the Saudi Chemical Society,18, 5,712-721, 2014.
[33] J. Hu. R.G. Gordon,"Textured aluminum-doped zinc oxide thin films from atmospheric pressure chemical-vapor deposition," Journal of Applied Physics, 71,880-890, 1992.
[34]Yang,W. et al.,"Room temperature deposition of Al-doped ZnO films on quartz substrates by radio-frequency magnetron sputtering and effects of thermal annealing," Thin Solid Films, 519,1, 31-36, 2010.

[35]T.L. Chenet al.," Highly stable Al-doped ZnO transparent conductors using an oxidized ultrathin metal capping layer at its percolation thickness," Applied Physics Letter, 99, 093302, 2011.
[36] L. Znaidi , G.J.A.A. Soler-Illia, S, Benyahia , C. Sanchez, A.V. Kanaev," Oriented ZnO Thin Films Synthesis by Sol-Gel Process for Laser Application,"Thin Solid Films, 428, 1-2, 257-262 , 2003.
[37]B. Stieberovaet al.,"Application of ZnO Nanoparticles in a Self-cleaning Coating on a Metal Panel: An Assessment of Environmental Benefits,"ACS Sustainable Chemistry and Engineering, 5,3, 2493–2500, 2017.
[38] J.N. Hasnidawaniet al.," ZnO Nanoparticles for Anti-Corrosion Nanocoating of Carbon Steel," Material Science Forum, 894, 76-80, 2017.
[39] S. Pisoniet al.," Impact of interlayer application on band bending for improved electron extraction for efficient flexible perovskite mini-modules," Nano Energy, 49,300-307, 2018.
[40] C. Delerue,"Minimum Line Width of Surface Plasmon Resonance in Doped ZnO Nanocrystals," Nano Letters, 17 ,12, 7599–7605, 2017.
[41] X. Zi-qiang, D.Hong, L.Yan, C. Hang, "Al-doping defects on structure, electrical and optical properties of c-axis-orientated ZnO: Al thin films," Journal of Optoelectronics Laser,17(3):257-260 , 2006.
[42] B. R. Bennett, R. A. Soref, and J. A. Del Alamo,"Carrier-induced change in refractive index of InP, GaAs and InGaAsP," IEEE. Journal of Quantum Electronics, 26,113-122 , 1990.
[43] D. Djouadi, A. Chelouche, A. Aksas, " Amplification of the UV emission of ZnO: Al thin films prepared by sol-gel method," Journal of Material and Environmental Science, 3(3), 585-590, 2012.
[44] S. Tabassum, ..E.Yamasue, H. Okumura, K.N. Ishihara,"Sol-gel and rf sputtered AZO thin films: analysis of oxidation kinetics in harsh environment," Journal of material Science: Mater Electron. 25,11),4883-4888 , 2014.
[45] B.T. Jheng, P.T. Liu, M.C.Wang, M.C. Wu, "Effects of ZnO-nanostructure antireflection coatings on sulfurization-free Cu2ZnSnS4 absorber deposited by single-step co-sputtering process,"Applied Physics Letters, 103, 5, 2904,1-4, 2013.
[46] C. Guillen, J. Herrero, " Optical, electrical and structural characteristics of Al: ZnO thin films with various thickness deposited by DC sputtering at room temperature and annealed in air or vacuum," Vacuum, 84 ,914-929 , 2010.
[47] G.Z Lee, "Optical and Structural Properties of Al-ZnO Nanocomposites," Journal of Nanoscience and Nanotechnology, 14, 3661–3666 , 2014.
[48] Ondo-Ndong, R. *et al.*"Capacitive properties of zinc oxide thin films by radiofrequency magnetron sputtering,"Journal of Theoretical and Applied Physics, 12,309–317, 2018.
[49] M. Cavas,"Investigation morphological, electrical, and optical properties of Mn-doped ZnO thin film by sol–gel spin-coating method,"Journal of Theoretical and Applied Physics, 11, 325-331, 2017.
[50] A. Sharmin, S. Tabassum, M. S. Bashar, Z. H. Mahmood, "Depositions and characterization of sol gel processed Al-Doped ZnO (AZO) as Transparent Conducting Oxide (TCO) for solar cell application," Journal of Theoretical and Applied Physics, 13, 2,123-132, 2019. https://doi.org/10.1007/s40094-019-0329-0

Chapter 5: Fabrication and characterization of Cu_2ZnSnS_4(CZTS)Thin Film

5.1.CZTS thin film with variance of annealing temperature

After ternary semiconductors emerged widely in 1980, cadmium telluride (CdTe), copper indium selenide (CIS), and copper indium gallium selenide (CIGS) [1-3] has garnered substantial attention in the areas of Absorber layer of thin film solar cells in the last several decades [4-5]. Highly toxic [6,7] of Cadmium(Cd) and Selenide(Se), as well as the limitation of Indium(In), Gallium(Ga), and Tellurium(Te) in the earth crust, non-toxic, environmentally acceptable, and element-rich other light absorber materials are required. On this premise, quaternary materialse.g. Cu_2ZnSnS_4 (CZTS) and $Cu_2ZnSnSe_4$ (CZTSe) have been regarded as one of the utmost prospective photovoltaic resources. With p type conductivity, CZTS have a near-optimal direct bandgap energy of 1.4-1.6 eV and a significant absorption coefficient of greater than 10^4 cm^{-1}[8]. Furthermore, as paralleled to the elements In and Ga, Zn and Sn are harmless and plentiful in nature (Cu: 50 ppm, Zn: 75 ppm, Sn: 2.2 ppm, S: 260 ppm). As a result, CZTS is one of the best materials to be utilized in the absorption layer of a solar cell, with a speculative maximum power conversion efficiency of 32.2 % [9-11].

The first CZTS thin film solar cell was stated in 1988 by Ito and Nakazawa [12]. Ito and Nakazawa[13] investigated the consequence of utilizing an ethanol and water combination as a solvent in 1996, and found that near-stoichiometric CZTS films could be generated at temperatures up to 360°C. Power conversion efficiency (PCE) of CZTS based solar cell was improved to 6.7% in 2008[14] and then to 9.6% in 2010 with the improvement of the Sulfurization technique [15]. Instead of hydrogen sulfide gas, Jiang et al. [16] confirmed a nitrogen environment for heat treatment in 2011. Barkhouse et al.[17] used a hybrid solution-particle slurry approach to developa CZTS-based solar cell with a PCE of 10.1% in 2012. At the 38th IEEE PVSC conference in 2013, Todorov et al.[18] claimed a PCE of 11.1%. Rajeshmon et al. reported 1.85 % efficiency on spray pyrolyzed CZTS/In_2S_3 solar cells in the same year [19]. Solar Frontier, IBM, and Tokyo Ohka Kogyo (TOK), a Japanese thin-film solar firm, jointly unveiled their record-breaking CZTSSe solar cell adept to renovating 12.6 % of solar energy to electricity in 2013. [20].

Numerous CZTS thin film preparation methods has been described such as sol-gel spin coating [21], spray pyrolysis [24] , sputtering [25],thermal deposition [23], pulsed laser deposition [22], chemical vapor deposition[27], electro-deposition [28] and thermal evaporation[26] etc. High temperature and high vacuum processes are more appropriate to attain high efficiency solar cells with some downsides such as luxurious precursors, complex instruments, and techniques. Henceforth, a non-vacuum process like the sol-gel method are mostly chosen for eco-friendly and inexpensive simple technique and large scale manufacturing. Researchers around the world are trying to progress the enactments of CZTS thin film with the variation of the concentration of precursor[32], deposition method, pH value, annealing temperature [29-30], sulfurization temperature[31] and other process parameters. CZTS films necessitate sulfurization to prevent the damage of S during the annealing process which makes it luxurious. The effect of grain size, stoichiometric ratios, morphology, pinholes and degree of roughness, etc. acts significantly in the enactment of solar cells [29]. In this investigation, CZTS thin film is fabricated on SLG by utilizing a modest and economical sol gel process. The CZTS thin film is annealed in the air without sulfurization to trail a low cost method. Morphological, structural, electrical and optical features has been investigated for changeable annealing temperatures

from 300 to 500°c. This study is issued in the International Journal of Thin Film Science and Technology in 2019[44].

5.1.1. Growth of CZTS by sol-gel spin coating

Materials

Zinc Chloride ($ZnCl_2.2H_2O$), Cupric Chloride ($CuCl_2.2H_2O$)Stannic Chloride ($SnCl_2.2H_2O$), and Thiourea ($SC(NH_2)_2$) are used as the precursor for CZTS. 2 Methoxyethanol is employed as a solvent. The concentration of precursor was upheld as 2M, 1M, 1M, and 7M respectively for $ZnCl_2.2H_2O$, $CuCl_2.2H_2O$, $SnCl_2.2H_2O$, and $SC(NH_2)_2$. Monoethanolamine (MEA) performs as a complexing agent.

Methods

The soda-lime glass (SLG) substrates are scrubbed with detergent and pounded with DI water. Then it is washed with methanol, ethanol, and DI water in an ultrasonic bath successively. Precursors are liquefied in 2 Methoxyethanol. A scarce amount of MEA is poured. The solution isagitated at 55-60 ºC for 30 minutes by a magnetic agitator to obtain a yellow homogeneous solution. The precursor solution is sieved if needed and fabricated on soda lime glass (SLG) by spin-coating (SPS SPIN 150) with 2500 rpm for the 30s at room temperature. Produced films were warmed at 200 °C for 5 min after each coating. It is then organically desiccated and chilled. To enhance the thickness, this operation was performed three to five times. So samples with 3 layers were prepared and annealed at diverse temperatures as 300º, 350º, 400º, 450º, and 500ºc for 30 minutes and titled as 300_3, 350_3, 400_3, 450_3, 500_3 respectively. Similarly, samples with 5 layers were termed as 300_5, 350_5, 400_5, 450_5, 500_5 with temperature difference.

5.1.2. Result and Discussion

Structural properties

The XRD configurations of CZTS thin film placed by sol gel spin coating are revealed in Fig.5.1.1 and Fig.5.1.2. Fig.5.1.1 displays the XRD configurations with 3 layers for temperature varied from 300º -500ºC. And Fig.5.1.2 reveals the XRD configuration for 5 layers with the same temperature variance. The thickness of 3 and 5 layers of film is 1.61 and 2.53 μm respectively.

The acuity of the peak rises with annealing temperature, as shown in Fig.5.1.1 and Fig.5.1.2. The acuity of the peak specifiesdecent crystallinity for CZTS films. It also can be detected that films with 5 layers (Fig.5.1.2) show more peaks than films with 3 layers (Fig.1). The major peaks are at 28.74°, 47.7°, and 56.6°, respectively, with the (112), (220), and (312) planes. [29-30]. With the (112) plane at 28.74°, the most desired orientation was observed. The characteristics peaks specify tetragonal body-centered polycrystalline kesterite CZTS according to JCPDS-26-0575 which is the most stable.

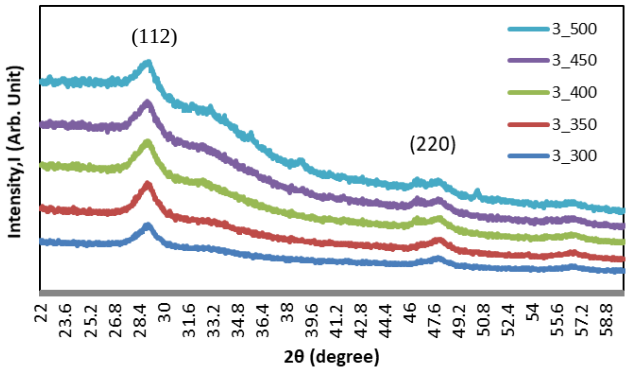

Fig. 5.1.1. *XRD patterns for CZTS for 3 layers film.*

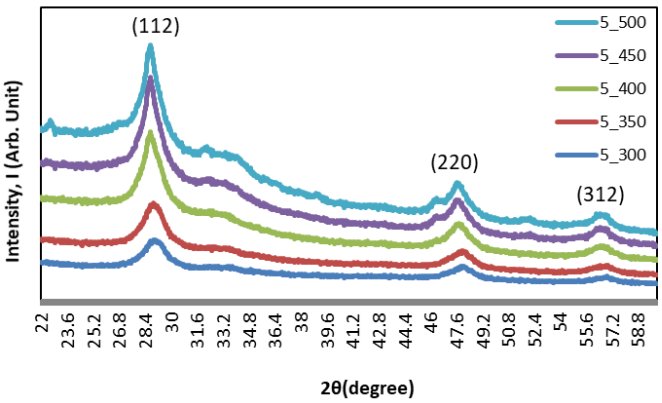

Fig. 5.1.2. *XRD patterns for CZTS for 5 layers film*

Nevertheless, lattice parameters of particular secondary phase i.e. SnS, tetragonal Cu_2SnS_3 and cubic ZnS is almost identical to CZTS film [30]. The secret to producing CZTS film without a secondary phase is a carefully executed annealing process combined with a strictly regulated concentration of precursor solution.

In Fig.5.1.1 there is no noticeable alteration in peak sharpness for the (112) plane. In Fig.5.1.2, peak sharpness improves as the annealing temperature rises from 300 ° to 500°c for (112),(220), and (312) planes due to crystalline nature[29]. Sharper peak and lesser FWHM values indicate improved crystallinity and greater grain size. The conversion efficiency of the CZTS photovoltaic cell is unswervingly associated with the size of grain. The minority carrier diffusion length increases as grain size increases. Additionally, it maximizes the polycrystalline solar cells' intrinsic potential [33].

The crystallite size (D) can be gained from the Debye-Scherrer Formulae [34]

$$D = \frac{0.9\lambda}{\beta Cos\theta} \qquad (5.1.1)$$

Where β is the line thickness at full width at half maximum (FWHM) of the diffraction peak at 2θ, λ is X-ray wavelength (0.15406 nm) and θ is the Bragg Diffraction angle.

Optical properties

Fig.5.1.3 depicts the absorption coefficients spectra versus photon energy (hν) for CZTS film annealed at diverse temperatures. The nature of absorption of the film has been determined by using the classical Tauc equation [35] for the absorption coefficient

$$\alpha = \frac{A(h\nu - E_g)^n}{h\nu} \qquad (5.1.2)$$

here, n is an index and n=1/2 for allowed direct transition and n=2 for allowed indirect transition. The absorption coefficient is found to be in the range of ~$10^4 cm^{-1}$ which is comparable to previous reports [10]. As an absorber layer, CZTS is very promising for its strong absorption over a broad solar spectrum. The optical band gap energy, E_g of direct transition is measured by the Tauc plot depicted in Fig.5.1.4 (a),(b), and (c). Table 5.1.1 lists the calculated band gap standards for samples annealed at various temperatures. From Table 5.1.1, that bandgap energy for all samples is in decent settlement with the theoretical standards [10]. Therefore, it can be assumed that it will act as an ideal absorber for applications such as photovoltaic solar cells. It is also detected that the bandgap inclines to lessening with rising annealing temperature. The disparity in inhomogeneity and crystallinity with temperature might be the reason for this transformation [30,36].

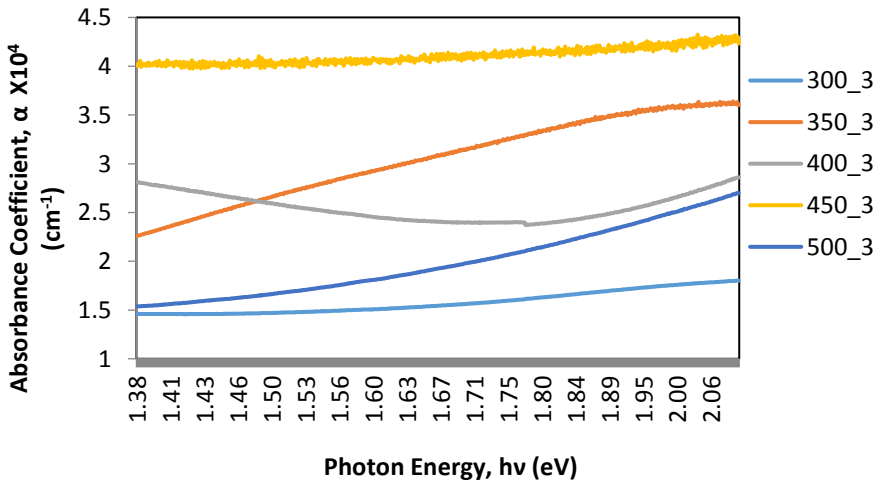

Fig.5.1.3. *Absorption coefficient (α) spectra of CZTS*

Refractive index (**n**), static dielectric constant (ε_0), and high-frequency dielectric constant(ε_∞) is recorded in Table1 which is reliable with other records [37]. For semiconducting materials, the refractive index (**n**) and dielectric constant (ε) play a vital role in optical and electrical characteristics that are obligatory for solar cell applications. These belongings of

semiconductor hetero-junctions is also significant for scheming some nano-electronic and optoelectronic devices. The refractive index (n) is considered from Moss relation [38]

$E_g n^4 = k$ (5.1.3)

Here k is a constant with a value of 108 eV. Both the high and static frequency dielectric constant is measured for CZTS film. High frequency dielectric constant (ε_∞) is obtained as

$\varepsilon_\infty = n^2$ (5.1.4)

Where *n* is the refractive index. Static dielectric constant (ε_0) is calculated as

$\varepsilon_0 = 18.52 - 3.08E_g$ (5.1.5)

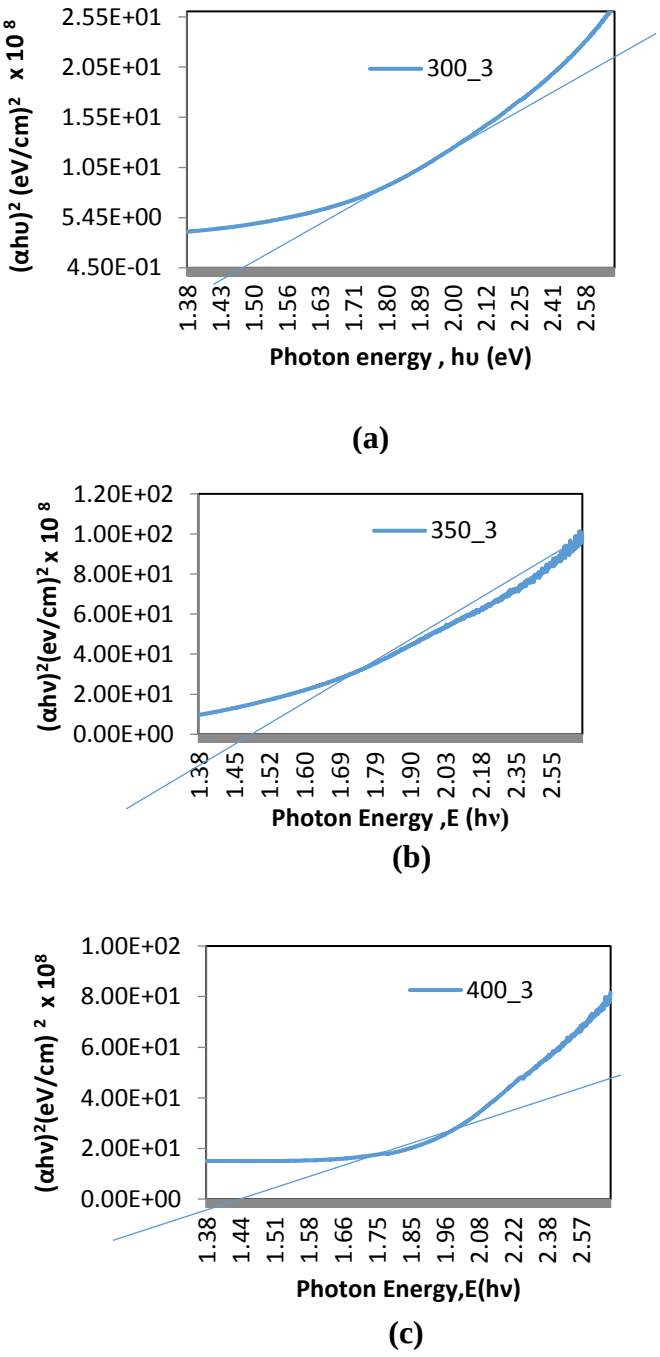

Fig.5.1.4*. Taut plot of the CZTS film annealed at (a)300º, (b)350º and (c) 400ºc*

***Table 5.1.1**. Band gap energy (E_g), Refractive index (n), static dielectric constant ($\mathcal{E}_0$) and high frequency dielectic ($\mathcal{E}_\infty$) constant*

sample	Bandgap Energy, E_g (eV)	Refractive index, **n**	Optical Static dielectric constant, $\mathcal{E}_0$	Optical high frequency dielectric constant, $\mathcal{E}_\infty$
300_3	1.49	2.91	13.93	8.46
350_3	1.46	2.93	14.02	8.58
400_3	1.46	2.93	14.02	8.58
450_3	1.44	2.94	14.08	8.64
500_3	1.42	2.95	14.15	8.70

Electrical properties: Hall Effect measurement

Hall effect measurement system is a consistent apparatus to examine the electronic possessions of semiconductor and compound semiconductors. The hall coefficient, R_H delivers the evidence of a semiconductor as n or p-type as it lies on positive values. Hall measurements for CZTS film reveal p type conductivity. Hall measurement standards of prepared CZTS film are depicted in Table 2.

From Table 5.1.2, With the growth in annealing temperature, the mobility improves and the carrier concentration reduces. Carrier electrons are produced when the number of charge carriers rises. Then mobility of the ion is induced. When mobility increases, there is a decrease in carrier concentration [29, 39]. The highest mobility, μ is establish for the CZTS thin film annealed at 500°c.

***Table 5.1.2**. Hall measurement values of CZTS thin films annealed at changed temperature*

Sample	Carrier concentration, N_b /cm^3	Hall mobility, μ cm^2/Vs	Hall Coefficient, R_H cm^3/C
300_3	5.828e13	4.3e1	+
350_3	9.783e12	6.2e1	+
400_3	4.806e11	1.4e2	+
450_3	3.699e11	2.1e2	+
500_3	3.285e11	3.9e2	+

It can be noted that with the rise in film thickness, mobility may also decrease. Consequently, enhancements in the crystallinity of CZTS thin films might be linked to the thickness of the layer, mobility, carrier concentration, and so on. The fewer structural flaws and larger crystal grain size can result in better crystallinity of the thin film [29].

Morphological properties

Fig.5.1.5 (a),(b),(c),(d),(e) respectively reveals the SEM image of CZTS thin films annealed at 300-500ºc. It can be seen that the substrate's surface has not been entirely submerged, and that the roughness rises with temperature [29]. And with the rise of temperature, the layer of the film became thinner and cracks are seen in Fig.5.1.4(d) and (e). Due to the evaporation of volatile materials in CZTS at higher temperatures, the film contracted, causing this to happen [40]. This kind of non-uniform dispersion of the agglomerated particles after 100oC annealing was achieved by Mali et al. [36]. Based on the nucleation growth mechanism proposed by Shinde et al.[30], this growth method is explained. In the beginning, all the metal ions of Zn^{2+}, $Cu^{+,}$ and Sn^{4+} come closer to create cationic nuclei on a glass substrate. S^{2-} ions are adsorbed over this to produce a CZTS molecule. By the successive aggregation more CZTS molecules are formed on each other. This phenomenon is defined as coalescence. Crystal growth revenues abode by continuous coalescence of the CZTS molecule.

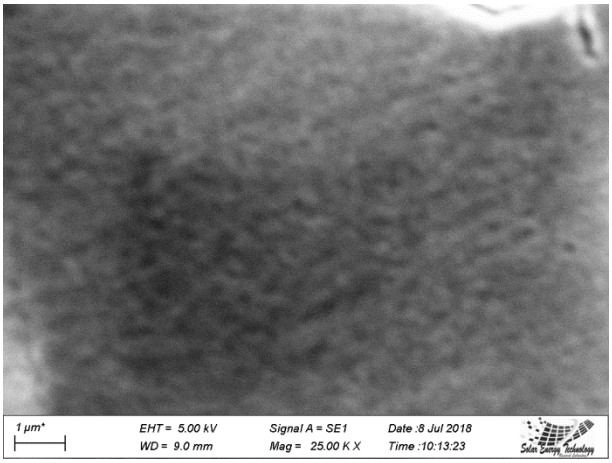

(a)

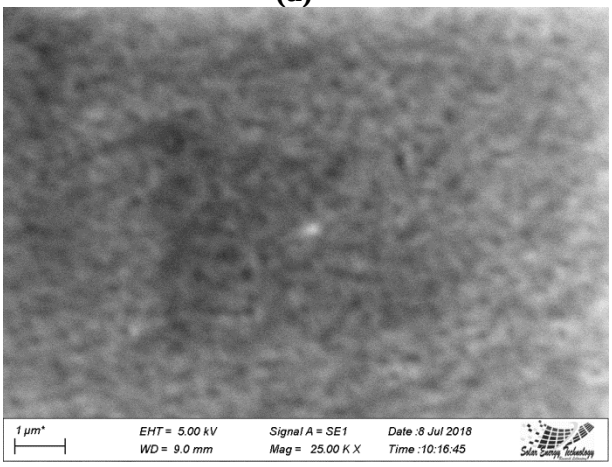

(b)

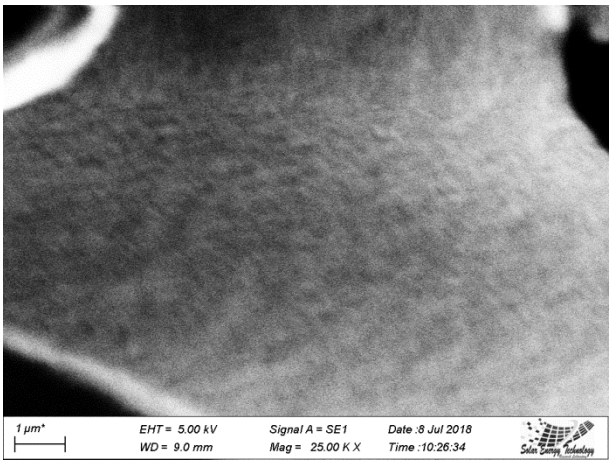
1 µm*
EHT = 5.00 kV
WD = 9.0 mm
Signal A = SE1
Mag = 25.00 K X
Date :8 Jul 2018
Time :10:26:34

(c)

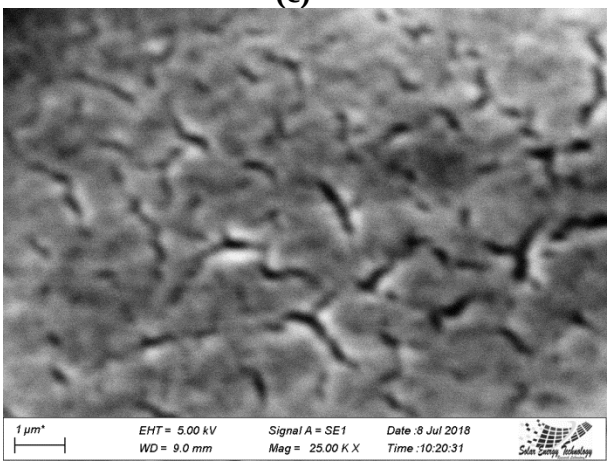
1 µm*
EHT = 5.00 kV
WD = 9.0 mm
Signal A = SE1
Mag = 25.00 K X
Date :8 Jul 2018
Time :10:20:31

(d)

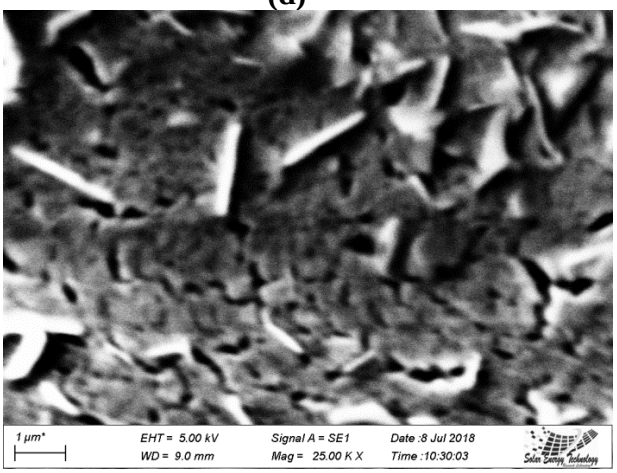
1 µm*
EHT = 5.00 kV
WD = 9.0 mm
Signal A = SE1
Mag = 25.00 K X
Date :8 Jul 2018
Time :10:30:03

(e)

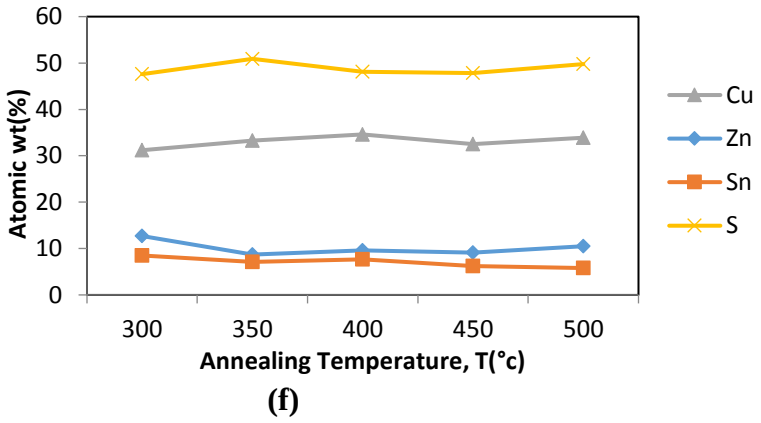

Fig. 5.1.5. *SEM images of CZTS thin film at (a)300º, (b)350º, (c)400º, (d)450º and (e) 500ºc temperature, (f) Atomic weight t(%) of CZTS sample as the role of annealing temperature.*

The EDX measurement for CZTS thin films in Fig. 5.1.5(f) confirms the formation of CZTS. The films are clearly Cu-rich and Zinc-deficient. Cu is a lighter-weight element with a faster flow rate than heavier elements. It indicates to the enriching of Cu in CZTS film[41]. Zn and S are also lighter elements. However, as they are volatile, CZTS films generally are to be Zn and S deficient. This composition of Cu rich and Zn deficient condition is appropriate for single-phase development of CZTS films recorded by Chen *et al.*[42-43]. However, in 2010, Torodov et al. [15] revealed that CZTS thin films with opposite compositional needs, i.e. Zn rich and Cu deficient, would have maximum power conversion efficiency. Park et al. [40] also stated the same compositions of sol gel processed CZTS in 2013 without sulfurization.

5.1.3.Remarks

Merits

- Quaternary CZTS thin film is fabricated on SLG by a modest non-vacuum sol-gel spin coating technique. The experiment was conducted at room temperature. Additionally, because there is no sulfurization involved in the deposition process, the substance utilized is both abundant on Earth and non-toxic. So the new method is both economical and environmentally benign.
- The samples were air annealed at temperatures varies from 300° to 500°C to explore structural, optical, electrical, and morphological aspects. No sulferization of selenization process is introduced which make the method economic.
- The CZTS's exquisite kesterite structure is evident in the XRD pattern, which also reveals that as temperature rose, sharper peaks appeared. Sharper peaks hence denote better crystallinity of CZTS thin films.
- The absorption coefficient is exposed to be in the range of ~10^4 cm^{-1} and band gap energy, E_g fluctuates from 1.42-1.49 eV which are effortlessly equivalent with previous statements.

- Hall effect investigation shows that the CZTS thin film is a p-type semiconductor. The data of mobility is maximum for the film annealed at 500° C. Additionally, Hall mobility() increases with the growth of annealing temperature.
- EDX study spectacles that synthesized films are Cu rich and Zn deficient with sufficient S.
- The observed property of CZTS thin-film implies that it should be utilized for the deposition of the absorber layer of the photovoltaic cell. It also shows that CZTS thin film needs to be improved even more in order to manufacture an efficient solar cell for low-cost electricity

Limitations

- However, EDX analysis shows the amount of Sn is quite less than expected in prepared CZTS thin film.
- No Raman study is conducted because of the unavailability of the instrument.
- It is detected from SEM image that the film has not shielded the substrate consistently.

To do next

- Another sol gel method may be employed to check its effect on film morphology
- Much work can be done to improve the stoichiometry i.e. with variance of precursor concentration, deposition consition, annealing condition etc.

Bibliography

[1] I. Repins , M. A. Contreras, B. Egaas, C. DeHart, J. Scharf, C. L. Perkins, B. To and R. Noufi, "19·9%-efficient ZnO/CdS/CuInGaSe$_2$ solar cell with 81·2% fill factor,Progress in Photovoltaics," 16 , 235-239, 2008.

[2] D. B. Mitzi, "Solution Processing of Chalcogenide Semiconductors via Dimensional Reduction, Advanced Materials," 21, 3141-3158, 2009.

[3] D. B. Mitzi, M. Yuan, W. Liu, A. J. Kellock, S. J. Chey, V. Deline, and A. G. Schrott, "A high efficiency solution deposited thin film photovoltaic device, "Advanced Materials; 20, 3657-3662, 2008.

[4] M. A. Green, K. Emery, Y. Hishikawa, and W.Warta, "Solar cell efficiency tables (version 41)," Progress in Photovoltaics, 21,1-11, 2013.

[5] A. N. Tiwari, D. Lincot, and M. Contreras, "The time for CIGS,"Progress in Photovoltaics; 18, 389, 2010.

[6] J. Britt and C. Ferekides, "Thin-film CdS/CdTe solar cell with 15.8% efficiency," Applied Physics Letter, 62, 2851-2852, 1993.

[7] M. A. Green, K. Emery, Y. Hishikawa, W. Warta, and W. D. Dunlop,"Solar cell efficiency tables (version 39)," Progress in Photovoltaics, 20, 12, 2012.

[8] X Song et al., "A Review on Development Prospect of CZTS Based Thin Film Solar Cells," International Journal of Photoenergy, Article ID 613173, 1-11, 2014.

[9]Q. Guo, H. W. Hillhouse, and R. Agrawal, "Synthesis of Cu_2ZnSnS_4 Nanocrystal Ink and Its Use for Solar Cells,"Journal of American Chemical Soceity, 131, 11672-11673, 2009 .

[10] C. Steinhagen, M. G. Panthani, V. Akhavan, B. Goodfellow, B. Koo, and B. A. Korgel,"Synthesis of Cu_2ZnSnS_4 Nanocrystals for Use in Low-Cost Photovoltaics," Journal of American Chemical Soceity, 131, 12554-12555, 2009.

[11]X. Li X, Z.Su , S. Venkataraj, S.K. Batabyal , L. H. Wong, “8.6% Efficiency CZTSSe solar cell with atomic layer deposited Zn-Sn-O buffer layer,” Solar Energy Materials & Solar Cells, 157, 101-107, 2016.
[12] K. Ito K and T. Nakazawa, “Electrical and Optical Properties of Stannite-Type Quaternary Semiconductor Thin Films,”Japanese Journal of Applied Physcis,27,2094-2097, 1988.
[13]K. Ito, T. Nakazawa, “Sprayed films of stannites Cu_2ZnSnS_4,” Applied Surface Science, 92, 171-175, 1996.
[14] H. Katagiri, K. Jimbo, S. Yamada, T. Kamimura, W. S. Maw, T. Fukano, T. Ito, and T. Motohiro, “Enhanced Conversion Efficiencies of Cu_2ZnSnS_4-Based Thin Film Solar Cells by Using Preferential Etching Technique,”Applied Physics Express,1, 041201, 2008.
[15] T.K. Todorov, K.B. Reuter, D.B. Mitzi, “High-efficieny solar cell with earth– abundant liquid-processed absorber,” Advanced Materials 22 , 1–4, 2010.
[16] M. Jiang, Y. Li, R. Dhakal , P. Thapaliya , M. Mastro , J.D. Caldwell , F Kub , X.Yan , “Cu_2ZnSnS_4 polycrystalline thin films with large densely packed grains prepared by sol–gel method,” Journal of Photonics for Energy, 1,019501, 2011.
[17]D.A.R. Barkhouse, O. Gunawan , T. Gokmen , T.K. Todorov T K, and D. B. Mitzi, “Device characterization of 10.1% hydrazine processed $Cu_2ZnSn(Se,S)_4$,”Progress in Photovoltaics, 20, 6-11, 2012.
[18]T. K. Todorov, J. Tang, S. Bag, O. Gunawan, T. Gokmen, Y. Zhu, and D. B. Mitzi, “Device Characteristics of CZTSSe Thin-Film Solar Cells with 12.6% Efficiency,”Advanced Energy Materials, 3, 34-38, 2013.
[19] V. G. Rajeshmon, N. Poornima, C. S. Kartha, K. P. Vijayakumar, “Modification of the optoelectronic properties of sprayed In_2S_3 thin films by indium diffusion for application as buffer layer in CZTS based solar cell,” Journal of Alloys and Compounds, 553, 239-244, 2013.
[20] W. Wang, M. T. Winkler, O.Gunawan, T. Gokmen, T. K. Todorov, Y. Zhu, D. B. Mitzi, "A 12.6% $Cu_2ZnSnS_xSe_{4-x}$ (CZTSSe) solar cell is presented with detailed device characteristics," Advanced Materials;4 ,7, 1301465, 2013.
[21] R. Liu *et al.*, "Impact of sol-gel precursor treatment with preheating temperature on properties of Cu_2ZnSnS_4 thin film and its photovoltaic solar cell," Journal of Alloys and Compounds, 655, 124-129, 2016.
[22] A. V. Moholkar *et al.*, "Development of CZTS thin films solar cells by pulsed laser deposition: Influence of pulse repetition rate," Solar Energy; 85,7, 1354-1363, 2011.
[23] C. Sripan , V.E. Madhavan, A.K. Viswanath , R. Ganesan R, "Sulfurization and annealing effects on thermally evaporated CZTS films," Materials Letters, 189, 110-113, 2017.
[24] S Patel S and J V Gohel, "Synthesis and characterization of Copper Zinc Tin Sulfide films prepared by spray pyrolysis deposition," International Conference on Sustainable Development for Energy and Environment, India,2017.
[25] M. Banavoth, S. Dias, and S. B. Krupanidhi, "Near-infrared photoactive Cu_2ZnSnS_4 thin films by co-sputtering," AIP Advances; 3, 082132, 2013 .
[26] C. W. Shi, G. Y. Shi, Z. Chen, P. F. Yang, and M. Yao,"Deposition of Cu_2ZnSnS_4 thin films by vacuum thermal evaporation from single quaternary compound source," Materials Letter, 73, 89-91, 2012..
[27] T. Washio, T. Shinji, S. Tajima, T. Fukano, T. Motohiro, K. Jimbo, and H. Katagiri, "6% Efficiency Cu_2ZnSnS_4-based thin film solar cells using oxide precursors by open atmosphere type CVD," Journals of Materials Chemistry, 22, 4021-4024, 2012.
[28] Khalil MI et al. ,"CZTS absorber layer for thin film solar cells from electrodeposited metallic stacked precursors (Zn/Cu-Sn),"Applied Surface Science; 379, 91-97, 2016.
[29] SK Shahenoor Basha, M.C. Rao, "Effect of annealing temperature on structural and morphological studies of electrodeposited CZTS thin films ," Ceramics International; 44,1, 648-656. 2018.

[30] N. M. Shinde, P.R.Deshmukh, S.V.Patil, C.D.Lokhande, "Aqueous chemical growth of Cu_2ZnSnS_4 (CZTS) thin films: Air annealing and photoelectrochemical properties,"Materials Research Bulletin, 48, 5, 1760-1766, 2013.
[31] J. Zhang, B. Long, S. Cheng, and W. Zhang, "Effects of Sulfurization Temperature on Properties of CZTS Films by Vacuum Evaporation and Sulfurization Method," International Journal of Photoenergy, 986076, 2013.
[32] M. Y. Yeh, P.H.Lei, S. H. Lin, C.D. Yang, "Copper-Zinc-Tin-Sulfur Thin Film Using Spin-Coating Technology," Materials (Basel); 9,526, 1-12, 2016.
[33] S M Pawar, B S Pawar, A V Moholkar, D S Choi, J H Yun, J H Moon, S S Kolekar, J H Kim, "Single step electrosynthesis of Cu_2ZnSnS_4 (CZTS) thin films for solar cell application," Electrochemica Acta, 55,12, 4057-4061, 2010.
[34] P. K. Nair, J. Cardoso, O. Gomez Daza, and M. T. S. Nair, "Polyethersulfone foils as stable transparent substrates for conductive copper sulfide thin film coatings," Thin Solid Films; 401, 243–250, 2001.
[35] R.R. Salunkhe, U.M. Patil, T.P. Gujar, C.D. Lokhande, "Synthesis and characterization of cadmium hydroxide nano-nest by chemical route," Applied Surface Science; 255,7, 3923-3926, 2009.
[36] S.S. Mali, P.S. Shinde, C.A. Betty, P.N. Bhosale, Y. W. Oh, P.S. Patil, "Synthesis and characterization of Cu_2ZnSnS_4 thin films by SILAR method," Journal of Physics and Chemistry of Solids; 73, 735-740, 2012.
[37] J. Henry, K. Mohanraj, G Sivakumar, "Electrical and optical properties of CZTS thin films prepared by Silar method," Journal of Asian Ceramic Societies, 4, 81-84, 2016.
[38] M.A. Yildrim, "The effect of copper concentration on structural, optical and dielectric properties of $Cu_xZn_{1-x}S$ thin films," Optics Communications, 285, 6 , 1215-1220, 2012.
[39] K L Chopra, P Paulsun, V Dutta, "Thin-Film Solar Cells: An Overview," Progress in Photovoltaics Research and Applications, 12, 69-92, 2004.
[40] H. Park , Y. H. Hwang , B. S. Bae, "Sol–gel processed Cu_2ZnSnS_4 thin films for a photovoltaic absorber layer without sulfurization," Journal of Sol-Gel Science and Technology 65,1, 23–27, 2013.
[41] L. Sun, J. He, H. Kong, F. Yue, P. Yang, J chu, "Structure, composition and optical properties of Cu 2ZnSnS 4 thin films deposited by Pulsed Laser Deposition method ," Solar Energy Materials and Solar Cells 95,10, 2907-2913, 2011.
[42]S. Chen, J.H. Yang, X. G. Gong, A. Walsh, S.H. Wei, "Intrinsic point defects and complexs in the quartenary kesterite semiconductor$Cu_2ZSn\ S_4$," Physical Review B; 819, 245204, 2010.
[43] S Chen, X G Gong, Aron Walsh, S H Wei, "Defect physics of the kesterite thin-film solar cell absorber Cu_2ZnSnS_4,"Applied Physics Letter, 96, 2, 021902(2010).
[44] A. Sharmin, M. S. Bashar, S.Tabassum, Z. H. Mahmood ,"Low Cost and Sol-Gel Processed Earth Abundant Cu_2ZnSnS_4Thin Film as an Absorber Layer for Solar Cell: Annealing without Sulfurization," International Journal of Thin Film Science and Technology, 8,2 ,65-74, 2019. http://www.naturalspublishing.com/ContIss.asp?IssID=1600

5.2. CZTS thin films with variance of precursor concentartion

Solar energy is naturally uncontaminated, carbon-free, and renewable sources, as it is produced by solar cells using sunshine. It has the prospective to encounter the world's terawatt energy requirements if we can make it available at a cost comparable to grid power. The current solar cells, which are made of silicon (Si), cadmium telluride (CdTe), or copper indium gallium selenide (CIGS), produce power that is still too lavish. As a result, there is a frenetic quest for novel solar cell materials that will create cost-effective electric power [1]. Earth-plentiful, cost effective, and nonpoisonous kesterite copper zinc tin sulfide is one such intriguing contender. CZTS is a natural mineral that has been discovered [2]. CZTS material, on the other hand, frequently emerges in the kesterite phase due to its greater thermodynamic stability than stannite-type materials [3]. Cu_2ZnSnS_4 (CZTS), a quaternary compound semiconductor, has received a lot of consideration for its potential as an absorber layer for thin-film solar cells [4-5] and thermoelectric power generators now a day [6]. In the chromatic spectrum, copper zinc tin sulfide (CZTS) is a notable case of a p-type semiconductor with a direct bandgap of 1.5 eV and an absorption coefficient greater than 10^4 cm^{-1} [7]. These elements together have resulted in rapid progress in CZTS-based thin-film PV study in recent times, as exemplified by the achievement of a new high of 12.6 % power conversion efficiency [8]. Although CZTS is quite remarkable for its attributes, the PCE value remains well underneath the Schockley-Quessier limit (30%) for a single-junction cell based on CZTS [9].

The p-type photoactive absorber layer of a thin film solar cell (photovoltaic device) is the CZTS film. Because the key activities mandatory for the photovoltaic effect take place here, the absorber layer is the furthermost important section of a solar cell. This absorber layer is responsible for the absorption of solar radiation, the creation of electron-hole pairs, and the departure of charges. As a result, the influence of light on conductivity (photoconductivity) of CZTS films is as significant as dark conductivity in this regard. The absorber's bandgap should be enough little to permit absorption of a substantial fraction of the solar spectrum while still being adequate huge to prevent reverse saturation current density. For this study, direct bandgap semiconductors (1–1.7 eV) with a high absorption coefficient are chosen [10]. As a result, p-type semiconductors are commonly employed as absorber layers. To create device-quality CZTS thin films, many groups have used wet chemical techniques such as spray pyrolysis [11], Sol-gel [12], spin coating [13], electrodeposition [14], Successive Ionic Layer Adsorption and Reaction (SILAR) [15], dip coating [16], and others.

The Sol method is linked with the sol-gel process since after manufacturing the sol; a successive gel might be produced in singlepace. The sol-gel method is the development of an oxide network through polycondensation reactions of a molecular precursor in a liquid [17]Amorphous or crystalline particles are possible outcomes. The Van der Waals forces or hydrogen bonds govern particle suspensions in sol or colloidal suspensions. Sol-gel synthesis permits to make multi-component systems with a regulated stoichiometry by mingling sols of various compounds [18], avoiding co-precipitation issues, and achieving intimate reagent mixing at the atomic level, resulting in tiny particles.

Submerging a base in a container holding coating liquid, withdrawing the item from the container, and offering it to trench are all processes of dip coating. Under organized temperature and atmospheric conditions, the method is carried out at a set pace. The coating thickness is determined by the liquid's viscosity, solid content, and withdrawal speed. This strategy is heavily reliant on automation due of its simplicity. The final state of a thin film's dip coating is determined by a number of factors [19]. Many parameters, such as submersion time, the number of dipping cycles, solution composition, concentration and temperature, and ambient humidity, can be controlled to produce several types of dip-coated films on various structures with different thicknesses. Even on bulky, complex structures, the dip coating process can produce homogeneous, high textured films [20]. Dip coating is an easy, cost effective technology that has the potential to speed up commercial production. It primarily comprises of two steps: (i) substrate immersed into the precursor solution and (ii) film thermolysis. These processes must be repeated several times to get the required film width. Furthermore, as the procedure is repeated, voids and porosity might form in the structure, necessitating post-growth heating [21].

There have been some recent reports on research into the CZTS thin film dip coating process. P. Prabeesh also assessed the effect of sulfurization at 550°C for 30 minutes after producing Cu_2ZnSnS_4 thin films using a dip coating process using nonpoisonous ingredients [22]. Fischereder et al. [23] employed a pyridine-based solution with Cu, Zn, and Sn salts, as well as thioacetamide as a sulfur source. Pure CZTS films, on the other hand, could only be created by air annealing the precursor film at temperatures exceeding 250°C. Thiourea is yet another frequent sulfur source that may quickly deposited with development with Cu, Zn, and Sn, yielding sulfides when heated [24]. Tapas Kumar et al used a methanolic solution of metal-thiourea complex to dip coat phase pure CZTS films [25]. Yuxin et al used ethylene glycol and metal-thioacetamide to stack CZTS films in this approach [26]. The impact of pH on the structural, optical, and electrical attributes of a CZTS thin-film absorber coated by dip method was studied by Ferhat et al [27]. Patel et al. made CZTS thin films utilizing thiourea as a sulfur base and explored the effects of annealing in a sulfur atmosphere withseveral temperatures [28].

In this research work Cu_2ZnSnS_4, thin films have been prepared using copper(II) chloride dehydrate ($CuCI_2.2H_2O$), zinc (II) chloride ($ZnCI_2$), tin (II) chloride ($SnCI_2$), and thiourea ($CS(NH_2)_2$) as the precursor material and 2-methoxyethanal as the solvent material using the simple dip coating method. Here we varied the Cu/(Zn+Sn) ratios keeping Zn/Sn and S/(Cu+Zn+Sn) ratios fixed so that we can observe the proper variation that takes place in the characterization. Properties that we witnessed were crystallographic structure, morphology, and optical features of the thin CZTS nanocrystalline films in detail. A journal article is published in 2019 [35] along with a conference paper[36] from this study.

5.2.1. Growth of CZTS by sol-gel dip coating

Sample preparation

Soda-lime glass (SLG) substrates of 2.5 cm x 2.5 cm are washed with detergent and distilled water earlier to fabricate of CZTS thin films. They are ultrasonically washed with methanol and DI water again followed by the flow of nitrogen to dry. The sol-gel solution for CZTS absorber layers was arranged to contain copper(II) chloride dehydrate ($CuCI_2.2H_2O$), zinc (II) chloride ($ZnCI_2$), tin (II) chloride ($SnCI_2$), and thiourea ($CS(NH_2)_2$). The solution of 3.335M metal ions and 6.665 M thiourea was dissolved in 35 ml of 2-methoxyethanal. The assortment was agitated on the hotplate with a magnetic stirrer at 45-55 °C for ½ h. Simultaneously, a few drops of mono-ethanolamine (about 3 ml) were added to the stabilizer. The combination was then incubated for at least 24 hours at room temperature to produce a homogeneous clear yellow mixture. Finally, the sol-gel mixture was applied on soda lime glass (SLG) substrates. The CZTS film is fabricated on the cleaned soda lime glass substrates using a PTL-MM01 dip coater at a withdrawn speed of roughly 150 mm per minute. The wet films were then heated for 10 minutes in a Binder ED53 Drying Oven at 200°C. After the sample has been heated for drying, it is placed in the environment for natural cooling for 10 minutes, and the process is repeated three times more to provide an appropriate thickness of CZTS film. For the Cu/(Zn+Sn) ratio modifications from 0.7 to 1, the samples were labeled A-3, B-3, C-3, and D-3. After that, the samples were annealed by Thermoconcept, KLS 10/12 at 250°C for 15 min.

Table 5.2.1. *Chemical statement of base solution***.**

Cu/(Zn + Sn)	**Zn/Sn**	**Metal ion**	**S/metal ion**	**Stirred**	**No. of deposition times**	**Name of sample**
1	1.15	3.335M	2M	30 min	3	A-3
0.9	1.15	3.335M	2M	30 min	3	B-3
0.8	1.15	3.335M	2M	30 min	3	C-3
0.7	1.15	3.335M	2M	30 min	3	D-3

Where A, B, C, D is the variation of Cu/(Zn + Sn) ratio and 3 is denoted for the deposition times.

5.2.2. Results and Discussion

Structural properties

Fig.5.2.2 shows the XRD configuration of sample A, B, C, and D for three times deposited CZTS films produced by dip coating process. Broad peaks are depicted for the annealed films at the 2θ locations 28.00°, 47.28°, and 55.24°, which correspond to the (112), (220), and (312) planes of CZTS thin films and are typical of the tetragonal kesterite structure of Cu_2ZnSnS_4 (ICDD: 26-0575) [29]. XRD confirmed the films annealed at 250°C as a kesterite CZTS containing Zn_2SnO_3[30], which matches to the (200) and (220)planes. As the films were treated with low annealing temperature, the films had poor adherence to the base.

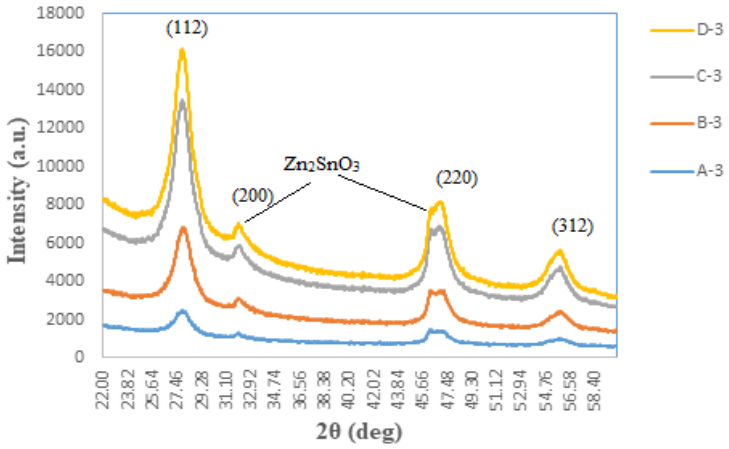

Fig.5.2.1: XRD pattern of sample A, B, C, D for 3 times deposited CZTS films

Morphological Characterization

The surface SEM micrograph is shown in Fig.5.2.2 and EDX composition in Fig.5.2.3. The textural structures for the CZTS thin films are visible in the SEM images, along with specific cavities and voids are seen across the whole surface of the CZTS thin film.[Fig.5.2.2].

It can be predict that as the copper content drops and that of zinc rises, there is a certain modification in the formation of particles [Fig5.2.3 and Table 5.2.2].

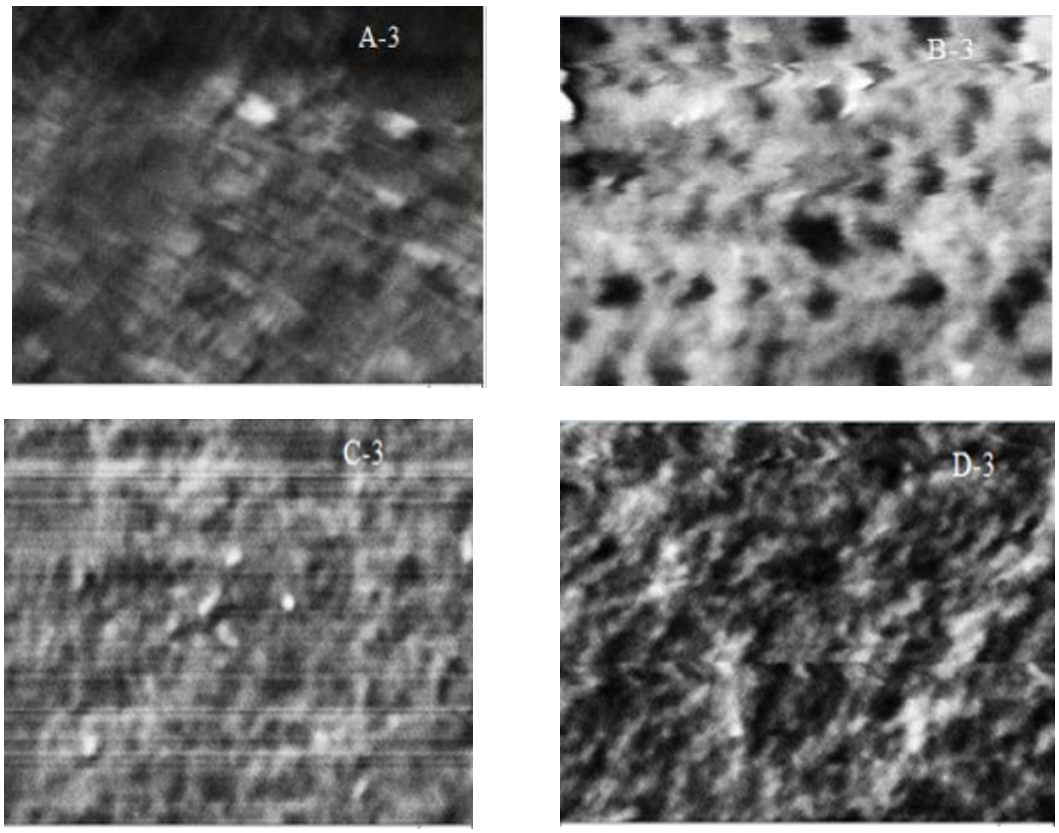

Fig.5.2.2. *SEM images of CZTS films with various Cu/(Zn+Sn) ratios*

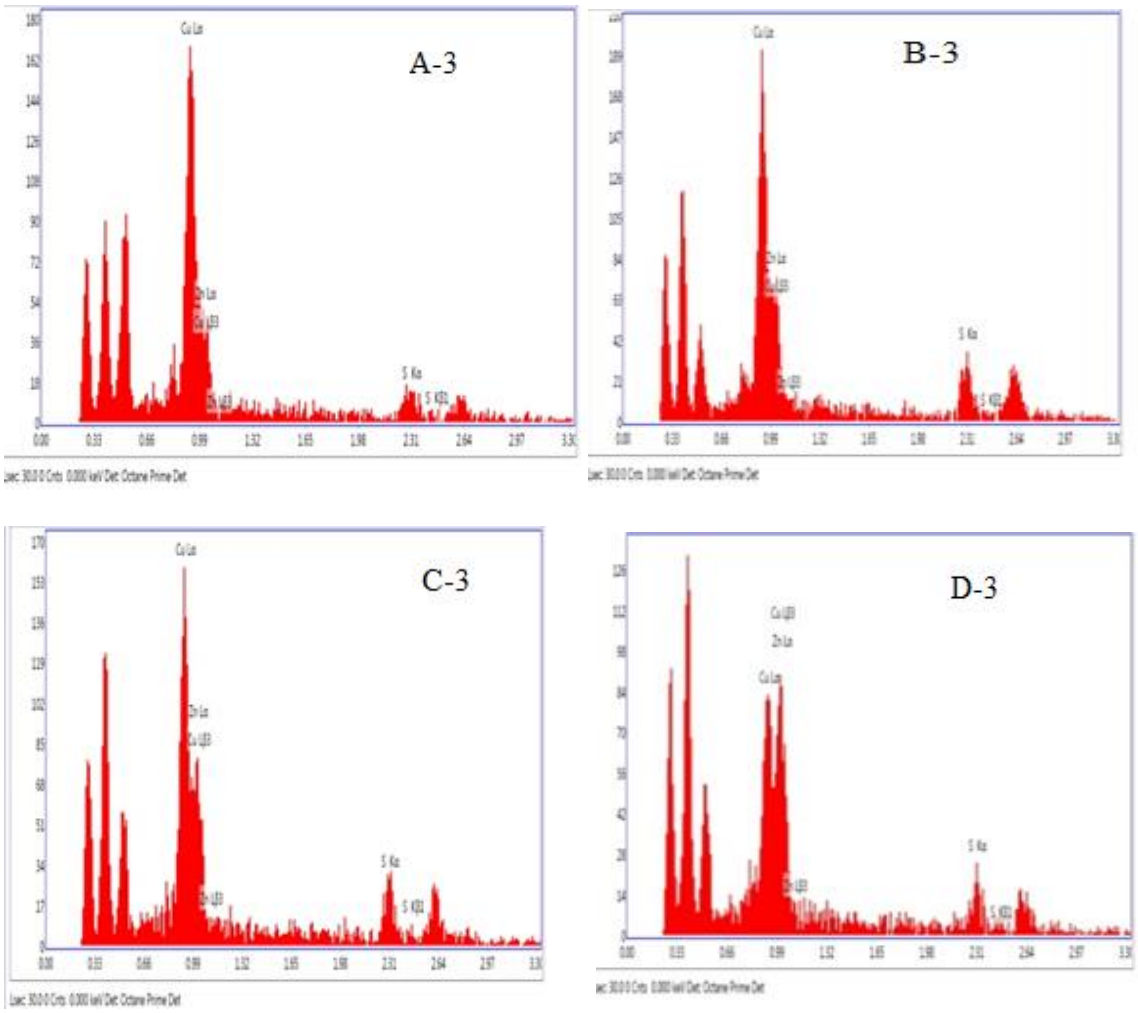

Fig.5.2.3. *EDX spectrum of CZTS thin film for 3 times deposited.*

Table 5.2.2. *Chemical composition (At %) of the CZTS films analysis.*

Sample	**Cu**	**Zn**	**Sn**	S
A-3	25.69	10.41	14.25	49.65
B-3	24.84	10.52	14.13	50.51
C-3	23.59	10.93	14.19	51.29
D-3	22.84	10.84	15.17	51.15

Measurement of thickness

The film width measurements attained by the surface profilometer shown that the film width by dip coating system was found to be as 3.65, 3.55, 3.40, 3.14µm respectively. It can be observed that thickness is proportionately improved with the Cu/(Zn+Sn) ratio.

Optical properties

The optical attributes were investigated using a UV–VIS Spectrophotometer to obtain transmittance spectra for various Cu/(Zn+Sn) ratios at wavelengths varies from 400 to 1200 nm. For low-temperature annealing, the CZTS films have been shown to have poor transmittance in the observable area. Small transmittance is intended for the CZTS absorber layer. Other optical properties showed variation, though allowing for comparable outcomes.

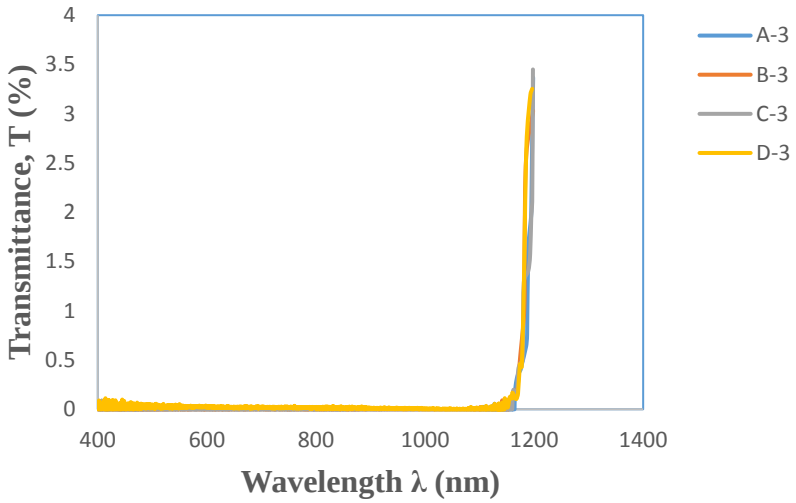

Fig.5.2.4. *Transmittance Vs Wavelength of CZTS Thin Film for 3 times deposited CZTS films.*

The absorption coefficient (α), of CZTS films, is calculated from the transmittance data as revealed in Fig5.2.5[31].

$$\alpha=\left(\frac{1}{d}\right)\ln\left(\frac{1}{T}\right) \qquad (5.2.1)$$

Where d is film width and T(%) is transmittance, the absorption coefficient is 5.4x104 cm^{-1}, 5.5x104cm^{-1}, 5.8xl04 $cm^{-1,}$ and 6.3x104 cm^{-1}correspondingly of A-3, B-3, C-3, and D-3 in the wavelength 400nm.

The optical band gap of CZTS films is obtained using Tauc's formula, as illustrated in Figure 5.2.6, as the absorption coefficient for diverse samples diminishes with growing thickness. [32].

$$(\alpha h\nu)=A(h\nu-Eg)^{m} \qquad (5.2.2)$$

Where A is a constant, the exponent "m" can take values ½ for direct allowed, 2 for indirect allowed, 3/2 for direct forbidden, and 3 for indirect forbidden. The band gap energy was determined by plotting $(ahv)^2$ versus the hv of Figure 6, thus, the direct band gaps (Eg) of CZTS annealed at 250°C during 15 minutes are obtained to be 1.50 eV, 1.49 eV, 1.48 eV, and 1.48 eV respectively of samples A-3, B-3, C-3, and D-3.

The band gap rises with the growth of film width and the ratios of Cu/(Zn+Sn). Finally, the calculated band gap energy of all samples corresponds well with that of previous records (1.4-1.6 eV)[33] but the band gap of sample A-3, B-3, C-3, D-3 are near to the optimal for solar cell devices.

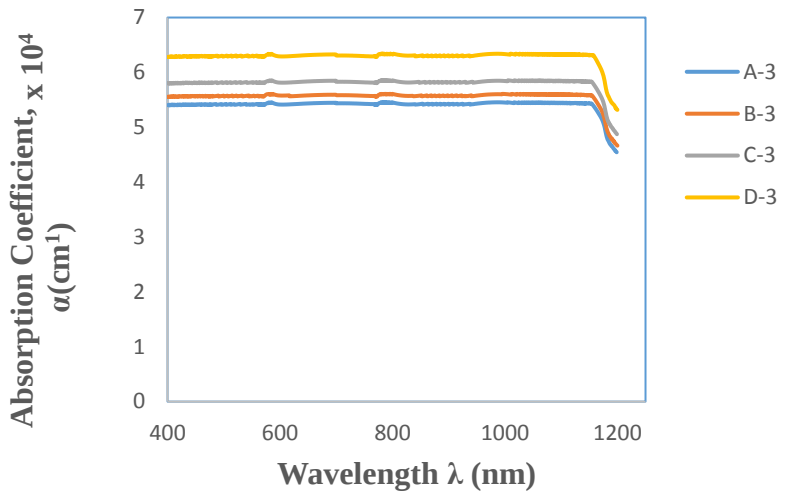

Fig.5.2.5. *Absorption coefficient of CZTS Thin Film for 3 times deposited,*

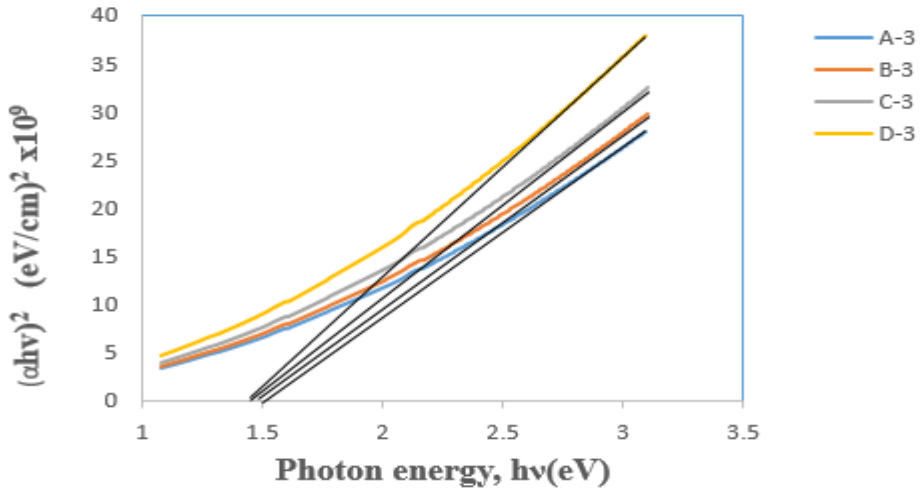

Fig.5.2. 6 *$(\alpha h\nu)^2$ in terms of hν, for 3 times deposited CZTS film.*

The extinction coefficient (k), is calculated as [34]

$k=\alpha\lambda/4\pi$ (5.2.3)

Fig.5.2.7 shows that the extinction coefficient for all three samples deposited in the wavelength array of 400nm to 1200nm spans between 0.18 and 0.55.

Curves appear to behave similarly when the value of Extinction coefficient, k grows with growing wavelength. Because Extinction coefficient, k is proportionate to absorption

(Eq.5.2.3). Additionally, because the CZTS has a higher absorption coefficient (10^4 cm^{-1}), Extinction coefficient, k will be high.

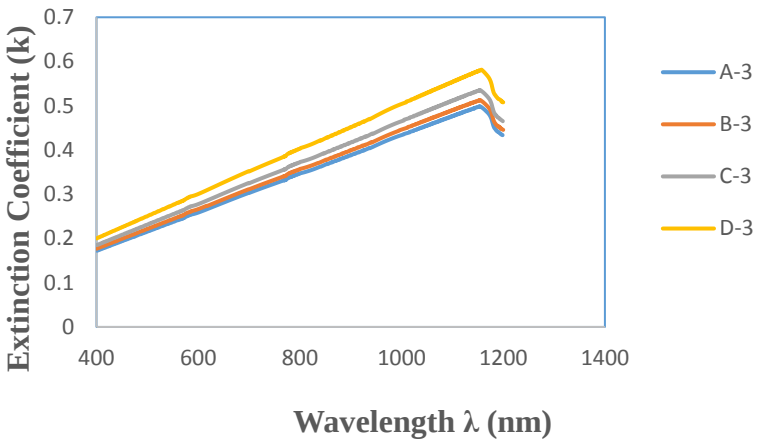

Fig.5.2.7 *Extinction coefficient of CZTS thin films for 3 times deposited*

Table 5.2.3. *Optical properties of CZTS with various Cu/(Zn+Sn) ratios*

Sample	A-3	B-3	C-3	D-3
Thickness (µm)	3.65	3.55	3.40	3.14
Optical band gap (eV)	1.50	1.49	1.48	1.48
Absorption coefficient (cm^{-1})	$5.4x10^4$	$5.5x10^4$	5.8xl0^4	$6.3x10^4$

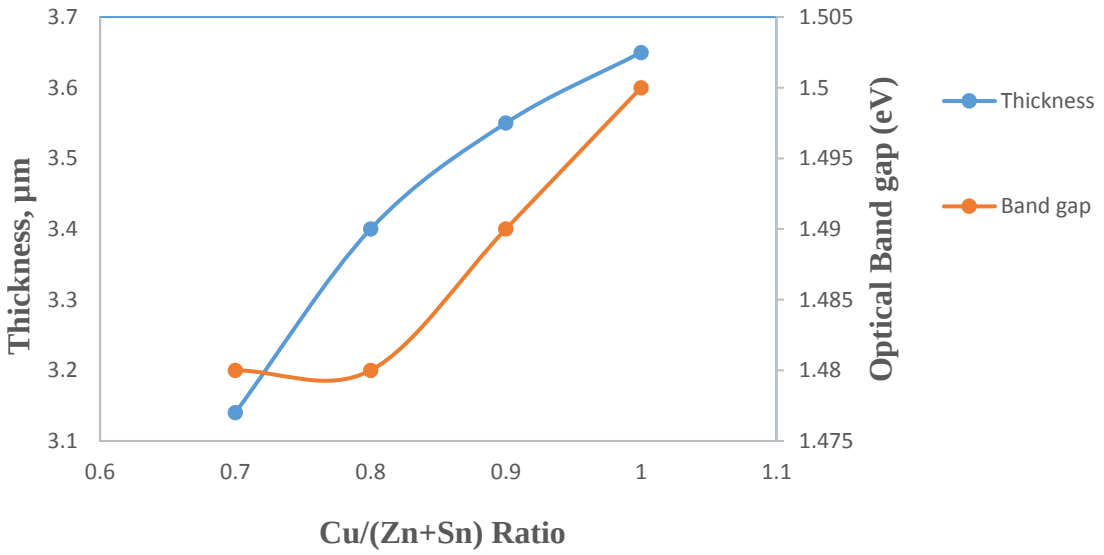

Fig.5.2.8*.Variation of thickness and band gap energy with Cu/(Zn+Sn) ratio.*

Here it is revealed that film thickness is proportionally enlarged with band gap energy (E_g) as a function of Cu/(Zn+Sn) Ratio. It is evident that most of the samples exhibited a band gap energy (E_g) close to ~1.5 eV, appropriate for photovoltaic devices.

5.2.3. Remarks

Merits

- CZTS absorber layer were successfully produced in this study by sol-gel method accompanying with the dip coating process.
- In perspective of XRD configuration, band gap energy, extinction coefficient, and absorption coefficient, the flexibility to alter the structural and optical attributes of CZTS thin film is explored adopting Cu/(Zn+Sn) precursor ratios varies from 0.7 to 1.0 and Zn/Sn and S/(Cu+Zn+Sn) ratios of 1.15 and 2 respectively.
- Dip coating of the precursors and annealing in an air atmosphere proved to be a facile method for developing kesterite CZTS thin films using soda lime glass as substarte.
- CZTS possesses a kesterite structure with a privileged orientation along the (112) plane, according to X-ray diffraction.
- Here the Cu/(Zn+Sn) ratio also varied and band gap energy was found around 1.4-1.5 eV which is suitable for photovoltaic applications.
- Structural and optical properties demonstrated better output when Cu/(Zn+Sn) ratio is increased.
- Here it is revealed that bandgap energy (E_g) upsurges with the film width.
- EDAX analysis reveals that Cu content drops and that of Zn rises, whereas Sn content is stable with concentration variations.

Limitations

- Because of the low-temperature annealing, the films had poor adherence to the substrates.
- A secondary phase was revealed by XRD analysis.
- Though bandgap energy (E_g) upsurges with the film width, absorption coefficient(α) reduces with the growth of thickness. As a result, the extinction coefficient (k) also drops with thickness because α is proportional to k.

To do next

- Sn content is stable for dip coated CZTS thin film in this study. But we need to focus on film adhesion to substarte to achieve good quality CZTS film. So a more sophisticated fabrication method needs to employ.
- Raman analysis is necessary for confirmation of Phase purity.
- Detailed analysis of topography and surface roughness of thin film can be revealed by influential surface analysis technique of AFM.

References

[1] H. Azimi, Y. Hou, C.J. Brabec," Towards low-cost, environmentally friendly printed chalcopyrite and kesterite solar cells,"Energy Environ. Sci. 7, 1829 ,2014.

[2] S. A. Kissin, "A Reinvestigation of the stannite (Cu2FeSnS4)—kesterite (Cu2ZnSnS4) pseudobinary system," Canadian Mineralogist, 27, 689–697, 1989.

[3] S. Schorr, “Structural aspects of adamantine like multinarychalcogenides,” Thin Solid Films, 515, 15, 5985– 5991, 2007.
[4] L. A. Wahab, M. B. El-Den, A. A. Farrag, S. A. Fayek and K. H. Marzouk. ," Electrical and optical properties of chalcopyrite compounds," J. Phys. Chem. Solids, Vol. 70, p. 604, 2009.
[5] J. Zhang, L. Shao, Y. Fu, and E. Xie, "Cu2ZnSnS4 thin films prepared by sulfurization of ion beam sputtered precursor and their electrical and optical properties," Rare metals, Vol. 25, p. 315, 2006.
[6] M. Liu, F. Huang, L. Chen and I. Chen., " A wide-band-gap *p*p-type thermoelectric material based on quaternary chalcogenides of Cu2ZnSn*Q*4Cu2ZnSnQ4 (*Q*=S,Se)," Appl. Phys. Lett., Vol. 94, p. 202103, 2009.
[7] K. Ito, "Copper zinc tin sulfide-based thin-film solar cells,"Wiley, Chichester, 2015.
[8] W. Wang, M. Winkler, O. Gunawan, T. Gokmen, T. Todorov, Y. Zhu, D. Mitzi, " Device Characteristics of CZTSSe Thin-Film Solar Cells with 12.6% Efficiency,"Advanced Energy Materials 4, 1301465, 2014.
[9] W. Shockley, H. Queisser," Detailed Balance Limit of Efficiency of p-n Junction Solar Cells," Journal of Applied Physics 32, 510-519, 1961.
[10] R.H. Bube, "Photovoltaic materials," Series on properties of semiconductor materials, 1 ,Imperial College Press, London, 1998.
[11] O. Galán, M. Courel, M. Rodriguez, D. Olarte, M. Frutis, E. Saucedo, " Electrical properties of sprayed Cu_2ZnSnS_4 thin films and its relation with secondary phase formation and solar cell performance," Solar Energy Materials and Solar Cells 132 , 557-562, 2015.
[12] B. Long, S. Cheng, Y. Lai, H. Zhou, J. Yu, Q. Zheng, "Effects of sulfurization temperature on phases and opto-electrical properties of Cu2ZnSnS4 films prepared by sol–gel deposition," Thin Solid Films 573 , 117-121, 2014.
[13] G. Ilari, C. Fella, C. Ziegler, A. Uhl, Y. Romanyuk, A. Tiwari, "Cu2ZnSnSe4 solar cell absorbers spin-coated from amine-containing ether solutions," Solar Energy Materials and Solar Cells 104, 125-130, 2012.
[14] E. Mkawi, K. Ibrahim, M. Ali, M. Farrukh, A. Mohamed, " Influence of triangle wave pulse on the properties of Cu_2ZnSnS_4 thin films prepared by single step electrodeposition," Solar Energy Materials and Solar Cells 130 (2014) 91-98.
[15] K. Patel, D. Shah, V. Kheraj, " Influence of deposition parameters and annealing on Cu2ZnSnS4 thin films grown by SILAR," Journal of Alloys and Compounds 622, 942-947, 2015.
[16] Y. Sun, K. Zong, H. Zheng, H. Wang, J. Liu, H. Yan, M. Zhu, " Ethylene glycol Based dipcoating route for the synthesis of Cu2ZnSnS4 thin film," Materials Letters, 92 , 195-197, 2013.
[17] G. Korotcenkov, "Handbook of Gas Sensor Materials: Properties, Advantages and shortcoming for applications ,2, new trends and technologies(Integreted analytical systems) , 2014.
[18] R. D’Angelo, C. L. Azanza Ricardo, A. Mittiga, P. Scardi, M. Leoni, " A water- and sulphurization- free solution route to $Cu_{2-x}Zn_{1+x}SnS_4$," J. Sol-Gel Sci. Technol. 72, 490-495, 2014.
[19] M. N. Rahaman, " Ceramic Processing," Boca Raton: CRC Press. pp. 242–244, 2007. ISBN 0-8493-7285 2.
[20] D Quéré, "FLUID COATING ON A FIBER". Annual Review of Fluid Mechanics. 31 (1): 347–384, 1999. ISSN 0066-4189. doi:10.1146/annurev.fluid.31.1.347.
[21] Kinjal Patel, VipulKheraj, Dimple V. Shah, C.J. Panchal, Neelkanth G. Dhere, “Cu2ZnSnS4 thin-films grown by dip-coating: Effects of annealing, ”JALCOM 36088 .
[22] P. Prabeesh, P. Saritha I.Packia Selvam and S N Potty “Fabrication Of CZTS Thin Films By Dip Coating Technique For Solar Cell Applications," Materials Research Bulletin, 86, 295-301, 2017
[23] A. Fischereder et al.," Investigation of Cu2ZnSnS4 formation from metal salts and thioacetamide," Chem Mater 22:3399, 2010.
[24] J. Madarasz, P. Bombicz, M. Okuya , S, Kaneko ," Thermal decomposition of thiourea complexes of Cu(I), Zn(II), and Sn(II)chlorides as precursors for the spray pyrolysis deposition of sulfide thin films," Solid State Ionics 439:141, 2001
[25] T. K. Chaudhuri, D. Tiwari,,"Earth-abundant non-toxic Cu2ZnSnS4 thin films by direct liquid coating from metal–thiourea precursor Solution," Sol. Energy Mater. Sol. Cells., 101,46-50, 2012.

[26] Y. Sun, K. Zong, H. Zheng, H. Wang, J. Liu, H. Yan, M. Zhu, "Ethylene glycol-based dip coating route for the synthesis of Cu_2ZnSnS_4 thin film," Mater. Lett. 92 ,195-197,2013.
[27] F. Aslan, A. Göktaş, A. Tumbul, "Influence of pH on structural, optical and electrical properties of solution processed Cu2ZnSnS4 thin film absorbers," Mater. Sci. Semicond. Process, 43,139-143, 2016.
[28] K. Patel, V. Kheraj, D. V. Shah, C. J. Panchal, N. G. Dhere, "Cu2ZnSnS4 thin-films grown by dip-coating: Effects of annealing," J. Alloys. Compd., 663 (2016) 842-847, 2016.
[29] ICDD, card no: 26-0575
[30] N. Nakayama, K. Ito, "Sprayed films of stannite Cu_2ZnSnS_4," Applied Surface Science 92 , 171-175, 1996.
[31] D.E. Milovzorov, AM. Ali, T. Inokuma, Y. Kurata, T. Suzuki, S. Hasegawa "Optical properties of silicon nanocrystallites in polycrystalline silicon films prepared at low temperature by p!asmaenhanced chemical vapor deposition" Thin Solid Films, 382 Z200 I. 47_55.
[32] J.Tauc, RGrigorivic , and A.vancu "Optical properties and Electronic structure of Amorphous Germanium," phys. Stat. sol .15,627, 1996.
[33] D. Seo , S. Lim, "Effect of sulfur and copper amounts in sol- gel precursor solution on the growth, crystal properties, and optical properties of Cu2ZnSnS4 films," J Mater Sci: Mater Electron, 2013. DOI 10.1007/sI0854-013-1314-z.
[34] S. Islam, M. A. Hossain, H. Kabir, M. Rahaman, M. S. Bashar, M. A. Gafur, A. Kabir, M. M. R. Bhuiyan, F. Ahmed, N. Khatun, "Optical, Structural and Morphological Properties of Spin Coated Copper Zinc Tin Sulfide Thin Films".Int. J. Thin. Fil. Sci. Tec. 4, 3, 155-161. 2015.
[35] S. Dilruba, T. P. Ananna, A. Sharmin, M. S. Bashar, Z. H. Mahmood,'Properties of Cu_2ZnSnS_4 Thin Films Fabricated by Dip Coating Technique for Solar Cell Application'; American International Journal of Research in Science, Technology, Engineering & Mathematics, 26(1), 170-178, 2019. http://www.iasir.net
[36] S. Dilruba, A. Sharmin, T. P. Ananna, Z. H. Mahmood, " Aspects ofNumeral Value of Cu_2ZnSnS_4 (CZTS) Absorber Layer Fabricated in Sol-gel Process by Dip Coating Technique ," 1st International Conference on Advances in Science, Engineering and Robotics Technology (ICASERT), 2019.

5.3. CZTS thin film with variance of annealing temperature and pressure

Driven by the rising energy consumption, solar power output has increased dramatically in recent time. Scientists in this discipline have focused on developing cost economic, high-efficiency solar devices. High power conversion efficiencies above 24.5% are achieved by the most extensively used Si-based solar cell [1]. Thin film solar cells are gaining popularity because of its high power conversion efficiencies (PCEs) and tunable and direct band gap (E_g), as well as the fact that they employ less material than traditional Si-based solar cells. Solar cells founded on copper indium selenide (CIS), copper indium gallium selenide (CIGS), and cadmium telluride (CdTe) have greater PCEs of up to 22%, but amorphous silicon (a-Si) thin film possesses a power conversion efficiency (PCE) of 13.6% [2,3]. The p-type chalcogenide semiconductor Cu_2ZnSnS_4 (also known as CZTS), that is produced from the chalcopyrite structure of CIGS by substituting In and Ga with the cost effective and plentiful material Zn and Sn, is another promising solar absorber material [4,5,6,7]. This material also has the benefit of not containing the hazardous metal cadmium. CZTS solar cells have a lot of potential since they have high absorption coefficients[8] ($>10^4$ cm^1) and an adjustable band gap (E_g~1.45–1.6 eV) that improve the PCE [9].

Vacuum and non-vacuum (i.e., solution-based) deposition process for generating CZTS films has been documented. The employment of vacuum-based technologies including thermal evaporation,[10] sputterings[11,12] electron beam evaporation,[13] and pulsed laser deposition (PLD) [14,15] raises manufacturing costs while producing high-quality thin films. Solution-based processes such as sol-gel dip16 and spin [17] coating, chemical bath deposition,18 screen printing,19,20 spray pyrolysis21and electrodeposition,22and sequential ionic layer adsorption and reaction(SILAR) can reduce manufacturing costs [23].

Yan et al. [24] observed heterojunction heat exposer of a CZTS cell allowed for a PCE of >10%. Green et al. [25] used a CZTS-based solar cell to attain a PCE of 11% and an open circuit voltage of 730.6 mV. Wang et al. used a pure hydrazine solution method to build a Cu_2ZnSnS_4 solar cell with the best PCE of roughly 12.6 % [26] According to optoelectronic simulations, a silver mixed CZTS (ACZTS) cell with a CdS/ACZTS/CZTS/ITO structure may achieve a maximum efficiency of 17.59 % at 550 nm and an open-circuit voltage of 940 mV [27]. Nonetheless, the PCEs of CZTS solar cells have not reached the levels of CIGS and CdTe solar cells till now.CZTS could accomplish a maximum PCE of 32.2 %, according to the Shockley–Queisser theory [28]. Therefore, further study into CZTS solar cells is desirable to enhance their PCEs, as a result, CZTS solar cells would play a larger part in energy generation in the future.

Though the other direct band gap absorbers such as CdTe, CIS, and CIGS/Se successfully scores in the PV market, the use of kesterite in solar cells has achieved a lot of interest. CZTS absorber has higher defect levels, resulting in short carrier lifetimes, hence great effort has gone into constructing an optimal device structure that can accommodate them. The application of an ultrathin crystalline absorber coating is required when using minimized material. The problem of optical losses [29] and the use of light trapping [30,31] can help CZTS films achieve higher PCE.

The present work is unique in that it optimizes post-annealing parameters after growing a quaternary CZTS thin film on a translucent substrate (SLG) with a solitary sputtering apparatus at 200°C and a sensitive CZTS target. The proper absorber layer width for light trapping might be found when developing a highly efficient solar cell considering the absorption length along with the carrier diffusion length [32] This layer thickness has an impact on the overall design of the device [29]. The current research shows that modifying the annealing factors (pressure and temperature) to achieve CZTS films of the correct film width for usage in PV cells is effective. Sulfurization is a crucial step because sulfur deficiency is common in most circumstances, making the system expensive. For some deposition procedures, sulfurization is required to obtain the anticipated stoichiometry. Furthermore, the selenization approach may offer certain benefits in terms of producing smooth, uniform, and compact films. However, in order to use a low-cost technique, the selenization and sulfuration processes are avoided. CZTS is a quaternary compound with several binary and ternary phases that must be handled in order to achieve solely the pure phase. Furthermore, when attempting to develop a greatly textured CZTS film with adequate coverage, various factors are taken into account, including grain size, surface smoothness, roughness, stoichiometric ratio, tin volatility, and pinholes in the layer formed. The crystal structure, morphology, composition, and optical characteristics of post-annealed CZTS thin film is examined in depth in order to truly comprehend and enhance CZTS thin film growth and phase formation. This knowledge will assist researchers create CZTS thin films with the best stoichiometry and photovoltaic characteristics for employing in PV devices. This study has been published in AIP Advances in 2020 [56].

5.3.1. Growth of CZTS film by sputtering

SLG substrates (3×3 cm^2) are splashed with detergent, scrubbed, and treated in an ultrasonic bath for 10 minutes each in methanol, ethanol, acetone, and deionized water. After that, the glass substrates are disinfected in deionized water and dehydrated. A radiofrequency (RF) magnetron sputtering apparatus (NSC-4000, NANO-MASTER, Inc., USA) is utilized to fabricate the quaternary CZTS, which is operated at 80W for 2 hours. Kurt J. Lesker Co. (USA) produced the target in this study, which was 2" in diameter and 0.125" width. The target's purity is 99.99 % and its composition is 2:1:1:4 C:Zn: Sn:S. Concerning the target compund (cathode) and the substrate (anode), a voltage is introduced. The process gas is ionized by electrons from the target's surface, causing in the generation of a plasma. To avert background gases from engaging with the film or sputter target, the chamber pressure was adjusted as much as feasible. Sputtering is used to develop a thin coating on the substrate by carefully controlling the partial pressures of the reactive gases. The spaceamid the target and the base is secured to 7 cm. Precursors are coated on the substratewith a sputter gun at a pressure applied of 4.5 mTorr while the base pressure reaches 6.3×10^{6} Torr. Throughout the procedure, a 5 SCCM Ar flow is maintained. To enhance film consistency and maximum utilization of target material, the substrate holder is revolved at 20 rpm. During accumulation, the chamber's temperature is kept at 200°C.

A two-stage heat exposer technique for CZTS has been reported, where precursor is generated at a base temperature of <300 °C and annealed at a higher temperature (about 500 °C).[15] In this study, post annealing is carried out inside a tube furnace with two distinct temperatures, 470°C and 560°C, in a N_2 environment (GSL-1100X, MTI Corporation, USA). For 30 minutes,

CZTS filmsare kept at the chosen temperature at four different base pressures (150, 250, 350, or 450 Torr). The samples were then allowed to chill gradually inside the annealing chamber.

The annealing conditions and usual film width of the film is determined with a surface profilometer and SEM are listed in Table 5.3.1. The thickness of the samples annealed at varied circumstances did not differ much. An average thickness estimated from 5 values in shown in the table. An SEM image of a cross-section of a CZTS thin film is shown in Fig.5.3.1.

Table 5.3.1*.CZTS thin film annealed under diverse conditions*

Sample	Annealing temperature (°C)	Base pressure for annealing(Torr)	Filmwidth via surface profilometer (μm)	Filmwidth Via SEM (μm)
S-560-150	560	150	2.112	2.156
S-560-250		250		
S-560-350		350		
S-560-450		450		
S-470-150	470	150		
S-470-250		250		
S-470-350		350		
S-470-450		450		

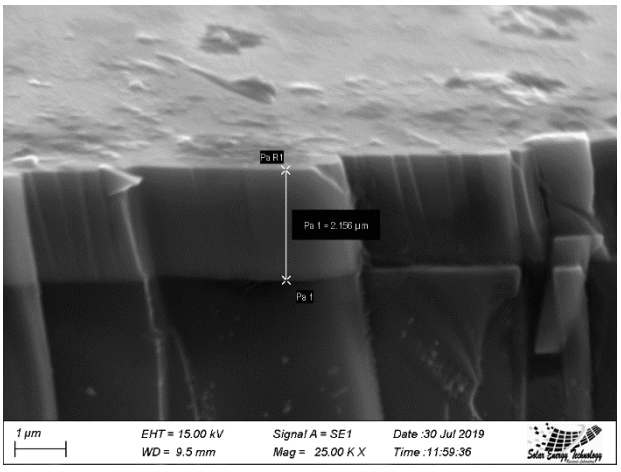

Fig.5.3.1. *Exploitation of SEM to obatin filmwidth of CZTS sample S-560-450.*

5.3.2. Results and Discussion

Structural properties

The fabricated CZTS films that were developed were amorphous. Annealing process provides with polycrystalline CZTS films with a kesterite crystal arrangement. The annealing process yields the crystal structure to migrate from a non-equilibrium to a more thermodynamically stable state. Figure 5.3.2 reveals the XRD configuration of CZTS films annealed at numerous circumstances (JCPDS-004751). All of the samples have a strong (112) peak and weaker (200), (220), and (312) peaks in their XRD profiles. It's worth noticing that the peak positions remain constant regardless of annealing settings, demonstrating that the CZTS phase is steady.

From XRD analysis of thin films annealed at 470°C, Bragg peaks from the $Cu_{2-x}S$ (x=1) phase are found (JCPDS-06-0464). Although the existence of a $Cu_{2x}S$ contaminated phase suggests a noteworthy growth in Cu ratio in the CZTS film, it favors single-phase CZTS development. This impurity was found in CZTS films fabricated at 350–400°C, according to Sun et al. [33] Tang et al. discovered a Cu_xS phase diffraction peak in a film that has been sulfurized at 450°C. [34] When the CZTS film is annealed at 500, 525, or 550°C, the peak vanished. Similarly, Bragg peaks from a CuS phase are observed in the current study for films annealed at a higher temperature (560°C). It's probable that the Cu:Zn:Sn:S ratio has approached the ideal stoichiometric condition at this annealing temperature, reducing impure phases like CuS. Consequently, when the annealing temperature is raised, the Bragg peaks vanish.[35]

The XRD configuration of the CZTS thin film displays Bragg peaks [36] in the (112), (200), (220), and (312) planes, as shown in Fig.5.3.3[16,17]. In addition to the two kesterite peaks evident in Fig. 5.3.2 at 2 = 38.07° and 52.06°, Fig. 5.3.3 shows two more kesterite peaks at 2θ = 38.07° and 52.06°. This picture also reveals that the (112) peak of S-560- 450 is intensed than S-470- 450's, demonstrating that peak acuity rises with annealing temperature, which is consistent with earlier observations [33,37].

Furthermore, as crystallite size decreases, the full width at half maximum (FWHM) of a diffraction peak surges. The Scherrer formula can be utilized to estimate the typical crystallite size from the FWHM of the furthermost strong peak (112)[38] as

$$D = \frac{k\lambda}{\beta\cos\theta} \qquad (5.3.1)$$

here β is the FWHM in radians, λ is the wavelength and k is Scherrer constant. The estimated average crystallite size, *D*, is listed in Table 5.3.2. The films annealed at a higher temperature (560°C; samples S-560-150, S-560-250, S-560-350, and S-560-450) strongly indicate lesser FWHMs and greater crystallite sizes compared to that of the films annealed at a lesser temperature (470 °C). The final structure and surface texture is strongly influenced by the crystallization temperature. As the temperature rises, so does the mobility and surface diffusion of the fabricated copound, allowing it to travel and amalgamate into larger islands, resulting in a bigger crystallite size, *D* and a lesser FWHM. The dislocation density is likewise lesser for films annealed at a higher temperature, indicating that they possess lesser lattice defects provided with less stress [39,40]. The crystallite size, on the other hand, does not tend to change appreciably as the base pressure rises.

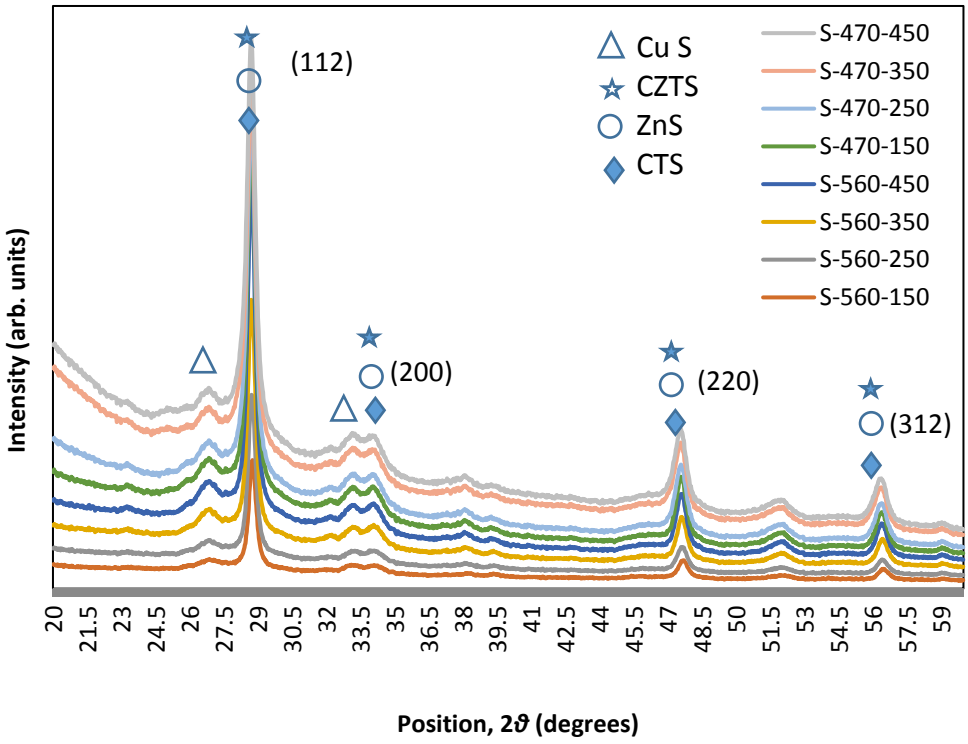

Fig.5.3 2. *XRD profiles of CZTS films annealed under diverse conditions.*

The number of dislocations in a unit volume of a crystal is called the dislocation density and estimated as

$$\delta = \frac{1}{D^2} \qquad (5.3.2)$$

In nanostructured materials, crystal dislocation enhances strain. The crystallite size and lattice strain is invariant in the Williamson–Hall isotropic strain model (W-HISM) [42]. When the crystallites are really tiny, the Williamson–Hall anisotropic uniform deformation energy density model (W-HUDEDM) predicts that there will be more volume defects near grain borders. If there is a volume defects inside a crystal structure, a surface tension is generated. This surface tension creates internal pressure which results in stress field inside a crystal. Thus strain is appeared. For the sake of simplicity, the thin film's strain, ε is quantified as [41]

$$\varepsilon = \frac{\beta \cot\theta}{4} \qquad (5.3.3)$$

Because their lattice characteristics are so close, it's hard to differentiate between tetragonal CTS, cubic CTS, sphalerite (ZnS), and CZTS in the lab. 36.43. The Raman spectra in the wave number region 140–495 cm^{-1} was acquired for a CZTS film at ambient temperature to identify classic difficulties of phase separation (secondary phases); Raman spectrum is exposed in Fig. 5.3.4. It has distinct peaks at 288, 334, and 361 cm^{-1}, which correlate to polycrystalline kesterite films' reported distinctive peaks[44]. Furthermore, there is no additional peaks attributable to the occurrence of other materials e.g. SnS_2 (314 cm^{-1}), Cu_2SnS_3 (352 and 374 cm^{-1}), cubic ZnS (352

and 275 cm^{-1}), or orthorhombic Cu_2SnS_3 (318 cm^{-1}), indicating that the sample is solitary phase CZTS [45,46].

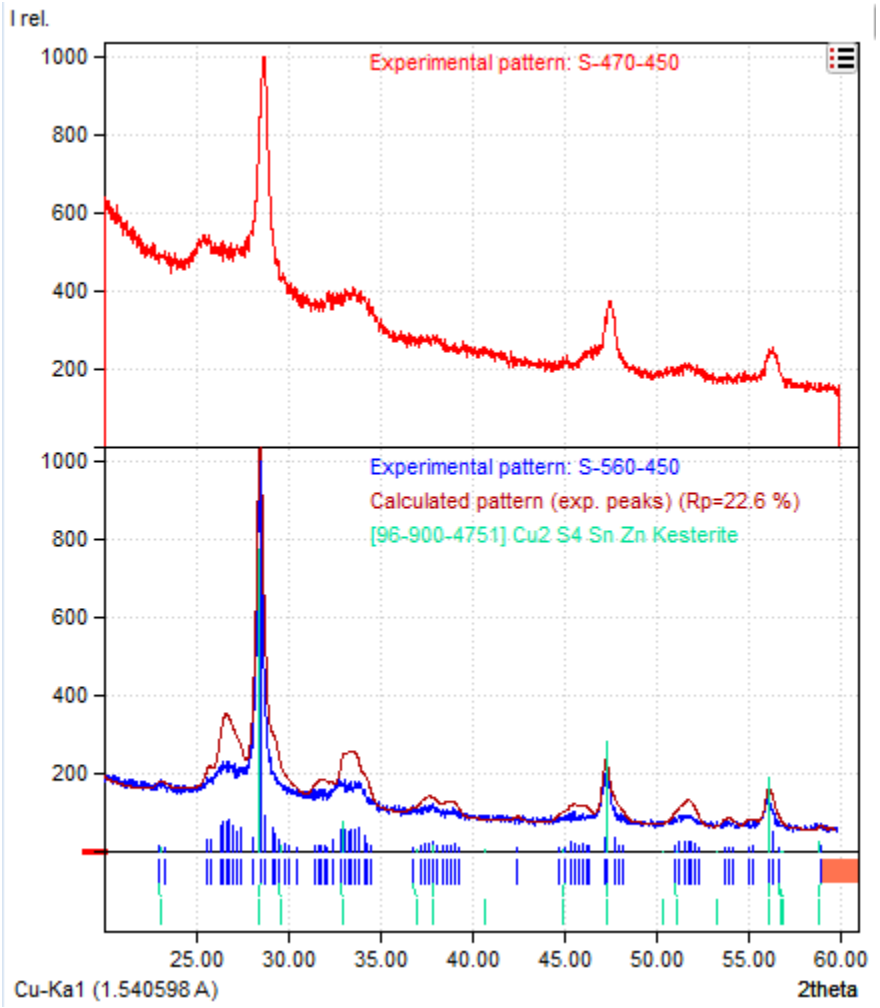

Fig.5.3.3. *X-ray diffraction configuration of two CZTS thin film(JCPDS 00-4751) annealed at the same base pressure (450 Torr) but at different temperatures: 470°C (top) and 560°C (bottom).*

Table 5.3.2. *Microstructural parameters of the CZTS thin film samples in the (112) plane*

Sample	*d* spacing, Δ (Å)	FWHM,*β* (°)	Crystallite size, *D* (nm)	Dislocation density,δ (10^{15}line/m^2)	Strain, *ε* (× 10^{-3})
S-560-150	3.162	0.38	21.32	2.20	6.60
S-560-250	3.096	0.41	19.78	2.55	6.97
S-560-350	3.092	0.466	17.41	3.30	7.91
S-560-450	3.116	0.404	20.07	2.48	6.91
S-470-150	3.159	0.524	15.46	4.18	9.10
S-470-250	3.147	0.488	16.61	3.63	8.43
S-470-350	3.161	0.514	15.76	4.03	8.93
S-470-450	3.119	0.564	14.38	4.84	9.66

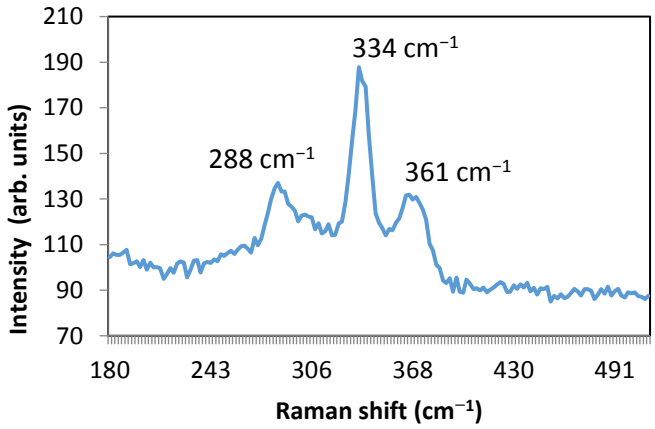

Fig.5.3.4. *Raman spectrum of a CZTS thin film sample (S-560-450) annealed at 560°C.*

Morphology

One of the most significant features for understanding surface phenomena is thin film morphology. AFM micrographs of a 25μm^2 area of the surface of each annealed CZTS film are shown in Fig.5.3.5.The sputtered films possess similar surface topographies and film width, and the Volmer–Weber mode was the dominating growth mode, according to these images. The films have significantly better coverage comparing to the film produced by using the spin coating method.Figure 5.3.6 depicts the fluctuation in the root mean square (RMS) surface roughness of the thin film taken from an AFM picture with different annealing pressure and temperature. The surface roughness increases dramatically as the annealing temperature rises, as shown in this

graph. When the annealing temperature is 470°C, the surface roughness hardly alters. But for the samples annealing at 560°C, it changes dramatically when the base pressure varies between 350 to 450 Torr. The phase transition of the CZTS film is shifted when the annealing temperature is altered [37]. The average grain size grows as the annealing temperature rises [47]. Grain coalescence and restructuring occur at high temperatures due to enhanced surface mobility. Based on AFM measurements, Figure 5.3.5(i) depicts the topography of the sample S-470-150. Table 5.3.2 illustrates that as the temperature rises above 500°C, the grain size expands.

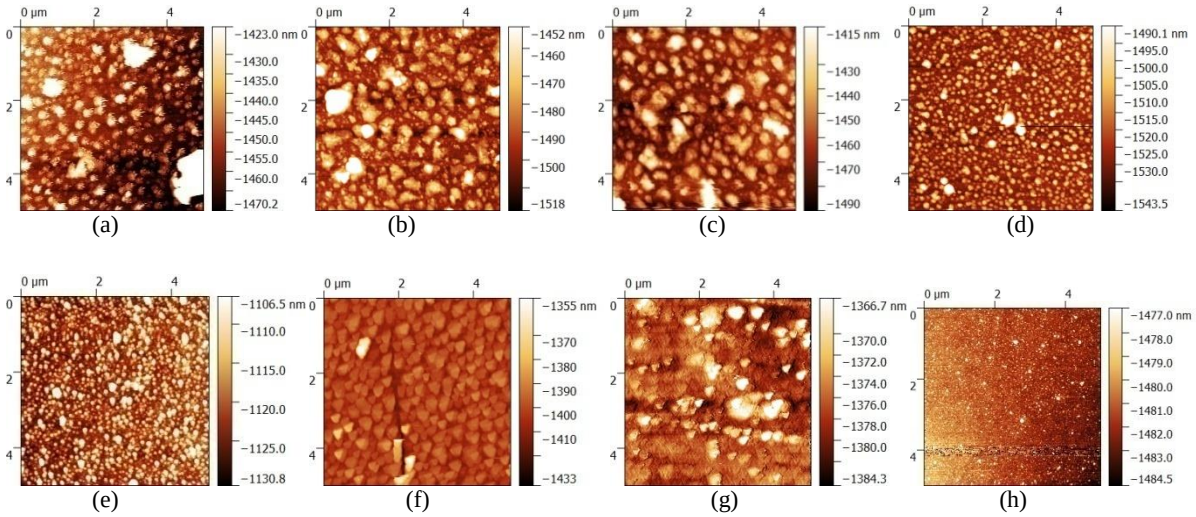

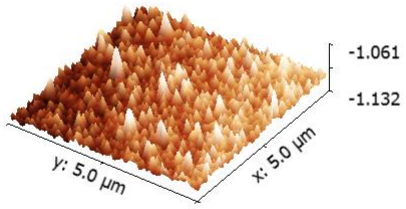

Fig.5.3.5. *AFM images of CZTS thin film samples: (a) S-560-150, (b) S-560-250, (c) S-560-350, (d) S-560-450, (e) S-470-150, (f) S-470-250, (g) S-470-350, (h) S-470-450, (i) AFM topographic image of the CZTS thin film sample S-470-150*

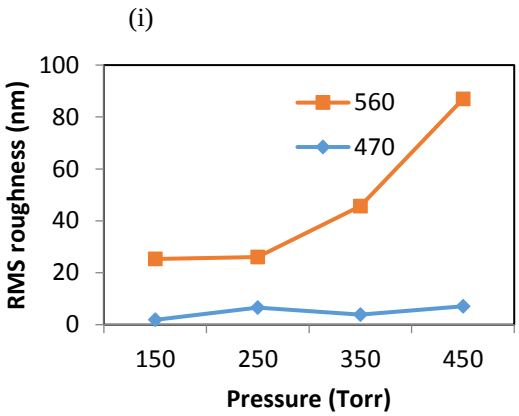

Fig. 5.3.6.*Deviation in the RMS roughness with annealing pressure and temperature (560 and 470 °C).*

The grain dimension and film roughness of the sputtered CZTS film rises with rising annealing temperature, as demonstrated in the AFM pictures in Fig. 5.3.6. However, small cavities were discovered on the film's surface. This was because of the increased annealing temperature which results in a considerable amount of Sn reduction [48]. Nonetheless, annealing process seems to be helpful in improving the crystallinity and phase development of the film, which is favorable for module features. According to our findings, CZTS thin films could be annealed at a temperature of 500°C as it facilitates larger grain and even power conversion efficiency.

Composition analysis

Table 5.3.3 shows the atomic percentages (at. %) of the CZTS film evaluated by employing EDX. The ratio as Cu:Zn:Sn: S=2:1:1:4 is the theoretical stoichiometry of CZTS. Table 5.3.3 shows that the films are Cu sufficient and Zn deficient in comparison to the anticipated stoichiometry. Cu-sufficient and Zn- deficient conditions are ideal for the formation of solitaryphase CZTS films, according to Chen et al.[49,50] Cu is a lighter element, hence it possess faster flow rate comparing to that of Zn, resulting in Cu enrichment in the CZTS film[33]. In CZTS thin films, Zn and S are comparatively combustible and have inferior melting temperatures comparing to other two components, resulting in Zn and S shortage[51]. However, without any sulfurization, the current samples' sulfur-to-metal ratios are consistent with those reported in prior studies [45,46]. The films annealed at 560°C (S-560-150, S-560-250, S-560-350, S-560-450) are Sn poor than the other films. At higher crystallization temperatures, there is a greater loss of volatile components, which shows a substantial impression on the ultimate composition. The likelihood of diffusion via substrate surfaces, which could offer the development of solid solutions, is another downside of using a significantly higher annealing temperature. According to Weber *et al.*,[48] the evaporation rates from various phases upsurge as following arrangement: Cu_2ZnSnS_4<Cu_4SnS_4<Cu_2SnS_3<SnS. At temperatures of 550 °C and above, SnS is rapidly degraded from CZTS thin films. Torodov et al., instead, found that CZTS absorber films with a Zn-sufficient but Cu-deficient composition has the maximum power conversion efficiency [52].

Table 5.3.3*. Chemical composition data for the annealed CZTS thin films.*

Sample	Cu (at.%)	Zn (at.%)	Sn (at.%)	S (at.%)	Zn/Sn	Cu/(Zn+Sn)	S/(Cu+Zn+Sn)
S-560-150	28.98	10.04	10.2	50.78	0.98	1.43	1.03
S-560-250	28.23	10.44	9.57	51.76	1.09	1.41	1.07
S-560-350	29.2	8.66	11.4	50.74	0.76	1.46	1.03
S-560-450	29.66	9.12	9.34	51.88	0.98	1.61	1.08
S-470-150	27.01	12.07	12.38	48.54	0.97	1.10	0.94
S-470-250	28.21	11.81	11.09	48.89	1.06	1.23	0.96
S-470-350	28.3	8.01	11.52	52.17	0.70	1.45	1.09
S-470-450	28.41	10.25	12.73	48.61	0.81	1.24	0.95

Optical properties

In the visible region, the UV-Vis absorption spectra of the CZTS thin film shown in Fig.5.3. 7 reveal that the films have a higher optical absorbance and a larger absorption coefficient (disregarding reflection and transmission losses). The phenomena of the absorption related transition might be established employing the absorption coefficient's classic equation [21]

$$\alpha = \frac{A(h\nu - E_g)^n}{h\nu} \qquad (5.3.4)$$

In this case, n=1/2 for a direct transition and n=2 for an indirect transition.. The absorption coefficient, α could be derived using[53]

$$I = I_o e^{-\alpha d}, \text{ or}$$

$$\alpha = 2.303\left(\frac{A}{d}\right) \qquad (5.3.5)$$

*I*s the transmitted intensity, I_o is the incident intensity, *A* is the absorbance, and *d* is the film width. The absorption coefficients of the CZTS film is expected to be larger than 10^4 cm^{-1}, which is reliable with earlier records [17,21,23]. Evaluating the materials' optical absorption allows us to investigate features like band structure, refractive index, and high-frequency dielectric constant [46], all of which have a noteworthy impression on PV cell efficiency.

The optical band gap energy influences how much of the solar spectrum is absorbed by a solar cell. Extrapolating the linear component of the $(\alpha h\nu)^2$ versus $h\nu$ plot yields the band gap energy E_g for direct transitions, and the determined band gap energies of CZTS film are provided in Table 5.3.4. The band gap energy of the samples have been measured to range between 1.47 and 1.51 eV. Variances in the homogeneity and crystallinity of the samples, that lead to differences in crystallite size among the samples, account for a major part of the variation in band gap [54]. The computed band gap values for solar cells are adjacent to the desirable band gap[55].

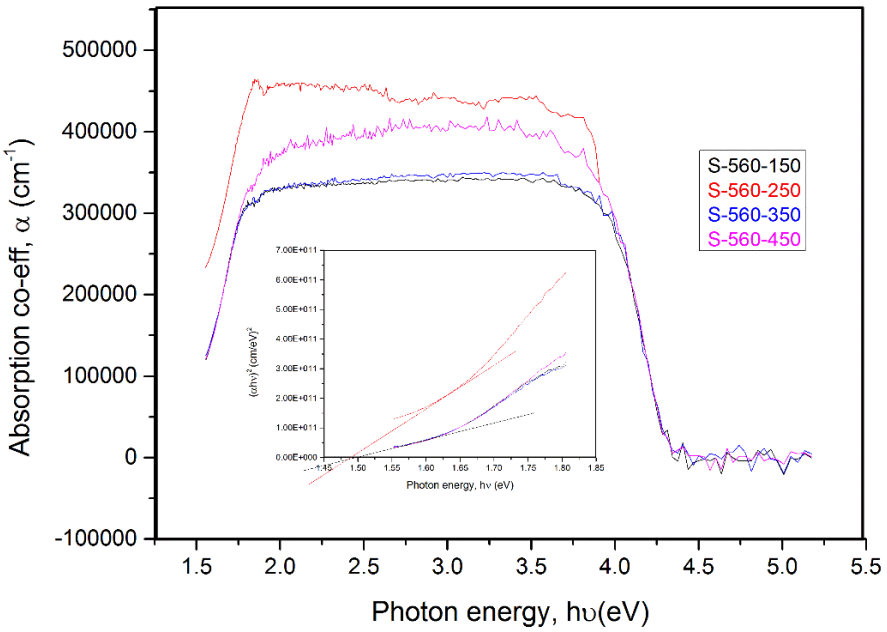

(a)

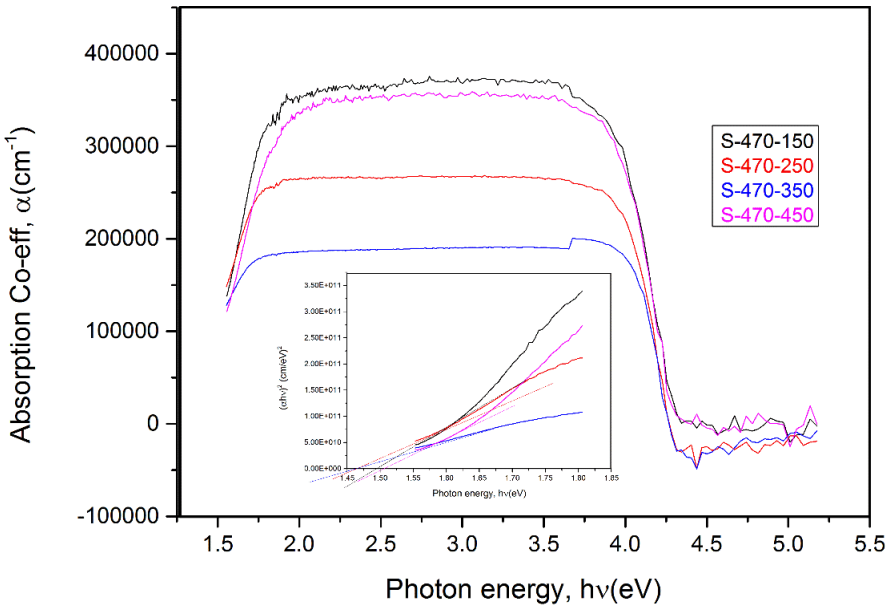

(b)

Fig. 5.3.7. *Absorption coefficient (α) versus photon energy plots and Tauc plots (inset) for CZTS thin films annealed at (a) 560 °C and (b) 470 °C.*

Table 5.3.4*. Estimated values of the band gap energy (E_g), refractive index(n), and dielectric constant for the CZTS thin film annealed under diverse conditions.*

Sample	Band gap E_g (eV)	Refractive index *n*	High-frequency dielectric constant ε_∞	Dielectric constant ε_o
S-560-150	1.5	2.913	8.485	13.900
S-560-250	1.48	2.923	8.542	13.962
S-560-350	1.5	2.913	8.485	13.900
S-560-450	1.5	2.913	8.485	13.900
S-470-150	1.49	2.918	8.514	13.931
S-470-250	1.47	2.928	8.571	13.992
S-470-350	1.47	2.928	8.571	13.992
S-470-450	1.51	2.908	8.457	13.869

The thin film's refractive index (n) is a crucial feature to achieve the potential of total internal reflection within the PV cell [31] The Moss relation was used to compute the refractive index of CZTS thin films [50]

$$E_g n^4 = k \qquad (5.3.6)$$

k is a constant with a value of 108 eV.

When a material is polarized under the presence of external electric field, its dielectric characteristics refer to its ability to obstruct electron transport. To build effective solar devices, semiconductors with appropriate dielectric constants are required.

The high-frequency dielectric constant,ε_∞ is calculated as[17,23]

$$\varepsilon_\infty = n^2 \qquad (5.3.7)$$

The static dielectric constant,ε_o,[23] is calculated using the relation

$$\varepsilon_o = 18.52 - 3.08E_g \qquad (5.3.8)$$

Table 5.3.4 shows band gap, refractive index, and dielectric constant data for CZTS thin films annealed under various circumstances, which are all in fair accord with earlier records.[23]

5.3.3. Remark

Merits

- This study presents the sputtering of thin (2000 nm) Se-free kesterite CZTS films with no noticeable phase separation or voids.

- After post-annealing treatment, sample properties were examined to investigate the best annealing conditions for CZTS thin films.The appearance of a prominent peak at 334 cm^{-1} and other weaker peaks at 288 and 361 cm^{-1} in the Raman spectra confirmed that the sputtered films are definitely kesterite.
- The XRD spectra of thin films annealed at 560 °C showed sharper peaks than those annealed at 470 °C, indicating that the CZTS films annealed at 560 °C had larger crystallites compared to those annealed at 470 °C. The grains in the films are dense, and as the annealing temperature rises, agglomeration increased, increasing the absorption coefficient as well.
- In addition, the deposiiton base pressure plays important role in film morphology. The RMS roughness of thin films annealed at 560 °C changed dramatically when the base pressure was increased from 350 to 450 Torr, according to AFM investigation.
- The CZTS films are Cu and S sufficient even without sulfurization but Zn and Sn deficient, according to EDX analysis. At temperatures above 500 °C, considerable SnS losses were discovered. This leads to the development of cavities or voids on the film and disrupts the stoichiometry of the film.
- The direct band gap energies (E_g) of the thin films spanned amid 1.47 to 1.51 eV, according to UV-Vis absorption spectra.
- Nonetheless, **with post-annealing parameter modification**, a much better CZTS film was achieved in this study, which could permit increased production efficiency. We may deduce that films annealed at higher temperatures (560° C) have superior crystallinity, as expected.

References

[1] J. Zhao, A. Wang, and M. A. Green, "24.5% efficiency silicon PERT cells on MCZ substrates and 24. 7% efficiency PERL cells on FZ substrates," Prog. Photovoltaics**7**(6), 471–474, 1999.

[2] H. Sai et al.,"Triple-junction thin-film silicon solar cell fabricated on a periodically textured substrate with a stabilized efficiency of 13.6%," Appl. Phy. Lett., **106**, 213902 , 2015.

[3] M.A. Green et al., "Solar cell efficiency tables (version 50),"Prog. Photovoltaic, **25**(7), 668–676 ,2017.

[4] M. Jiang and X. Yan, "Cu_2ZnSnS_4 thin film solar cells: present status and future prospects," in Solar Cells—Research and Application Perspectives, edited by A. Morales-Acevedo, Intech, London, 107–143, 2013.

[5] X. Song, X. Ji, M. Li,W. Lin, X. Luo, and H. Zhang, "A review on development prospect of CZTS based thin film solar cells," Int. J. Photoenergy, **2014**, 613173 ,2014.

[6] A. Haddout, A. Raidou, and M. Fahoume, "A review on the numerical modeling of CdS/CZTS-based solar cells," Appl. Phy. A, **125**, 124, 2019.

[7] A. Kowsar, et al., "Progress in major thin-film solar cells: growth technologies, layer materials and efficiencies," Int. J. Renew. Energy Res., **9**, 2, 579–597, 2019.

[8] D. B. Mitzi, O. Gunawan, T. K. Todorov, K. Wang, and S. Guha, "The path towards a high-performance solution-processed kesterite solar cell," Sol. Energy Mater. Sol. Cells, **95**, 1421–1436, 2011.

[9] T. Maeda, S. Nakamura, and T. Wada, "Electronic structure and phase stability of In-free photovoltaic semiconductors, $Cu_2ZnSnSe_4$ and Cu_2ZnSnS_4 by first-principles calculation," MRS. Proc., **1165**, 1165-M04-03,2011.;https://doi.org/10.1557/PROC-1165-M04-03.

[10] B. Shin, O. Gunawan, Y. Zhu, N. A. Bojarczuk, S. J. Chey, and S. Guha, "Thin film solar cell with 8.4% power conversion efficiency using an earth-abundant Cu_2ZnSnS_4 absorber," Prog. Photovoltaics, **21**(1), 72–76 ,2013.

[11] F. Jiang, H. Shen, and W. Wang, "Optical and electrical properties of Cu_2ZnSnS_4 film prepared by sulfurization method," J. Electron. Mater.**41**(8), 2204–2209 ,2012.
[12] N. Muhunthan, O. P. Singh, S. Singh, and V. N. Singh, "Growth of CZTS thin films by cosputtering of metal targets and sulfurization in H_2S,"Int. J. Photoenergy, 752012 ,2013.
[13] H. Katagiri et al., "Development of thin film solar cell based on Cu_2ZnSnS_4 thin films," Sol. Energy Mater. Sol.Cell., **65**, 141–148, 2001.
[14] A. V. Moholkar et al., "Development of CZTS thin films solar cells by pulsed laser deposition: Influence of pulse repetition rate," Sol. Energy **85**, 1354–1363 , 2011.
[15] A. Cazzaniga et al., "Ultra-thin Cu_2ZnSnS_4 solar cell by pulsed laser deposition," Sol. Energy Mater. Sol. Cells **166**, 91–99 ,2017.
[16] S. Dilruba, T. P. Ananna, A. Sharmin, M. S. Bashar, and Z. H. Mahmood, "Properties of Cu_2ZnSnS_4thin films fabricated by dip coating technique for solar cell application," AIJRSTEM **26**, 1, 170–178 ,2019.
[17] A. Sharmin, M. S. Bashar, S. Tabassum, and Z. H. Mahmood,"Low cost and sol-gel processed earth abundant Cu_2ZnSnS_4thin film as an absorber layer for solar cell: Annealing without sulfurization,"IJTFST, **8**,2, 65–74, 2019.
[18] N. M. Shinde, C. D. Lokhande, J. H. Kim, and J. H. Moon, "Low cost and large area novel chemical synthesis of Cu_2ZnSnS_4 (CZTS) thin films," J. Photochem. Photobiol. A, **235**, 14–20 , 2012.
[19] X. Sheng, L. Wang, Y. Tian, Y. Luo, L. Chang, and D. Yang, "Low-cost fabrication of Cu_2ZnSnS_4 thin films for solar cell absorber layers," J. Mater. Sci.: Mater. Electron., **24**(2), 548–552 ,2013.
[20] W. Wang, H. Shen, F. Jiang, X. He, and Z. Yue,"Low-cost chemical fabrication of Cu_2ZnSnS_4microparticles and film," J. Mater. Sci.: Mater. Electron.,**24**(6), 1813–1817, 2013.
[21] N. M. Shinde, R. J. Deokate, and C. D. Lokhan, "Properties of spray deposited Cu_2ZnSnS_4(CZTS) thin films,"J. Anal. Appl. Pyrol., **100**, 12–16 ,2013.
[22] M. Jeon, T. Shimizu, and S. Shingubara, "Cu_2ZnSnS_4 thin films and nanowires prepared by different single-step electrodeposition method in quaternary electrolyte," Mater. Lett., **65**, 15–16, 2364–2367,2011.
[23] J. Henry, K. Mohanraj, and G. Sivakumar, "Electrical and optical properties of CZTS thin films prepared by SILAR method," J. Asian Ceram. Soc.**4**,1, 81–84 , 2016.
[24] Yan et al., "Cu_2ZnSnS_4 solar cells with over 10% power conversion efficiency enabled by heterojunction heat treatment," Nat. Energy,**3**,9, 764–772 ,2018.
[25] M. A. Green, Y. Hishikawa, E. D. Dunlop, D. H. Levi, J. Hohl-Ebinger, and A. W. Y. Ho-Baillie, "Solar cell efficiency tables (version 51)," Prog. Photovoltaics, **26**, 3–12 ,2018.
[26] W.Wang, M. T. Winkler, O. Gunawan, T. Gokmen, T. K. Todorov, Y. Zhu, and D. B. Mitzi, "Device characteristics of CZTSSe thin film solar cells with 12.6% efficiency,"Adv. Energy Mater. ,**4**,7, 1301465,2014.
[27] U. Saha and M. K. Alam, "Boosting the efficiency of single junction kesterite solar cell using Ag mixed Cu_2ZnSnS_4 active layer," RSC Adv.**8**, 4905–4913,2018.
[28] W. Shockley and H. J. Queisser,"Detailed balance limit of efficiency of pn junction solar cells," J. Appl. Phys. **32**, 510–519 ,1961.
[29] B. Vermang et al.,"Employing Si solar cell technology to increase efficiency of ultra-thin $Cu(In,Ga)Se_2$ solar cells,"Progr. Photovoltaics, **22**, 1023–1029, 2014.
[30] C. Van Lare, G. Yin, A. Polman, and M. Schmid, "Light coupling and trapping in ultrathin $Cu(In,Ga)Se_2$ solar cells using dielectric scattering patterns,"ACS Nano, **9**, 9603–9613 , 2015.
[31] R. S. Dubey et al., "Performance enhancement of thin film silicon solar cells based on distributed Bragg reflector & diffraction grating," AIP Adv., **4**, 127121, 2014.
[32] F. Liu et al., "Beyond 8% ultrathin kesterite Cu_2ZnSnS_4 solar cell by interface reaction route controlling and self organized nanopattern at the contact," NPG Asia Mater., **9**, e401, 2017. https://doi.org/10.1038/am.2017.103.
[33] L. Sun, J. He, H. Kong, F. Yue, P. Yang, and J.Chu, "Structure, composition and optical properties of Cu_2ZnSnS_4 thin films deposited by pulsed laser deposition method," Sol. Energy Mater. Sol. Cells, **95**,10, 2907–2913, 2011.

[34] D. Tang et al., "An alternative route towards low-cost Cu_2ZnSnS_4 thin film solar cells", Surf. Coat. Tech.,**232**, 53–59, 2013.
[35] X. Lin et al., "Structural and optical properties of Cu_2ZnSnS_4 thin film absorbers from ZnS and Cu_3SnS_4 nanoparticle precursors," Thin Solid Films **535**, 10–13 ,2013.
[36] N.M. Shinde et al., "Aqueous chemical growth of Cu_2ZnSnS_4(CZTS) thin films: Air annealing and photoelectrochemical properties," Mater. Res. Bull., **48**, 1760–1766, 2013.
[37] Sk. Shahenoor Basha and M.C. Rao, "Effect of annealing temperature on structural and morphological studies of electrodeposited CZTS thin films," Ceram.Int.,**44**(1), 648–656, 2018.
[38] P. K. Nair, J. Cardoso, O. Gomez Daza, and M. T. S.Nair, "Polyethersulfone foils as stable transparent substrates for conductive copper sulfide thin film coatings," Thin Solid Films **40**,1–2, 243–250, 2001.
[39] R. Rafique,K. N. Tonny, A. Sharmin, and Z. H. Mahmood,"Study on the effect of varying film thickness on the transparent conductive nature of aluminum doped zinc oxide deposited by dip coating," Mater. Focus, **7,** 5, 707–713 ,2018.
[40] K. N. Tonny, R. Rafique, A. Sharmin, M. S. Bashar, andZ. H. Mahmood, "Electrical, optical and structural properties of transparent conducting Al doped ZnO (AZO) deposited by sol-gel spin coating," AIP Adv., **8**, 065307,2018.
[41] A. Sharmin, S. Tabassum, M. S. Bashar, and Z. H. Mahmood, "Depositions and characterization of sol gel processed Al-doped ZnO (AZO) as transparent conducting oxide (TCO) for solar cell application," JTAP ,**13**(2), 123–132 ,2019.
[42] P. M. Shafi and A.C. Bose, "Impact of crystalline defects and size on X-ray line broadening: A phenomenological approach for tetragonal SnO_2 nanocrystals,"AIP Adv.,**5**, 057137 ,2015.
[43] A. Irkhina et al., "Metal acetate based synthesis of small sized Cu_2ZnSnS_4 nanocrystals: effect of injection temperature and synthesis time," RSC Adv., **7**,11752–11760 ,2017.
[44] N.M. Shinde et al., "Development of polyaniline/Cu_2ZnSnS_4(CZTS)thin film based heterostructure as room temperature LPG sensor," Sens. Actuator. APhys., **193**, 79–86, , 2013.
[45] A. G. Kannan, T. E. Manjulavallia, and J. Chandrasekaran, "Influence of solvent on the properties of CZTS nanoparticles," Procedia Eng.,**141**, 15–22 , 2016.
[46] R. Sun et al., "$Cu_2ZnSNSSe_4$ solar cells with 9.6% efficiency via selenizing Cu-Zn-Sn-S precursor sputtered from a quaternary target," Sol. Energy Mater. Sol.Cells, **174**, 42–49 , 2018.
[47] G.D. Surginaet al., "Effect of annealing on structural and optical properties of Cu_2ZnSnS_4 thin films grown by pulsed laser deposition," Thin Solid Films, **594**(A),74–79 ,2015.
[48] A. Weber, R. Mainz, and H.W. Schock, "On the Sn loss from thin films of the material system Cu-Zn-Sn-S in high vacuum," J. Appl. Phys.,**107**, 013516 , 2010.
[49] S. Chen, J.H. Yang, X. G. Gong, A. Walsh, and S.H. Wei, "Intrinsic point defects and complexes in the quartenary kesterite semiconductor Cu_2ZnSnS_4," Phys. Rev.B, **819**, 245204 2010.
[50] S. Chen, X. G. Gong, A. Walsh, and S. H. Wei, "Defect physics of the kesterite thin-film solar cell absorber Cu_2ZnSnS_4," Appl. Phys. Lett., **96**(2), 021902, 2010.
[51] V. Kheraj et al., "Synthesis and characterization of copper zinc tin sulphide(CZTS) compound for absorber material in solar cells," J. Cryst. Growth ,**362**, 174–177 ,2013.
[52] T.K. Todorov, K.B. Reuter, and D.B. Mitzi, "High-efficiency solar cell with earth-abundant liquid-processed absorber," Adv. Mater.**22**, 1–4,2010.
[53] J. H. Lambert, D. A. Lightner, H. F. Shurvelland, and R. G. Cooks, "Introduction to Organic Spectroscopy ," Macmillan, New York, 1987.
[54] M.C. Rao and Sk. Shahenoor Basha, "Structural and electrical properties of CZTS thin films by electrodeposition,"Results Phys., **9**, 996–1006, 2018.
[55] S.M.Power et al., "Single step electrosynthesis of Cu_2ZnSnS_4 (CZTS) thin film for solar cell application,"Electrochim. Act,a **55**,12, 4057–4061,2010.
[56] A. Sharmin, M. S. Bashar, M. Sultana, S.M. M. A. Mamun,"Sputtered single-phase kesterite Cu_2ZnSnS_4 (CZTS) thin film for photovoltaic applications: Post annealing parameter optimization and property analysis," AIP Advances, 10,1, 015230, 2020. https://doi.org/10.1063/1.5129202

Chapter 6: Modelling, Simulation and Fabrication of CZTS Solar cell

6.1.Modelling and Fabrication of CZTS Solar Cell

6.1.1. Growth of Mo Back contact

Low resistivity, chemical and mechanical inertness during high-temperature operations, and great stability are all characteristics of molybdenum. With CIGS solar cells, there is a slight lattice mismatch as well. For CZTS thin-film solar cells, the Mo layers have been employed as suitable back contact layers. High photo-conversion efficiency thin-film solar cells are made primarily at the interface between the back and absorber layers. Mo films have columnar microstructure that are particularly fit for back contact and are extremely conductive and sticky. The surface shape and lattice orientation of Mo films are also crucial in the development of the absorber layers' favored development. Direct current (DC) magnetron sputtering has been used relatively extensively to form Mo layers [1-3]. RF magnetron sputtering was an approach that some people tried [87]. In order to investigate the hole transport characteristics for c-Si solar cells, Bivour et al. [88] build the molybdenum oxide layer by the atomic layer deposition process and discover it does have a low work function, making it difficult to make an efficient hole interface.

Back contact was primarily influenced by two factors: Mo's resistivity and adherence to the absorber layer and substrate. Low resistivity and adhesion were mostly dependent on the pressure of the working gas used to create the Mo layer [1]. The general finding from earlier research was that, with sputtering gas pressure, resistivity and sticky state were the opposite of each other. The well turns sticky and resistant depending on the working gas pressure. When the pressure is high, the well becomes resistive. Chelvanathan P. et al. [3] meticulously followed the production process' instructions.

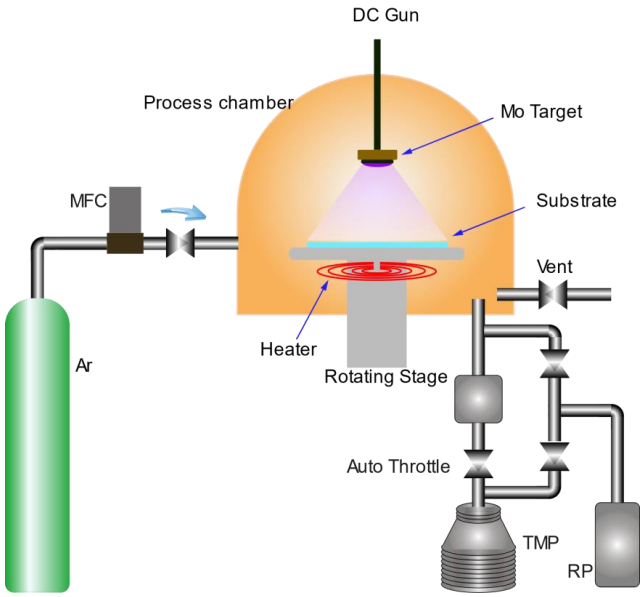

Fig. 6.1: Schematic diagram of the back-contact deposition of CZTS Solar Cell

The pictorial representation is illustrated in Fig. 6.1, and this study carefully examined the impact of sputtering variables on the morphological and microstructural characteristics of Mo layers formed by DC sputtering.

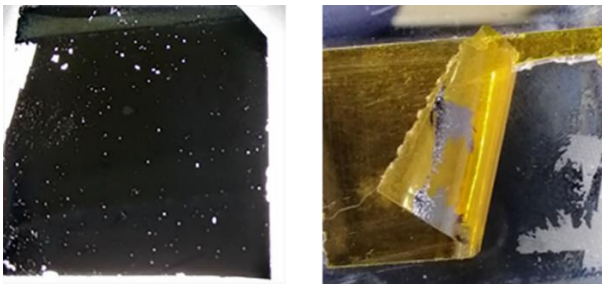

(a) (b)

Fig.6.2. (a) Mo thin film (b) Kapton tape test of Mo films.

Mo thin films were deposited on soda-lime glass measuring 30 mm by 30 mm using a DC magnetron sputtering technique (SLG). Followed by subsequent dipping and ultrasonically cleaning with methanol, acetone, methanol, deionized water, all SLG substrates were then dried with a jet stream of dry air. The source material, a 50.8 mm diameter target of Mo (purity 99.95%) acquired from Angstrom Sciences, Inc. in the USA, was positioned 95 mm away from the substrates.

Prior to the film growth, the target was pre-sputtered to clean off any potential contaminants from its surface. The deposition processes were carried out in a deposition chamber that was roughly vacuumed to 4.510-6 Torr, at 200°C, with a substrate rotation speed of 20 rpm. Variations in the argon gas flow rate and DC power led to different operating pressures ranging from 4.21 to 7.95 torr and DC powers ranging from 50 to 90 with a 10 W increment. Sputtered Mo thickness in the range of 300 to 600 nm was obtained after an average deposition period of 40 min. Additionally, the Kapton tape evaluation method is used to specifically investigate and assess the adhesive characteristics of RF sputtered Mo layers. The accumulation of internal compressive stress during the nucleation process is associated with the failure of Mo adherence to the SLG substrates. Compressively stressed films have a propensity to buckle and separate from the SLG substrate beneath them.

6.1.2. Growth of CZTS Absorber Layer

Cu2ZnSnS4, a quaternary semiconductor with high absorption coefficients (10^4 cm-1) in the terrestrial solar spectrum, and a direct band gap of around 1.4 to 1.6 eV, is composed of earth abundant copper, zinc, tin, and sulfur. On 30mm x 30mm soda-lime glass, thin coatings of CZTS were simultaneously deposited using an RF magnetron sputtering. Following initial deposition and ultrasonically cleaning with methanol, acetone, methanol, deionized water, all SLG substrates were then dried with a jet stream of dry air. The RF power was changed while the argon gas flow rate was maintained, resulting in a fixed working pressure of $4.5x10^{-3}$ Torr. During the deposition procedure, the substrate holder was heated to 200°C and rotated at 20 rpm. To achieve improved crystallinity, the CZTS films were annealed after deposit at 450°C for 30 minutes in a

N2 environment at 375 Torr pressure using a thermal annealing chamber made by MTI Corporation with Model GSL-1100X-LD.

6.1.3. Growth of CdS Buffer Layer

Chemical bath deposition has been used to generate a thin film of cadmium sulfide (CdS) film as a buffer layer for solar cell. The buffer layer of a solar cell must be composed of a n type material in order for the p type absorber layer to function at the p-n junction. Solar cells use thin films of CdS, ZnS, ZnSe, and other materials as buffer layers.

The growth parameters, such as the bath temperature, the relative concentrations of the various reactants in the solution, the pH level, and the kind of substrate, affect the physical characteristics of the chemically deposited CdS films [9]. Typically, an alkaline aqueous solution (high pH) with a majority of Cd compounds (such as chloride, nitrate, sulfate salts, etc.), thiourea as the sulfide source, and ammonia as the complexing agent is used to deposit CdS thin films via CBD. Through the formation of complexes with Cd ions, ammonia aids in preventing the unwanted homogeneous sedimentation.

6.1.4. Growth of TCO

The use of transparent conducting oxide thin films is widespread. TCO layer serves as a transparent electrode for organic light-emitting diodes, solar cells, plasma display panels, and transparent heat-reflecting windows, surface heaters for cameras, gas sensors, lenses, mirrors, and car windows, as well as ohmic connections for surface-emitting diodes [6-9]. The TCO layer is composed topically of zinc oxide [95, 96], tin oxide, cadmium oxide, indium tin oxide [12-15], and cadmium tin oxide. Indium oxide doped with tin (ITO) and florin doped tin oxide (FTO) are two TCO thin films that are frequently employed because of their distinct electrical and optical attributes.

ITO thin films were deposited on a 30 mm x 30 mm SLG using a confocal RF magnetron sputtering setup. Following initial coating and ultrasonically cleaning with methanol, acetone, methanol, deionized water, all SLG substrates were then dried with a jet stream of dry air. As a source material, a 50.8 mm diameter ITO target with an In_2O_3/SnO_2 composition of 90/10 wt% and a purity of 99.99 % was positioned about 80 mm away from the worktops. Prior to the depositing procedure, the target was pre-sputtered to clean off any potential contaminants from its surface. The deposition process were carried out in a deposition chamber that was roughly vacuumed to $6.0x10^{-6}$ Torr, at a temperature of 250°C, with a substrate rotation speed of 20 rpm. Sputtered ITO thicknesses in the range of 80 to 100 nm were obtained after an estimated deposition time of 30 min.

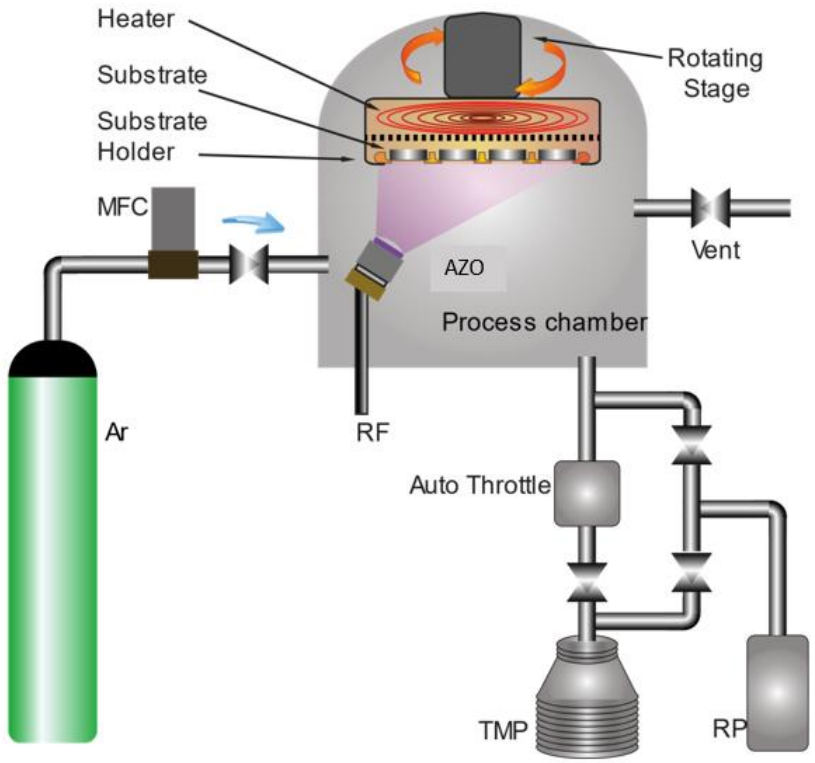

Fig. 6.3: Schematic diagram of the front contact deposition of CZTS Solar Cell.

6.2. Assembly of Solar Cell

The thin-film solar cell structure can be divided into two classes, substrate type and superstrate type, depending on the choice of layer deposition. A solar cell's substrate (glass, metal, or polymer) is a passive element, but it could have a significant impact on the PCE of the solar cell. A suitable glass or ceramic substrate is used for thin film solar cells that need thin films to be processed at high temperatures. A soda-lime glass (SLG) measuring 30 x 30 mm and 1.5 mm thick was used as the substrate. It was sonicated in an ultrasonic bath for 10 minutes before being degreased with methanol-acetone-methanol and de-ionized water. After that, compressed dry air was used to dry the substrate. As a method for depositing substrate cells, the entire cell manufacturing process is employed. According to the instructions from section 6.1 to 6.4, the front contact TCO, the absorber layer, the buffer layer, and the back-contact layer is fabricated. A molybdenum layer with a thickness of around 350 microns was deposited as the back-contact layer on top of it. The remaining layers are then fabricated one by one. A mask (a) for absorber layer and grid mask (b) for front contact, as illustrated in Fig.6.4, with dimensions of 30 x 30 mm and nine apertures of 5 x 5 mm each is applied to form a solar cell with a surface area of 25 mm^2.

The grid was fastened to the TCO's top using silver (Ag). The grid's architecture has significantly improved the photo-conversion efficiency of solar cells. The grid must gather the most generated

carriers with the least amount of cell shadowing possible [16-17]. The grid shouldn't cover more than 10% of the solar cell's active surface area.

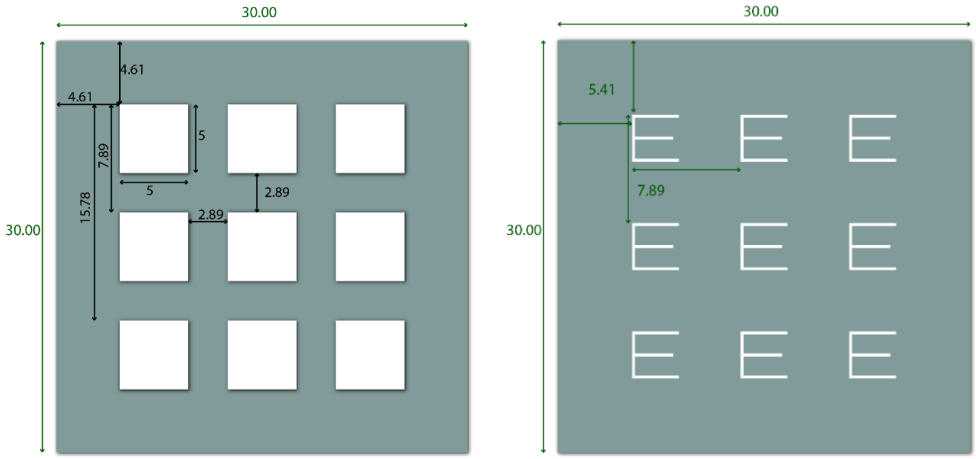

(a) (b)

Fig.6.4 (a) Mask for CZTS absorber Layer and (b) Grid mask for front contact

With the aid of an electron beam evaporator, silver, the grid material, was coated. For optimal ohmic contact with the TCO layer, an electron beam evaporator can achieve deposition rates of a few nanometers per minute.

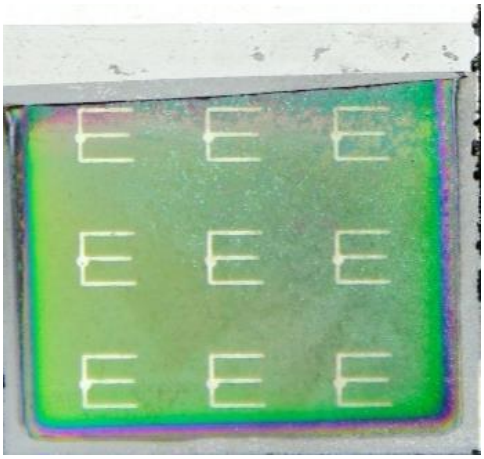

Fig. 6.5. SLG/Mo/CZTS/CdS/i-ZnO/AZO/Ag solar cell

6.3. Practical Device

On a clean piece of sola lime glass(SLG), a solar cell comprised of sputtered Mo for the back contact, sputtered CZTS absorber layer, chemical bath deposited CdS buffer layer, sputtered AZO and ITO as the window layer, and e-beam evaporated silver(Ag) for the grid front contact layer was subsequently deposited. The practical device's outcome is not thought to be particularly spectacular. The High series resistance value suggests that the subjective layer junction was not

made effectively. After each layer of fabrication, the vacuum was broken. The sample must be removed from the machinery used to anneal and modify the target materials. The interval between layer depositions was another reason of deteriorating film quality and effectiveness. The data from the sun simulator analysis are displayed in Table 6.1.

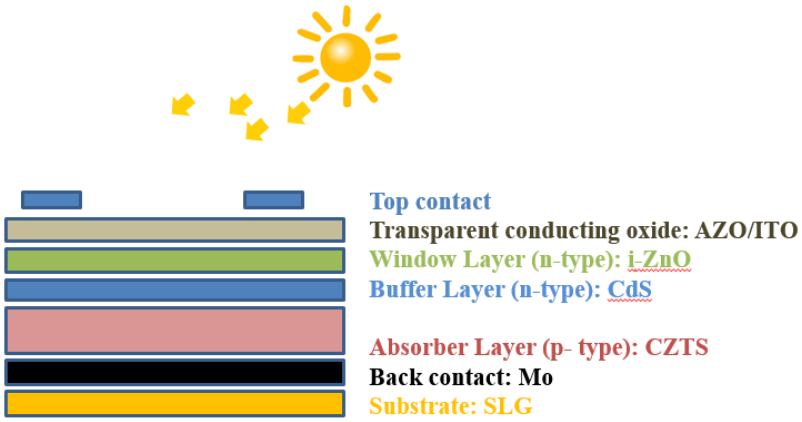

(a)

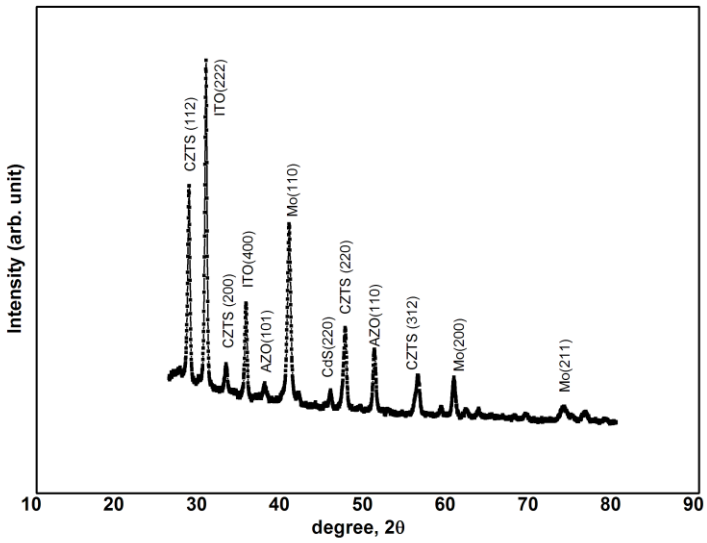

(b)

Fig.6.6. (a) *Schematic diagram of CZTS solar cell and (b) XRD pattern of a CZTS Photovoltaic cell.*

Table 6.1. Electrical parameter of CZTS thin-film solar cell

Open-circuit voltage, V_{oc}	0.209 V
Short-circuit current, I_{sc}	0.031 mA
Short-circuit current density, J_{sc}	0.212 mA/cm^2
Maximum power, P_{max}	0.002 mW
Maximum voltage, V_{max}	0.105 V
Maximum Current, I_{max}	0.02 mA
Fill Factor (FF)	23.3388 %
Photo-conversion efficiency, η	0.00245 %
Shunt resistance, R_{sh}	4635.11 Ω
Series resistance, R_s	5478.98

6.4. Modelling and Simulation of CZTS Solar Cell under illumination

A numerical method for estimating various parameters using theoretical or practical characteristics of various layers is called simulation of the solar cell. The Department of Electronics and Information Systems (ELIS) at the University of Gent developed SCAPS, a one-dimensional modeling and simulation tool for solar cells [18]. The fundamental tool for simulating real systems is modeling. Analyzing the effects of various elements on solar cells and taking into account the specifications provided by the manufacturers are important for modeling. Table 6.2 contains a list of the standard parameters that is utilized to complete our computations. And Table 6.3 shows a comparison between experimental and simulated PCE incorporating the properties of samples with best experimental results from Chapter 4 and 5. The values are either calculated or extrapolated from earlier publications [19-25].

Table 6.2. Simulation parameters of different layers of CZTS thin-film solar cell

PARAMETERS	**Mo**	**MoS_2**	**p-CZTS**	**CdS**	**i-ZnO**	**n-AZO**
Thickness (nm)	200-800	100	**500-3000**	50	80	**100-900**
Bandgap (eV)	0	1.7	**1.5**	2.4	3.3	**3.6**
Electron affinity (eV)	0.75	4.2	**4.5**	4.5	4.6	**4**
Dielectric permittivity	-	13.6	**10**	10	9	**9**
Electron mobility (cm^2/V_s)	-	100	**100**	100	100	**50**
Hole mobility (cm^2/V_s)	-	25	**25**	25	25	**5**
Shallow uniform donor density, N_D (cm^{-3})	-	0	**1.00E+01**	1.00E+18	1.00E+18	**1.00E+19**
Shallow uniform acceptor density, N_D (cm^{-3})	-	1.00E+16	**1.00E+16**	0	0	**0**

Table 6.3. Variance of performance metrics of CZTS thin-film solar cell

	Voc (V)	Jsc (mA/cm^2)	FF%	PCE%
Experimental	0.209	0.212	23.33	0.00245
Simulation	1. 6268	28.2047	51.64	23.69

6.5. Result and Discussion

i. Effect of Film thickness of Absorber layer

Calculating the photocurrent density while accounting for the solar radiation's spectrum distribution will yield qualitative features of the solar cell efficiency for absorber layer thicknesses. The effectiveness of the CZTS/CdS/i-ZnO/AZO solar cell is demonstrated in Table 6.3 for different thickness of the CZTS Absorber layer. Interface defects between absorber/buffer and buffer/window are ignored. For the experiment of CZTS thin film deposition (Section 5.1, 5.1 and 5.3), three process such as sol gel spin coating, dip coating and sputtering system is employed to achieve better quality film. For sol gel spin and dip coating, its not convenent to obtain a specific thickness. However, sputtering sytem offers a good control on film growth and confirms crystallinity and better coverage film as well.

As CZTS thickness increases from 500 to 3000 nm, a very small increase is observed in V_{oc}, J_{SC}, Fill Factor, and PCE(%). A crucial aspect affecting cell performance is the fill factor (FF), which measures the parasitic resistance and p-n junction quality of a completed solar cell. The I-V curve's squareness is judged by the fill factor. As can be observed, the current density, J_{sc} is influenced by the absorber layer width. The efficiency increases when the thickness of the CZTS layer is increased because more light is absorbed. Consequently, more electron hole pairs are generated which improves carrier production as seen by the rise in Jsc [29, 31]. When the CZTS layer's thickness is increased, at first, the Voc also rises before becoming saturated [30]. Voc is dependent on both the saturation current and the photocurrent. With expanding absorber film thickness, the quantity of photogenerated carriers also increases, driving up photocurrent and, ultimately, the initial rise in Voc. Again, all metrics significantly improve when the minority carrier lifespan grows along with the thickness of the absorber layer. Therefore, there is a strong correlation between the thickness optimization and the minority carrier lifetime [28]. In addition, the acceptor concentration of the CZTS layer is assumed to be 10^{16} cm^{-3} for numerical analysis which varied from10^{16} ~10^{17} cm^{-3}. For acceptor concentration >5x10^{16} cm^{-3}, the PCE(%) generally rises because the reduction in Jsc is compensated by the rise in Voc and fill factor(FF)[32].

As thicker layer needs much materials, makes it much expensive, so thickness of around 2µm of absorber layer is an optimum choice for the configuration. The maximum photo-conversion efficiency of the Mo/CZTS/CdS/i-ZnO/AZO solar cell is 23.74%, along with a 51.55% fill factor, V_{oc} = 1.62 V, and J_{sc} = 28.37 mA/cm^2 when CZTS and AZO film thickness is 3000 and 900 nm respectively.

Table 6.4. Variance of performance metrics of modified CZTS solar cell with thickness of CZTS

Thickness (nm) of CZTS	Thickness of AZO (nm)	Voc (V)	J_{SC}(mA/cm^2)	FF(%)	PCE (%)
500	900	1.6927	28.2047	49.63	23.69
1000		1.6977	27.9984	49.72	23.63
1500		1.7056	27.4760	50.11	23.48
2000		1.7386	25.4366	51.52	22.78
2500		1.6268	28.3062	51.51	23.72
3000		1.6244	28.3668	51.55	23.74

ii.Effect of film thickness of Transperent conductive Oxide (TCO)

The effect of TCO layer thickness on the performance of CZTS/CdS/i-ZnO/AZO solar cell is shown in Table 6.4. Again, interface defects between absorber/buffer and buffer/window is disregarded. For this project, different deposition process is employed for achieving high quality thin film with better coverage, crystallinity and optoelectronic properties. However, From section 4.1, 4.2 and 4.3, its clear that film thickness of AZO around 900-1000 µm shows better coverage and lower resistivity. Results further indicate that as film thickness increases, crystallinity of the films improves, electrical conductivity rises while optical transmittance falls. Additionally, film thickness and confinement effects cause the optical band gap energy to drop [33]. So for the simulation, thickness of AZO film is varied from 1.0-1.1 µm to estimate the qualitative features of aforementioned configuration. the maximum photo-conversion efficiency (PCE%) of the Mo/CZTS/CdS/i-ZnO/AZO solar cell is 23.72% with FF= 51.55%, V_{oc} = 1.62 V, and J_{sc} = 28.37 mA/cm^2 when AZO film thickness is around 300-500 nm.

Table 6.5. Variance of performance metrics of modified CZTS solar cell with thickness of AZO

Thickness (nm) of CZTS	Thickness (nm) of AZO	Voc (V)	J_{SC}(mA/cm^2)	FF(%)	PCE (%)
2000	100	1.6939	28.4770	51.25	23.70
	300	1.6261	28.3743	51.41	23.72
	500	1.6269	28.3003	51.51	23.72
	700	1.6246	28.2558	51.66	23.71
	900	1. 6268	28.2047	51.64	23.69
	1100	1.6264	28.1729	51.67	23.68
	1300	1.6258	28.1479	51.71	23.66

iii.Effect of Band Gap of Absorber layer

The effect of the CZTS's energy band gap on cell performance is also examined in this numerical simulation. The band gap was increased from 1.40 to 1.55 eV while the thickness of the CZTS was left unaltered (2000 nm). The simulation results are displayed in Fig.6.7. As can be seen, the Voc

increases from 1.618 to 1.646 V when the CZTS band gap is increased. Greater quasi Fermi energy level splitting is the cause of the higher Voc at higher band gaps. In contrast, Jsc dramatically falls as the CZTS band gap widens due to a reduction in the absorption coefficient. The value of FF(%) is shown as 46.77%, 49.86%, 51.63% and 53.77% when band gap varies from 1.40 to 1.55 eV.

The increase in band gap from 1.40 to 1.55 eV enhances FF, which follows the same trend as Voc. The reduction of J_{sc} brought on by the absorption loss may be the reason of the increase in FF shown in Fig 6.8. The formation of flaws in the absorber volume might help explaining the reason of the PCE declines as the band gap increases [34]. Fig 6.8 reveals that the maximum value of J varies from 32-26 mA/cm^2 when band gap, E_g is varied from 1.40 to 1.55 eV. As seen in Fig.6.8, the resulting J-V curve under illumination is frequently represented as output power.

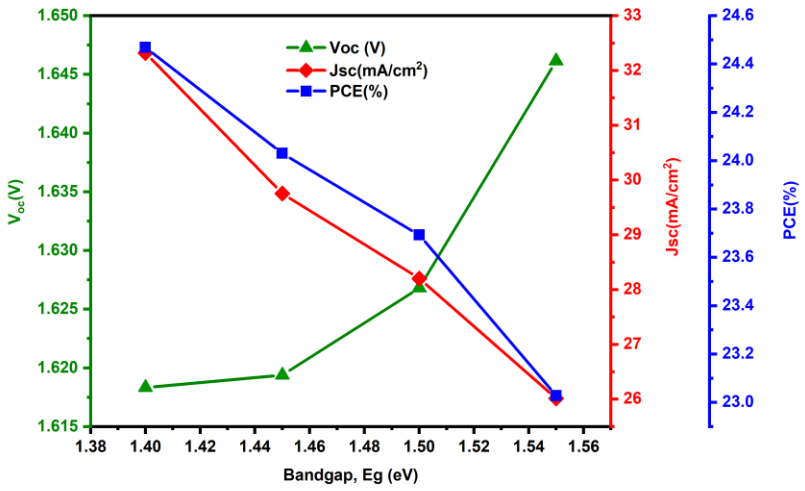

Fig.6.7. Effect of the CZTS film's band gap on cell's qualitative performance

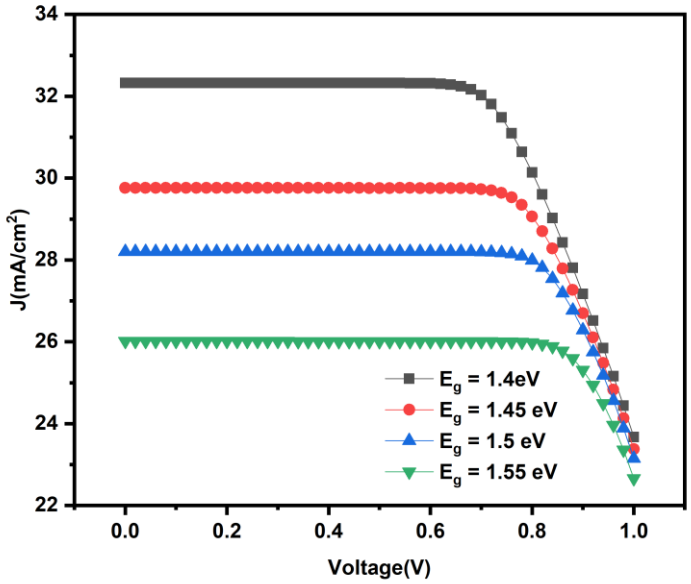

Fig.6.8. Effect of the CZTS band gap on J-V Characteristics of simulated CZTS solar cell.

Fig. 6.9 displays the External Quantum Efficiency (EQE) of simulated CZTS solar cells. In essence, the band gap of the absorber layer is connected to the changes in shape and structure in the long wavelength (800-900 nm). Short wavelength quantum efficiency has a form and range that depend on the device's construction and window layers. The range of optical response varies with changes in E_C. The aforementioned findings will serve as a guide for producing CZTS-based thin film solar cells with improved efficiency.

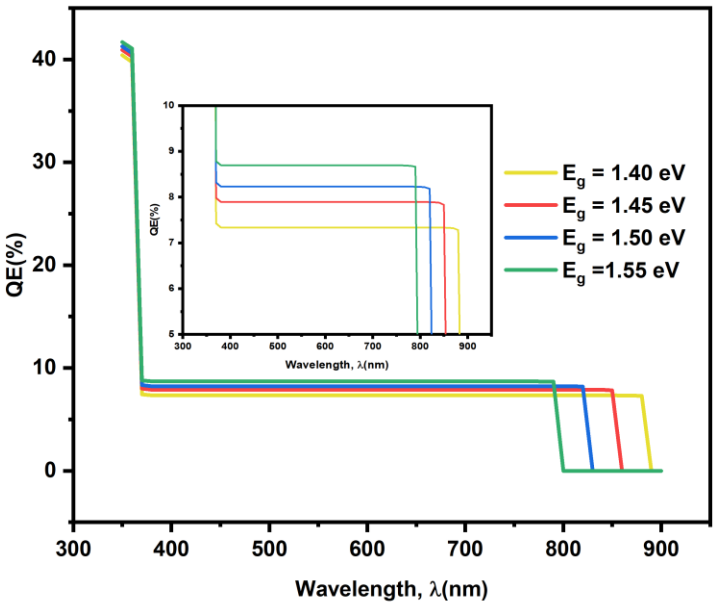

Fig.6.9. Effect of the CZTS band gap on Quantum Efficiency (QE) of CZTS solar cell

iv. Effect of Band Gap of TCO layer

The effect of the AZO's energy band gap on cell performance is examined. The band gap was increased from 3.20 to 3.40 eV while the thickness of the AZO was left unaltered (900 nm). The simulation results are displayed in Fig.6.10. As can be seen, the Voc decreases from 1.618 to 1.646 V when the AZO band gap is increased. In addition, Jsc falls as the AZO band gap widens. The value of FF(%) is shown as 18.31%, 52.32%, 52.00%, 51.68% and 51.60% and when band gap varies from 3.20 to 3.40 eV.

The increase in band gap enhances FF, which follows the same trend as J_{sc}. Fig 6.11 reveals that the value of J_{sc} varies from 27.90 -28.20 mA/cm^2 when band gap, E_g is varied from 3.20 to 3.40 eV. Fig. 6.12 displays the External Quantum Efficiency (EQE) of simulated CZTS solar cells with variance of band gap of AZO. As we discussed earlier, QE at short wavelength possesses a form and range depending on the device's construction and window layers.

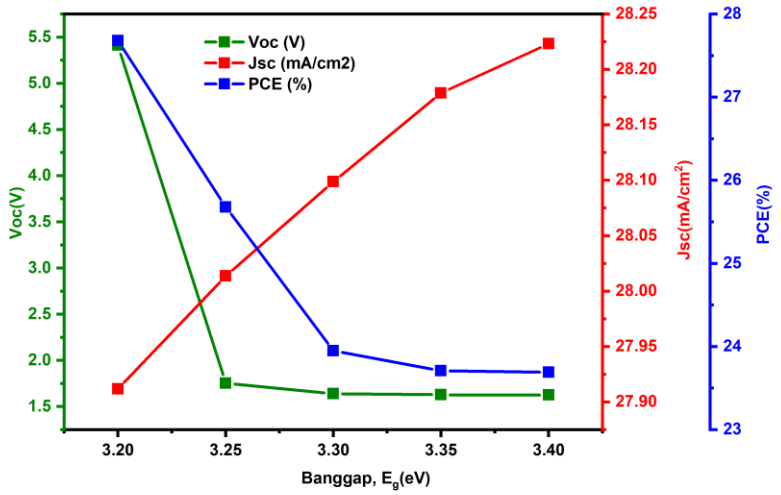

Fig.6.10. Effect of the AZO band gap on cell's qualitative performance

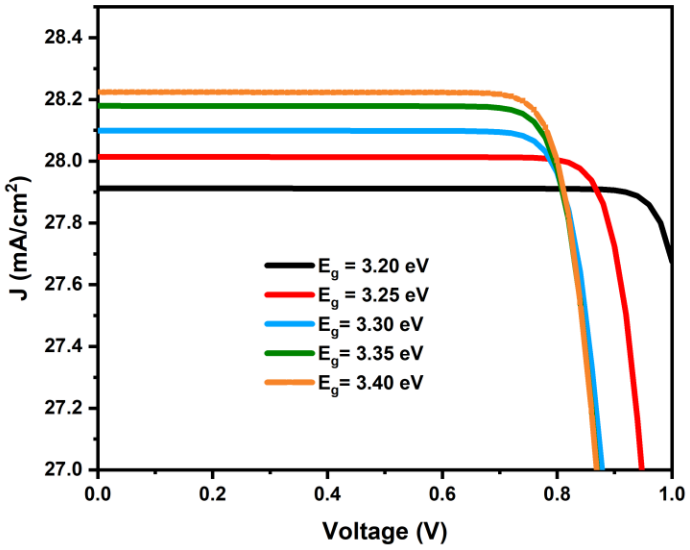

Fig.6.11. Effect of the CZTS band gap on J-V Characteristics.

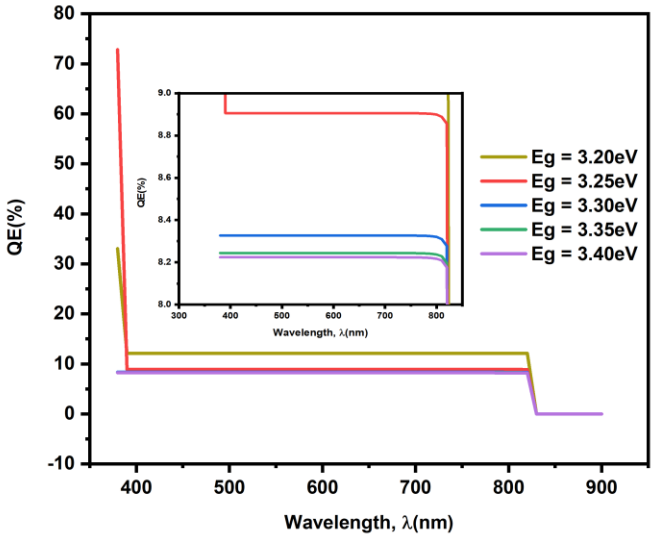

Fig.6.12. Effect of the AZO band gap on Quantum Efficiency (QE) of CZTS solar cell

v.Band Diagram of CZTS Solar Cell

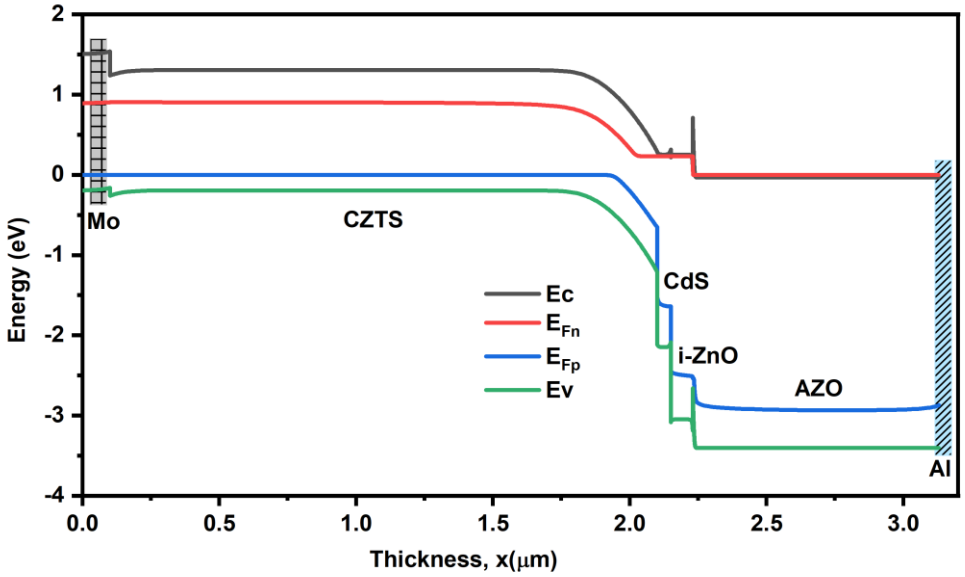

Fig.6.13. Band diagram of simulated of CZTS soalr cell

The energy band diagram is drawn (Fig 6.13) using the outcome of our simulation. To analyze the solar cell in non-equilibrium state under illumination, quasi-Fermi levels (E_{Fn} for electrons and E_{Fp} for holes) are used [35].

The Mo/CZTS interface exhibits a Schottky contact. The Schottky contact develops because Mo's work function (4.6–4.9 eV) is lower than CZTS's (5.15 eV) [26]. As a result, the cell's inherent potential is decreased, which raises the dark current. Due to its inverse relationship with the logarithm of dark saturation current, Voc likewise declines as a result [26]. Additionally, optically produced minority carriers in CZTS are drawn to the Mo interface and are subjected to surface recombination, which lowers the Jsc, because of the band bending near the Mo/CZTS interface (Fig. 6.13). Additionally, Mo contact reduces the Voc and Jsc of CZTS solar cells, hence lowering the cell's overall PCE.

Furthermore, a conduction band offset at the CdS/CZTS interface prevents optically produced minority carriers (electrons) in CZTS from moving into the CdS(n) region when there is no back-surface-Field (BSF) layer shown in Fig.6.13.

However, Mo can be substituted by ITO as the back contact based on the aforementioned observations. As ITO's work function can be adjusted to match that of CZTS by changing its doping and the undesirable Schottky contact with the CZTS layer can be removed as a result [26]. ITO with a work function of 5.25 eV, which is adequate for forming ohmic contact with CZTS, offers a new insight toward enhancing the absorbance efficiency. This makes it a possible substitute for fabricating highly effective CZTS thin-film solar cells for photovoltaic applications.

Last and not the least, investigating the stability of the cell at various operating temperatures is necessary since the cell can be warm up by the sun. Liturratures show that with temperatures ranging from 280 K to 360 K, Voc and power conversion efficiency(PCE) are significantly impacted by changes in operating temperature, while JsC and fill factor are largely unaffected. The energy of the electrons in the cell increases as the operating temperature rises. The electrons then become unstable and are more likely to pair again with holes before they are gathered in the depletion area. As a result, V oe and fill factor will decline [36].

6.6. Issues to be addressed

In this PhD work, there is various challenges associated with solar cell materials, focusing on crystal defects, morphology, stoichiometry, and mixed phases. From literature review, the highest PCE for CZTS is observed from solution based method like sol gel spin coating. However, in this case, PVD system like Magnetron Sputter shows the best performance for film depositions. Better coverage and stoichiometry is observed from Sputter coated film. There are several reasons which may effect for low PCE solar cell.

In case of film fabrication, there is issues of poor coverage and non uniformity of film. Unavailability of pure chimicals is one of the major reason behind this. Stacking faults is another issue which arises in most of the cases and alter films intrinsic properties i.e.

i. improve charge carrier transport
ii. may increase recombination center
iii. form localized electric field

In case of cell fabrications, there is interrupted use of clean room due to time constraints. It occurs contamination and degradations of thin films over time. Interface defect plays a key role during fabrication of one film on another. A lots of issues arises from interface defects i.e.

i. Contact resistance
ii. Indices carrier localization which can alter electronic properties
iii. Alter Band alignment
iv. Carrier recombination (trap)
v. Chemical reaction and degradation

There are some other possible reasons-

i. Material and Device Quality
ii. Measurement and Calibration Errors
iii. Light Absorption
iv. Temperature Effects
v. Surface reflection and anti reflection coating
vi. Modelling Assumptions (i.e thickness of buffer layer)

To determine the exact reasons for the low efficiency, a detailed analysis of the experimental setup, material properties, and measurement procedures would be necessary. Additionally, comparing the results with multiple simulations using different models and input parameters could provide further insights into the discrepancies.

6.6. Bibliography

[1] Z.H. Li, E.S. Cho, S.J. Kwon, "Molybdenum thin film deposited by in-line DC magnetron sputtering as a back contact for Cu(In,Ga)Se_2 solar cells," Appl. Surf. Sci., 257, 9682–9688, 2011.

[2] J.H. Yoon, S. Cho, W.M. Kim, J.K. Park, Y.J. Baik, T.S. Lee, T.Y. Seong, J.H. Jeong, "Optical analysis of the microstructure of a Mo back contact for Cu(In,Ga)Se_2 solar cells and its effects on Mo film properties and Na diffusivity," Sol. Energy Mater. Sol. Cells., 95, 2959–2964, 2011.

[3] P. Chelvanathan, S.A. Shahahmadi, F. Arith, K. Sobayel, M. Aktharuzzaman, K. Sopian, F.H. Alharbi, N. Tabet, N. Amin, "Effects of RF magnetron sputtering deposition process parameters on the properties of molybdenum thin films," Thin Solid Films, 638, 213–219, 2017.

[4] G. Zoppi, N.S. Beattie, J.D. Major, R.W. Miles, I. Forbes, "Electrical, morphological and structural properties of RF magnetron sputtered Mo thin films for application in thin film photovoltaic solar cells," J. Mater. Sci. 46, 4913–4921, 2011.

[5] "M. Bivour, B. Macco, J. Temmler, W.M.M. Kessels, M. Hermle, Atomic Layer Deposited Molybdenum Oxide for the Hole-selective Contact of Silicon Solar Cells," Energy Procedia. 92, 443–449, 2016.

[6] M.A. Matin, D.E. Lacklison, T.M. Benson, J.W. Orton, A.F. Jezierski, T.S. Cheng, C.T. Foxon, S.A. Bashar, A.A. Rezazadeh, J.S. Roberts, T.E. Sale, "Optically transparent indium-tin-oxide (ITO) ohmic contacts in the fabrication of vertical-cavity surface-emitting lasers," Electron. Lett., 30, 318–320, 1994.

[7] C.W. Tang, S.A. Vanslyke, "Organic electroluminescent diodes," Appl. Phys. Lett., 51 , 913–915, 1987.

[8] Z. Tang, P.C.H. Chan, R.K. Sharma, G. Yan, I.M. Hsing, J.K.O. Sin, "Investigation and control of microcracks in tin oxide gas sensing thin-films," Sensors Actuators, B Chem. 79 , 39–47, 2001.

[9] K.W. Whang, J.K. Kim, "Discharge physics of alternating current Plasma Display Panels (PDPs)," IEEE/OSA J. Disp. Technol. 1 (2005) 295–303, 2005.

[10] A. Sharmin, S. Tabassum, M.S.B. Zahid, H. Mahmood, "Depositions and characterization of sol – gel processed Al ‑ doped ZnO (AZO) as transparent conducting oxide (TCO) for solar cell application," J. Theor. Appl. Phys., 13, 123–1322019.

[11] K.N. Tonny, R. Rafique, A. Sharmin, M.S. Bashar, Z.H. Mahmood, "Electrical, optical and structural properties of transparent conducting Al doped ZnO (AZO) deposited by sol-gel spin coating," AIP Adv. 8, 065307, 2018.

[12] O. Tuna, Y. Selamet, G. Aygun, L. Ozyuzer, "High quality ITO thin films grown by dc and RF sputtering without oxygen," J. Phys. D. Appl. Phys. 43 2010.

[13] M.K.M. Ali, K. Ibrahim, O.S. Hamad, M.H. Eisa, M.G. Faraj, F. Azhari, "Deposited Indium Tin Oxide (ITO) thin films by dc- magnetron sputtering on Polyethylene Terephthalate substrate (PET)," Rom. Reports Phys. 56, 730–741, 2011.

[14] Z. Qiao, D. Mergel, "Comparison of radio-frequency and direct-current magnetron sputtered thin In2O3: Sn films," Thin Solid Films. 484, 146–153, 2005.

[15] V.S. Reddy, K. Das, A. Dhar, S.K. Ray, "The effect of substrate temperature on the properties of ITO thin films for OLED applications," Semicond. Sci. Technol. 21, 1747–1752, 2006.

[16] M.M. Shabana, M.B. Saleh, M.M. Soliman, "Optimization of grid design for solar cells at different illumination levels," Sol. Cells., 26, 177–187, 1989.

[17] W. Liu, Y. Li, J. Chen, Y. Chen, X. Wang, F. Yang, "Optimization of grid design for solar cells," J. Semicond. 31, 2010.

[18] A. Niemegeers, M. Burgelman, K. Decock, J. Verschraegen, S. Degrave, "SCAPS Manual 2,", Man. SCAPS-1D, 2013.

[19] C. Mebarkia, D. Dib, H. Zerfaoui, R. Belghit, "Energy efficiency of a photovoltaic cell based thin films CZTS by SCAPS," J. Fundam. Appl. Sci. 8, 363, 2016.

[20] M.D. Wanda, S. Ouédraogo, F. Tchoffo, F. Zougmoré, J.M.B. Ndjaka, "Numerical Investigations

and Analysis of Cu_2ZnSnS_4 Based Solar Cells by SCAPS-1D," Int. J. Photoenergy. 2152018, 2016.

[21] A. Haddout, A. Raidou, M. Fahoume, "A review on the numerical modeling of CdS/CZTS-based solar cells," Appl. Phys. A Mater. Sci. Process. 125,2, 2019.

[22] A. Kumar, A.D. Thakur, "The simulation of CZTS solar cell for performance improvement," AIP Conf. Proc. 1953, 1–4, 2018.

[23] W. Zhao, W. Zhou, X. Miao, "Numerical simulation of CZTS thin film solar cell," 2012 7th IEEE Int. Conf. Nano/Micro Eng. Mol. Syst. NEMS 2012, 502–505, 2012.

[24] V. Gavryushin, A. Kazlauskas, G. Raciukaitis, "Direct Study of Local Electron-Phonon Interaction in Semiconductors," Journal of the Society for Information Display, 1–6, 1998.

[25] M.S. Jamal, S.A. Shahahmadi, P. Chelvanathan, N. Asim, H. Misran, M.I. Hossain, N. Amin, K. Sopian, M. Akhtaruzzaman, "Effect of defect density and energy level mismatch on the performance of perovskite solar cells by numerical simulation," Optik (Stuttg). 182, 1204–1210, 2019.

[26] Uday Saha and Md. Kawsar Alam, "Boosting the efficiency of single junction kesterite solar cell using Ag mixed Cu_2ZnSnS_4 active layer," RSC Adv., 8, 4905, 2018.

[27] Farjana Akter Jhuma, Marshia Zaman Shaily, Mohammad Junaebur Rashid, "Towards high‐efficiency CZTS solar cell through buffer layer Optimization," Materials for Renewable and Sustainable Energy, 8,6, 2019.

[28] M. Courel, O. Vigil-Galán, Advanced Ceramic and Metallic Coating and Thin Film Materials for Energy and Environmental Applications,Springer, Cham, 2018.

[29] A.D. Adewoyin, M.A. Olopade, M.A. Chendo, Enhancement of the conversion efficiency of Cu2ZnSnS4thin film solar cell through the optimization of some device parameters. Optik 133,122–131, 2017.

[30] I. Bouchama, S.A. Saoucha, Effect of wide band-gap TCO properties on the bifacial CZTS thin-films solar cells performances.Optik 144, 370–377, 2017.

[31] H. Arbouz, A. Aissat, J.P. Vilcot, "Simulation and optimization of CdS-n/Cu2ZnSnS4 structure for solar cell applications structure for solar cell applications," Int. J. Hydrog. Energy 42(13), 8827–8832, 2017.

[32] Theoretical investigations on enhancement of photovoltaic efficiencyof nanostructured CZTS/ZnS/ZnO based solar cell device, S. Vallisree1 · R. Thangavel1 · T. R. Lenka2, Journal of Materials Science: Materials in Electronics, 29:7262–7272, 2018.

[33] Khamsa Necib et al., Investigation of the effects of thickness on physical properties of AZO sol-gel films for photonic device applications, Journal of Alloys and Compounds 735, 2017.

[34] Journal of Energy and Power Engineering 13 (2019) 32-36 doi: 10.17265/1934-8975/2019.01.003Effect of CZTS Parameters on Photovoltaic Solar Cell from Numerical Simulation, Abdellah Benami.

[35] Yuguo Tao and Ajeet Rohatgi, "High-Efficiency Front Junction n-Type Crystalline Silicon Solar Cells," Nanostructured Solar Cells, Ch 6.

[36] Wenhao Zhao, Wenli Zhou, Xiangshui Miaol, "Numerical Simulation of CZTS Thin Film Solar Cell," NEMS 2012, Kyoto, JAPAN, March 5-8,2012

Chapter 7: Conclusions

Photovoltaics (PV) is a renewable and environmentally friendly source of energy. It is widely recognized as one of the leading future resources of renewable energy. Currently, the PV industry is a "booming" business with an annual growth of 30-40 %. A drop in the cost per kWh can be accomplished by boosting module conversion efficiency or lowering production costs. The partial absorption of the solar spectrum, which leads to a severe drop in efficiency, is a key issue with thin-film photovoltaic cells. To comprehend and solve the issues that vitiate the solar cells for improving overall efficiencies may result in great photovoltaic process exploitation.

The work described within this Ph.D. dissertation has focused on five major objectives (Sec 1.3). By addressing those, the main contribution of this research work is summerised below.

The purpose of the thesis is to construct and regulate the high quality CZTS **deposition process** on the one hand, and to acquire a better discernment of the role of **fabrication parameters** in film growth on the other. Moreover, there are numerous challenges like grain size, smoothness of the surface, roughness, stoichiometric ratio, volatility of tin (Sn), pinholes that confront the approach of the highly textured film. In this investigation, crystal structure, surface morphology, composition, and optical features have been studied rigorously to comprehend and enhance the progression and phase formation of CZTS thin film to obtain preferred stoichiometry and photovoltaic properties. The novelty of the work is the efficacious production of quaternary CZTS film (~200nm) on see through glass substrate by a single sputtering unit at 200° C with an elusive CZTS target followed by annealing treatment at 470° and 560° C in N_2 atmosphere. And base pressure is varied as 150, 250, 350, 450 Torr. There have been a lot of studies done on annealing temperature this far. It's the first time, however, that the effect of a shift in base pressure has been documented. It has been discovered that annealing in a N_2 atmosphere is required for better grain development. This investigation establishes the performance of annealing parameters (i.e. pressure, temperature, and atmosphere) to obtain high quality CZTS film with the anticipated film thickness and stoichiometry. The study of surface morphology reveals that the sputtered film has much even topography and thickness instigate from Volmer-Weber mode than that of sol-gel method. In addition, the film has much better covering and stoichiometry and larger crystallite size than the film produced by sol gel method. It is depicted that surface roughness upsurges with rising annealing temperature. rms Roughness hasn't changed much with base pressure for the sample annealed at 470° C. However, for the films annealed at 560° C, it changes drastically at 350-450 Torr. Mechanical properties will be affected by nano roughness. Interestingly enough, rough films have an improvement in several properties that are directly connected with an increase of surface area e.g. mechanical stability, emittance, dielectric functions. Finally, it is evident that both the spin coated and sputtered films are Cu sufficient and Zn deficient. SnS loss arises at considerable rates in CZTS thin films at temperatures of 550 °C and above. However, the sulfur to metal ratio is compatible with previous reports even without sulfurization.So we can conclude that sputtering will be the best option for producing a complete CZTS solar cell because it is both manufacture compatible and moderately inexpensive compared to other vacuum deposition processes.

This thesis, on the other hand, looked into the properties of **AZO** as a plausible alternative to more expensive ITO or FTO. However, the electric property of AZO could be better to achieve a higher efficiency solar cell. Chemical Vapor Deposition (CVD) and Physical Vapor Deposition (PVD) process with higher annealing temperature might be a great way for far better AZO film. Annealing (after heat exposer) with Argon (Ar) or pure Hydrogen (H_2) flow results in improved and more

consistent electric characteristics. A further increase in total current through a mere optimization (annealing with pure H_2 or a mix of Ar and H_2 atmosphere) should be possible.

According to research objectives, a complete and optimized **SLG/ Mo/CZTS/CdS/i-ZnO/AZO** solar cell fabrication process is developed. It comprised of subsequently deposited sputtered Mo for the back contact, sputtered CZTS absorber layer, chemical bath deposited CdS buffer layer, sputtered AZO and ITO as the window layer, and e-beam evaporated silver(Ag) for the grid front contact. Due to the issues of non uniform texture of AZO and poor electric property, the final PCE is not as it is expected. Issues i.e. stacking fault, interfacial defects, interrupted use of clean room, time constrains and film degradation over time plays a key role for low range of PCE from the practical devices. Finally, we use numerical simulations through Solar Cell Capacitance Simulator-1 Dimension (SCAPS-1D) to investigate the performance of a CZTS thin film solar cell. A vast numerical analysis has been performed to investigate the effect band gap,E_g and film thickness of CZTS and AZO thin film on PCE of theoretical model. From the Simulations of CZTS thin film solar cell, the maximum PCE is shown as 23.74% with V_{oc}= 1.62 V, J_{sc}= 28.37 mA/cm^2 and FF= 51.55% for CZTS absorber layer of 3000 nm. The results definitely paves the way towards understanding the performance and operation mechanism of proposed CZTS thin film solar cells. In the future, there is scope of research to improve the junction properties of successive layers of thin-film solar cells. Furthermore, efforts should be made to develop and quantify the electron injection efficiency between the layers to achieve higher efficiency for fabricated solar cell. Overall, we may conclude that by addressing crystal defects, morphology, stoichiometry, and mixed phases, this research contributes valuable insights and practical solutions for advancing solar cell technology. The findings from this project definitely have the potential to lead to more efficient and cost-effective solar energy harvesting, paving the way for a greener and sustainable future.

Future Work

- For sputter growth CZTS thin film, change in Sn composition with annealing temperature and pressure arises instantaneous curiosity for a vast study as it is associated with band gap energy (E_g).
- Roughness has changed drastically for higher annealing temperature (560° C) from 350-450 Torr which recommends high mechanical stability of the upper buffer layer of CdS.
- Microsturctural parameters i.e. dislocation density (δ) and starin (ε) can be determined using Reciprocal Space mapping from XRD which is more reliable. AFM can also be utilized to determine quantitative dislocation density by observing singularities in atomic structure.
- An addition of Back Surface Field (BSF) layer in solar cell would help to increase the efficiency.
- Modelling, simulation and fabrication of p+/p/n/n+ configuration catches much interest in recent times.
- Performing defect analysis and stability and reliability studies over time for commertial purpose.